Linear and nonlinear electron-acoustic waves in plasmas with two electron components

RICHARD LESTER MACE

Submitted in partial fulfilment of the requirements for the degree of Doctor of Philosophy in the Department of Physics, University of Natal

Durban
December 1991

Preface

The work described in this thesis was carried out by the author from January 1988 to December 1991, in the Department of Physics, University of Natal, Durban, under the supervision of Professors M.A. Hellberg and R. Bharuthram (University of Durban-Westville).

These studies represent original work by the author and have not been submitted in any form to another university. Where use was made of the work of others, it has been duly acknowledged in the text.

Acknowledgements

Firstly, I would like to thank Professor Manfred Hellberg, my supervisor, whose advice, enthusiasm and encouragement is worthy of special mention. Working with Professor Hellberg has been a thoroughly enjoyable, enlightening and invaluable educational experience.

I extend my sincere thanks to Professor Ramesh Bharuthram, for kindly standing in as my supervisor during Professor Hellberg's absence, for his encouragement and for the valuable discussions we held.

My thanks to Dr. Rod Greaves, Eldridge Van Niekerk and Dr. Mike Alport, whose unselfish assistance in the computing laboratory is greatly appreciated.

Discussions with Dr. Satya Baboolal, Prof. A.D.M. Walker, Prof. M.J. Scourfield, Prof. Jim McKenzie and Dr. Sunil Maharaj have been most valuable.

I would like to extend my thanks to fellow students of past (Dr. John Waltham, Dr. Mark Notcutt, Richard Gaunt, Richard Cazalet, Neil Frank and Bradley Hansen) and present (Ricardo Buccellato and Clemens Dempers) for useful discussions and generally making life in the plasma laboratory more congenial.

The financial support of the Council for Scientific and Industrial Research, F.R.D. is acknowledged.

Finally, I would like to thank Hamming, whose motto, "the purpose of computing is insight, not numbers", *loudly* exclaimed, proved to be an indispensable aid in venting frustration at the computer terminal.

Abstract

Measurements of broadband electrostatic wave emissions in conjunction with particle distributions in the earth's magnetosphere, have provided motivation for a number of studies of waves in plasmas with two electron components. One such wave—the electron-acoustic wave—arises when the two electron components have widely disparate temperatures (Watanabe & Taniuti 1977), and has a characteristic frequency that lies between the ion and electron plasma frequencies. Because of this broadband nature and because it is predominantly electrostatic, it provides a likely candidate for the explanation of the electrostatic component of "cusp auroral hiss" observed in the dayside polar cusp at between 2 and 4 earth radii as well as the broadband electrostatic noise (BEN) observed in the dayside polar regions and in the geomagnetic tail. The electron-acoustic wave and its properties provide the subjects for much of the investigation undertaken in this thesis.

The thesis is divided into two parts. Part I is concerned with certain aspects of the linear theory of the electron-acoustic wave and is based on a kinetic description of the plasma. The dispersion relation for plane electrostatic waves obtained via linearisation of the Vlasov–Poisson system is studied in detail using analytical and numerical/geometrical techniques, and conditions under which the electron-acoustic wave arises are expounded. This work represents an extension of earlier works on Langmuir waves (Dell, Gledhill & Hellberg 1987) and the electron-acoustic wave (Gary & Tokar 1985).

The effects of electron drifts and magnetization are investigated. These result, respectively, in a destabilization of the electron-acoustic wave and a modification of the dispersive properties. In this plasma configuration the model more closely replicates the conditions to be found in the terrestrial polar regions. We extend the parameter regimes considered in earlier works (Tokar & Gary 1984) and in addition, identify another electron sound branch related to the electron-cyclotron wave/instability.

Effects of ion-beam destabilization of the electron-acoustic wave are also investigated briefly with a view to explaining BEN in the geomagnetic tail and also to provide a comparison with the electron-driven instability.

In part II the nonlinear electron-acoustic wave is studied by employing a warm hydrodynamic model of the plasma components. We first consider weak nonlinearity and employ the asymptotic reductive perturbation technique of Washimi & Taniuti (1966) to render the hydrodynamical equations in the form of simpler evolutionary equations describing weakly-nonlinear

electron-acoustic waves. These equations admit solitary-wave or soliton solutions which are studied in detail.

Wherever possible we have justified our small amplitude results with full numerical integration of the original hydrodynamical equations. In so doing we extended the range of validity of our results to arbitrary wave amplitudes and also find some interesting features not directly predicted by the small amplitude wave equations. In this respect we were able to determine the important role played by the cool-to-hot electron temperature ratio for soliton existence. This important effect is in accordance with linear theory where the electron temperature ratio is found to be critical for electron-acoustic wave existence.

The effects of magnetization on electron-acoustic soliton propagation is examined. We found that the magnetized electron-acoustic solitons are governed by a Korteweg–de Vries–Zakharov–Kusnetsov equation. In addition, it is shown that in very strong magnetic fields ion magnetization can become important yielding significant changes in the soliton characteristics. Multi-dimensional electron-acoustic solitons, which have greater stability than their plane counterparts, are also briefly discussed.

Employing a weakly-relativistic hydrodynamic model of the plasma, the effect of a cool, relativistic electron beam on such soliton parameters as width, amplitude and speed is studied in detail. Both small- and large-amplitude solitons are considered. The arbitrary-amplitude theory of Baboolal *et al.* (1988) is generalised to include relativistic streaming as well as relativistic thermal effects. The importance of the cool electron (beam)-to-hot electron temperature in conjunction with the beam speed is pointed out.

Finally, we derive a modified Korteweg–de Vries (mKdV) equation in an attempt to establish whether electron-acoustic double layers are admitted by our fluid model. Although double layers formally appear as stationary solutions to the mKdV equation, the parameter values required are prohibitive. This is borne out by the full fluid theory where no double layer solutions are found.

Contents

Part I

Linear theory

We must therefore discover some method of investigation which allows the mind at every step to lay hold of a clear physical conception, without being committed to any theory founded on the physical science from which that conception is borrowed, so that it is neither drawn aside from the subject in pursuit of analytical subtleties, nor carried beyond the truth by a favourite hypothesis.
(The Scientific Works of James Clerk Maxwell, Vol. I, p. 156.)

Chapter 1

Introduction to part I

The study of plasmas dates back to the 19th century when Michael Faraday investigated electrical discharges through gases. Modern plasma physics, however, had its beginnings in 1957 and 1958 when the Soviet *Sputnik* and American *Explorer* spacecrafts discovered that space near earth is filled with plasma. At the same time, till then secret research on controlled thermonuclear fusion conducted by the U.S., Soviet Union and Europe was revealed at the *Atoms for Peace* conference in Geneva, greatly increasing the freely available information on plasmas.

The richness and diversity of wave modes supportable by plasmas has provided much of the stimulus for their study. In pace with the ever-increasing body of experimental and observational data, has been the complexity of plasma models. Nowadays plasmas with multiple ion species (Fried *et al.* 1971), multiple electron components (Watanabe & Taniuti 1977), negative ions (Verheest 1988), positrons (Lominadze, Melikidze & Pataraya 1984, and references cited therein) and charged dust particles (de Angelis, Formisano & Giordano 1988; Rao, Shukla & Yu 1990) etc. are not uncommon in the literature. This has led to the recognition of an ever-increasing number of plasma wave modes and instabilities, making a full review an impossibility in a work such as this.

In this chapter we shall, however, point out some of the applications of plasma wave theory, with special emphasis on collisionless shock waves, polar cusp hiss and broadband electrostatic noise (BEN), which have direct relevance to the electron-acoustic wave/instability. We conclude this introduction with a brief review of pertinent work on the linear electron-acoustic wave and an outline of the work to be presented in part I.

1.1 Applications of plasma wave theory

Without doubt, one of the most important applications of man-made plasmas is the control of thermonuclear fusion reactions, which holds a vast potential for the generation of power.

The basic problem in achieving controlled thermonuclear fusion is to generate a plasma at very high temperature (with thermal energies at least in the 10 keV range) and confine its particles long enough for a substantial number of fusion reactions to take place. The need for the high temperature comes from the fact that the particles must come sufficiently close together, $\sim 10^{-12}$ cm, for significant wave-function overlap, which requires sufficient thermal energy to surmount the Coulomb barrier.

Since plasma waves determine the magnetohydrodynamic (MHD) instability time scale, and fusion plasmas are fraught with microinstabilities and the ensuing turbulence, the understanding of both linear and nonlinear waves and instabilities has played an important part in the development of wave theory. Plasma wave heating has also recently come to the forefront, leading to even more refinement in wave theory as one tries to model successfully the scenarios for using plasma waves to raise the plasma temperature to ignition levels.

Natural plasmas are ubiquitous. Modern astrophysics and especially radio astronomy have uncovered numerous sources of radiation that are likely to originate from plasmas. The archetypal Crab nebula is a rich source of plasma phenomena because it is known to possess a magnetic field. In addition it contains a visual pulsar. The pulsar, which commonly emits radiation in the radio-wavelength regime, is a veritable goldmine of plasma phenomena. Current theories of pulsars generally picture them as rapidly rotating neutron stars (Gold 1969) with very strong electric and magnetic fields (Sturrock 1971). Although theories of the pulsar magnetosphere may differ in certain aspects they all have one common feature: the presence of a relativistic electron-positron plasma (see Lominadze, Melikdze & Pataraya (1984) and references cited therein). It is from wave processes in these plasmas that the radio wave emission is thought to originate (Lominadze *et al.* 1984).

In addition to those examples cited above there are numerous other applications of plasma wave theory, but for want of space we shall not go into those here. We shall, however, elucidate three of the more important cosmic/space applications of plasma waves that are relevant to the application of electron-acoustic wave theory.

1.2 Collisionless shock waves

In an ordinary gas or aerodynamic shock wave the faster moving fluid particles in the denser regions of the fluid rush ahead of the others, colliding with the slower particles ahead of the shock and so bringing these particles up to the speed of the moving wave. In a collisionless shock, as the name implies, this process ceases to dominate. In a collisionless shock wave the collisional process is replaced by the combined effects of wave dispersion and wave-particle interations (Sagdeev (1966) and references cited therein).

A collisionless shock is defined as one in which the shock width is significantly less than the characteristic Coulomb collisional mean free path. The dissipation mechanism which permits such a relatively sharp transition to be maintained is generally considered to be wave-particle interactions, i.e. the scattering of plasma particles by fluctuating fields driven to enhanced amplitudes by plasma instabilities. If it were not for such interactions the competition between wave dispersion and nonlinearity (see part II) would lead to the formation of infinitely long trains of solitons. However, given such dissipation mechanisms the train of solitons is damped leading to the formation of an oscillatory shock front. The strength of this dissipation mechanism effectively determines the shock or transition width.

Ness *et al* (1964), using data collected from the *IMP-1* spacecraft, detected clear signs that a collisionless shock exists where the solar wind encounters the earth's magnetic field—the so-called bow shock—so providing the first experimental evidence for this phenomenon. More recent research has demonstrated that collisionless shocks abound in cosmic and astrophysical settings (see e.g. Kirk & Schneider 1987; Begelman & Kirk 1990). An important part of the understanding of collisionless shocks is the understanding of the dissipation mechanisms. This has led to the investigation of many wave and instability problems including those involving the electron-acoustic wave.

Thomsen *et al.* (1983) undertook a study of electrostatic wave instabilities generated by observed nonequilibrium particle distribution functions in an effort to explain the significant electric field component parallel to the static background magnetic field (Rodriguez & Gurnett 1975) in the earth's bow shock. They modelled the electron distribution by two components: a modified Lorentzian distribution and a convected Maxwellian component. It was found that both the electron-acoustic and ion-acoustic waves were destabilised by the field-aligned free energy source, and furthermore, that these instabilities appear to be good candidates for explaining the most

intense waves at near 3 kHz.

Intense electrostatic waves with frequencies ranging up to and above the electron plasma frequency are often observed upstream of the earth's bow shock in conjunction with energetic ions and electrons. It was suggested (Gurnett & Frank 1978) that this broadband electrostatic noise (BEN) is due to highly (upward) Doppler-shifted ion-acoustic waves. In a study of the electron-acoustic instability Marsch (1985) demonstrated that the electron-acoustic wave provides an alternative explanation for this BEN (or at least a complementary theory).

1.3 Cusp Auroral hiss

As remarked by Gary (1987), perhaps one of the most convincing applications of electron-acoustic wave theory concerns its application to cusp hiss—enhanced electrostatic and electromagnetic field fluctuations extending up to the local electron gyrofrequency in the terrestrial polar cusp.

First observations of intense electric field noise along the auroral field lines were made by the *OV1-10* spacecraft (Heppner 1969). These waves were later studied in greater detail by the *Hawkeye 1* and *IMP 6* satellites (Gurnett & Frank 1977), by the *Dynamics Explorer-1* (*DE-1*) spacecraft (Gurnett *et al.* 1976) and by the *Viking* satellite (Pottelette *et al.* 1988; 1990).

The *DE-1* satellite made *in situ* plasma and field measurements across the polar cusp at radial distances of between 2 and 5 earth radii. In the nightside auroral zone (Gurnett *et al.* 1983) the hiss observed by the *DE-1* spacecraft was mainly electrostatic and believed to consist primarily of whistler waves propagating upward from a wave source whose lower boundary lay between 0.7 and 0.9 earth radii. At altitudes lower than about 3000 km the auroral hiss is electromagnetic and frequently detected by satellites as downward propagating whistler waves (Gurnett & Frank 1972; Shawhan 1979). Auroral hiss at these lower altitudes has been found to be closely correlated with intense fluxes of low energy (100 eV to 1 keV) precipitating electrons in the dayside auroral zone (Gurnett 1966; Hoffman & Laaspere 1972). In the nightside auroral zone Gurnett & Frank (1972) specifically showed that an auroral hiss event occurred in direct association with an intense inverted V electron precipitation event. It is well known that intense inverted V electron fluxes are characterised by downward beams with a beam energy typically about several keV (Lin & Hoffman 1982).

In the dayside polar cusp the electron beams correlated with hiss emission are not related to inverted V events because these beams are moving in the upward direction (Lin *et al.* 1984). These upward electron beams occur just equatorward of, and extend up into the polar cusp region. Lin *et al.* (1984) demonstrated a strong correlation of low-energy electron beams with auroral hiss emission at a few kHz, at altitudes above two earth radii near the polar cusp. They reported the occurrence of both upward and downward electron beams with energies less than 100 eV but the upward beams were generally more intense than the downward by an order of magnitude in the number density. These electron beams are believed to be charge carriers of the dayside region 1 field-aligned currents (Tokar & Gary 1984).

Tokar & Gary (1984) showed that the electron-acoustic instability is a very likely candidate for the explanation of cusp auroral hiss in the dayside polar cusp. Plasma in the polar cusp consists of three electron components: a cool component whose temperature is $\sim$ 1 eV, a warm beam component $T_b \sim 20$ eV and a much hotter component with a temperature of 100 eV and above. By solving the full electromagnetic dispersion relation for electromagnetic waves in a plasma with constituents modelled on *DE-1* data, they showed that the electron-acoustic wave was unstable for polar cusp parameters. Furthermore, they demonstrated that the whistler wave is stable for these same parameters and hence cannot account for the electrostatic component of cusp hiss. Tokar & Gary (1984) calculated the group velocity of the electron-acoustic wave and demonstated its consistency with the "funnel-shaped" frequency-time profiles observed by *DE-1*. Lin *et al.* (1985), Roth & Hudson (1986) and Lin *et al.* (1987) performed particle simulations which further supported the view that electron-acoustic waves are responsible for the electrostatic component of cusp hiss.

1.4 Auroral BEN

In addition to auroral hiss, impulsive electrostatic wave emissions extending over a broad range of frequencies are also frequently observed in the auroral magnetosphere. Although, in opposition to auroral hiss, these emissions have neither a well-defined cut-off frequency nor a fixed polarization (which could be explained by the fact that they have different physical origins (Dubouloz *et al.* 1991a)), they are often referred to by the same name: broadband electrostatic noise (BEN).

The physical context of BEN in the auroral zone is quite different from

that in the magnetotail, which justifies a separate study. In particular the electron plasma frequency in the low density region of the auroral magnetosphere is smaller than the electron gyrofrequency, and the highly energetic (between 1 and 40 keV) field-aligned ion beams are not observed to be correlated with BEN emissions, as is the case in the magnetotail (Schriver & Ashour-Abdalla 1987).

The first observations of BEN in the auroral magnetosphere were reported by Gurnett & Frank (1977), but after the launch of the Swedish satellite *Viking* in 1986 it has been possible to study these wave emissions with a higher degree of time resolution. *Viking* has revealed the presence of intense and impulsive BEN in the low-density region along the auroral field lines in the 2000 to 10000 km altitude range (Pottelette *et al.* 1988; 1990), which is somewhat lower than the altitude range covered by *DE-1* ($\sim$ 13000 to 32000 km). The characteristic variation time of the emission is of the order of a few hundred milliseconds and the total electric field amplitude can reach up to $100\,\mathrm{mV\,m^{-1}}$. The range of wave frequencies is found to extend up to and even higher than the electron gyrofrequency, however, most of the wave power is concentrated in the lower frequencies near the ion plasma and lower hybrid frequencies (Dubouloz *et al.* 1991b).

The plasma composition in this region consists of a cool electron component (temperature of a few eV), a warm drifting component, and a hot component whose temperature lies between 100 and 200 eV. As discussed by Dubouloz *et al.* (1991b) and previously reported by Tokar & Gary (1984) and Gary (1987), such conditions highly favour the destabilization of the electron-acoustic wave. Furthermore, the intense bursts of BEN are usually associated with strong depletions of the cool electron density (Dubouloz *et al.* 1991b) which further favours the destabilisation of the electron-acoustic wave. Under quiescent conditions, however, plasma data suggest that the cool and hot electron densities are equal.

Dubouloz *et al.* (1991a) showed that nonlinear effects must play a significant role in the generation of BEN in the dayside auroral zone. Evidence supporting the latter includes: (i) the very high electric field amplitudes involved, and (ii) the power law shape of most of the BEN spectra above a few kHz. In fact, Douboloz *et al.* (1991b) showed that electron-acoustic solitons passing by the satellite would generate spectra that can explain the high-frequency part of BEN, above the plasma frequency, in the dayside auroral zone.

1.5 A brief review of electron-acoustic waves

Electron-acoustic waves are by no means new. They were first identified as strongly damped acoustic-like solutions of the dispersion relation for electrostatic waves in the work of Fried & Gould (1961). However, because of their very strong damping under most circumstances, they have not been deemed worthy, by the majority of researchers in the field, of extensive research, receiving only passing attention in the literature (Stix 1962; Denavit 1965).

In contrast to the usual criterion for weakly-damped ion-acoustic waves, when the ion temperature is very much larger than the electron temperature, Sizonenko & Stepanov (1967), Aref'ev (1970) and Lashmore-Davies & Martin (1973) showed that a weakly-damped electron-acoustic wave may arise, which propagates quasi-perpendicularly to the magnetic field. The wave was found to be destabilised by a perpendicular ion drift u_{0i}, even if the perpendicular velocity is less than the ion thermal velocity v_i, (Sizonenko & Stepanov 1967). The dispersion relation for this electron-acoustic wave is given by

$$\omega = k_\perp u_{0i} + \frac{k_\parallel v_{se}}{(1 + k^2 v_i^2/\Omega_e \Omega_i)^{1/2}}, \tag{1.1}$$

(Aref'ev 1970), where Ω_e and Ω_i are the electron and ion gyrofrequencies, respectively; and the electron sound speed is given by $v_{se} \equiv (T_i/m_e)^{1/2}$.

Further investigation of this wave/instability by a number of authors, took place in subsequent years. Goedbloed, Pyatak & Sizonenko (1973) investigated the electron-acoustic and drift instabilities in a plasma with a perpendicular current, allowing for electromagnetic effects. Kitsenko, Panchenko & Stepanov (1974a, 1974b) considered the excitation of the electron-acoustic and ion cyclotron parametric instabilities by an alternating electric field perpendicular to the magnetic field.

Mohan & Yu (1983) showed that drift dissipative instabilities could occur between the ion and electron gyrofrequencies $\Omega_i \ll \omega \ll \Omega_e$. They further demonstrated that these instabilities are associated with the electron-acoustic and lower-hybrid waves. Dash, Sharma & Buti (1984) generalised the analysis to include a second hot ion component. Contrary to their own expectations they found no mode conversion between the electron-acoustic and ion-ion hybrid resonance waves.

A common factor in all the abovementioned works, is the large ion temperature relative to that of the electrons, necessary for weak Landau damping of the electron-acoustic wave. Unfortunately, this condition is difficult

to fulfil in the laboratory but may arise naturally in some regions of the terrestrial magnetosphere. In support of the latter remark we cite the plasma models of Grabbe & Eastman (1984) and Grabbe (1985), which were based on particle data from the *ISEE-1* satellite. Today still, however, the comment by Montgomery (1971) that "they (electron-acoustic waves) have not played an important role in any theories or experiments to date" seems to hold true—at least as far as plasmas with a single electron component are concerned.

It was some years after the initial works of Sizonenko & Stepanov (1967), Aref'ev (1970) and Lashmore-Davies & Martin (1973) that the suggestion of Watanabe & Taniuti (1977) was put forward. They proposed that if the electron component was nonisothermal, i.e. it comprised two separately isothermal populations with widely disparate temperatures, then an electron-acoustic wave which suffered only weak Landau damping could occur without the necessary presence of a magnetic field, and apparently independently of the ion temperature.

Two approaches to the investigation of the electron-acoustic wave ensued: the first was to treat the ions as a hot isothermal component (Yu & Shukla 1983) yielding the so-called modified electron-acoustic wave; and the second was to assume cold/cool ions and examine an electron-acoustic wave due solely to the electron dynamics (Tokar & Gary 1984). The latter approach rendered interesting results applicable to the understanding of cusp auroral hiss as well as the broadband electrostatic noise observed upstream of the earth's bow shock, as discussed previously.

Yu & Shukla (1983) investigated the linear and nonlinear behaviour of the modified electron-acoustic wave in a plasma consisting of hot isothermal ions, a cool fluid electron component and a hot isothermal electron component. They derived the following dispersion relation for the modified electron-acoustic wave

$$\omega = \frac{\omega_c}{(1 + 1/k^2\lambda_{Dh}^2 + 1/k^2\lambda_{Di}^2)^{1/2}}, \tag{1.2}$$

where ω_c is the plasma frequency of the cool electron component and λ_{Dh}, λ_{Di} are the Debye lengths of the hot electron and ion components, respectively. In addition, they derived a Korteweg–de Vries equation for the nonlinear wave. The analysis was extended to include a second hot ion component by Guha & Dwivedi (1984). They noted the effects of the second ion species, but conceded that the electron parameters had the more profound effect on the characteristics of the wave.

Ashour-Abdalla & Okuda (1986) and Schriver & Ashour-Abdalla (1987) investigated the modified electron-acoustic instability in a magnetized plasma, driven by a hot, field-aligned ion beam. The former authors also performed a particle simulation of the instability. Both sets of authors noted the broadband nature of the instability and pointed out its possible application to the explanation of the Broadband Electrostatic Noise (BEN) observed in the magnetotail. In fact, ion beam driven instabilities have played an important part in the understanding of BEN in the magnetotail (Grabbe & Eastman 1984; Dusenbery & Lyons 1985; Dusenbery 1986).

The other route to the electron-acoustic wave and instability was taken, initially, by Thomsen, Barr, Gary, Feldman & Cole (1983). By modelling the electron distributions observed within the earth's bow shock with modified Lorentzian and drifting Maxwellian distributions, respectively, and incorporating a cool ion species, they identified two instabilities driven by the field-aligned free energy of the drifting electrons: the ion-acoustic instability whose real frequency lay below the ion plasma frequency; and the electron-acoustic instability with a real frequency of several times the ion plasma frequency.

Simultaneous plasma and wave observations in the cusp auroral region (*DE-1*) at altitudes between 2 and 4 earth radii have shown that there is a strong correlation between upward electron beams and electrostatic auroral hiss emissions (Lin, Burch, Shawhan & Gurnett 1984). Undertaking an instability analysis based on observed electron distribution functions that were modelled by hot, warm beam, and cool Maxwellian components, Lin *et al.* (1984) concluded that the whistler wave near resonance was responsible for the observed electrostatic emissions.

This conclusion was refuted by Tokar & Gary (1984). Using particle distributions similar to those of Lin *et al.* (1984), but employing the full electromagnetic dispersion relation, they showed that the whistler mode was stable for parameters relevant to the polar cusp and that it is the electron-acoustic wave that is unstable. Furthermore, they demonstrated that the dispersion of the electron-acoustic wave can account for the funnel shaped frequency-time spectra observed by the *DE-1* satellite in the high-altitude cusp auroral region.

A comprehensive parameter survey for the electron-acoustic wave was carried out by Gary & Tokar (1985). They showed that it was distinct from the electron plasma wave and demarcated regions in parameter space in which the electron-acoustic wave is weakly Landau damped. Among the more important results were the approximate existence criteria for the

electron-acoustic wave $T_h/T_c > 10$ and $n_{0c} < 0.8n_{0e}$. They showed that the dispersion relation for the wave is given by

$$\omega = kv_{se}, \tag{1.3}$$

at small wavenumbers $k\lambda_{Dh} \ll 1$, where $v_{se} \equiv (n_{0c}/n_{0h})^{1/2}v_h$, and satisfies

$$\omega^2 = \omega_c^2 \frac{1 + 3k^2\lambda_{Dc}^2}{1 + 1/k^2\lambda_{Dh}^2}, \tag{1.4}$$

at larger wavenumbers.

The electron-acoustic instability was investigated by Gary (1987). It was shown that a relative drift between the two electron components was able to provide the free energy necessary to destabilise the electron-acoustic wave. Two models were employed in the study: the zero-current model in which the total plasma current was zero, $n_{0h}\mathbf{v}_{0h} + n_{0c}\mathbf{v}_{0c} = 0$; and the hot electron current model in which the hot electrons bore a drift relative to the ions and cool electrons. The salient observations were: (i) in both models the electron-acoustic wave was unstable; (ii) in the zero-current model the ion-acoustic wave is also destabilised, and for a range of parameter values has a lower threshold than the electron-acoustic instability.

Particle simulations of the electron-acoustic wave in the polar cusp have been carried out by Lin, Winske & Tokar (1985), Roth & Hudson (1986) and Lin & Winske (1987). In all the simulations it was shown that the electron-acoustic instability always strongly heats the cool electron component, and that under many circumstances, this heating leads to saturation of the instability. Further, Lin, Winske & Tokar (1985) demonstrated that the electron-acoustic instability generated by observed distribution functions can indeed generate the electrostatic component of cusp hiss.

Recently, Bharuthram (1991a) investigated the electron-acoustic instability driven by a field-aligned anisotropic hot electron beam. It was found that increasing the temperature anisotropy of the beam and/or the cool electron component reduced wave growth. Furthermore, it was found that the electron-acoustic instability could only be excited for beam densities greater than $0.2n_{0e}$ where n_{0e} is the total electron density. This result is in agreement with the existence criteria for the electron-acoustic wave reported in earlier works (Gary & Tokar 1985; Mace & Hellberg 1990).

Bharuthram (1991b) also investigated the electron-acoustic instability driven by a cross-field hot electron beam. An important difference from the previous work (Bharuthram 1991a) is that in this case the electron-acoustic instability transforms into the modified two-stream instability as

obliqueness of the propagation angle increases relative to the magnetic field. Furthermore, whereas in the field-aligned scenario (Bharuthram 1991a) the anisotropy of the beam played a significant role, its effects are less important when the beam is perpendicular to the magnetic field.

1.6 Outline of part I

We begin with an introductory chapter (chapter 2) introducing the physical model of the electron-acoustic wave that shall concern us for the main part of this thesis. The basic wave properties, dispersion relation, damping and wave frequency are discussed.

Chapter 3 sees the introduction of a novel analytical geometrical technique of investigating wave behaviour through the topology of the dielectric function. Such techniques have been used before to investigate ion-acoustic waves in multi-ion plasmas (Fried *et al.* 1971; Gledhill & Hellberg 1986), and Langmuir waves in multi-electron plasmas (Dell, Gledhill & Hellberg 1987). Our work represents an extension of that of the latter. Moreover, we elucidate the relationship between the electron plasma wave and the electron-acoustic wave. The work presented in this chapter has appeared in *Journal of Plasma Physics.*

In chapter 4 the magnetized electron-acoustic instability driven by a field-aligned hot electron drift is investigated. The instability in this form was considered for an unmagnetized plasma by Gary (1987) and for a magnetized plasma, by Tokar & Gary (1984). The latter work, however, only covered a small region of parameter space. In this chapter not only is the strongly magnetized limit considered, as was the case before, but we also consider the situation when the electron gyrofrequency is less than the cool electron plasma frequency, $\Omega_e < \omega_c$, leading to some interesting results. In addition, the ion driven electron-acoustic instability is also investigated in this limit and results compared with those for the electron driven case.

This part ends with a brief conclusion summarising the results and bringing attention to possible extensions of the present theory. The derivations of some of the more important results are provided in the appendices.

Chapter 2

The electron-acoustic wave

This chapter serves as an introduction to the electron-acoustic wave. The dispersion, damping and wave dynamics are discussed in some detail. A more thorough parameter survey for the electron-acoustic wave has been carried out by Gary & Tokar (1985). The basic electrostatic dispersion relation derived here shall be the subject of further investigation in chapter 3.

2.1 Basic equations and plasma model

Consider a charge-neutral plasma comprising cool electrons, hot electrons and cool massive ions. We adopt a kinetic description of each plasma component based on the collisionless Boltzmann or Vlasov equation. Furthermore, we consider only electrostatic waves and make the electrostatic approximation

$$\mathbf{E} = -\nabla\phi. \tag{2.1}$$

Then the plasma may be described by the Vlasov–Poisson system:

$$\frac{\partial f_j}{\partial t} + \mathbf{v}\cdot\nabla f_j - \frac{q_j}{m_j}\nabla\phi\cdot\nabla_{\mathbf{v}} f_j = 0, \tag{2.2}$$

$$\nabla^2\phi = -4\pi\sum_j n_{0j} q_j \int f_j \,\mathrm{d}\mathbf{v}, \tag{2.3}$$

where the subscript j refers to the jth plasma component and in this case takes on the values $j = (i, h, c)$, and the operator $\nabla_{\mathbf{v}} = \partial/\partial\mathbf{v}$ is the gradient with respect to velocity. In the above form the Vlasov-Poisson system

is highly intractable and in order to gain further ground analytically it becomes necessary to make some approximations. We assume that the wave amplitude is so small that it introduces only a small perturbation to the plasma and the macroscopic electric field, i.e. we suppose

$$\left.\begin{aligned} f_j(\mathbf{x},\mathbf{v},t) &= f_j^{(0)}(\mathbf{v}) + f_j^{(1)}(\mathbf{x},\mathbf{v},t) \\ \phi(\mathbf{x},t) &= 0 + \phi^{(1)}(\mathbf{x},t), \end{aligned}\right\} \tag{2.4}$$

where only the perturbations have spatial and temporal dependence. Substitution of (2.4) into (2.2) and (2.3), and ignoring terms quadratic in small quantities leads to the linearised equations

$$\frac{\partial f_j^{(1)}}{\partial t} + \mathbf{v}\cdot\nabla f_j^{(1)} = \frac{q_j}{m_j}\nabla\phi^{(1)}\cdot\nabla_{\mathbf{v}} f_j^{(0)}, \tag{2.5}$$

$$\nabla^2\phi^{(1)} = -4\pi\sum_j n_{0j}q_j\int f_j^{(1)}\,\mathrm{d}\mathbf{v}. \tag{2.6}$$

Fourier and Laplace transforming equations (2.5)–(2.6), performing the necessary analytic continuation to the lower half of the complex ω–plane (Krall & Trivelpiece 1973), and assuming that the undisturbed particle distributions are Maxwellians yields the linear dispersion relation

$$\epsilon(\mathbf{k},\omega) = 0, \tag{2.7}$$

where

$$\epsilon(\mathbf{k},\omega) = 1 - \sum_{j=i,c,h}\frac{1}{2k^2\lambda_{Dj}^2}Z'\Big(\frac{\omega}{\sqrt{2}\,kv_j}\Big). \tag{2.8}$$

The subscripts i, h, c refer to the ions, hot electrons and cool electrons, respectively and $Z'(\zeta)$ is the derivative of the plasma dispersion function. It is conveniently written in the form

$$Z'(\zeta) = -2\left(1 + 2i\zeta\mathrm{e}^{-\zeta^2}\int_{-\infty}^{i\zeta}\mathrm{e}^{-t^2}\,\mathrm{d}t\right),$$

(Fried & Conte 1961) and clearly is related to the complex error function. Temperatures are understood to be measured in energy units throughout. The parameters are defined as follows: $\lambda_{Dj} = (T_j/4\pi n_{0j}e^2)^{1/2}$, the Debye length of species j; $v_j = (T_j/m_j)^{1/2}$, the thermal speed of species j; and $\omega = \omega_r + i\gamma$, is the complex wave frequency.

2.2 The dispersion relation for electron-acoustic waves

Watanabe & Taniuti (1977), employing a fluid treatment of a plasma consisting of ions, cool and hot electrons, showed that if the temperature of the hot electrons greatly exceeds that of the cooler, then the dynamical equations admit wave solutions whose phase velocity satisfies

$$v_i,\, v_c \ll \frac{\omega}{k} \ll v_h, \tag{2.9}$$

and are therefore weakly Landau-damped. They called this wave mode the electron-acoustic wave. In the context of (2.9) we can expand the relevant terms in (2.7) in their power or asmptotic series, whichever is the appropriate, to yield an approximate dispersion relation for electron-acoustic waves. The following expansions of the Z' function are employed:

$$\begin{aligned} Z'(\zeta) &\simeq -2(1 + i\pi^{1/2}\zeta \mathrm{e}^{-\zeta^2}), \qquad |\zeta| \ll 1; \\ Z'(\zeta) &\simeq \zeta^{-2} - 2i\pi^{1/2}\zeta \mathrm{e}^{-\zeta^2}, \qquad |\zeta| \gg 1. \end{aligned}$$

Furthermore, we assume that the damping is weak, i.e. that $|\gamma| \ll \omega_r$. Then using an expansion of the above form for each of the terms in (2.7) and separating the resultant equation into real and imaginary parts we obtain the dispersion relation for electron-acoustic waves (cf. Gary & Tokar 1985)

$$\omega_r^2 = \frac{\omega_c^2}{1 + 1/k^2\lambda_{Dh}^2} = \frac{k^2 v_{se}^2}{1 + k^2\lambda_{Dh}^2}, \tag{2.10}$$

where the electron sound speed is defined here by $v_{se} = (n_{0c}/n_{0h})^{1/2} v_h$, and the plasma frequency of the cool electrons, ω_c, is given by $(4\pi n_{0c} e^2/m_e)^{1/2}$. The damping rate is given by

$$\begin{aligned} \gamma \;=\; & -\left(\frac{\pi}{8}\right)^{1/2} \frac{n_{0c}}{n_{0h}} \frac{k v_h}{(1 + k^2\lambda_{Dh}^2)^2} \\ & \cdot \left[1 + \frac{n_{0c}}{n_{0h}} \left(\frac{T_h}{T_c}\right)^{3/2} \exp\left\{\frac{-1}{2k^2\lambda_{Dc}^2(1 + 1/k^2\lambda_{Dh}^2)}\right\}\right]. \end{aligned} \tag{2.11}$$

Equation (2.11) demonstrates that the Landau damping of the electron-acoustic wave depends critically on the cool-to-hot electron density ratio: the larger this ratio, the greater will be the wave damping. Therefore in

order to observe the electron-acoustic wave the cool electron density should ideally be less that that of the hot. This was also remarked by Watanabe & Taniuti (1977), but from a different argument.

In the small-wavenumber regime $k\lambda_{Dh} \ll 1$ the dispersion relation (2.10) can be written

$$\omega_r \simeq k v_{se} \tag{2.12}$$

and indicates that at sufficiently long wavelengths the waves all propagate at the same phase and group velocities—hence the name "electron-acoustic". At such wavelengths, however, equation (2.11) shows that the wave is strongly-damped by the hot electrons unless the cool electron number density is substantially less that that of the hot electrons.

At larger wavenumbers where the frequency approaches the cool electron plasma frequency, ω_c—the so-called cool plasma regime—the wave damping begins to decrease with wavenumber approximately like k^{-3} and at these intermediate wavenumbers Landau damping by the hot electrons diminishes. In addition, the wave mode becomes more oscillatory in nature. The dispersion relation at these intermediate and larger wavenumbers satisfies (Gary & Tokar 1985):

$$\omega_r^2 \simeq \omega_c^2 \frac{1 + 3k^2\lambda_{Dc}^2}{1 + 1/k^2\lambda_{Dh}^2}, \tag{2.13}$$

and illustrates the similarity of the wave at these wavelengths, to a plasma wave based on the cool electron component. The dispersion relation (2.13) may be derived from (2.7) by expanding the cool electron Z'–term to higher order in k than was done when deriving (2.10).

At still larger wavenumbers the wave continues to be cool plasma-like, but Landau damping due to the cool electrons now becomes significant. This can be seen by observing the second term in (2.11) which increases with increasing wavenumber and eventually leads to quenching of the wave mode.

In figures 2.1 to 2.4 we illustrate the dispersion and damping of the electron-acoustic wave (obtained by numerical solution of (2.7)) for a number of cool electron density values with a common value of the temperature ratio $T_h/T_c = 100$. The dispersion at small wavenumbers is indeed acoustic and the damping is strongest when the cool electron density is greater than the hot electron density. In figure 2.5 we illustrate the dispersion relation over a large range of wavenumbers clearly displaying the three regions: (i) the strongly-damped acoustic regime; (ii) the weakly-damped cool plasma regime; and (iii) the short-wavelength, strongly damped regime.

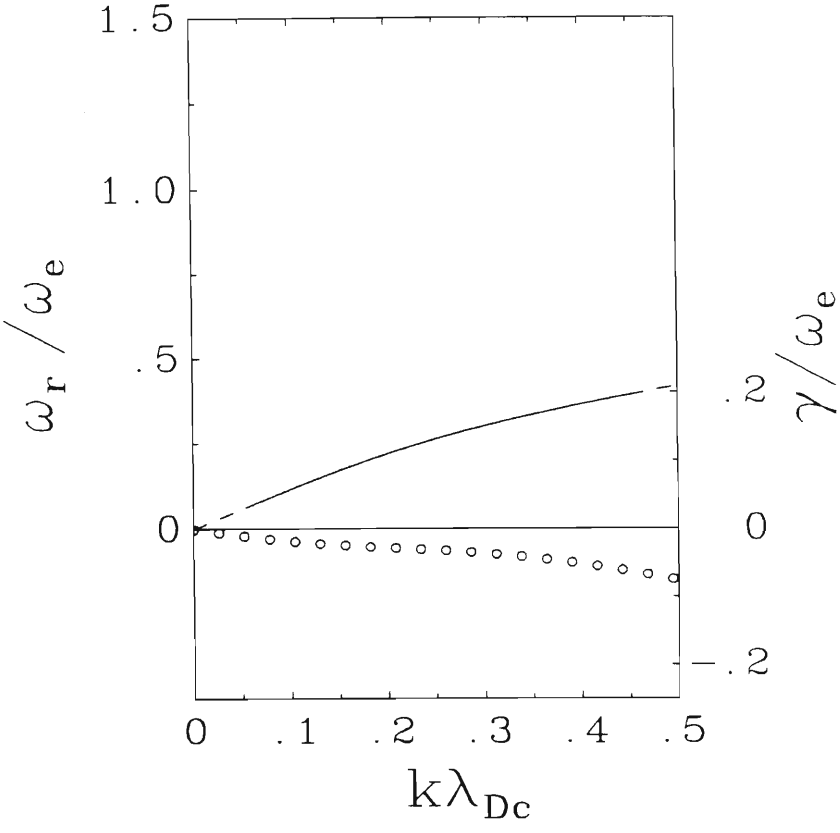

Figure 2.1: The dispersion relation (— or − − −) and damping rate (∘) of the electron-acoustic wave at a cool electron density of $n_{0c} = 0.1n_{0e}$. In this and other figures in this chapter the hot electron temperature is $T_h = 100T_c$ and ω_e denotes the plasma frequency calculated from the total electron density. In all figures the dashed portions of the curves for the real frequency indicate where $-\gamma > \omega_r/2\pi$.

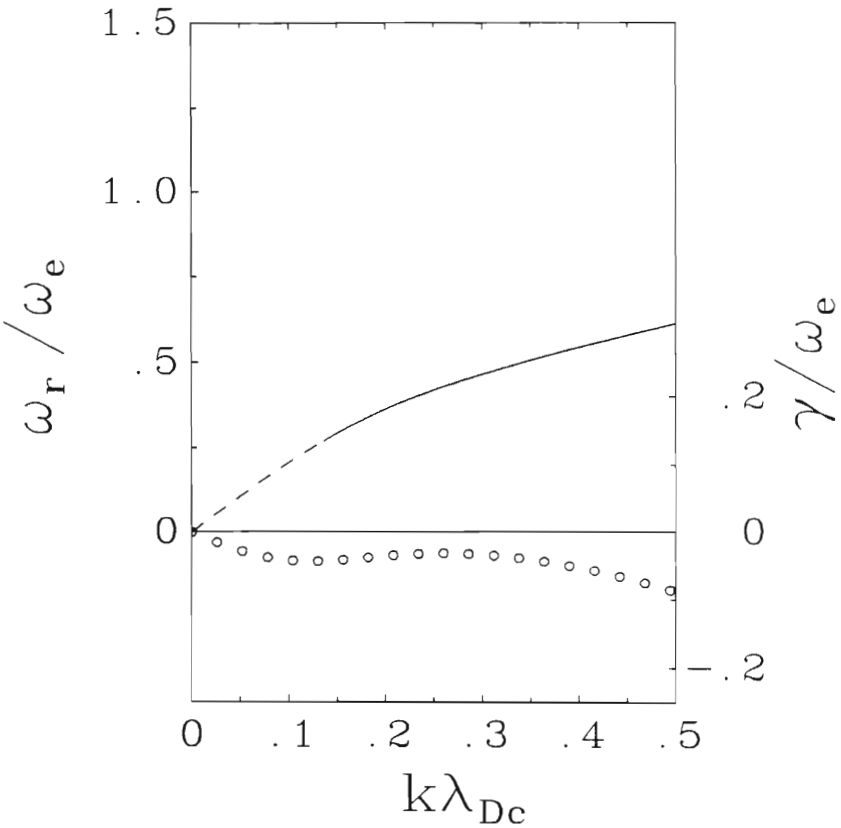

Figure 2.2: The dispersion relation and damping rate of the electron-acoustic wave for a cool electron density of $n_{0c} = 0.2n_{0e}$.

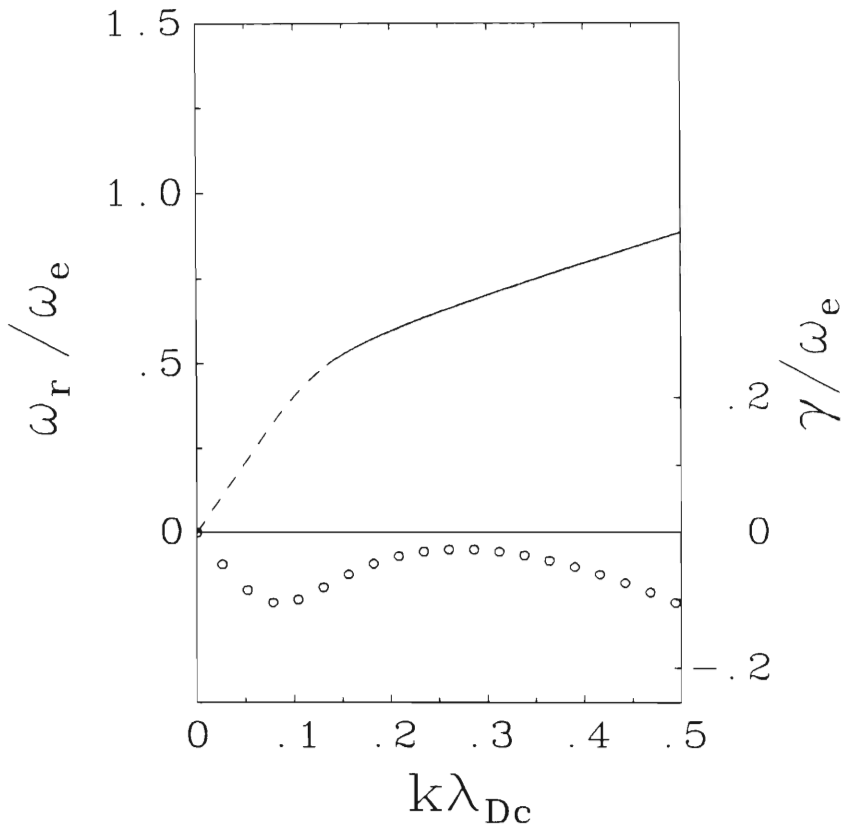

Figure 2.3: The dispersion relation and damping rate of the electron-acoustic wave for a cool electron density of $n_{0c} = 0.4n_{0e}$.

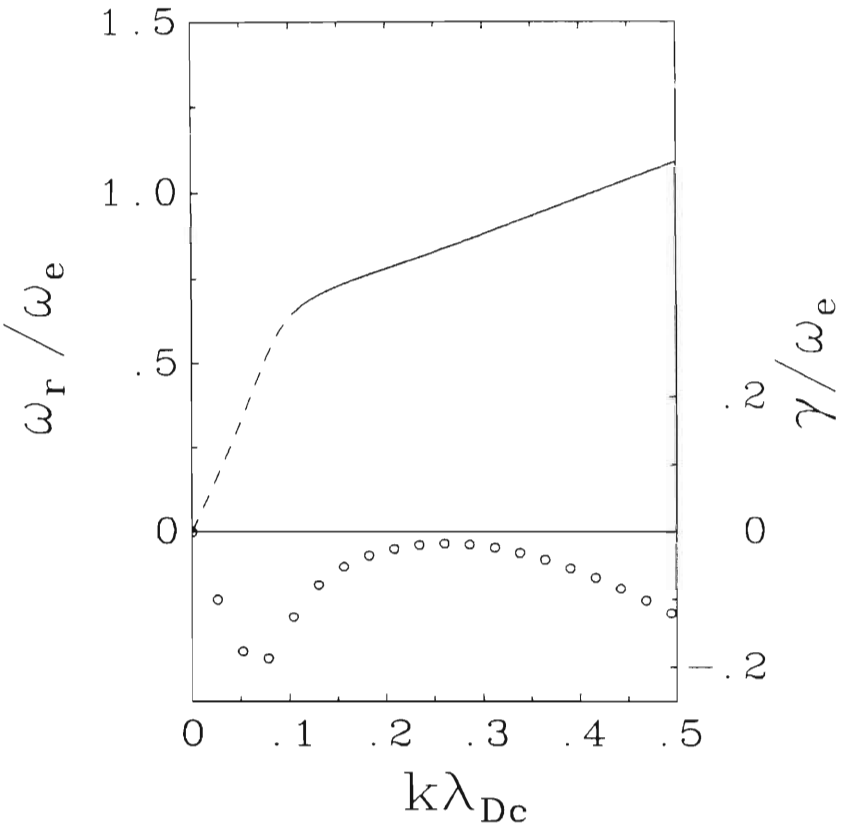

Figure 2.4: The dispersion relation and damping rate of the electron-acoustic wave for a cool electron density of $n_{0c} = 0.6n_{0e}$.

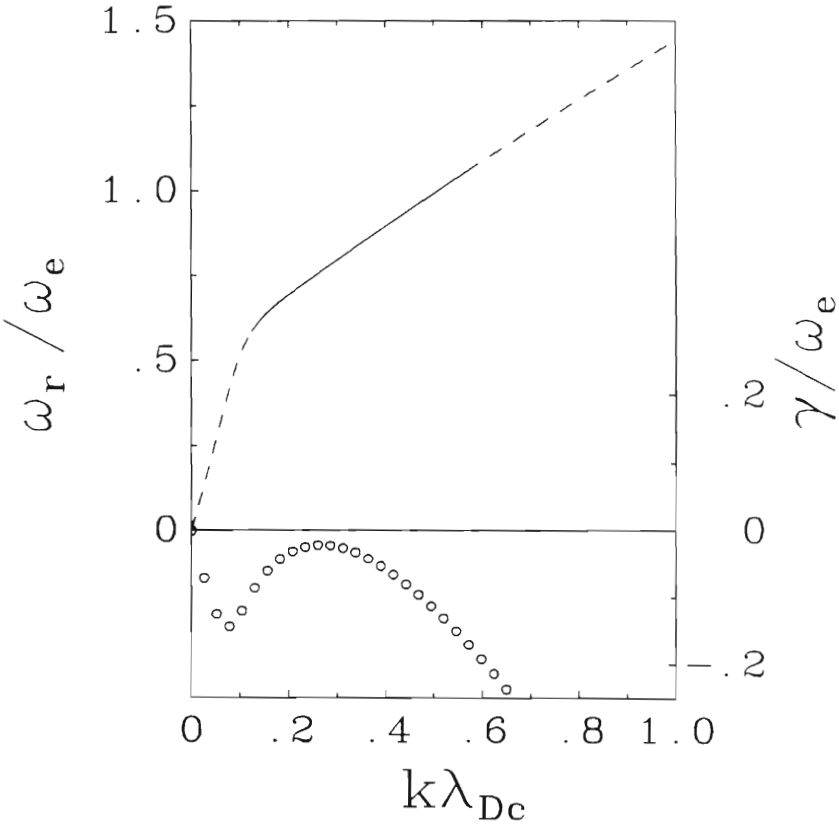

Figure 2.5: The dispersion relation and damping rate of the electron-acoustic wave for a cool electron density of $n_{0c} = 0.5n_{0e}$. The three regimes are clearly evident.

2.3 Comparison with the ion-acoustic wave

The electron-acoustic wave exhibits a number of properties similar to those of the ion-acoustic wave. The dispersion relation of the latter in a single electron–ion plasma is given by

$$\omega_r^2 = \frac{k^2 v_{si}^2}{1 + k^2 \lambda_{De}^2}, \tag{2.14}$$

where the subscript e refers to electron parameters and $v_{si} = (T_e/m_i)^{1/2}$ is the ion sound speed. Immediately one notices the similarity in form between (2.10) and (2.14). In fact, the dynamics of the electron-acoustic wave are analogous to those of the ion-acoustic wave if the following correspondence is made

$$\begin{aligned} \text{ions} &\longleftrightarrow \text{cool electrons}, \\ \text{electrons} &\longleftrightarrow \text{hot electrons}, \\ \text{vacuum/free space} &\longleftrightarrow \text{ions}, \end{aligned}$$

where the electron-acoustic wave plasma components occur on the right hand side of each relation. The ions and cool electrons provide the wave inertia in each case, which is coupled to the electric field, and the hot electrons in both cases provide dynamic neutralization of the charge imbalances. In the ion-acoustic wave no background neutralization is required because the plasma is already charge-neutral, but in the electron-acoustic wave, which is intrinsically an electron wave, a background of stationary cool ions is required to ensure overall charge-neutrality. These and other similarities are summarized in Table 2.1.

	electron-acoustic	ion-acoustic
dispersion rel.	$\frac{kv_{se}}{(1+k^2\lambda_{Dh}^2)^{1/2}}$	$\frac{kv_{si}}{(1+k^2\lambda_{De}^2)^{1/2}}$
sound speed	$\frac{\omega_c}{\omega_h}v_h$	$\frac{\omega_i}{\omega_e}v_e$
wave inertia	cool electrons	ions
dynamic neutr.	hot electrons	(hot) electrons
backgr. neutr.	cool ions	–

Table 2.1: The similarities/differences between the electron-acoustic and ion-acoustic waves.

Chapter 3

Higher-order electron modes in a plasma with two electron temperatures

It is well known that the electrostatic dispersion relation for waves in an unmagnetized, homogeneous, collisionless plasma of stationary ions and electrons admits an infinite number of complex solutions. The solutions that exhibit weak damping, i.e. their imaginary part is small with respect to their real part, are known as normal modes. It is these modes that govern the time-asymptotic behaviour of the plasma. The infinite set of solutions that excludes the normal modes are known as higher order modes (HOMs). These usually only play a role in the transient behaviour of the plasma, and are thus, in general physically unimportant.

Fried & Gould (1961) showed that in an electron-ion plasma the electron-acoustic wave is strongly damped and therefore does not appear as a normal mode under normal circumstances. The most common electrostatic normal modes in an unmagnetized plasma are the ion-acoustic and electron plasma or Langmuir waves/modes. It was pointed out by Watanabe & Taniuti (1977) that if the electron species consists of two separately isothermal populations then the Landau damping of the electron-acoustic wave is considerably decreased, possibly even to the extent that the electron-acoustic wave becomes a normal mode. They emphasized the roles of the electron densities and temperature ratio in bringing about this change.

In this chapter we investigate these criteria in detail by examining the geometrical properties of the dispersion function $\epsilon(\mathbf{k},\omega)$ in a manner similar

to that used originally by Gledhill & Hellberg (1986) in their study of ion-acoustic waves in two-ion plasma, and later by Dell, Gledhill & Hellberg (1987) in a study of Langmuir waves in two-electron plasmas.

We shall find that just as the heavy-to-light ion density ratio plays a role in determining which of the ion-acoustic waves in a two-ion plasma is prevalent (Gledhill & Hellberg 1986), so the hot-to-cool electron density ratio plays a role in the determination of whether the Langmuir or electron-acoustic wave in a two-electron-temperature plasma is weakly-damped. Furthermore, we show that the "Langmuir wave" investigated by Dell *et al.* (1987), whose frequency lies below ω_e, actually belongs to the electron-acoustic branch of the dispersion relation. We extend the temperature ratio to much higher values than have been investigated previously and reinterpret the results in terms of the electron-acoustic wave. In addition we calculate the regions in parameter space in which the waves will be only weakly Landau-damped.

3.1 Normal mode solutions of the dispersion relation

We define a normal mode as one that has $-\gamma < \omega_r/2\pi$ and therefore the amplitude damps by less than e^{-1} in one wave period τ. There are three electrostatic normal modes in a two-electron-component plasma. We review each in turn in the following.

The first normal mode solution to (2.7) is the high frequency electron plasma or Langmuir wave, which is characterized by a very high phase velocity, $\omega_r/k > v_h$. This wave has a real frequency that satisfies

$$\omega_r^2 = \omega_e^2 + 3k^2 v_e^2, \tag{3.1}$$

where $v_e \equiv (T_e/m_e)^{1/2}$ is the effective electron thermal speed calculated from the effective electron temperature $T_e \equiv (n_{0c}T_c + n_{0h}T_h)/n_{0e}$; and $\omega_e = (4\pi n_{0e}e^2/m_e)^{1/2}$ is the plasma frequency calculated from the total electron density $n_{0e} = n_{0h} + n_{0c}$. This wave is generally weakly damped at small wavenumbers because of the high phase velocity in this regime, with a progressive increase in the electron Landau damping as wavenumber is increased. The damping rate of the Langmuir wave is given approximately

by

$$\gamma \simeq -\frac{\pi^{1/2}\omega_r^2\omega_h^2}{\sqrt{8}k^3v_h^3}\left[\exp\left(\frac{-\omega_r^2}{2k^2v_h^2}\right)+\frac{n_{0c}}{n_{0h}}\left(\frac{T_h}{T_c}\right)^{3/2}\exp\left(\frac{-\omega_r^2}{2k^2v_c^2}\right)\right], \qquad (3.2)$$

where ω_r satisfies (3.1).

The second normal mode occurs for a relatively low phase velocity, $v_i < \omega_r/k < v_c$. This mode, the ion-acoustic wave in a two-electron-temperature plasma, is weakly damped if the effective temperature of the electrons (see below) is much greater than that of the ions. It has a real frequency that satisfies

$$\omega_r^2 = k^2\left(\frac{3T_i}{m_i}+\frac{T_e/m_i}{1+k^2\lambda_{De}^2}\right) \qquad (3.3)$$

and damping given by (3.2) with (3.3) incorporated. In equation (3.3) the effective electron temperature is defined as $T_e \equiv n_{0e}T_cT_h/(n_{0h}T_c + n_{0c}T_h)$ (Jones *et al.*, 1975). In the long wavelength limit the phase speed reduces to the ion sound speed $v_{si} = [(T_e + 3T_i)/m_i]^{1/2} \simeq [T_e/m_i]^{1/2}$.

The third normal mode has an intermediate phase velocity $v_c < \omega_r/k < v_h$, and arises for large temperature ratios $T_h/T_c > 10$ (Watanabe & Taniuti 1977; Tokar & Gary 1984). The frequency of this wave satisfies (Gary & Tokar 1985)

$$\omega_r \simeq kv_{se}, \qquad (3.4)$$

in the small wavenumber limit ($k\lambda_{Dh} \ll 1$) and is clearly dispersionless and thus acoustic in this regime. The electron sound speed is defined by $v_{se} = (n_{0c}/n_{0h})^{1/2}v_h$. We note that by our initial assumptions regarding the phase speed (3.4) is only strictly valid in the regime $n_{0c}/n_{0h} < 1$, but we have found it to hold approximately even for $n_{0c}/n_{0h} > 1$. However, the wave is found to be strongly Landau damped by the hot electron component (see chapter 2) unless $n_{0c} \ll n_{0h}$. At larger wavenumbers the frequency satisfies (Gary & Tokar 1985)

$$\omega_r^2 = \omega_c^2\frac{1+3k^2\lambda_{Dc}^2}{1+1/k^2\lambda_{Dh}^2}, \qquad (3.5)$$

and in this wavelength regime the dispersion relation strongly resembles that of a Langmuir wave based on the cooler electron component. The electron-acoustic wave has a damping rate given by (3.2) where ω_r satisfies either (3.4) or (3.5) depending on the magnitude of the wavenumber. The first term in (3.2) is the contribution to the Landau damping by the hot electrons and it dominates at small to intermediate wavenumbers. The second term is the

contribution from the cool electron component and only becomes substantial at larger wavenumbers where the phase velocity of the wave is nearer the cool electron thermal speed.

In addition to these normal modes there are three families of heavily damped solutions of (2.7). Each family of solutions can be associated with a Z' term in (2.7). These solutions are normally acoustic in nature in that their phase velocities are constant at small wavenumbers. The solutions associated with the ion term have smallest phase speed and $|\gamma|$, and those associated with the hot electrons have largest phase speed and $|\gamma|$. The roots associated with the cold electron term in (2.7) have phase speeds and damping that lie between these two extremes. It is these HOMs that concern us for the purposes of our investigation. Henceforth, unless otherwise stated, when we talk about a HOM we mean a HOM associated with the cold electron term in (2.7).

3.2 Double roots of the dispersion relation

We define the following parameters: $f \equiv n_{0h}/n_{0e}$, the concentration of hot electrons; $\lambda_{Dc} \equiv (T_c/4\pi n_{0c}e^2)^{1/2}$, the cold electron Debye length; $\beta \equiv T_h/T_c$, the electron temperature ratio; and $\zeta \equiv \zeta_c = \omega/\sqrt{2}kv_c$, is the complex wave phase speed normalized with respect to the cold electron thermal speed.

Since we are concerned only with high-frequency electron waves it is a valid approximation to neglect the ion contribution to the dispersion relation. This is readily seen by examining the leading term in the asymptotic expansion for the Z'–function, viz. $\sim kv_i/\omega$.

We define the complex function of complex, normalized phase velocity ζ,

$$G(\zeta) = \frac{f}{\beta} Z'\left(\frac{\zeta}{\beta^{1/2}}\right) + (1-f)Z'(\zeta) - 2(1-f)k^2\lambda_{Dc}^2, \qquad (3.6)$$

which is related approximately to the dielectric function ϵ by $G = 2(1-f)k^2\lambda_{Dc}^2\epsilon$ and provided $k > 0$ the roots of G correspond to the solutions of (2.7). Equation (3.6) is similar to that used by Dell *et al.* (1987) in their investigation. They write the last term in (3.6) in terms of $\lambda_D \equiv (T_c/4\pi n_{0e}e^2)^{1/2}$, rather than λ_{Dc}. We shall discuss the reasons for our choice of normalizing length later. The equation is also essentially equivalent in form to that employed by Gledhill & Hellberg (1986) in their study of ion-acoustic waves in a two ion component plasma. Some remarks about the

form of G are appropriate at this stage.

Note that the shape or topology of the surface $G_i = \mathrm{Im}\, G(\zeta_r, \zeta_i)$ is independent of the value of the wavevector k although it does depend on f. On the other hand the topology of the surface $G_r = \mathrm{Re}\, G(\zeta_r, \zeta_i)$ depends on both the magnitude of the wavevector and the hot electron fraction f. These observations imply that roots of the dispersion relation (which simultaneously must satisfy $\mathrm{Re}\, G = 0$ and $\mathrm{Im}\, G = 0$) traverse the zero-height contour of the "constant" (for f constant) surface, $\mathrm{Im}\, G$, as the wavenumber is varied. So by studying the topology of the zero-height contour of the imaginary G surface we have a geometrical method of investigating the dispersion relations of the various wave modes. However, if we trace root loci whilst varying f then the surface "dynamics" are more complex.

Gledhill & Hellberg (1986) showed that the topology of the root loci changes if the imaginary part of G possesses a saddle point with height less than or equal to zero. This defines a critical criterion for root behaviour: that of a saddle point at zero height in $\mathrm{Im}\, G$.

If $\mathcal{F}(x, y)$ is an arbitrary real function of real variables x and y then setting

$$A = \left.\frac{\partial^2 \mathcal{F}}{\partial x^2}\right|_{x_s, y_s}, \qquad B = \left.\frac{\partial^2 \mathcal{F}}{\partial y\, \partial x}\right|_{x_s, y_s} \qquad C = \left.\frac{\partial^2 \mathcal{F}}{\partial y^2}\right|_{x_s, y_s},$$

we require that the discriminant satisfy (Salas & Hille 1978)

$$D = B^2 - AC > 0, \tag{3.7}$$

if the function $\mathcal{F}$ is to have a saddle point at the coordinates x_s, y_s. In addition, if this saddle point occurs at zero height then $\mathcal{F}$ must further satisfy $\mathcal{F}(x_s, y_s) = 0$. That G_i satisfies all these conditions if G possesses a double root at ζ_S can be seen as follows.

By our hypothesis we require

$$G(\zeta_S) = 0, \quad \text{and} \quad \left.\frac{\mathrm{d}G}{\mathrm{d}\zeta}\right|_{\zeta_S} = 0, \tag{3.8}$$

for a double root at ζ_S. Application of the Cauchy–Riemann conditions then shows that at ζ_S

$$\left.\frac{\partial^2 G_r}{\partial \xi^2}\right|_{\zeta_S} = -\left.\frac{\partial^2 G_r}{\partial \eta^2}\right|_{\zeta_S}$$

and

$$\left.\frac{\partial^2 G_i}{\partial \xi^2}\right|_{\zeta_S} = -\left.\frac{\partial^2 G_i}{\partial \eta^2}\right|_{\zeta_S}$$

with $\zeta = \xi + i\eta$. Now since $B^2 \geq 0$ for all real G_i (or G_r) and $A = -C$ we obtain

$$D = B^2 + A^2 > 0,$$

and therefore G_i possesses a saddle point at zero height at ζ_S. Furthermore notice that G_r also has a saddle point at ζ_S.

From the point of view of wave modes admitted by G, this means that there will be a critical set of parameters (k^*, ω^*, and f^*) at which two wave modes with exactly the same frequencies, wavenumbers, and damping rates at ζ_S, simultaneously satisfying the dispersion relation. By varying the plasma parameters about these critical values we can determine which of the waves will Landau damp and which will emerge lightly damped. Therefore the critical curves defined by the parameters which satisfy (3.8) simultaneously, are important in that they delineate parameter regimes in which one of the wave modes, by virtue of its weaker Landau damping, predominates over the other.

Unfortunately it is not always the case that a double root defined by (3.8) occurs in a region of the complex plane where the waves are weakly-damped. Thus in addition to knowing parameter values at which saddle points occur we must also determine parameter domains in which the competing waves are weakly-damped. Parameter values that satisfy both of these criteria will be sought here.

To continue, as discussed by Gledhill & Hellberg (1986), there is a region in ζ–space, with small $|\zeta/\beta^{1/2}|$, where the function $Z_i'(\zeta/\beta^{1/2})$ ($Z_i'(\zeta) = ImZ'(\zeta)$) is negative, while $Z_i'(\zeta)$ has a large set of saddle points at positive height. Consequently it may be seen from equation (3.6) that near these positive saddle points associated with the cool electron Z_i', the function $G_i(\zeta)$ will have saddle points at zero height for small values of f, i.e. at a critical value, f^*, of f for given β. We label these saddle points derived from the cool electron term $S_0, S_1, S_2, \ldots$, where the modulus of Im S_j increases with j. By analogy with the saddle point called S_M by Gledhill & Hellberg (1986), there is also a saddle point S_β (see Dell *et al.*, 1987), which is not due to $Z_i'(\zeta)$, but arises solely out of the addition of the Z' terms in G. Its position in the complex plane is more dependent on the temperature ratio β than are the S_j, and it is often sited well away from that sequence. The

influence of this saddle point becomes more profound at larger temperature ratios where its damping is reduced.

3.3 Numerical results

Simultaneous numerical solution of (3.8) as a function of β renders families of critical curves, $f_S^*(\beta)$, $k_S^*\lambda_{Dc}(\beta)$, corresponding to the various saddle points ζ_S. These critical curves delineate regions of parameter space within which root behaviour remains qualitatively similar as f or $k\lambda_{Dc}$ is varied (Dell *et al.* 1987). Figure 3.1 (after Dell *et al.*, 1987), illustrates the change in the topology of root loci which occurs as f passes through f^*.

By investigating the root behaviour in complex phase velocity space, we were able to confirm the results of Dell *et al.* (1987), for the critical curves f^* and our equivalent curve $k^*\lambda_{Dc}$. We have extended the range of the temperature ratio β well beyond that considered earlier, and find no significant qualitative changes in the critical curves for higher values of β, although the damping of the waves is found to decrease as temperature ratio is increased (see later). The critical curves remain associated with the saddle point S_β for $\beta > 10$ (Dell *et al.* 1987), each exhibiting a slow monotonic decline with β in that regime. As our main concern shall be with the electron-acoustic wave it is the curves defining the trajectory of S_β that are of primary importance for us.

Figure 3.2 shows the critical curve in (β, f) space and 3.3 shows the critical curve in (β, $k\lambda_{Dc}$) space. These composite curves consist of the critical curves associated with S_0 and S_β (Dell *et al.* 1987). There are two types of root behaviour depending on whether the value of f lies above or below f^*. Consider the f^* critical curve. We hold f constant and vary $k\lambda_{Dc}$.

If f, the fraction of hot electrons, lies below the critical curve, then there will be no change in the root topology as $k\lambda_{Dc}$ is varied and we observe a continuous variation in wave phase velocity.

If $f \geq f^*$ then a change in root topology will occur: depending on the value of the temperature ratio β, the critical value of f occurs as either the S_0 or S_β saddle point in $\mathrm{Im}\, G$ is lowered below zero. As a result, the most weakly damped or principal mode (PM) at $k\lambda_{Dc} = 0$, undergoes progressively stronger damping as $k\lambda_{Dc}$ is increased, with a concomitant decrease in the damping of a HOM. This gives rise to an exchange of roles between HOM and PM. If one were to experimentally monitor the phase velocity of the PM while varying the wavenumber, then a discontinuous variation of the

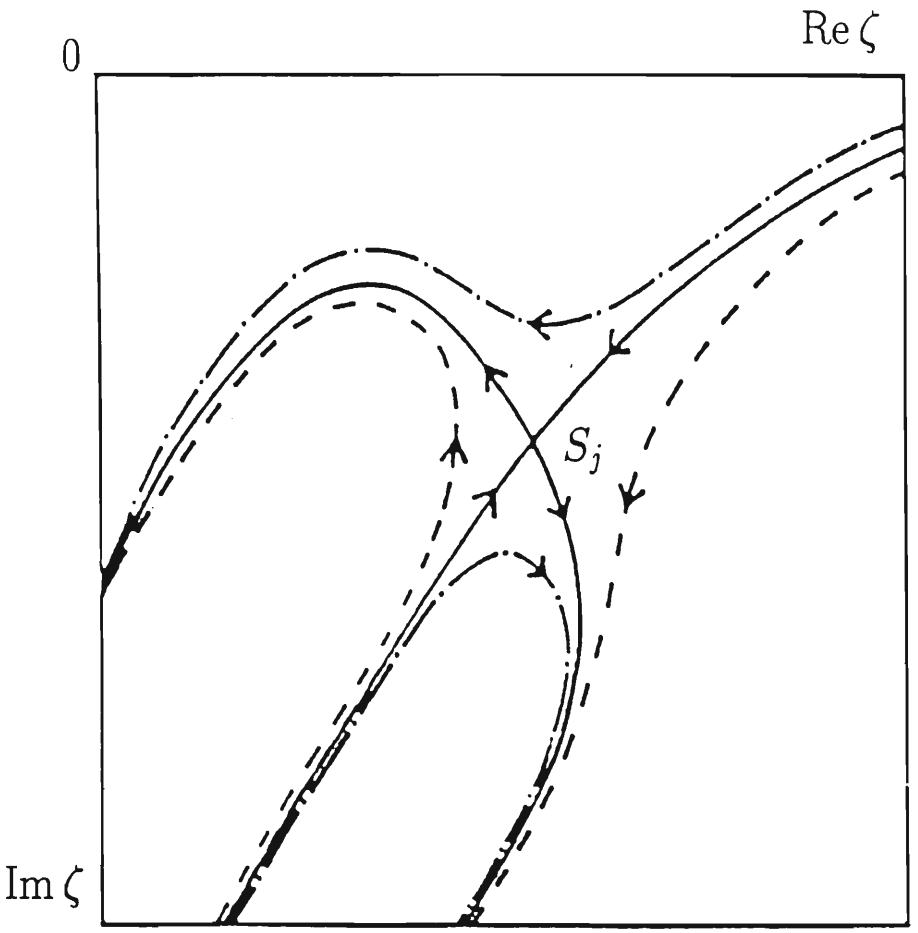

Figure 3.1: Influence of the saddle point S_j on paths traced by roots in the complex ζ–plane as $k\lambda_{Dc}$ is increased. Root trajectories are shown for three values of f: – · –, $f < f_j^*$; —, $f = f_j^*$; - - -, $f > f_j^*$. (After Dell *et al.* (1987).)

phase velocity of that wave would be observed. This case has been called the discontinuous transition by Gledhill & Hellberg (1986), and the case where no change in topology occurs has been called the continuous transition.

Figure 3.4 illustrates the topology of the root loci before, and figure 3.5 the topology after the lowering of the S_0 saddle point below zero, for low β. Figures 3.6 and 3.7 show the equivalent change when $\beta = 100$, where the saddle point S_β is critical. The S_β saddle point in the latter situation effects the promotion of a very strongly damped HOM to the status of PM. By examining the dispersion of this HOM (see later) we shall see that it approximately satisfies (3.5) in the weakly-damped wavenumber regime and we thus identify it as belonging to the electron-acoustic branch of the dispersion relation for electrostatic waves.

Analogous transitions occur for the case of varying f at constant $k\lambda_{Dc}$. In this case we vary the fraction of hot electrons so that we start with an initially cold plasma and end up with a plasma of hot electrons. The observed root behaviour depends on the value of $k\lambda_{Dc}$ in relation to the $k^*\lambda_{Dc}$ curve (figure 3.3).

If $k\lambda_{Dc} < k^*\lambda_{Dc}$ then no change in the topology of the root loci (generated by varying f) occurs and the phase velocity of the principal cold mode (PCM) varies continuously with increasing f until the wave becomes the (PHM). This behaviour is shown in figure 3.8 for low β ($\beta = 5$) and in figure 3.10 for higher β ($\beta = 100$).

If $k\lambda_{Dc} \geq k^*\lambda_{Dc}$, then the change in the topology of the root loci causes the PCM to quench as f is increased and a HOM emerges to become the PHM at $f = 1$. This is shown in figure 3.9 for $\beta = 5$ and in figure 3.11 for $\beta = 100$. As before the $\beta = 5$ case corresponds to a change in topology effected by the S_0 saddle point, while for $\beta = 100$ it is the S_β saddle point that effects the change in topology.

We found that with the definition of λ_D given by Dell *et al.* (1987), namely $\lambda_D = (T_c/4\pi n_{0e}e^2)^{1/2}$ based on the cold electron temperature and the total electron number density, the modes were not always observable at $f \simeq 0$ and $f \simeq 1$, i.e. they did not satisfy $-\mathrm{Im}\,\zeta < \mathrm{Re}\,\zeta/2\pi$. We have rather used $\lambda_{Dc} = (T_c/4\pi n_{0c}e^2)^{1/2}$, the cold electron Debye length, which varies with the density ratio f.

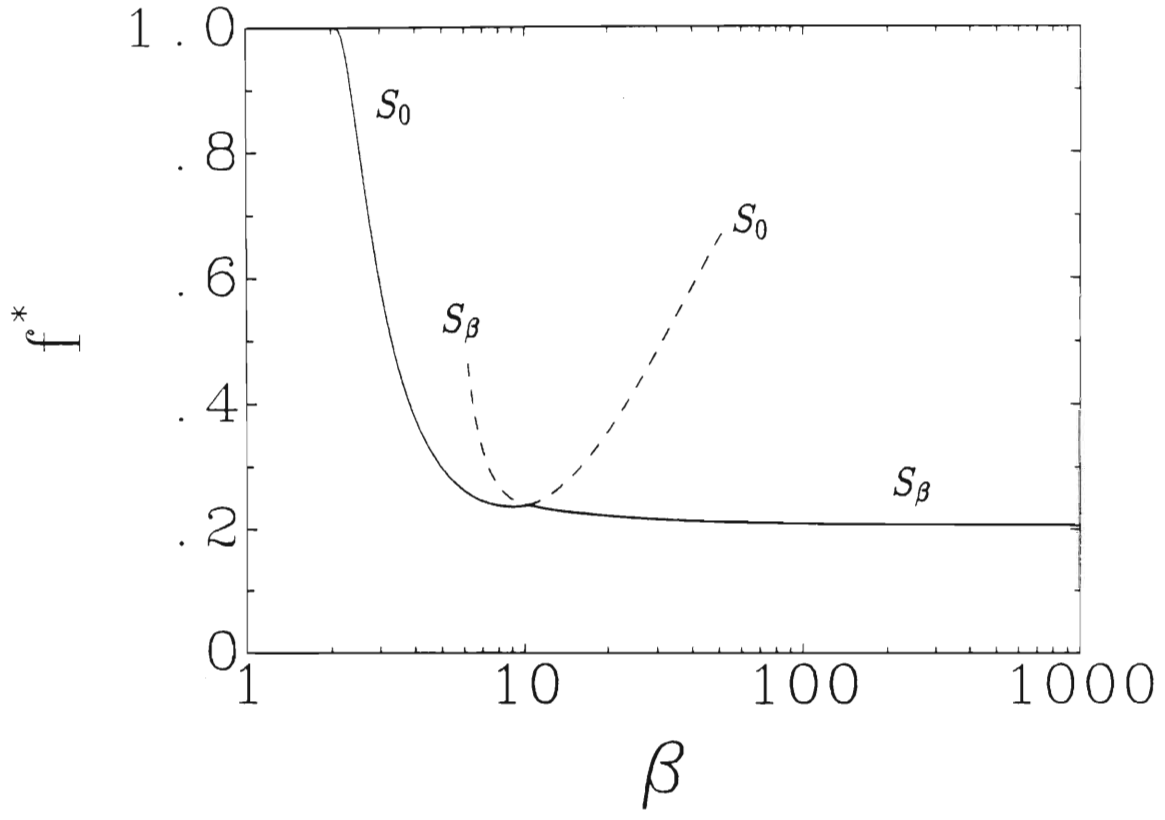

Figure 3.2: The critical value of f as a function of the temperature ratio β. The dashed portion of the curves show parts of the continuations of the $f^*_{S_0}$ and $f^*_{S_\beta}$ curves.

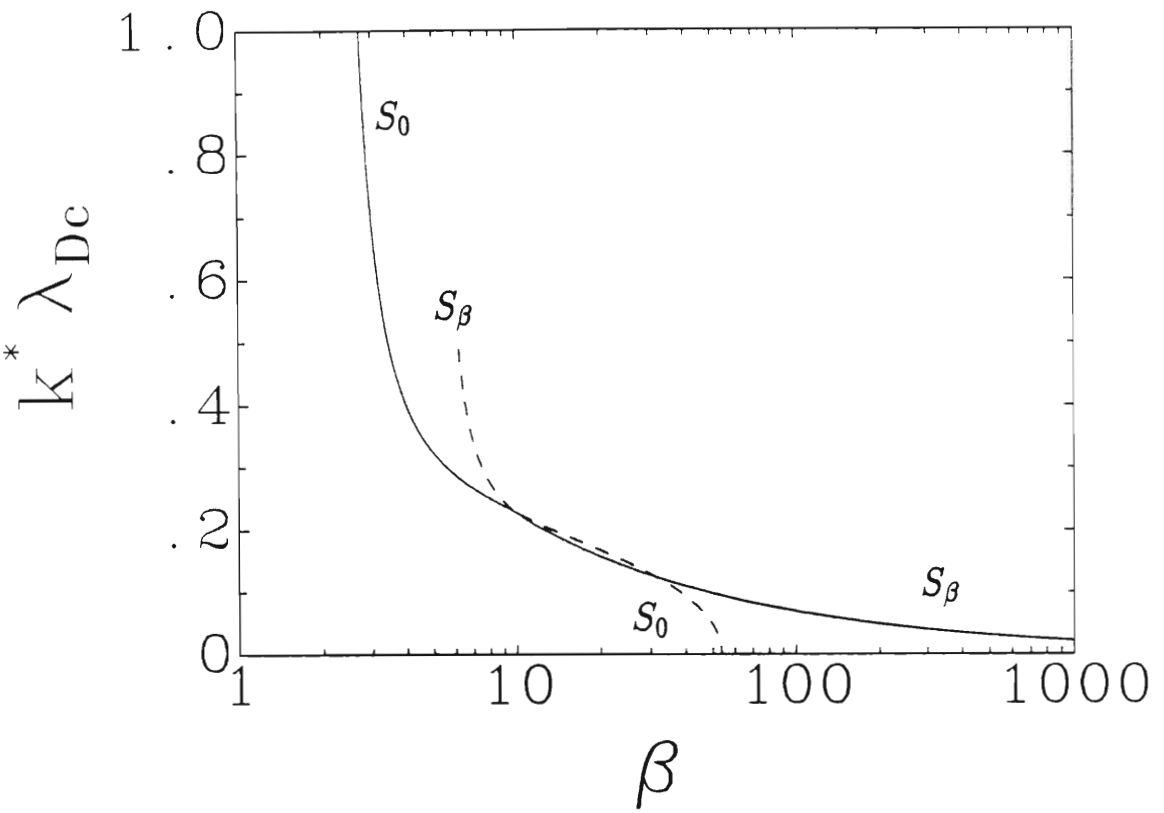

Figure 3.3: The critical value of $k^*\lambda_{Dc}$ as a function of the temperature ratio β. The dashed portion of the curves show parts of the continuations of the $k^*_{S_0}\lambda_{Dc}$ and $k^*_{S_\beta}\lambda_{Dc}$ curves.

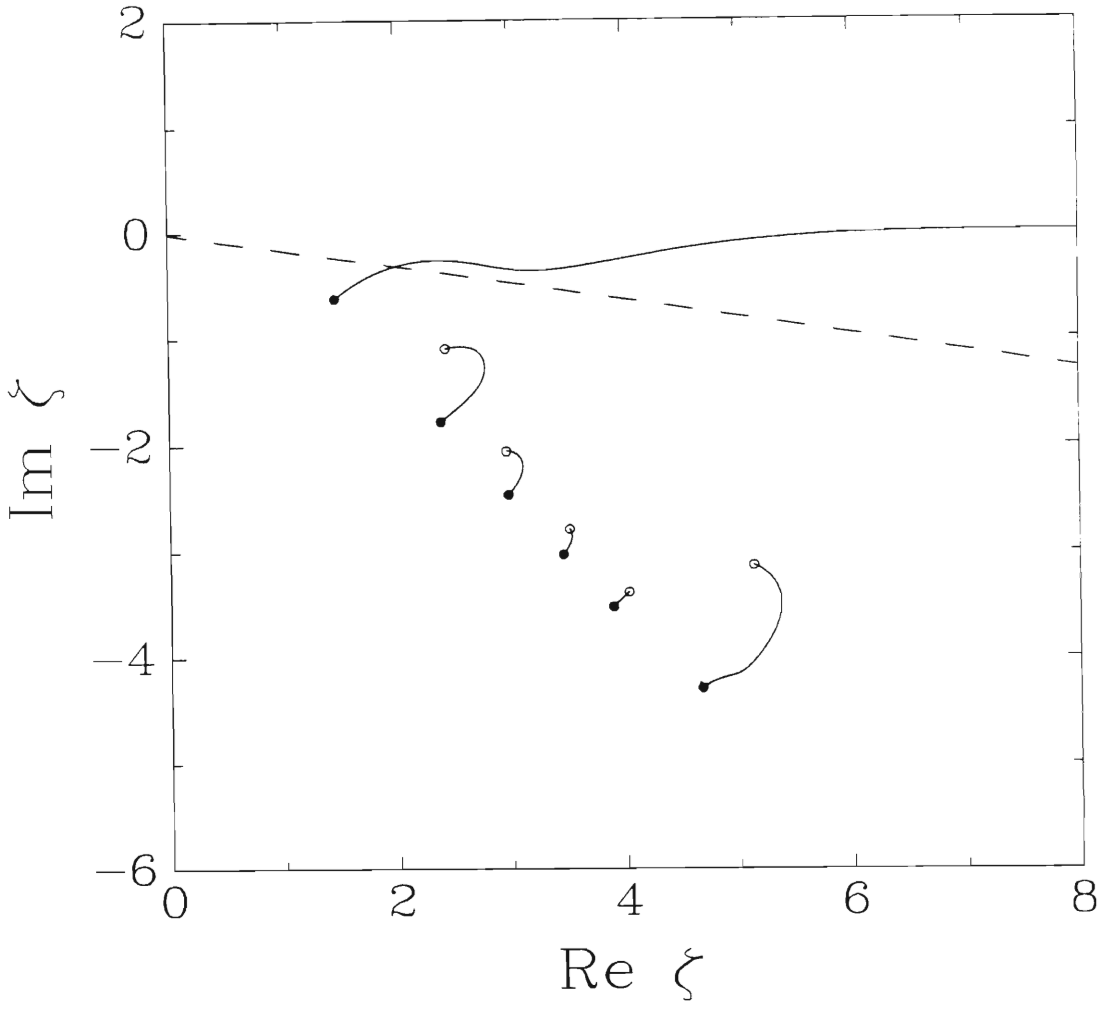

Figure 3.4: Root loci generated by varying $k\lambda_{Dc}$ for $\beta = 5$ and $f = 0.2 < f^*$: no change occurs in the topology of the PM. Here and in figures 3.5–3.11 the slanted dashed line represents the curve $-\mathrm{Im}\,\zeta = \mathrm{Re}\,\zeta$, and here and in figures 3.5–3.7 the open and full circles mark where $k\lambda_{Dc} = 0$ and 1, respectively.

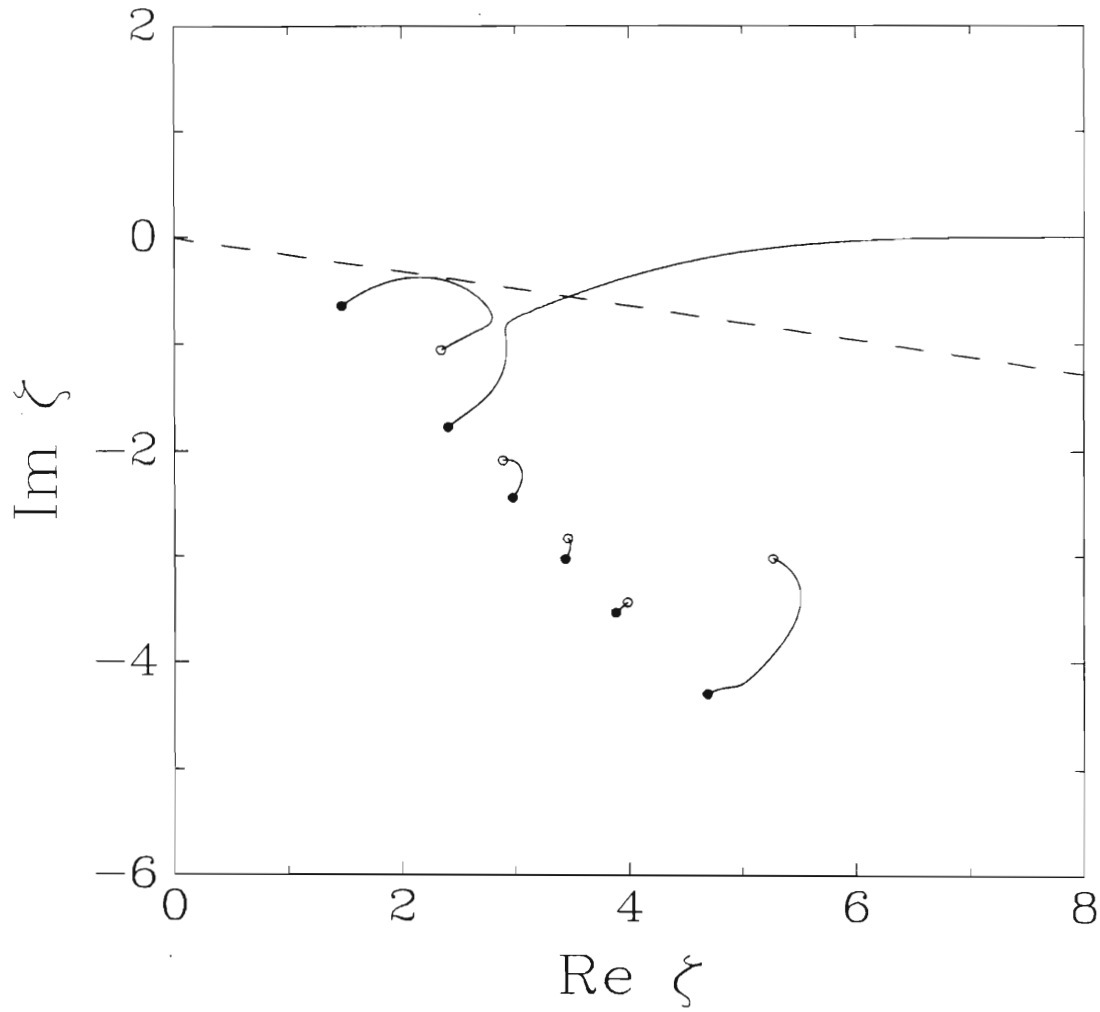

Figure 3.5: Root loci generated by varying $k\lambda_{Dc}$ for $\beta = 5$ and $f = 0.3 > f^*$: the topology of the PM changes.

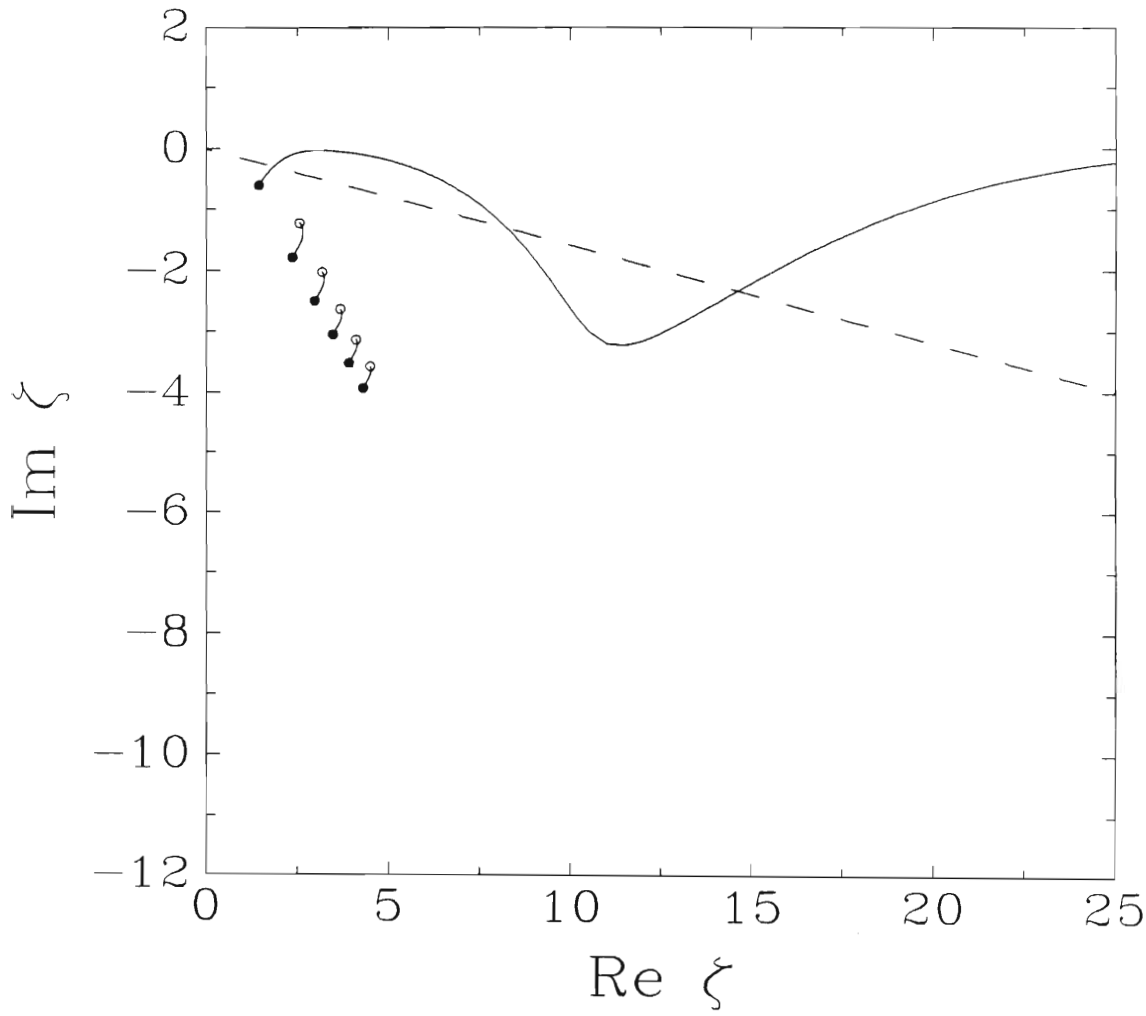

Figure 3.6: Root loci generated by varying $k\lambda_{Dc}$ for $\beta = 100$ and $f = 0.2 < f^*$.

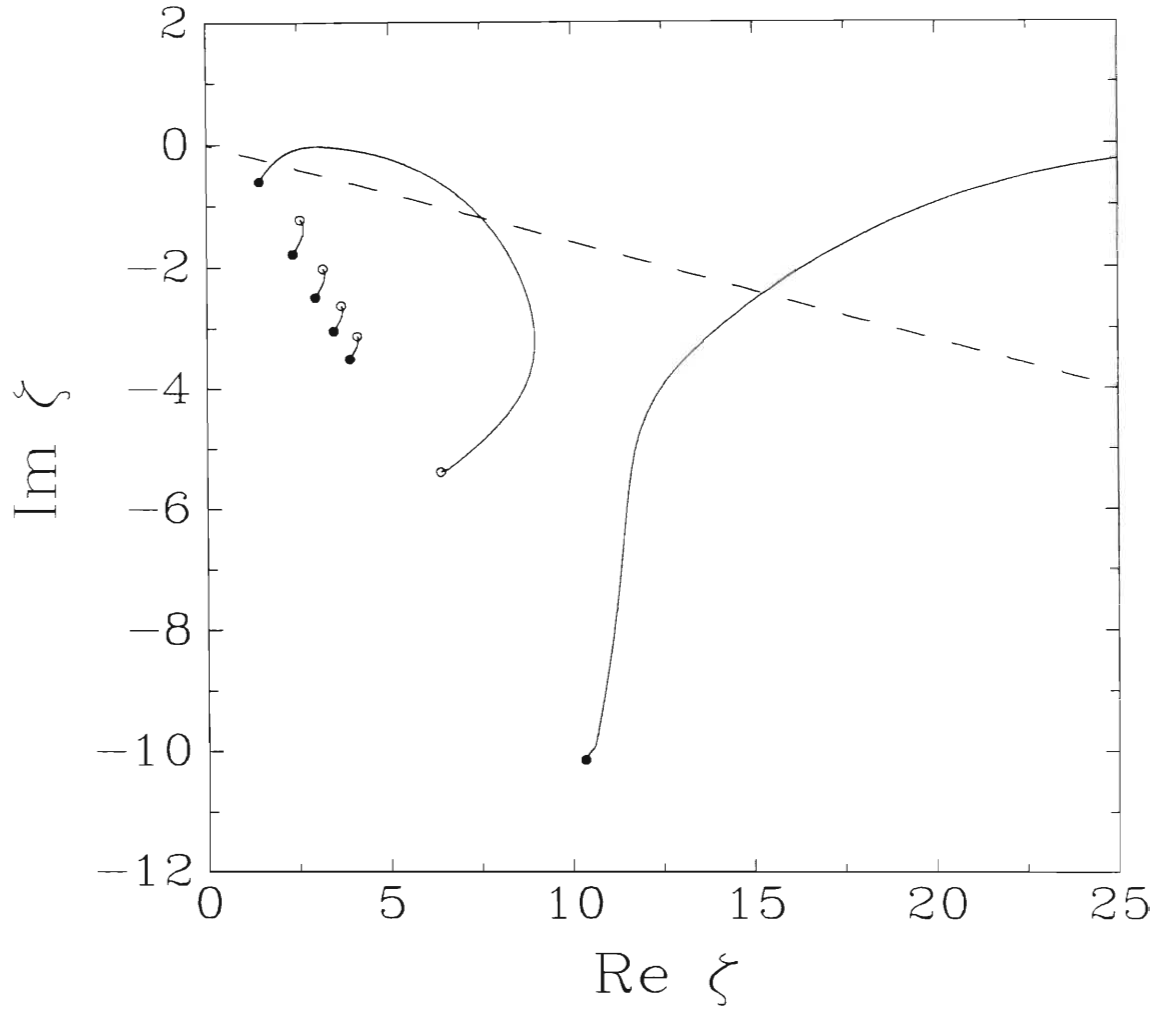

Figure 3.7: Root loci generated by varying $k\lambda_{Dc}$ for $\beta = 100$ and $f = 0.23 > f^*$.

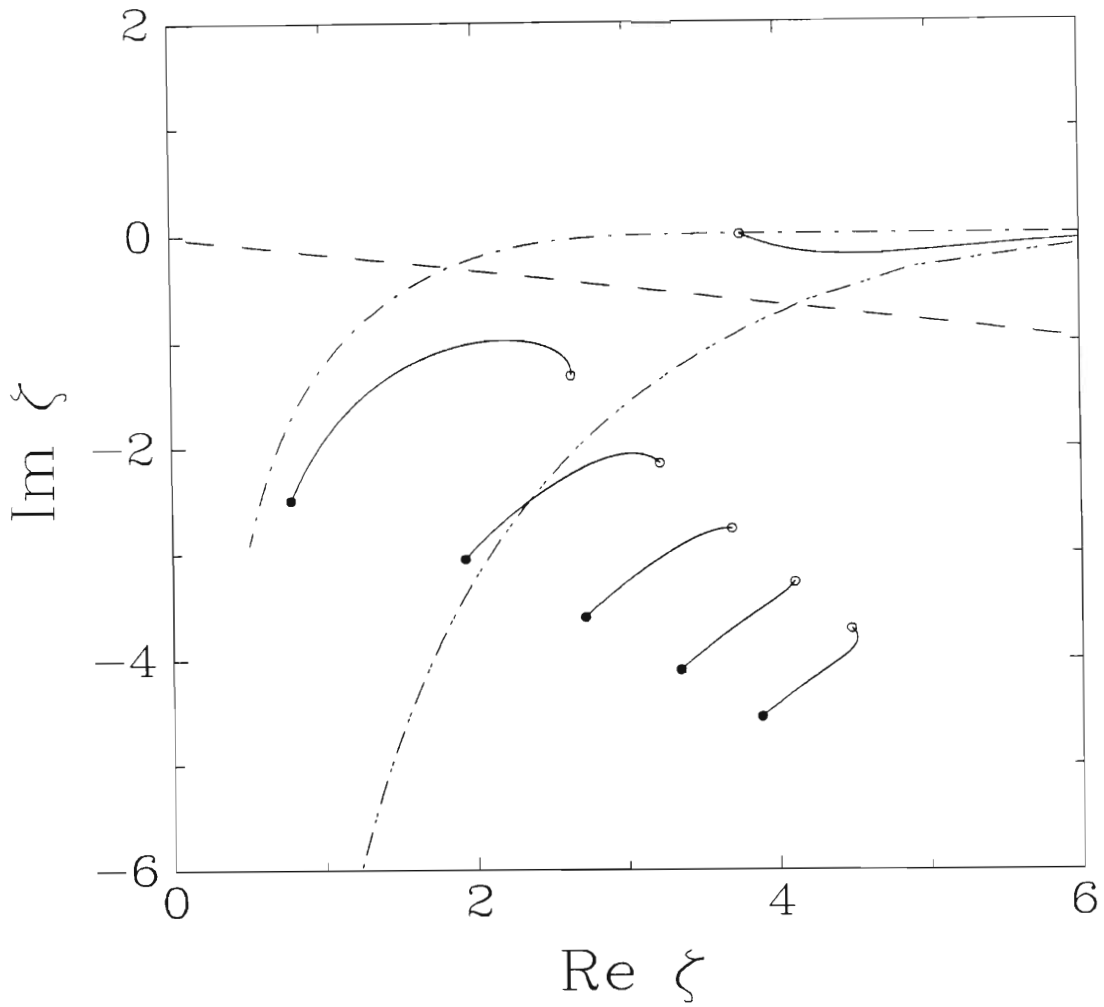

Figure 3.8: Root loci generated by varying f with $k\lambda_{Dc}$ and β constant. In the figure $k\lambda_{Dc} = 0.2 < k^*\lambda_{Dc}$ and $\beta = 5$. No change in the topology of the PM occurs. In figures 3.8–3.11 the open circles indicate points where $f = 0$ and the solid circles where $f = 1$, and also in these figures $- \cdot -$ denotes the locus of the PM (generated by varying $k\lambda_{Dc}$) at $f = 0$ and $- \cdot\cdot -$ the locus of the PM for $f = 1$.

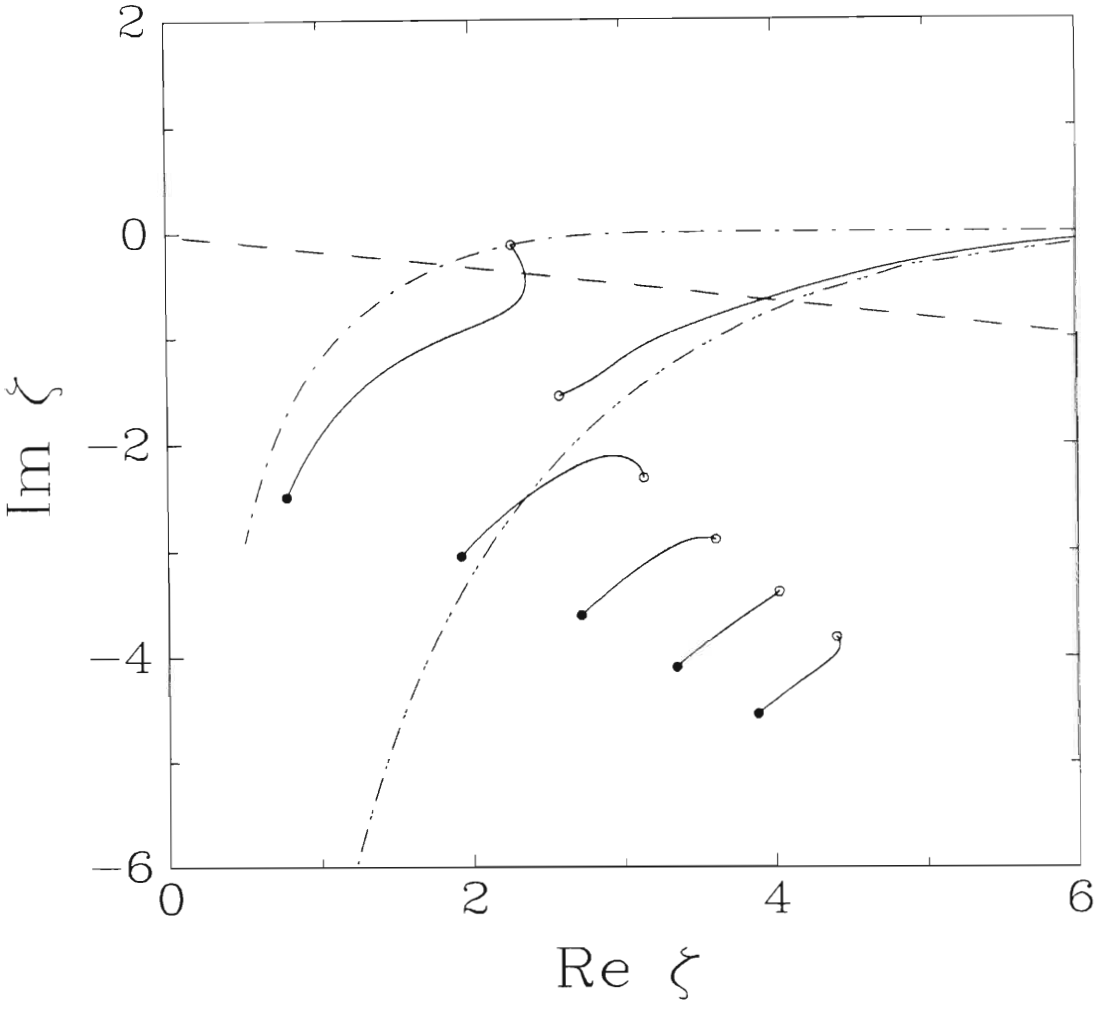

Figure 3.9: Root loci generated by varying f with $k\lambda_{Dc}$ and β constant. In the figure $k\lambda_{Dc} = 0.4 > k^*\lambda_{Dc}$ and $\beta = 5$. There is a change in the topology of the PM in this case.

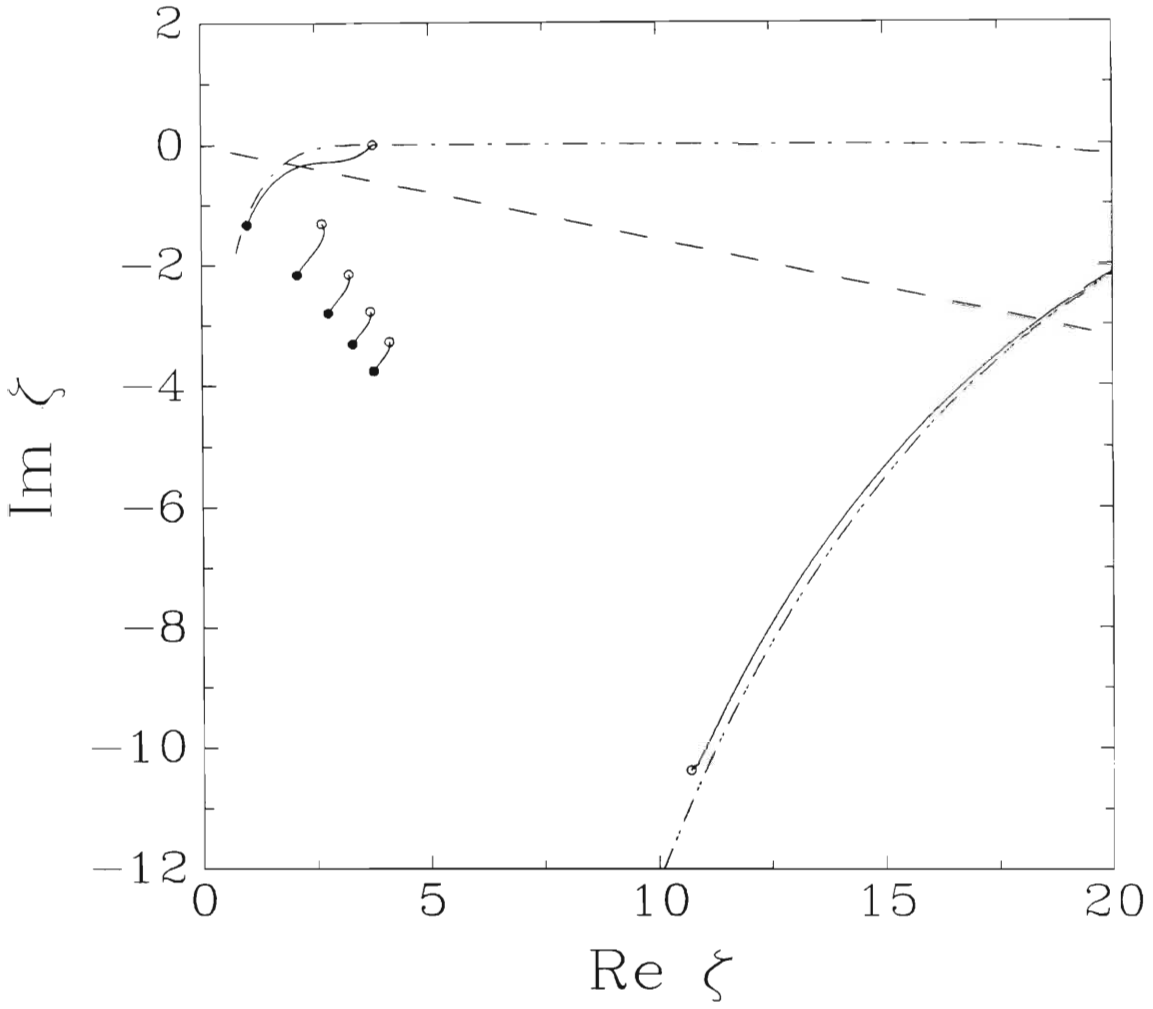

Figure 3.10: Root loci generated by varying f for $\beta = 100$ and $k\lambda_{Dc} = 0.05 < k^*\lambda_{Dc}$.

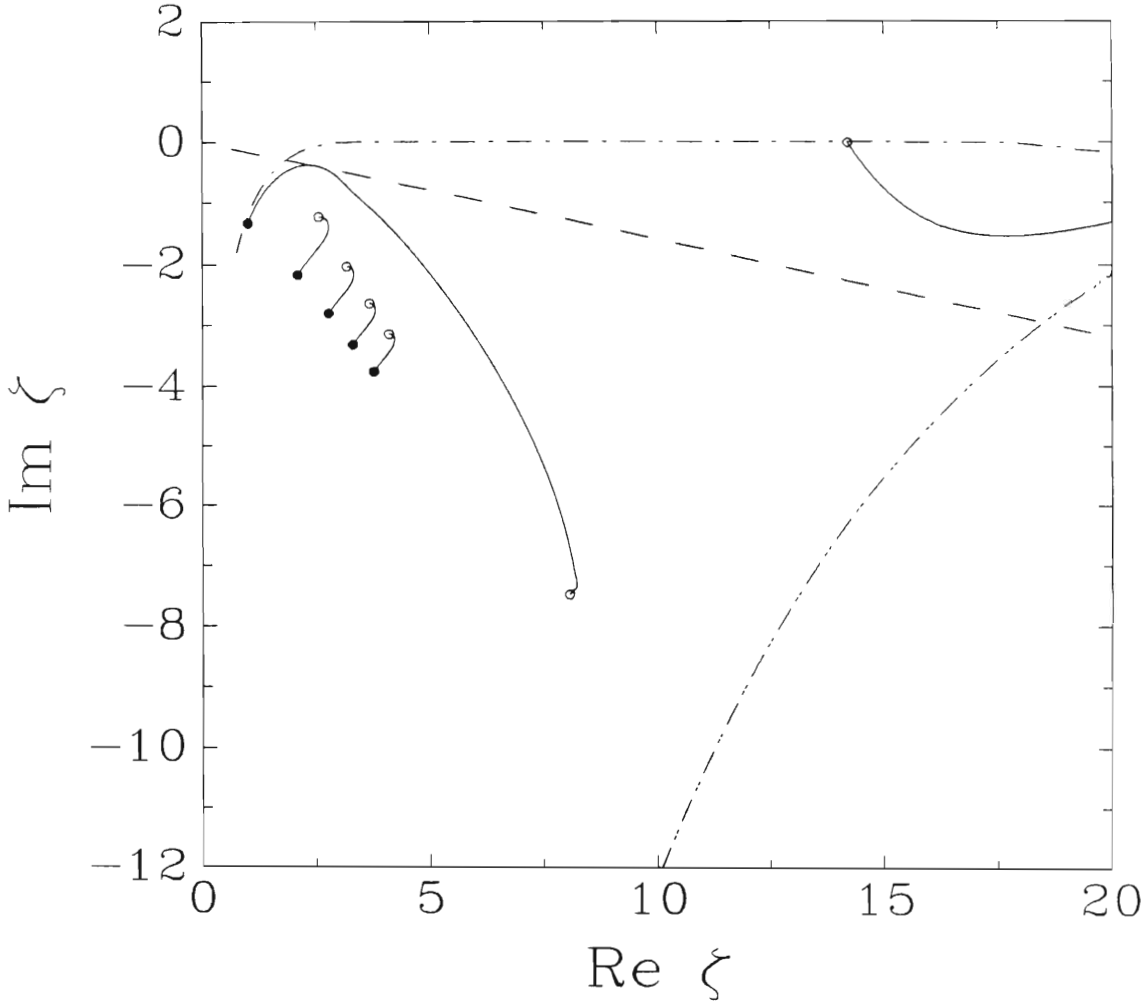

Figure 3.11: Root loci generated by varying f for $\beta = 100$ and $k\lambda_{Dc} = 0.2 > k^*\lambda_{Dc}$.

3.4 Wave dispersion of the PM and HOMs

It was mentioned previously that the principal mode is Langmuir-like and that the higher order modes are normally acoustic-like, i.e. they have $\omega_r/k \sim$ const. This is not always strictly true especially when the plasma parameters are near the critical values. The dispersion relations of the plasma wave modes actually depend on the parameter f in relation to the critical f^* curve.

If $f < f^*$ then indeed the PM is characterised by a dispersion relation similar to the Langmuir wave and the HOMs are acoustic. However, if $f \geq f^*$, then one of the HOMs will develop dispersive characteristics at intermediate wavenumbers that can be associated with Langmuir waves. Specifically, the mode develops a cold plasma regime, i.e. the frequency is related to the cold electron density (cf. equation (3.5)). These features are evident from our diagrams (figures 3.12–3.15).

In figures 3.12 and 3.13 we present the dispersion relations of the PM and first four HOMs for the two cases, $f < f^*$ and $f > f^*$, respectively, at low β. In figure 3.12 the principal mode is Langmuir-like (at least in the long wavelength regime) and the HOMs are all acoustic-like and strongly damped. In figure 3.13 ($f > f^*$) the principal mode remains Langmuir-like at small wavenumbers and a HOM develops a cold plasma regime at intermediate wavenumbers, in addition to an acoustic regime at small $k\lambda_{Dc}$. Examination of the curves for γ shows that in this case a change in the root topology has occurred. The HOM, however, does not satisfy the weak damping criterion $-\gamma < \omega_r/2\pi$ and hence will be unobservable. It is the S_0 saddlepoint that effects the change in the topology of the root loci in figure 3.13.

Figures 3.14 and 3.15 illustrate the dispersion relations for the PM and selected HOMs for the continuous (figure 3.14) and discontinuous (figure 3.15) cases at higher $\beta = 100$. The dispersive properties of the waves in this case are similar to those at a temperature ratio of $\beta = 5$. There is, however, one important difference: the HOM that exhibits reduced damping for $f \geq f^*$, is now weakly damped at intermediate wavenumbers. The appearance of this mode can be associated with a change in the topology of the root loci of G, brought about by the S_β saddle point.

For $\beta > 10$ and $f \geq f^*$, it was found that the HOM that exhibits weaker damping has a strongly damped acoustic regime at long wavelengths, a cold plasma regime at intermediate wavelengths and becomes strongly damped at shorter wavelengths. These properties of the wave are characteristic of

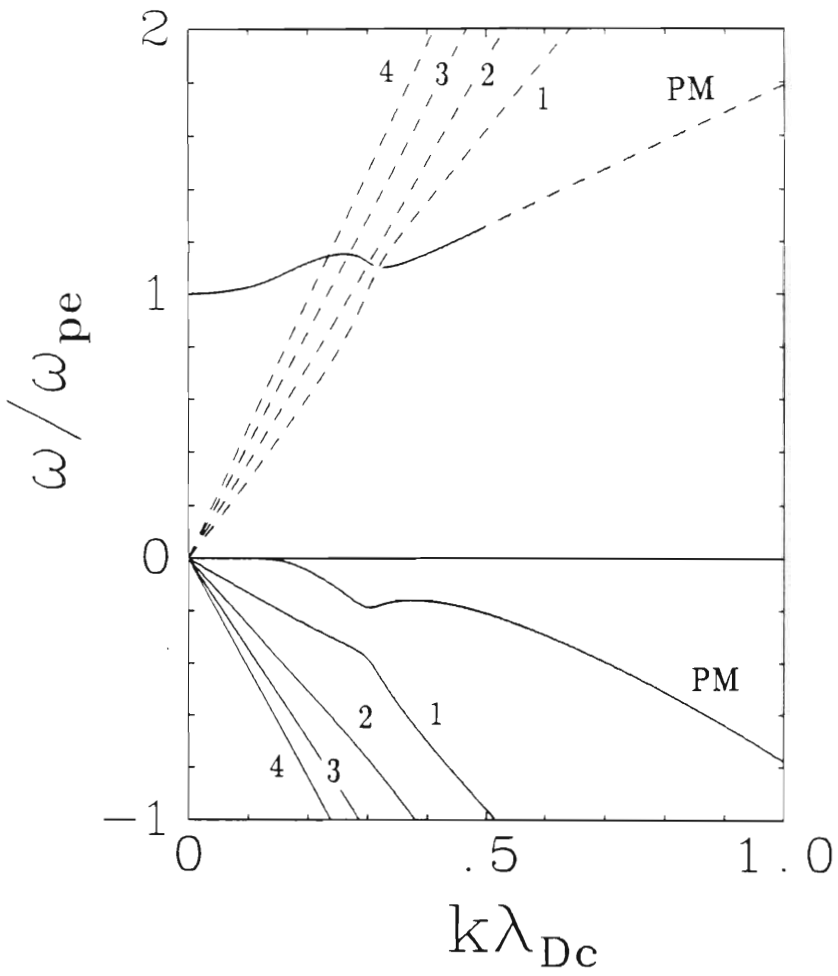

Figure 3.12: Complex frequency as a function of $k\lambda_{Dc}$ for the PM and first four HOMs for $f = 0.25$ and $\beta = 5$.

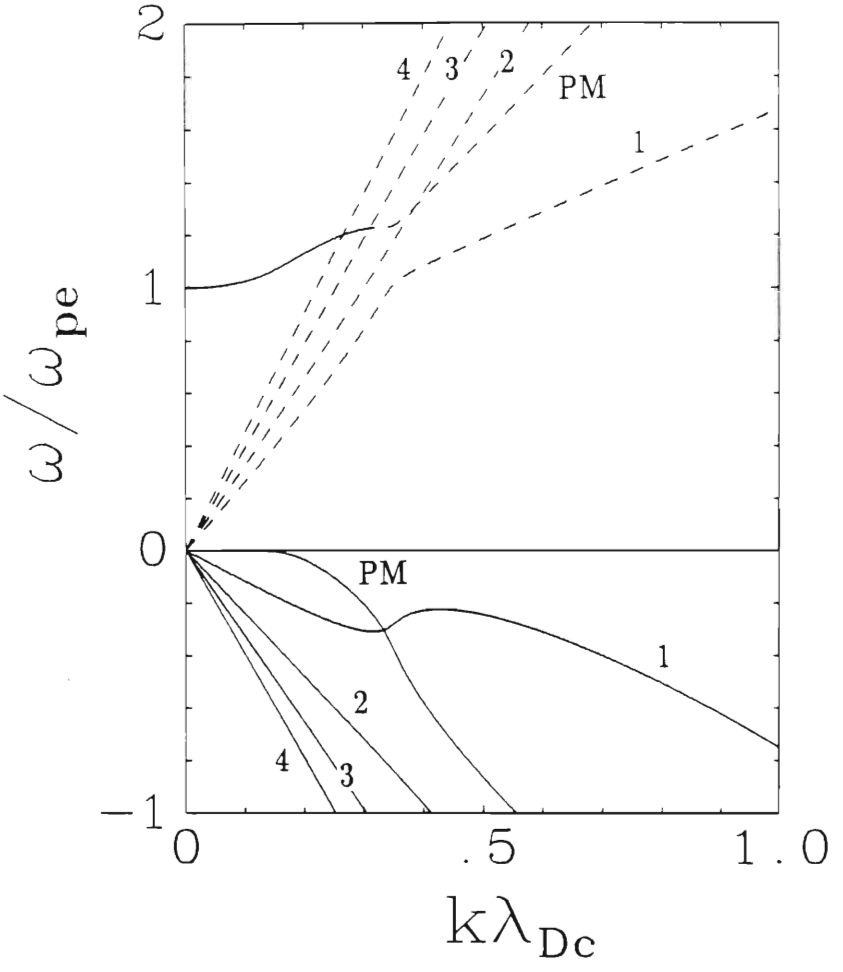

Figure 3.13: Complex frequency as a function of $k\lambda_{Dc}$ for the PM and first four HOMs for $f = 0.35$ and $\beta = 5$.

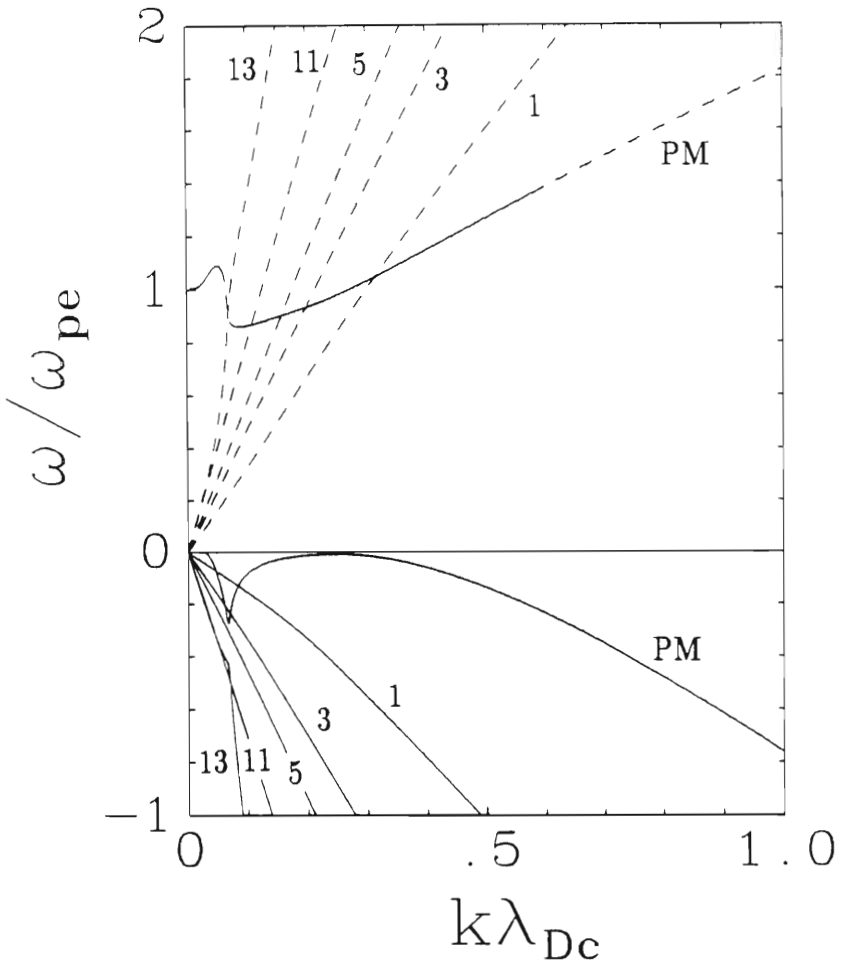

Figure 3.14: Complex frequency as a function of $k\lambda_{Dc}$ for the PM and selected HOMs for $\beta = 100$ and $f = 0.2 < f^*$. Only the 1, 3, 5, 11 and 13 HOMS have been shown for clarity.

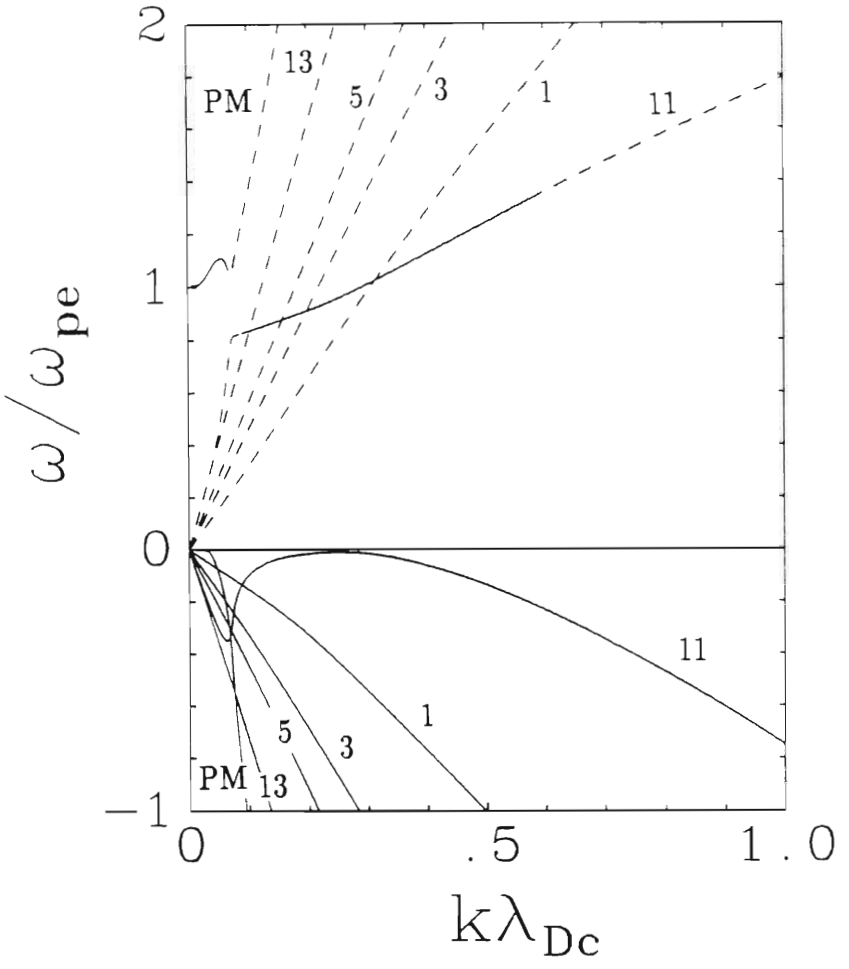

Figure 3.15: Complex frequency as a function of $k\lambda_{Dc}$ for the PM and selected HOMs for $\beta = 100$ and $f = 0.23 > f^*$. Only the 1, 3, 5, 11 and 13 HOMS have been shown for clarity.

the weakly damped electron-acoustic mode (Gary & Tokar 1985) and we thus identify the emergent HOM as such, rather than as a second electron plasma wave, as suggested by Dell *et al.* (1987). We hasten to add, however, that for values of $f \sim f^*$ both waves exhibit dispersive properties that make them identifiable with Langmuir waves. For values of f significantly larger than f^*, only the PM exhibits Langmuir-like behaviour, which now continues up to larger wavenumbers, and the electron-acoustic wave branch exhibits weak damping at smaller wavenumbers where the wave dispersion is given approximately by (3.4). Such behaviour can be seen in figure 3.21, however, we defer discussion of this figure till later.

Weak damping at small wavenumbers for large f was first predicted, using a fluid model, by Watanabe & Taniuti (1977) and verified numerically by Gary & Tokar (1985). Using (3.4) in (3.2), together with the condition $-\gamma < \omega_r/2\pi$, we can derive an analytical expression relating this minimum limit in $k\lambda_{Dc}$, to T_h/T_c and n_{0h}/n_{0c}, i.e.

$$k\lambda_{Dc} > \frac{\pi^{3/4}}{2^{1/4}} \left(\frac{T_c}{T_h}\right)^{1/2} \left(\frac{n_{0h}}{n_{0c}}\right)^{1/4}. \tag{3.9}$$

This equation shows good agreement with the lower branch of the curve for $k\lambda_{Dc}$, at $n_{0c}/n_{0e} = 0.5$, presented by Gary & Tokar (1985) in their figure 3.

Watanabe & Taniuti (1977) showed that a necessary condition for the existence of a weakly damped electron-acoustic wave, is that the plasma electrons consist of two species at widely different temperatures. Mathematically, the existence of two electron species gives rise to the presence of the S_β saddle point in G or its equivalent saddle point in $\epsilon(k,\omega)$. This saddle point, which arises out of the addition of the two electron Z' terms in G (or ϵ), is directly responsible for the appearance of the weakly damped electron-acoustic wave in a two-electron component plasma. The absence of this saddle point in the dispersion relation for a single electron-temperature plasma, is the reason why this mode remains strongly damped in such a plasma.

Thus, we conclude that a necessary condition for observation of a weakly damped electron-acoustic mode, is that $f > f^* \simeq 0.2$ and $\beta > 10$. Geometrically, in this temperature range, this corresponds to the lowering of the S_β saddle point in $\mathrm{Im}\, G$ (or $\mathrm{Im}\, \epsilon$) below zero height.

3.5 Weakly damped parameter regimes

In section 3 we presented conditions under which one might observe one or two electron modes as $k\lambda_{Dc}$ or f is varied. However, we said little about the damping of the modes. Gary & Tokar (1985) calculated the regions of weak damping in T_h/T_c, n_{0c}/n_{0e} space, for the electron-acoustic and ion-acoustic waves (figure 4 of Gary & Tokar 1985). They remark that the Langmuir mode is weakly damped, at small wavenumbers, for all parameters in this figure ($0 \leq n_{0c}/n_{0e} \leq 1$; $5 \leq T_h/T_c \leq 1000$). The upper branch of their existence curve, for $T_h/T_c > 20$, has $n_{0c}/n_{0e} \simeq 0.8$ which coincides with our value of $f^* \simeq 0.2$ for $\beta > 20$, and represents the maximum value of n_{0c} for which the electron-acoustic wave may occur (although the dispersion is more Langmuir-like in this regime).

The weakly damped wave regimes in (f, $k\lambda_{Dc}$)–space are illustrated in figures 3.16(a) to 3.16(f) for β values 5, 10, 20, 50, 60 and 100, respectively. The curves were calculated by solving the dispersion relation, $\epsilon(k,\omega) = 0$ and the equation $-\gamma(k) - \omega_r(k)/2\pi = 0$, simultaneously while varying f. The shaded regions indicate where $-\gamma < \omega_r/2\pi$, i.e. the amplitude of the wave damps by less than e^{-1} in one wave period and hence the waves will be sufficiently weakly damped to be observable. The cross-hatched areas define the regions in which the weakly damped electron-acoustic mode occurs. We define the left hand boundary of this region representing the maximum value of f at particular β for which the electron-acoustic wave occurs, by the value of $f^*(\beta)$ which was read off from figure 3.2 . For the β values that we have considered, we observe that the principal hot Langmuir mode (PHM), which is defined at $f = 1$, is weakly damped for all values of $k\lambda_{Dc}$ spanned by the diagrams. The principal cold Langmuir mode (PCM, $f = 0$), on the other hand, is only weakly damped at smaller wavenumbers, $0 \leq k\lambda_{Dc} < 0.58$. The regime of weak damping of the electron-acoustic wave encompasses a progressively larger region of parameter space with increasing β (figures 3.16(a) to (e)) and for high β and f, the wave exhibits weak damping at small wavenumbers (figure 3.16(f)) and hence the acoustic regime of the electron-acoustic mode will be observable (figure 3.21). In fact it is readily seen that there is an optimum electron density ratio that gives weak electron-acoustic wave damping even at small wavenumbers, viz. $n_{0c} \simeq 0.1 n_{0e}$ for a hot-to-cool electron temperature ratio of 100. The lower wavenumber limit, in units of the cool electron Debye length, λ_{Dc}, of the weakly damped region of the electron-acoustic mode, is well approximated for intermediate values of f by (3.9), which in terms of f and β may be

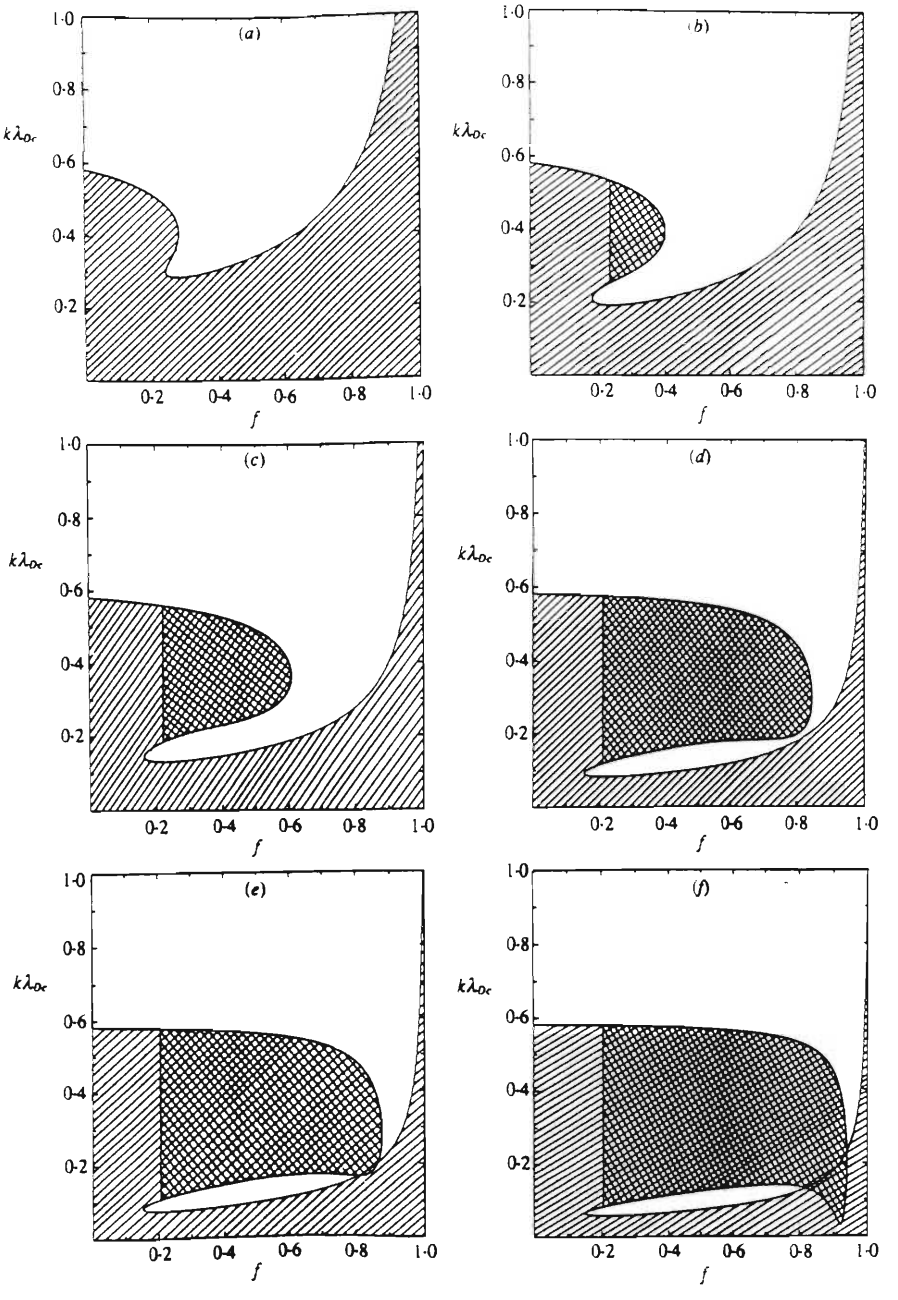

Figure 3.16: Regions of weak damping in $k\lambda_{Dc}$ versus f space. The shaded regions indicate regions in this parameter space in which the Langmuir and/or electron-acoustic mode(s) will be weakly damped. Cross-hatched regions indicate where the electron-acoustic wave will occur. (After Mace & Hellberg (1990).)

expressed as

$$k\lambda_{Dc} > \frac{\pi^{3/4}}{2^{1/4}\beta^{1/2}} \left(\frac{f}{1-f}\right)^{1/4}. \tag{3.10}$$

We note here that by the constancy of the f^* curve for $\beta > 20$, we obtain an approximate expression for $k^*\lambda_{Dc}$ as a function of β for $\beta > 20$ if we substitute $f = 0.2$ into (3.10). This yields the approximate expression,

$$k^*\lambda_{Dc} \simeq \frac{1.4}{\beta^{1/2}}, \tag{3.11}$$

which is in reasonable agreement with our numerically calculated curve (figure 3.3) for $\beta > 20$.

The utility of the diagrams presented in figure 3.16, is that they provide the range of wavenumbers $k\lambda_{Dc}$ at particular values of f and β, through which there will be weakly-damped waves. Alternatively they provide the range in f over which the plasma can sustain electrostatic oscillations at a particular wavelength and temperature ratio. By taking a vertical or horizontal slice through these diagrams one can predict, qualitatively, the dispersive behaviour of a wave mode as $k\lambda_{Dc}$ or f, respectively, is varied.

Consider figure 3.16(c), the curve for $\beta = 20$. It is seen from the critical f^* curve (figure 3.2) that the transition between the cases of one mode and a possible second mode occurs at $f \simeq 0.21$. We select slices through figure 3.16(c) at $f = 0.2, 0.4, 0.6$. At $f = 0.2$ we observe only one mode, which we know is Langmuir-like, and it will be weakly damped in the regions: $0 \leq k\lambda_{Dc} \leq 0.13$; and $0.17 \leq k\lambda_{Dc} \leq 0.56$. This may be confirmed by considering figure 3.17, which shows a plot of the dispersion relation. At $f = 0.4$ the hot electron fraction lies above the critical value and therefore it is possible to observe two wave modes. Figure 3.16(c) indicates that there is a finite range of wavenumbers over which these waves may be observed. Indeed, referring to figure 3.18, it is seen that we will observe a Langmuir-like mode for $0 \leq k\lambda_{Dc} \lesssim 0.15$ which damps out for higher $k\lambda_{Dc}$, and an electron-acoustic-like mode that emerges for $0.25 \lesssim k\lambda_{Dc} \lesssim 0.55$ (figure 3.18). Following a similar procedure it is found that for $f = 0.6$ (figure 3.19) we observe a Langmuir-like mode and, over a very small interval in $k\lambda_{Dc}$ and ω_r, the electron-acoustic mode. For $f > 0.6$ we observe only a Langmuir-like mode, although we have $f > f^*$, because the HOM that exhibits weaker damping does not satisfy $-\gamma < \omega_r/2\pi$ (figure 3.20).

Similar slices can be taken at various $k\lambda_{Dc}$ values and compared to $k^*\lambda_{Dc}$. A similar analysis can then be undertaken when f is varied yielding

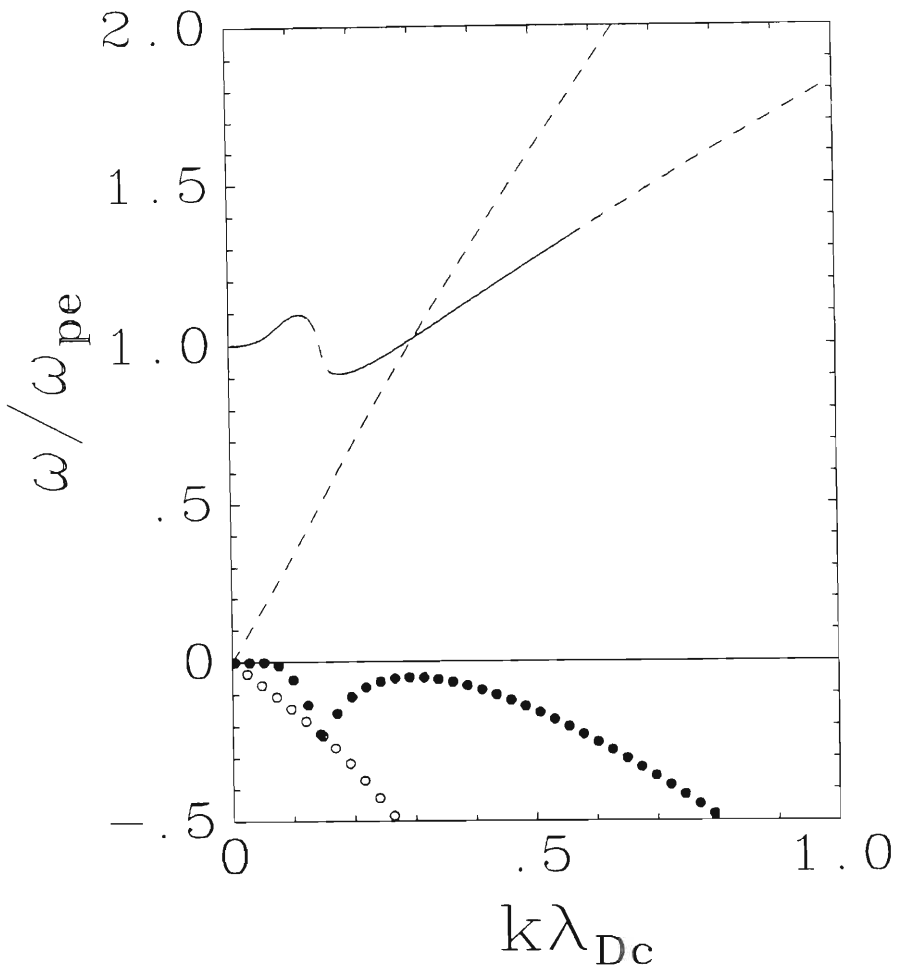

Figure 3.17: Complex frequency as a function of $k\lambda_{Dc}$ for the Langmuir-like mode and the electron-acoustic mode at a temperature ratio, β, of 20 and $f = 0.2$. Here and in figures 3.18–3.20 the dashed portions of the curves have $-\gamma > \omega_r/2\pi$, while open circles illustrate the damping rate of the electron-acoustic-like wave.

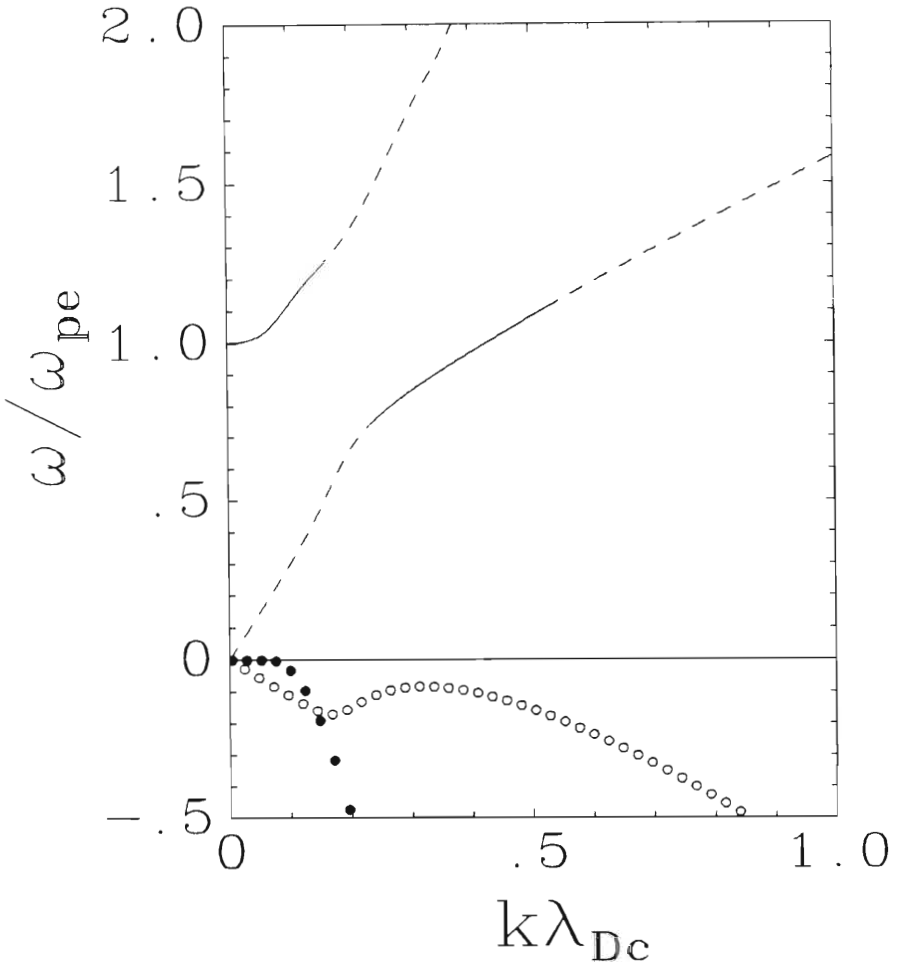

Figure 3.18: Complex frequency as a function of $k\lambda_{Dc}$ for the Langmuir-like mode and the electron-acoustic mode at a temperature ratio, β, of 20 and $f = 0.4$.

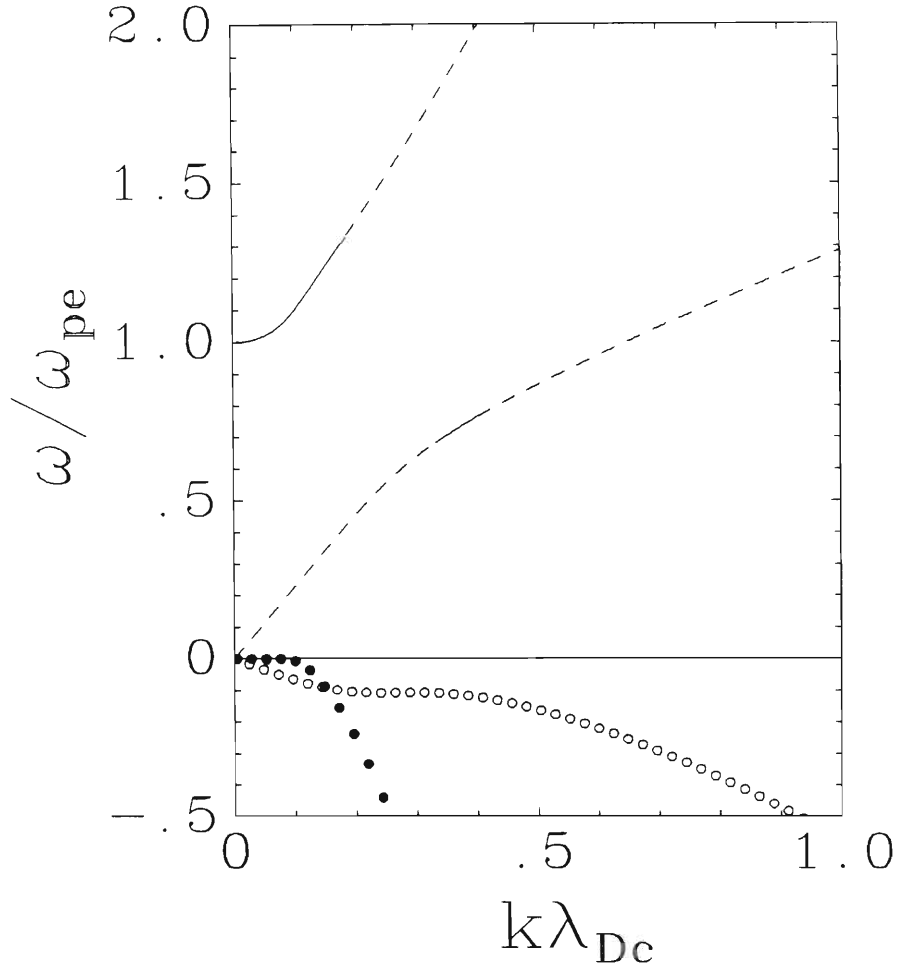

Figure 3.19: Complex frequency as a function of $k\lambda_{Dc}$ for the Langmuir-like mode and the electron-acoustic mode at a temperature ratio, β, of 20 and $f = 0.6$.

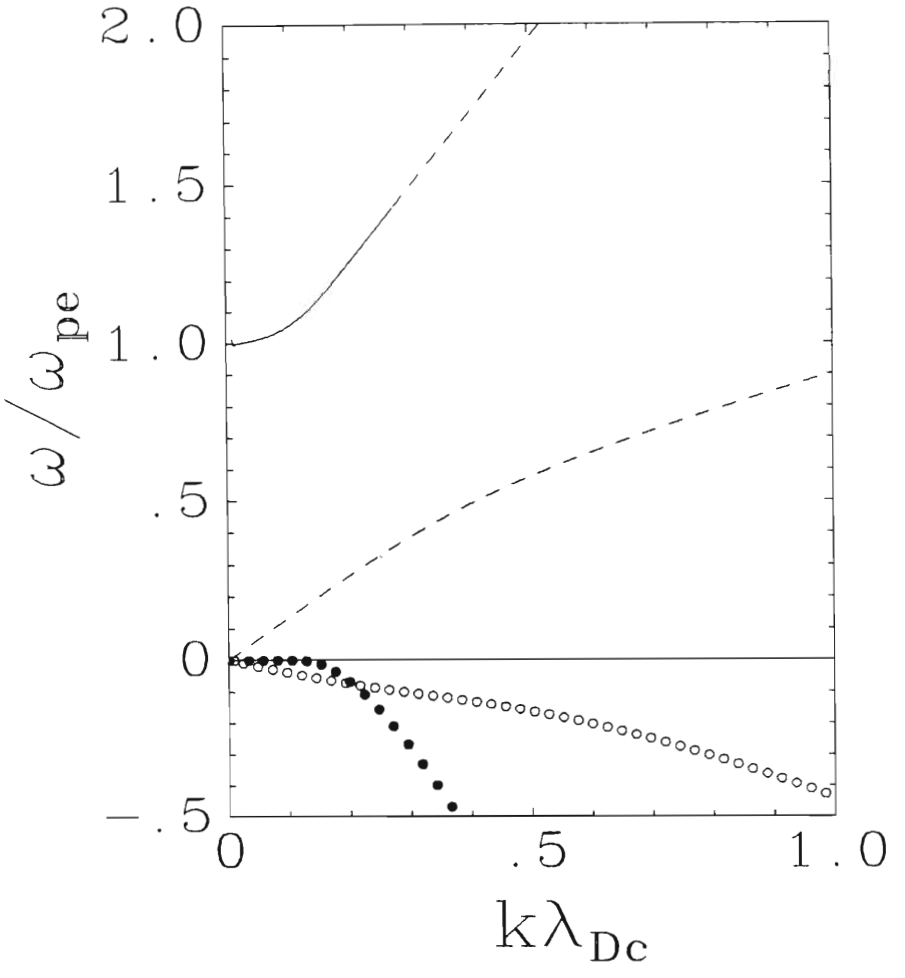

Figure 3.20: Complex frequency as a function of $k\lambda_{Dc}$ for the Langmuir-like mode and the electron-acoustic mode at a temperature ratio, β, of 20 and $f = 0.8$.

useful information about the damping and wave dispersion of the waves in such a scenario.

The onset of an interesting phenomenon takes place for β lying somewhere between 50 and 60 (figures 3.16(d) and 3.16(e)). The curve folds back on itself at larger values of f and smaller $k\lambda_{Dc}$, rendering a region of overlap in which one may observe an electron-acoustic and a Langmuir-like wave simultaneously. Experimentally this could give rise to beating, as two modes of the same wavelength but with different frequencies may propagate. As mentioned above, the critical lower limit of the temperature ratio β for this occurrence lies between 50 and 60, and is restricted to relatively large values of f (or alternatively small values of n_{0c} relative to n_{0e}) and thus occurs in a region of parameter space where the electron-acoustic wave is very weakly damped. Such a situation is illustrated in figure 3.16(f). We observe that for $0.8 < f < 0.95$ we can observe two modes, one belonging to the electron-acoustic ω-k spectrum and the other belonging to the Langmuir ω-k spectrum, for $0.062 \lesssim k\lambda_{Dc} \lesssim 0.18$. This is confirmed by examination of the dispersion relations presented in figure 3.21. Figure 3.21 is noteworthy also, from the point of view that the electron-acoustic wave clearly exhibits the dispersionless characteristics at these parameter values, as well as suffering only weak Landau damping in this regime.

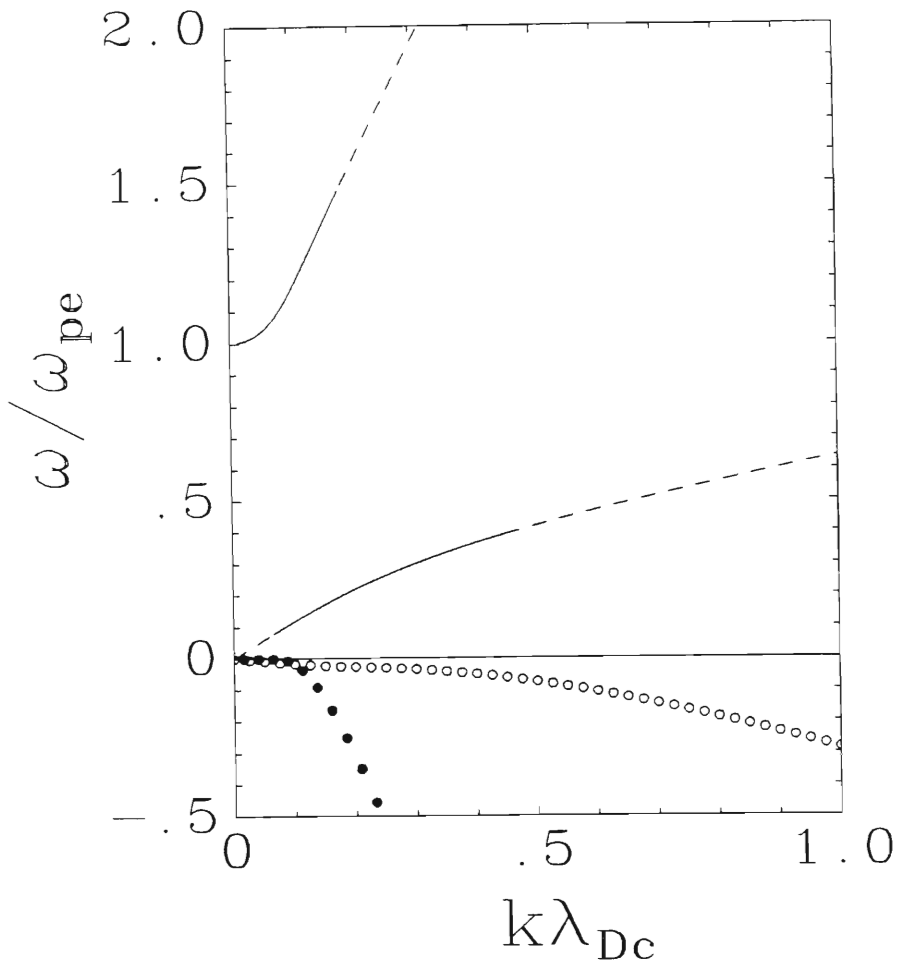

Figure 3.21: Complex frequency as a function of $k\lambda_{Dc}$ for the Langmuir and electron-acoustic waves at $\beta = 100$ and $f = 0.9$. There is a range of wavenumbers over which both waves exhibit weak damping and thus they may be observed simultaneously. The dashes and dots have the same meanings as in the previous diagrams.

Chapter 4

The magnetized electron-acoustic instability driven by field-aligned hot electron streaming

The work in this chapter provides an extension of the work of Tokar & Gary (1984) on the electron-acoustic instability in magnetized plasma. They solved the linear kinetic electromagnetic dispersion relation for a few fixed parameter values relevant to the polar cusp and deduced that the hot electron beams destabilise the electron-acoustic wave and not the whistler mode near resonance, as had previously been suggested (Lin *et al.* 1984). Furthermore, they show that the dispersion of the electron-acoustic wave can account for the frequency-time structures observed by satellites in that region (e.g. *Dynamics Explorer–1 (DE–1)*).

The work in this chapter provides a more complete view of the electron-acoustic instability than was presented by Tokar & Gary (1984) taking into account such factors as effect of the terrestrial magnetic field, direction of wave propagation and the possible competition with other electrostatic instabilities in or near the electron-acoustic frequency range.

4.1 Model and basic equations

Our plasma model is based upon the plasma constituents observed in the terrestrial polar cusp region, viz. cool ions, and electrons that consist of two separately isothermal components: a cool component; and a much hotter component that has mean drift speed directed along the magnetic field. The whole plasma is immersed in a constant homogeneous magnetic field $\mathbf{B} = B_0\mathbf{e}_z$, which crudely approximates the magnetic field in the polar region. This model represents a simplification of the model used by Tokar & Gary (1984), in which a third electron component was incorporated.

The distribution functions of the ion and cool electron components are approximated by Maxwellians to lowest order, and the hot electron velocity distribution is given by the drifting Maxwellian

$$f_h^{(0)}(\mathbf{v}) = (2\pi v_h^2)^{-3/2} \exp\left\{-\frac{v_x^2 + v_y^2 + (v_z - v_{0h})^2}{2v_h^2}\right\},$$

where v_{0h} is the mean drift speed of the hot electrons relative to the ions and cool electrons, and $v_h = (T_h/m_e)^{1/2}$ is the hot electron thermal speed. Furthermore, the ions are assumed to be unmagnetized on electron-acoustic timescales, due to their much larger mass and hence their much smaller gyrofrequency.

The wavevector $\mathbf{k}$ has components $k_{||}$ and $k_\perp$ parallel and perpendicular to $\mathbf{B}$, respectively, and the angle it makes with the magnetic field is defined by $\tan\theta = k_{||}/k_\perp$.

The dispersion relation for linear electrostatic waves in such a plasma may then be written (see appendix A)

$$1 + \sum_{j=i,c,h} K_j = 0, \tag{4.1}$$

where

$$K_i = -\frac{1}{2k^2\lambda_{Di}^2} Z'\left(\frac{\omega}{\sqrt{2}\,k v_i}\right), \tag{4.2}$$

and the electron contributions are:

$$K_c = \frac{1}{k^2\lambda_{Dc}^2}\left[1 + \frac{\omega}{\sqrt{2}\,k_{||}v_c}\exp\left(-\frac{k_\perp^2 v_c^2}{\Omega_e^2}\right) \cdot \sum_{n=-\infty}^{\infty} I_n\left(\frac{k_\perp^2 v_c^2}{\Omega_e^2}\right) Z\left(\frac{\omega - n\Omega_e}{\sqrt{2}\,k_{||}v_c}\right)\right]; \tag{4.3}$$

$$K_h = -\frac{1}{2k^2\lambda_{Dh}^2} Z'\left(\frac{\omega - k_{||}v_{0h}}{\sqrt{2}\,kv_h}\right). \tag{4.4}$$

For analytical purposes we assume that the hot electrons are unmagnetized which, by analysing the Gordeyev integral form for the hot electron susceptibilty, it can be shown requires $k_{||}^2 v_h^2/\Omega_e^2 > 4$ (Gary 1971). However, in the numerical calculations (see §4.3) we have employed the magnetized form for the hot electron susceptibility.

The definitions of symbols are as follows: $\lambda_{Dj} = (T_j/4\pi n_j e^2)^{1/2}$ is the Debye length; $\omega_j = (4\pi n_j e^2/m_j)^{1/2}$ is the plasma frequency; $v_j = (T_j/m_j)^{1/2}$ is the thermal speed; and $\Omega_j = |q_j|B/m_j c$ is the gyrofrequency of species j, where j denotes one of $\{i, h, c\}$. I_n is the modified Bessel function of order n, and Z is the plasma dispersion function. Temperatures are measured in energy units throughout.

4.2 The dispersion relation for magnetized electron-acoustic waves

Assuming, as in the unmagnetized case (Gary & Tokar 1985), that the phase velocity of the magnetized electron-acoustic wave lies between the thermal velocities of the cool and hot electrons we write

$$\left|\frac{\omega}{\sqrt{2}\,kv_i}\right| \gg 1, \quad \left|\frac{\omega - n\Omega_e}{\sqrt{2}\,k_{||}v_c}\right| \gg 1, \quad \left|\frac{\omega - k_{||}v_{0h}}{\sqrt{2}\,kv_h}\right| \ll 1. \tag{4.5}$$

Implicit in (4.5) above is the assumption that the wave frequency does not lie near any cyclotron harmonics. Were this to be the case, the second inequality in (4.5) would be reversed implying a power rather than asymptotic expansion of the relevant Z–function term. For the purposes of this analysis (a fuller derivation of the results of this section is provided in appendix A.4), however, we shall suppose that (4.5), as it stands, always holds.

Assuming further, that the cool electrons are strongly magnetized and hence have small Larmor radii $k_\perp^2 v_c^2/\Omega_e^2 < 1$, facilitates the expansion of the Z– and Z'–, as well as the Bessel functions, in their appropriate asymptotic/power series regimes.

Expanding (4.1) in conjunction with (4.2)–(4.4), retaining only lowest order terms, and summing between $n = -1$ and $n = 1$ (which takes into account only the effects of the cyclotron fundamental) yields the following

approximate dispersion relation in the context of (4.5) (see appendix A.4):

$$1 + \frac{1}{k^2\lambda_{Dh}^2} + \frac{\omega_c^2 \sin^2\theta}{\Omega_e^2 - \omega^2} - \frac{\omega_c^2 \cos^2\theta}{\omega^2} + i\pi^{1/2}\omega_h^2 \frac{\omega - k_\parallel v_{0h}}{\sqrt{2}k^3 v_h^3} \exp\left\{ -\frac{(\omega - k_\parallel v_{0h})^2}{2k^2 v_h^2} \right\} = 0. \qquad (4.6)$$

Equation (4.6) has a resonance at $\omega = \Omega_e$ for nonzero θ. This gives rise to two wave modes that have frequencies, respectively, above and below the electron gyrofrequency, Ω_e. If $\Omega_e \gg \omega$, or $\Omega_e \ll \omega$ then this resonance is avoided. We shall take the liberty of calling the case corresponding to the first inequality the strongly magnetized case, and the case corresponding to the latter, the weakly magnetized case. We deal with the former first.

4.2.1 Strongly-magnetized electron-acoustic waves

We seek weakly-damped or weakly-growing waves. Therefore it shall be supposed that $|\gamma| \ll |\omega_r|$ in addition to our fundamental assumption that $\Omega_e \gg \omega_r$. Solving (4.6) for ω_r in this parameter regime then yields (see appendix A.4):

$$\omega_r^2 = \frac{k_\parallel^2 v_{se}^2}{1 + k^2\lambda_{Dh}^2 + k_\perp^2 \rho_{se}^2}, \qquad (4.7)$$

where $\rho_{se} = v_{se}/\Omega_e$ is an effective electron Larmor radius based upon the electron sound speed $v_{se} = (n_{0c}/n_{0h})^{1/2} v_h$. The term in the denominator involving the latter is in most instances negligible in comparison to the others therein, and may be ignored for all but very oblique propagation, i.e. large $k_\perp$.

In the small wavenumber limit, $k\lambda_{Dh} \ll 1$, this equation clearly reduces to

$$\omega_r \simeq k_\parallel v_{se} = k v_{se} \cos\theta, \qquad (4.8)$$

which illustrates the acoustic nature of the wave at small wavenumbers.

At large wavenumbers $k\lambda_{Dh} \gg 1$ the wave frequency approximately satisfies

$$\omega_r \sim \omega_c \cos\theta,$$

(which can be seen from (4.7) by dividing through by $k^2\lambda_{Dh}^2$ and letting $k\lambda_{Dh} \to \infty$) and in this wavenumber-regime the mode behaves more like a plasma oscillation at a frequency commensurate with the natural frequency of the cool electrons.

4.2.2 Weakly-magnetized electron-acoustic waves

Here it is assumed that $\Omega_e < \omega_c$ and therefore the electrons are less strongly magnetized. Following an analysis similar to that of Melrose (1986), for ion-acoustic waves, we assume $|\gamma| \ll |\omega_r|$, and equate the real part of (4.6) to zero to obtain two roots for ω_r^2 (see appendix A.4),

$$\omega_r^2 = \tfrac{1}{2}(\omega_s^2 + \Omega_e^2)\left\{1 \pm \sqrt{1 - \frac{4\omega_s^2\Omega_e^2\cos^2\theta}{(\omega_s^2+\Omega_e^2)^2}}\right\}, \tag{4.9}$$

where $\omega_s(k) \equiv \omega_c/(1 + 1/k^2\lambda_{Dh}^2)^{1/2}$. To facilitate identification of these waves we investigate (4.9) in the small and large wavenumber regimes.

For those small wavenumbers, $k\lambda_{Dh} \ll (\omega_c^2/\Omega_e^2 - 1)^{-1/2}$, that enable $\omega_s(k) \ll \Omega_e$ to be satisfied, the upper and lower frequency solutions, respectively, reduce to (see appendix A.4)

$$\omega_r^{(+)} \simeq \Omega_e + \frac{k^2 v_{se}^2}{2\Omega_e}\sin^2\theta, \tag{4.10}$$

$$\omega_r^{(-)} \simeq kv_{se}\cos\theta. \tag{4.11}$$

For wavenumbers such that $\omega_s(k) \gg \Omega_e$, which reverses the sense of the above-mentioned wavenumber inequality, the upper and lower frequencies behave asymptotically like (see appendix A.4)

$$\omega_r^{(+)} \simeq \frac{\omega_c}{(1 + 1/k^2\lambda_{Dh}^2)^{1/2}}, \tag{4.12}$$

$$\omega_r^{(-)} \simeq \Omega_e\cos\theta. \tag{4.13}$$

It is evident then that the lower frequency solution $\omega_r^{(-)}$ behaves like an electron-acoustic wave at small wavenumbers (4.11), but has an upper frequency cut-off at larger wavenumbers given by (4.13).

The higher frequency solution, $\omega_r^{(+)}$, is bounded below by the electron gyrofrequency, Ω_e, and behaves like an electrostatic electron-cyclotron wave (4.10) at small wavenumbers. At intermediate wavenumbers the dispersion relation (4.12) is approximately acoustic:

$$\omega_r = \frac{kv_{se}}{(1 + k^2\lambda_{Dh}^2)^{1/2}}, \tag{4.14}$$

and therefore the cyclotron-like wave bears some resemblance to the electron-acoustic wave in unmagnetized plasma in this wavelength region. Akhiezer

et al. (1975) have called the ion-acoustic analogy of this wave the cyclotron-sound branch. In similar vein we shall refer to this wave as the electron-cyclotron-sound wave, or for brevity, just the cyclotron-sound wave.

At large wavenumbers the dispersion of the wave (4.12) is more like a cool electron plasma wave, the effects of the magnetic field becoming less apparent at these higher frequencies.

4.2.3 The instability and dynamics of the magnetized wave

From the aforementioned, the dispersion relation of the electron-acoustic wave in both the strongly- and weakly-magnetized regimes satisfies

$$\omega_r \simeq k_{||} v_{se}, \tag{4.15}$$

for small wavenumbers $k\lambda_{Dh} \ll 1$. At larger wavenumbers, $k\lambda_{Dh} \gg 1$ the dispersion relation ceases to be acoustic and the real frequency satisfies

$$\omega_r \simeq \min\{\omega_c, \Omega_e\} \frac{k_{||}}{k}, \tag{4.16}$$

in this wavelength regime. Equation (4.16) demonstrates the importance of the ratio Ω_e/ω_c in determining the dispersion at large wavenumbers.

The growth rate of the instability is easily obtained via (4.6) in the limit $|\gamma| \ll |\omega_r|$ (see appendix A.4):

$$\gamma = -\frac{\pi^{1/2}}{8^{1/2}} \frac{k^2}{k_{||}^2} \frac{\omega_h^2}{\omega_c^2} \frac{\omega_r^3}{k^3 v_h^3} (\omega_r - k_{||} v_{0h}) \exp\left[-\frac{(\omega_r - k_{||} v_{0h})^2}{2k^2 v_h^2} \right], \tag{4.17}$$

with ω_r given approximately by either of (4.15) or (4.16) above, depending on the magnitude of the wavevector. Numerical investigations of the unmagnetized instability (Gary 1987) have shown that growth near threshold occurs in the frequency regime $\omega_r \sim \omega_c$, which is the regime of weak damping of the electron-acoustic mode. In the magnetized instability it will be shown later that growth emerges at the frequency $\sim \min\{\omega_c, \Omega_e\} \cos\theta$. With this foresight it is probably more accurate to employ (4.16) in the above. When this is done it is not difficult to see that (4.17) has a $\cos^2\theta$ dependence and therefore the growth rate maximises for wave propagation parallel to the magnetic field. This monotonic decrease of the growth rate with wave propagation angle is confirmed by the numerical calculations (see later).

By (4.17) it is clear that the condition for instability is

$$v_{0h} \geq \frac{\omega_r}{k_{||}},$$

and therefore the wave is driven unstable when its phase velocity is in resonance with the positive slope of the hot electron distribution i.e. by inverse Landau damping. When the plasma is strongly magnetized then this condition can be written

$$v_{0h} \geq \frac{v_{se}}{(1 + k^2\lambda_{Dh}^2)^{1/2}}.$$

At this point it is appropriate to discuss the particle and wave dynamics of the magnetized electron-acoustic instability.

In the unmagnetized mode, the wave inertia is provided by the cool electrons. This motion is coupled to the restoring force of the hot electrons and the particles undergo roughly one-dimensional oscillatory motion in the direction of the wavevector $\mathbf{k}$.

In the magnetized wave, by contrast, the magnetic field, provided it is strong enough, effectively restricts electron trajectories to lie along it. The self-consistent wave $\mathbf{E}$ field, which is collinear with the wavevector $\mathbf{k}$, then gives rise to an $\mathbf{E} \times \mathbf{B}$ force which acts on the electrons in a direction perpendicular to both $\mathbf{B}$ and $\mathbf{E}$ (assuming $\mathbf{k} \times \mathbf{B} \neq 0$). Consequently the electron trajectories become ellipses with major axes parallel to $\mathbf{B}$ and minor axes perpendicular to both $\mathbf{B}$ and $\mathbf{k}$. The more oblique the angle of propagation, the smaller the angle made by the wavefronts with the magnetic field, and the further the distance along the magnetic field that the hot electrons must travel to neutralise any charge imbalances. For this reason the growth rate of the instability decreases with increasing angle θ.

The direction of energy propagation in the magnetized electron-acoustic wave can be established by considering the group velocity,

$$\mathbf{v}_g \equiv \frac{\partial \omega_r}{\partial \mathbf{k}} = \frac{\partial \omega_r}{\partial k_\perp}\mathbf{e}_\perp + \frac{\partial \omega_r}{\partial k_{||}}\mathbf{e}_{||}.$$

At small wavenumbers the group velocity of the electron-acoustic wave satisfies

$$\mathbf{v}_g = (0, v_{se}). \tag{4.18}$$

So too, does the direction of wave energy propagation (Melrose 1986). This means that independent of the direction of $\mathbf{k}$ the energy always propagates along the magnetic field, which contrasts strongly with the unmagnetized

wave in which the direction of energy propagation usually lies along the wavevector $\mathbf{k}$.

The group velocity in the large wavenumber limit is readily evaluated:

$$\mathbf{v}_g = -\min\{\omega_c, \Omega_e\}\frac{k_{||}}{k^3}(k_\perp, k_{||}) = -\min\{\omega_c, \Omega_e\}\frac{k_{||}}{k^3}\mathbf{k}. \tag{4.19}$$

In this wavenumber regime the energy propagation is in a direction opposite to that of the wavevector, which again contrasts with the unmagnetized wave. In the latter there is no energy propagation at all, at larger wavenumbers the wave reduces to a plasma oscillation at a frequency close to the cool electron plasma frequency (Gary & Tokar 1985).

4.3 Numerical

In this section we present numerical results based on the solution of the dispersion relation (4.1) incorporating (4.2)–(4.3) retaining their full analytical complexity and furthermore, including hot electron magnetization, i.e. incorporating

$$K_h = \frac{1}{k^2\lambda_{Dh}^2}\left[1 + \frac{\omega - k_{||}v_{0h}}{\sqrt{2}\,k_{||}v_h}\exp\left(-\frac{k_\perp^2 v_h^2}{\Omega_e^2}\right) \cdot \sum_{n=-\infty}^{\infty} I_n\left(\frac{k_\perp^2 v_h^2}{\Omega_e^2}\right) Z\left(\frac{\omega - n\Omega_e - k_{||}v_{0h}}{\sqrt{2}\,k_{||}v_h}\right)\right], \tag{4.20}$$

instead of (4.4). Since only the electrons are magnetized we henceforth omit the subscript e on Ω_e.

The dispersion relations and growth rates of the electron-acoustic and electron-cyclotron-sound instabilities are illustrated in figures 4.1–4.3 for a number of wave propagation angles θ. The magnetization of the electrons is weak, $\Omega/\omega_c = 0.25$, and the mean hot electron drift speed is $v_{0h} = 10v_c$. In this instance oblique wave propagation gives rise to two instabilities.

Based on the approximate dispersion relations (4.15) and (4.16) we identify the lower frequency wave, $\omega_r < \Omega$ for $\theta > 0$, with the electron-acoustic wave, where the acoustic nature $\omega_r/k = $ const. is clearly evident from figure 4.1. We identify the upper frequency mode as the cyclotron-sound-like wave (see figure 4.2). The latter mode may nevertheless exhibit a substantial acoustic regime depending upon the cyclotron harmonic onto which it connects. Indeed, the dispersion of this mode/instability at intermediate to

large wavenumbers reduces to the dispersion of the electron-acoustic mode in an unmagnetized plasma (cf. equation (4.14) and figure 4.2). Growth may occur in the acoustic regime for this mode also, giving rise to acoustic-like instability at frequencies greater than the electron gyrofrequency (see figure 4.2).

At this point it is appropriate to comment on the early ($k \neq 0$) termination of the dispersion curves for the cyclotron sound wave. The reason is numerical in origin and comes about because we have not considered full electromagnetic and relativistic effects in our dispersion relation (4.1). As demonstrated in Cuperman (1981), if one projects the full (nonrelativistic) electromagnetic wave tensor Λ_{ij}, where

$$\Lambda_{ij} E_j = 0,$$

is the wave equation and E_j are the electric field components, along the wavevector then one obtains (4.1) with additional contributions due to electron current-induced coupling to the transverse waves. Callen & Guest (1971) have shown that unless

$$\frac{\omega_e^2}{c^2 k^2} \ll 1,$$

these contributions should be considered. As is evident from the diagrams k is tending toward zero with $\omega_r \neq 0$ when the curves terminate and therefore this contribution would become important. In addition, the frequency of the cyclotron-sound wave tends toward a cyclotron harmonic at small k, where the arguments of the Z functions become indeterminate ($0/0$ as $k \rightarrow 0$) suggesting unphysical behaviour there. As discussed by Swanson (1989) this shortcoming can be overcome by employing a full relativistic treatment of the plasma particles.

A similar mode to the cyclotron-sound wave arises in a magnetized electron-ion plasma when the ions are much hotter than the electrons. Akhiezer *et al.* (1975) have called this latter wave the low-frequency electron sound branch and it is related to the electron-acoustic instability studied by Aref'ev (1970) and Lashmore-Davies & Martin (1973).

In each of the electron-acoustic and cyclotron-sound instabilities discussed above the growth rate is observed to decrease with increasing propagation angle in agreement with our earlier discussions. However, in contrast the real frequency of the electron-acoustic wave is observed to decrease, while the frequency of the cyclotron-sound wave is observed to increase with progressively larger propagation angles.

Figure 4.3 illustrates the dispersion relation and growth rate of the strongly magnetized electron-acoustic instability. The electron gyrofrequency in this case is $\Omega = 2\omega_c$ and lies well above the range of electron-acoustic frequencies—so avoiding any resonances. In this situation, also, the growth rate as well as the frequency, decreases with propagation angle.

In figures 4.4–4.9 we illustrate the effect of increasing the magnetization on the instability dispersion and growth rate, for oblique propagation angles. The drift velocity is $v_{0h} = 10v_c$ and the wavevector, $\mathbf{k}$, makes an angle of 20° with $\mathbf{B}$. In all the figures one observes a "coupling" between the electron-acoustic and cyclotron-sound waves at wavenumbers $k\rho_c \sim 0.1 - 0.2$ and frequencies lying just below Ω. This coupling, as is evident from the figures, becomes weaker as the ratio Ω/ω_c is increased.

The lower frequency acoustic instability is observed to span a progressively larger range of frequencies relative to the plasma frequency, as the gyrofrequency is increased. More important, however, is the dramatic decrease in the growth rate of the cyclotron-sound-like instability as the electron gyrofrequency is increased. This leads to the eventual stabilisation of the wave at $\Omega/\omega_c \sim 0.75$ (see figure 4.7). This phenomenon is shown clearly in figure 4.10. Here we cite cyclotron damping as the main reason for the suppression of the growth rate.

In contrast, the growth rate of the electron-acoustic instability appears to be less strongly affected by this parameter.

Figures 4.11 and 4.12 show a more detailed view of the growth rates of the instabilities at various θ values. As discussed earlier the waves grow by inverse Landau damping due to resonance with the positive slope of the hot electron distribution. Figure 4.11 illustrates the scenario when $\Omega < \omega_c$, and figure 4.12 the corresponding scenario when the inequality is reversed, $\Omega > \omega_c$. The former shows the far greater maximum growth rate of the cyclotron-sound-like instability at values of Ω/ω_c less than one. Nevertheless, at small wavenumbers $k\rho_c \ll 1$, the growth rate of the electron-acoustic instability is larger than that of the cyclotron-sound-like instability.

Figure 4.12 shows that at larger gyrofrequency–plasma frequency ratios $\Omega/\omega_c > 1$, i.e. stronger magnetization, the cyclotron-sound mode is stable for a wide range of propagation angles, and only the electron-acoustic instability prevails.

At quasi-parallel propagation, $0 < |\mathbf{k} \times \mathbf{B}| \ll 1$, and weak electron magnetization $\Omega/\omega_c < 1$, we find that the electron-acoustic instability is

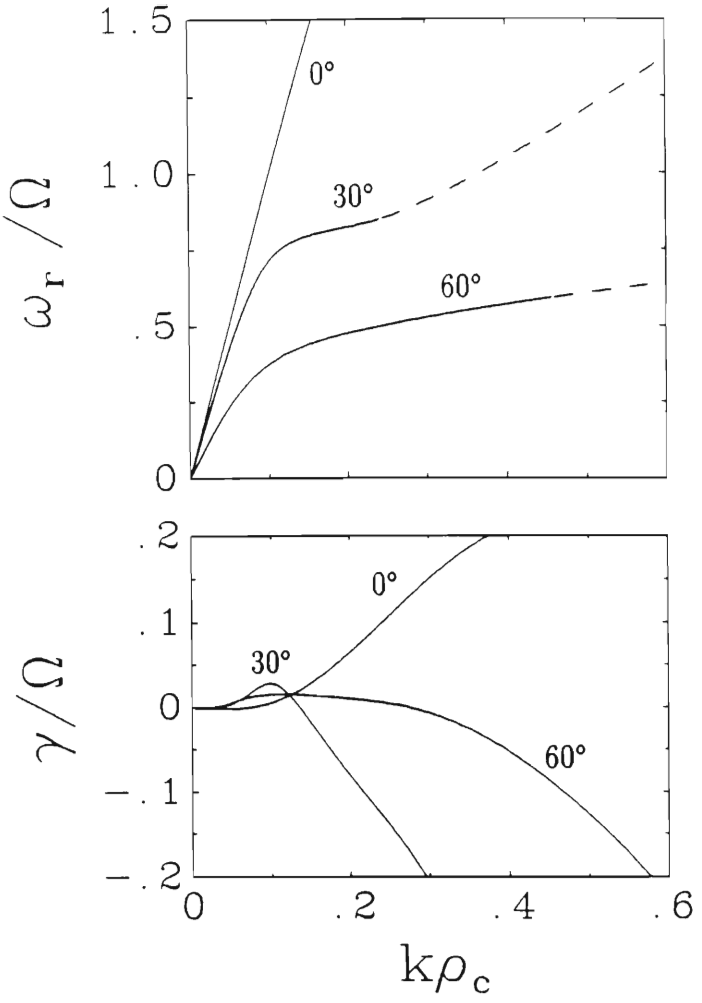

Figure 4.1: The dispersion relation and growth rate of the electron-acoustic instability. The parameter labelling the curves is θ. Other parameters are: $\Omega/\omega_c = 0.25$, $v_{0h} = 10v_c$. Unless otherwise stated, in all figures in this chapter $n_c = n_h$, $T_h = 100T_c$, $T_i = T_c$ and $m_i = 1836m_e$. Here and in figures 4.4–4.9, 4.14, and 4.20–4.22 the dashed section of the curves indicate strongly damped waves where $-\gamma < \omega_r/2\pi$.

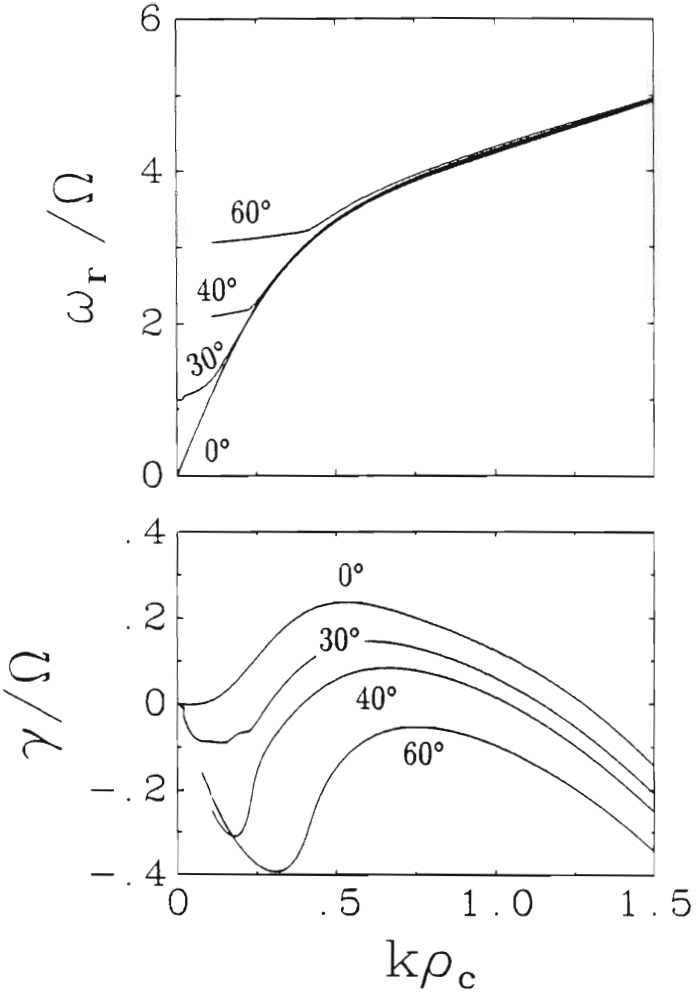

Figure 4.2: The dispersion relation and growth rate of the higher-frequency electron-cyclotron-sound-like instability. The parameter labelling the curves is θ; and $\Omega/\omega_c = 0.25$, $v_{0h} = 10v_c$.

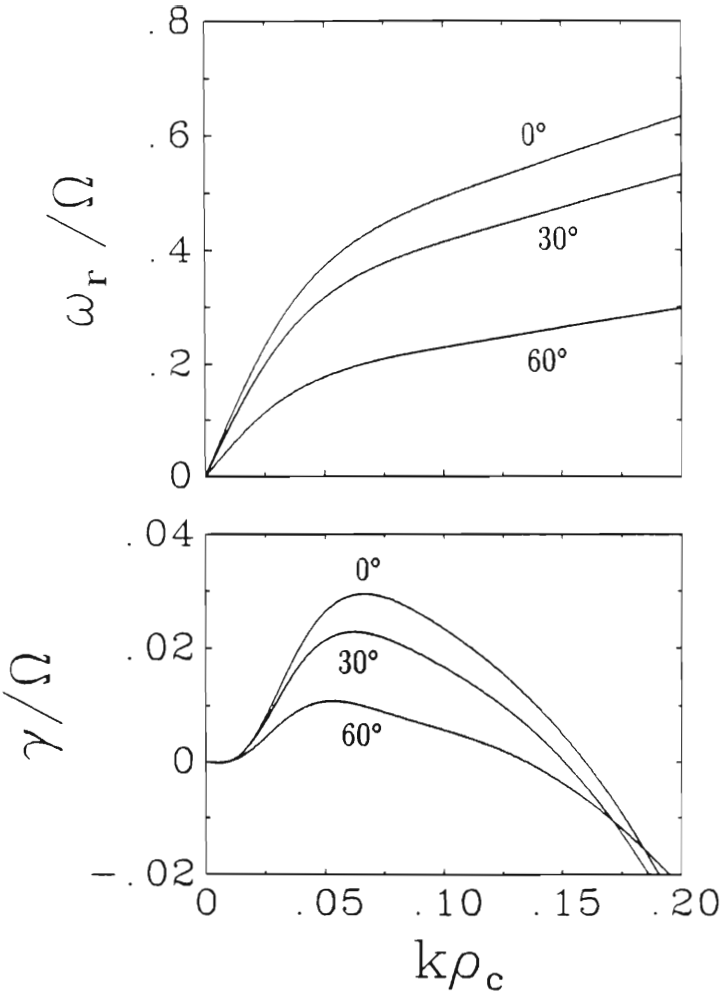

Figure 4.3: The dispersion relation and growth rate of the electron-acoustic instability in the strongly magnetized regime $\Omega/\omega_c = 2$. The parameter labelling the curves is θ; and $v_{0h} = 10v_c$.

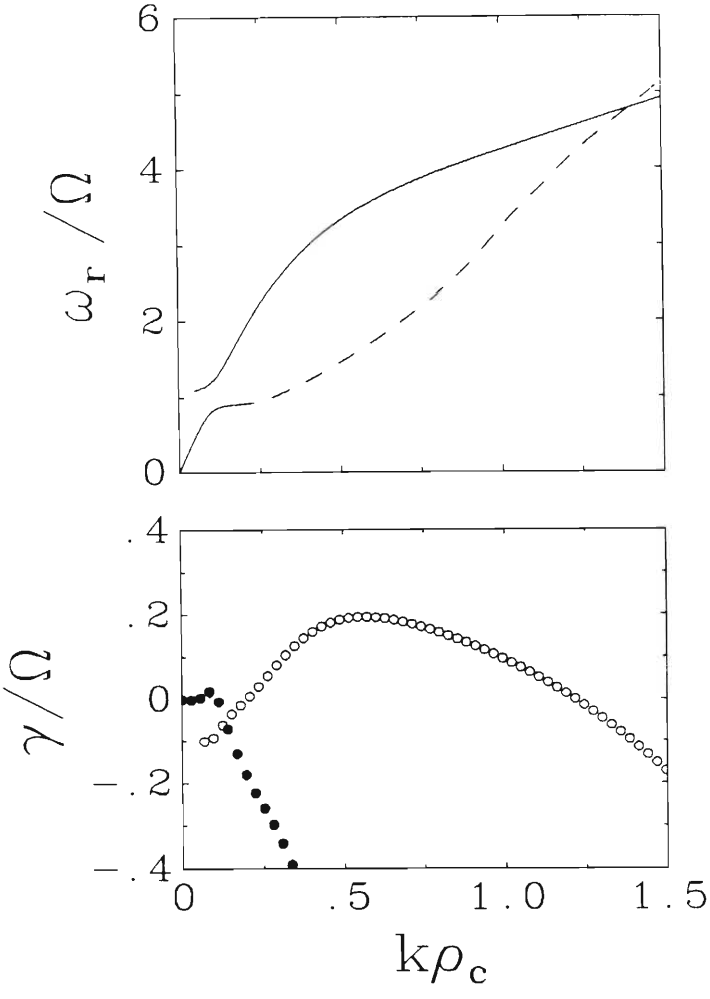

Figure 4.4: Figures 4.4–4.9 illustrate the dispersion relation and growth rate of the electron-acoustic- and electron-cyclotron-sound instabilities for various values of the ratio Ω/ω_c. The wavevector makes an angle $\theta = 20°$ with respect to the magnetic field. The open circles correspond to the growth rate for the electron-cyclotron-sound instability, whereas the shaded circles show the growth rate of the electron-acoustic instability. In the above figure Ω/ω_c has the value 0.25.

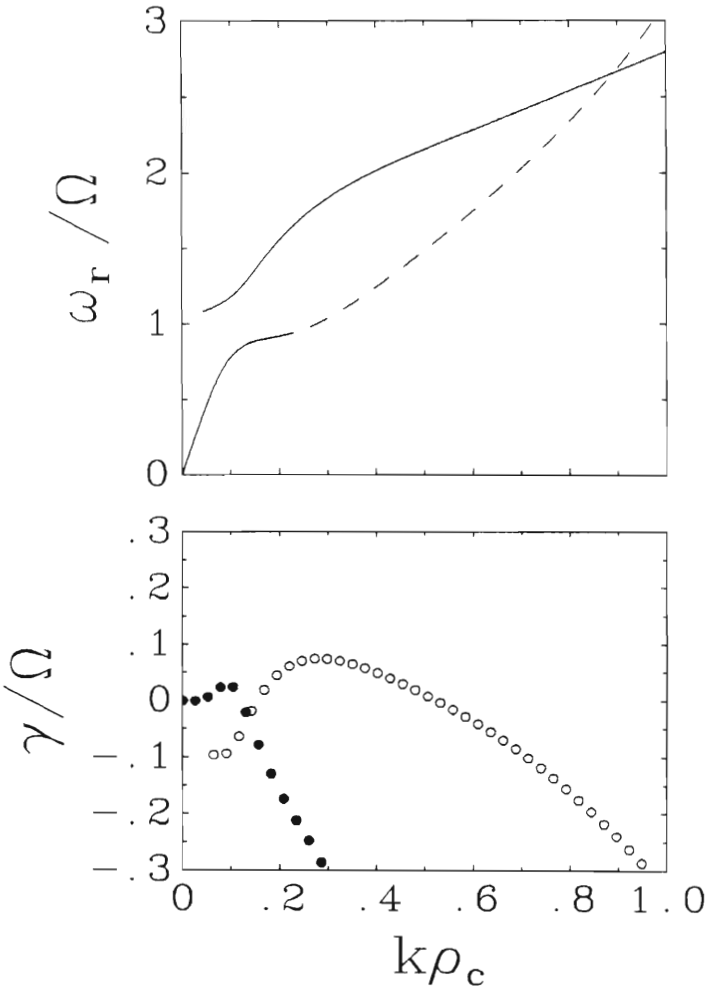

Figure 4.5: $\Omega/\omega_c = 0.5$

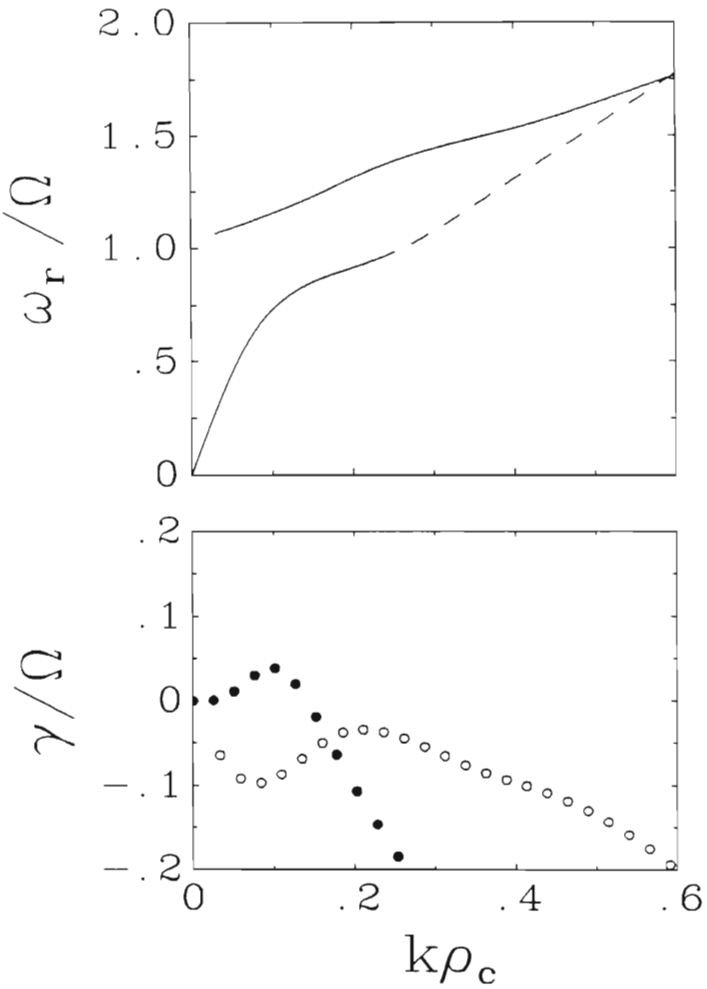

Figure 4.6: $\Omega/\omega_c = 0.75$

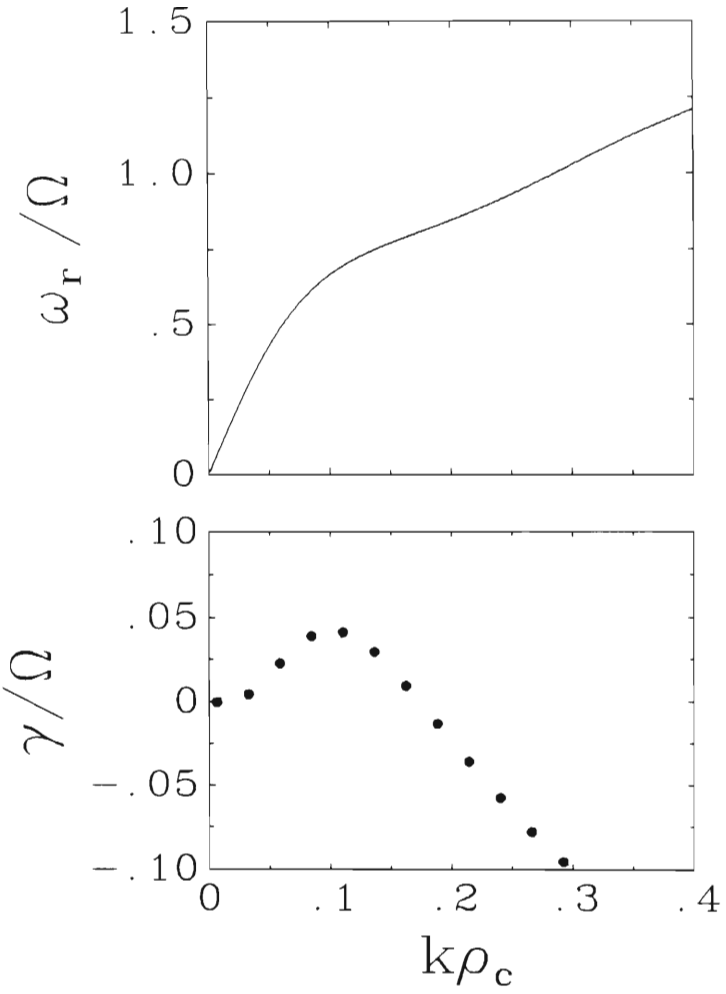

Figure 4.7: $\Omega/\omega_c = 1$

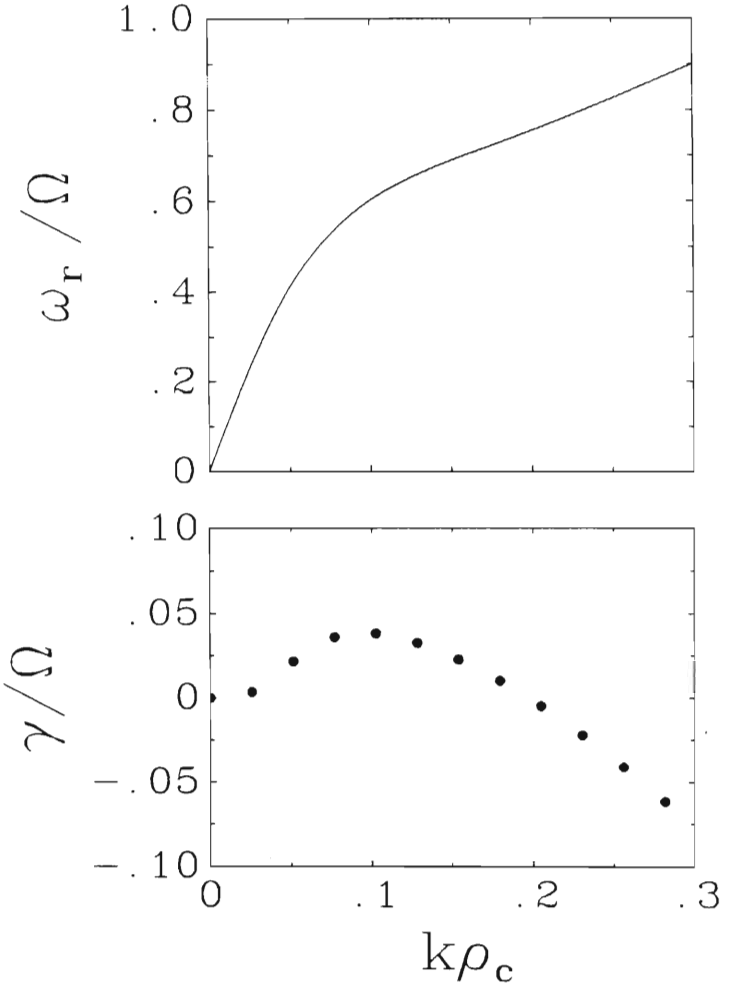

Figure 4.8: $\Omega/\omega_c = 1.25$

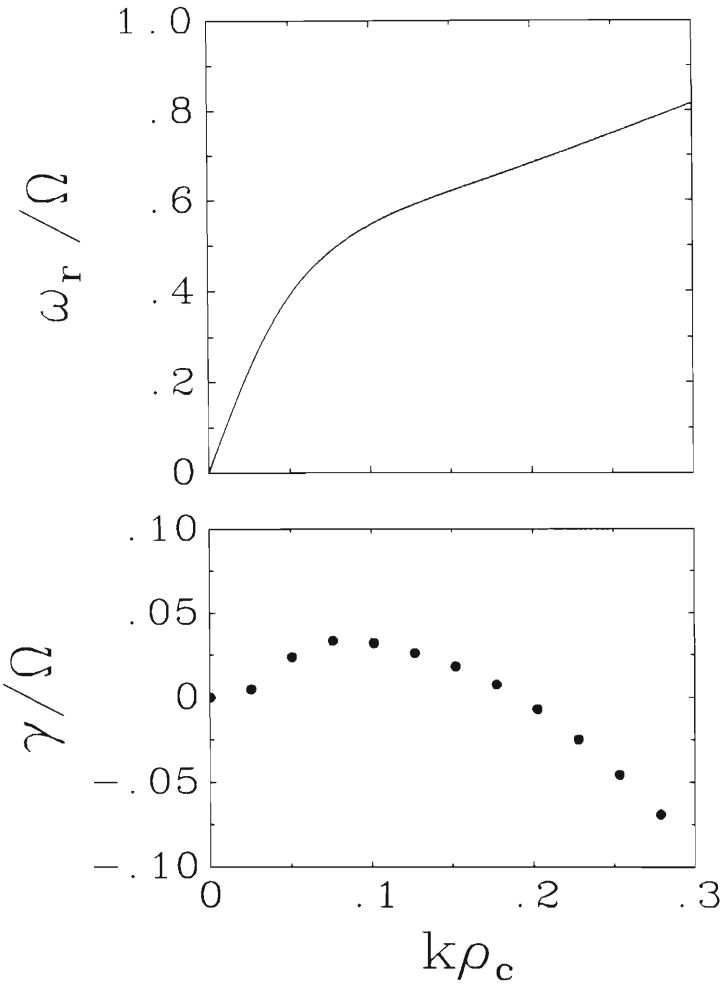

Figure 4.9: $\Omega/\omega_c = 1.5$

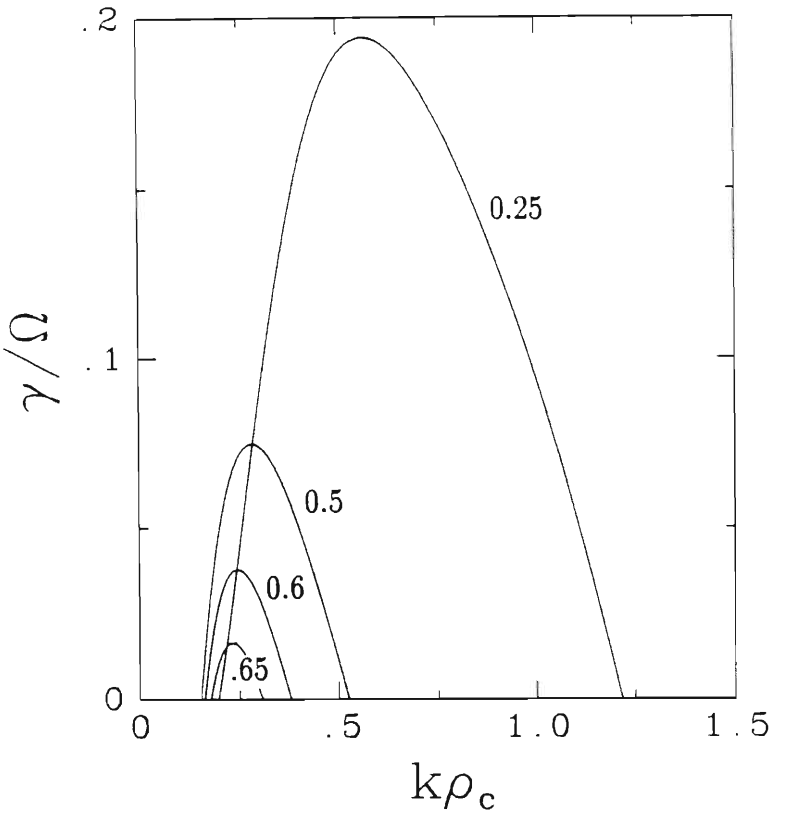

Figure 4.10: Growth rate of the electron-cyclotron-sound instability for various values of the ratio Ω/ω_c (on curves). The hot electron drift speed is $v_{0h} = 10v_c$ and the wavevector makes an angle of 20° with the magnetic field.

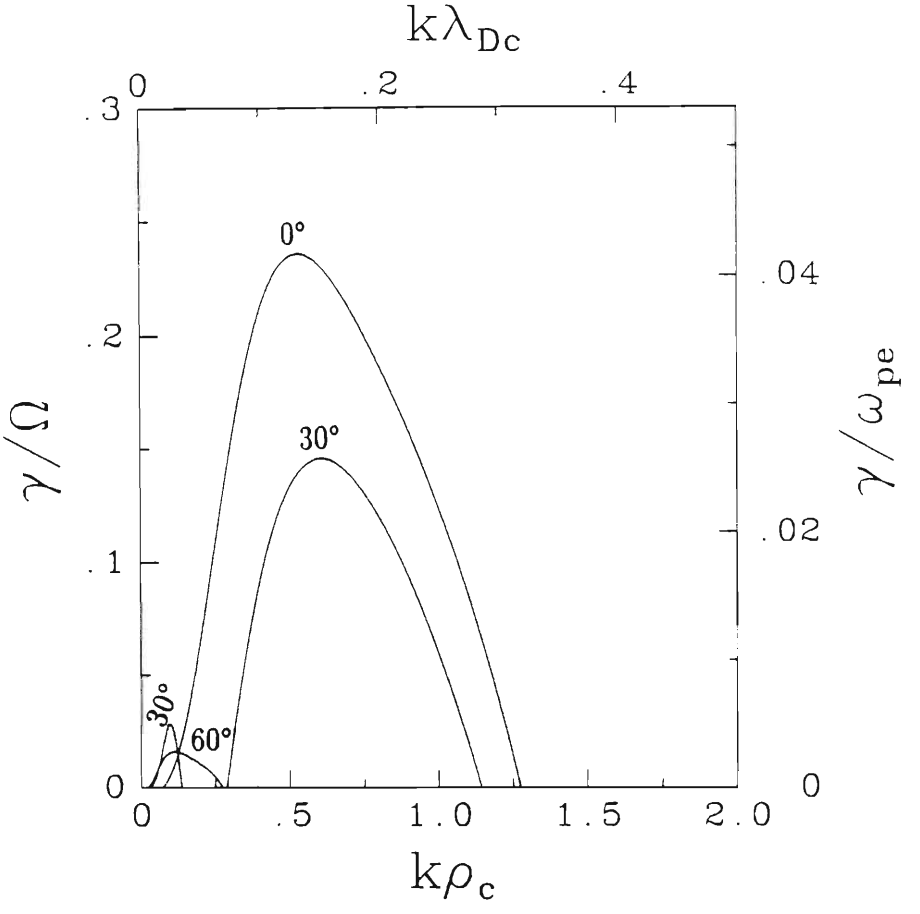

Figure 4.11: The growth rate of the instabilities at various angles, θ for $\Omega/\omega_c = .25$. The smaller peaks correspond to the growth rate of the electron-acoustic instability and the larger to the electron-cyclotron-sound instbility.

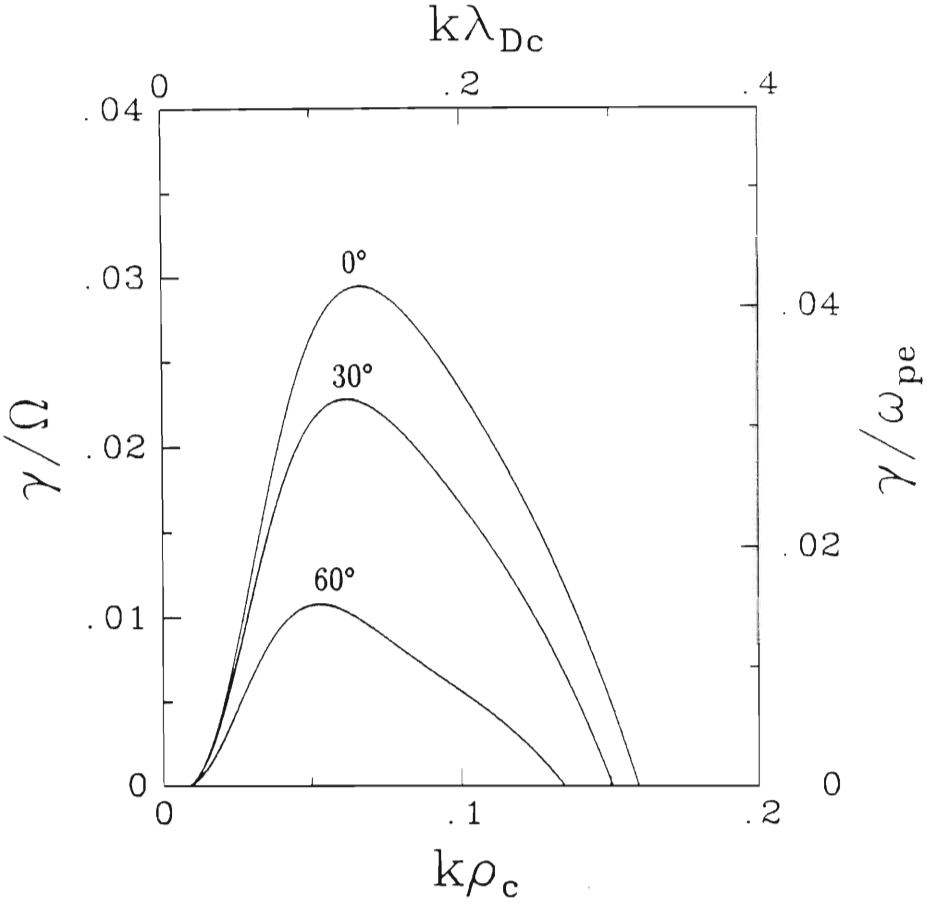

Figure 4.12: The growth rate of the electron-acoustic instability at various angles, θ, for $\Omega/\omega_c = 2$. The cyclotron-sound wave is stable.

unaffected by the magnetic field. The dispersion of the wave is given by

$$\omega_r^2 \simeq \frac{\omega_c^2}{1 + 1/k^2\lambda_{Dh}^2}.$$

and under these circumstances the results of Gary (1987) apply, approximately.

If $\theta > 2°$, however, and the hot electron drift speed is not too far from its threshold value, then there arises a local maximum in the growth rate corresponding to wave growth at frequencies $\sim \Omega \cos\theta$ (see figure 4.13). This peak signals the onset of the lower frequency electron-acoustic instability. For larger propagation angles the waves/instabilities are clearly distinct, each with its own separate dispersion curve one above and one below Ω (see figure 4.14).

Figure 4.15 illustrates the thresholds of the instabilities as a function of θ, for various values of Ω/ω_c. The instability with lower threshold as $\theta \to 0$ is electron-cyclotron-sound-like, and the other, corresponding to a larger threshold drift speed as $\theta \to 0$ is electron-acoustic-like. For sufficiently oblique propagation angles, however, the electron-acoustic instability becomes the instability with lower threshold (and larger growth rate—see later) and it becomes increasingly more difficult to destabilize the cyclotron-sound-like wave by a hot electron drift. As the ratio Ω/ω_c is increased towards ~ 1 we find only one threshold curve pertaining to an electron-acoustic-like instability. It is noteworthy that as $\theta \to 0$ the higher frequency instability, which reduces to the electron-acoustic instability in an unmagnetized plasma in this limit, has $v_{0h} > 4.7v_c$ at $\theta \to 0$, which agrees with the finding of Gary (1987), that the hot electron drift speed must be approximately $5v_c$ for the onset of the electron-acoustic instability.

At larger magnetization $\Omega/\omega_c > 1$, the threshold exhibits very weak dependence on the wave propagation angle. Consequently, a hot electron drift speed greater than $5v_c$ will excite electron-acoustic turbulence in all propagation directions. However, wave growth is non-isotropic and will be enhanced along the magnetic field direction (cf. §4.2.3 and figure 4.12). Furthermore, Tokar & Gary (1984) have solved the full electromagnetic dispersion relation and shown that the electron-acoustic mode has a lower threshold than the whistler mode for both $\Omega/\omega_e > 1$ and $\Omega/\omega_e < 1$—the latter is more usually destabilised by strong temperature anisotropies in the particle distribution functions. Therefore field-aligned electrostatic turbulence between the ion and electron plasma frequencies in a strongly magnetized plasma, could be a

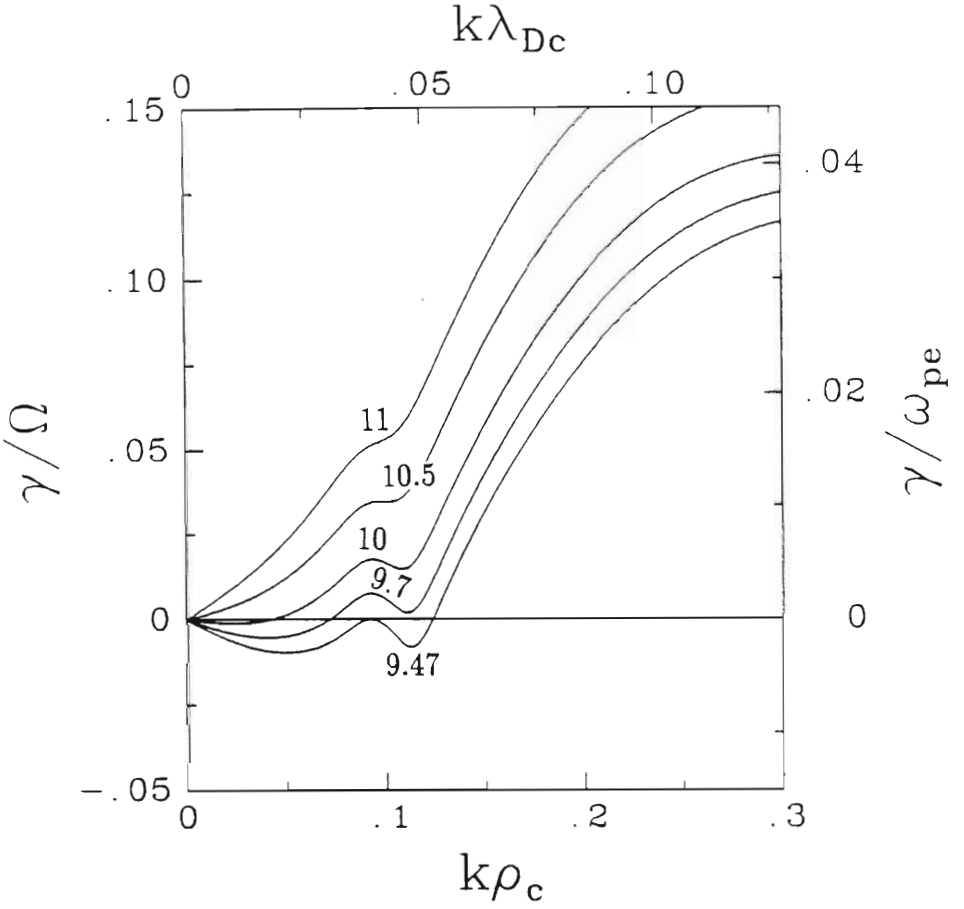

Figure 4.13: The local maximum in the growth rate of the electron-acoustic instability that occurs for $\Omega/\omega_c < 1$ and $0 < |\mathbf{k} \times \mathbf{B}| \ll 1$. $\theta = 5°$ and $\Omega/\omega_c = 0.424$. The parameter labelling the curves is v_{0h}/v_c.

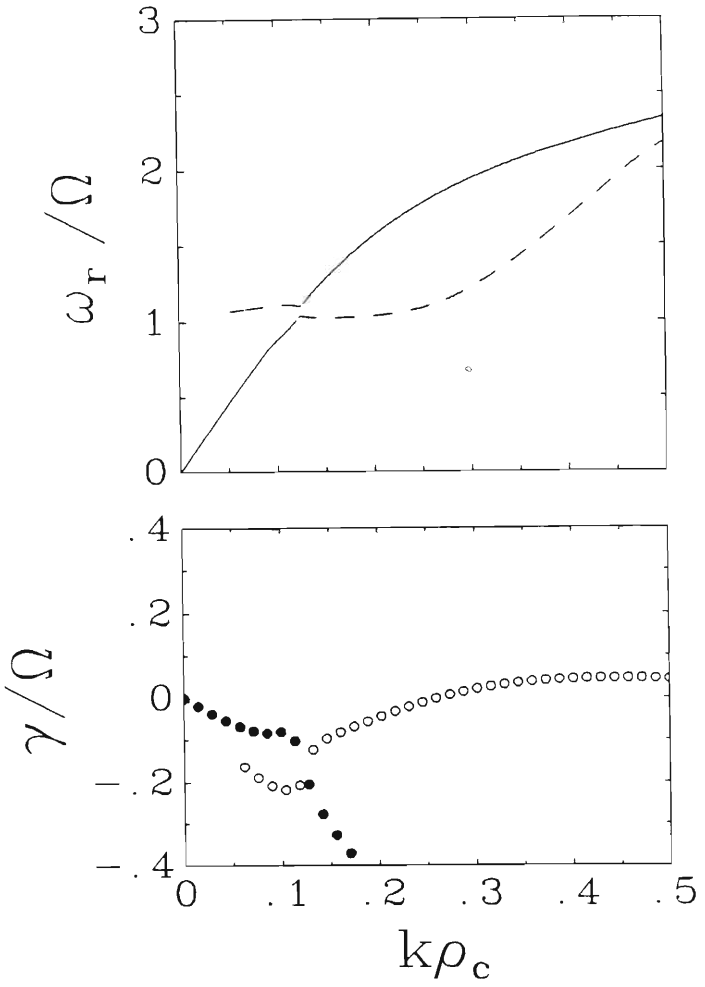

Figure 4.14: The dispersion relation and growth rate of the electron-acoustic and higher frequency cyclotron-sound instabilities for $\theta = 5°$ near the critical value at which the "unmagnetized" electron-acoustic instability couples to the cyclotron-sound wave giving rise to instabilities above and below Ω. The hot electron drift velocity, v_{0h}, is $7v_c$. Open circles correspond to the growth rate of electron-cyclotron-sound-like instability, whereas the shaded circles indicate the growth rate of the electron-acoustic instability.

strong indication of the occurrence of the electron-acoustic instability (Gary 1987).

In figures 4.16 and 4.17 we illustrate the maximum growth rates of the instabilities under conditions of weak magnetization, at wave propagation angles of 20° (figure 4.16), and 40° (figure 4.17). Here and in figures 4.18–4.19 the growth rates have been maximized with respect to $k = |\mathbf{k}|$. In figures 4.16–4.18 the ratio $\Omega/\omega_c = 0.424$ and this corresponds to $\Omega/\omega_e = 0.3$.

In figure 4.16 the propagation angle is such that the cyclotron-sound-like instability has lower threshold (cf. previous figure) and it also has larger maximum growth rate for hot electron drift speeds of just above $6v_c$ to over $20v_c$.

In figure 4.17 the situation is reversed: the electron-acoustic wave has lower threshold and also larger maximum growth rate for a drift speed such that $6v_c < v_{0h} < 13v_c$. For $v_{0h} > 13v_c$ the cyclotron-sound instability has the larger maximum growth rate. This means that for such angles the electron-acoustic instability will appear as an instability "island" which for this particular case takes the form $6v_c < v_{0h} < 13v_c$, being swamped by the electron-cyclotron-sound instability at larger beam speeds due to its larger growth rate there. Because it has the lower threshold of instability, however, the electron-acoustic wave could grow to such a large amplitude that it sufficiently scatters the plasma components, thus preventing the emergence of the electron-cyclotron-sound instability. In the event of this occuring the hot electron drift-induced turbulence would be dominated by electron-acoustic waves.

Figure 4.18 illustrates the maximum growth rate of the lower frequency electron-acoustic instability for $\Omega/\omega_c = 0.424 < 1$ and a number of wave propagation angles θ. Clearly, for large drift speeds there is a monotonic decrease in the maximum growth rate of this instability as the propagation angle increases. This trend breaks down for drift speeds close to their threshold values where the behaviour of the maximum growth rate curves is more complex, but is in keeping with the threshold predictions.

In the strongly magnetized plasma, $\Omega/\omega_c = 4.24$, the behaviour of the maximum growth rate with θ is strictly monotonic (see figure 4.19); there being very little variation in the threshold drift speed with the angle of wave propagation. In addition we point out that, as discussed by Gary (1987), the electron-acoustic instability transforms into the electron/electron two-stream instability at large values of the electron drift speed $\sim 20v_c$.

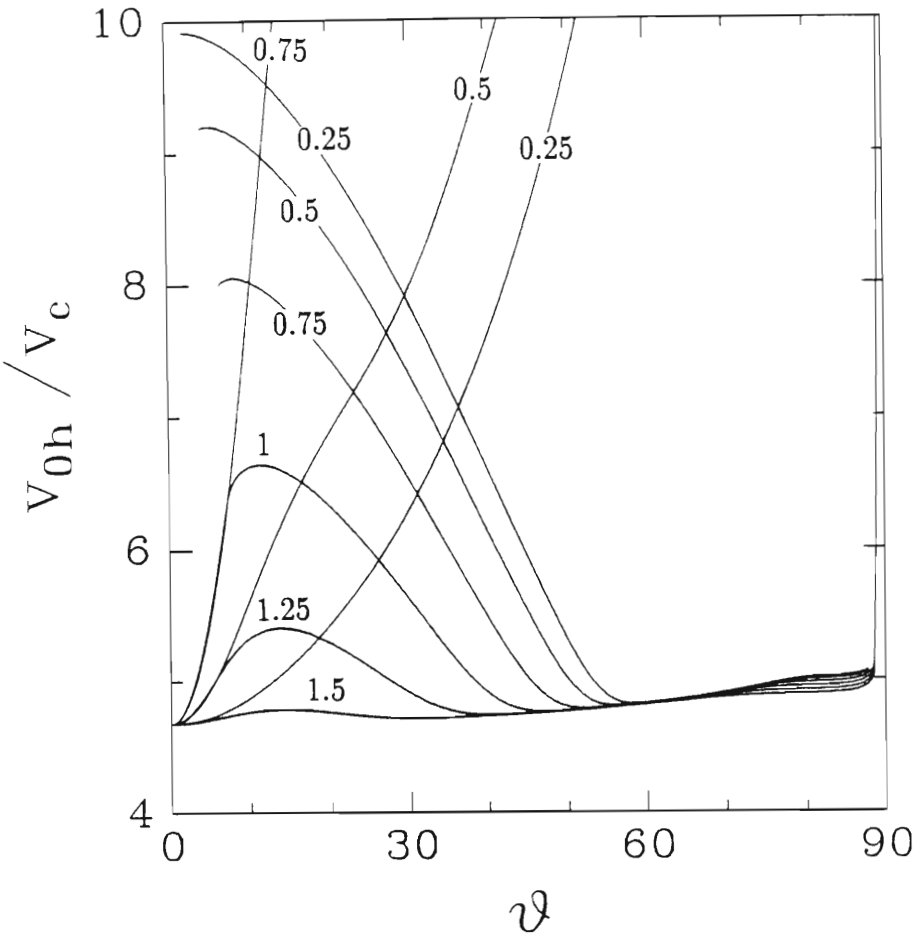

Figure 4.15: The thresholds of the instabilities that arise for various values of Ω/ω_c as a function of wave propagation angle θ. The parameter labelling the curves is the ratio Ω/ω_c.

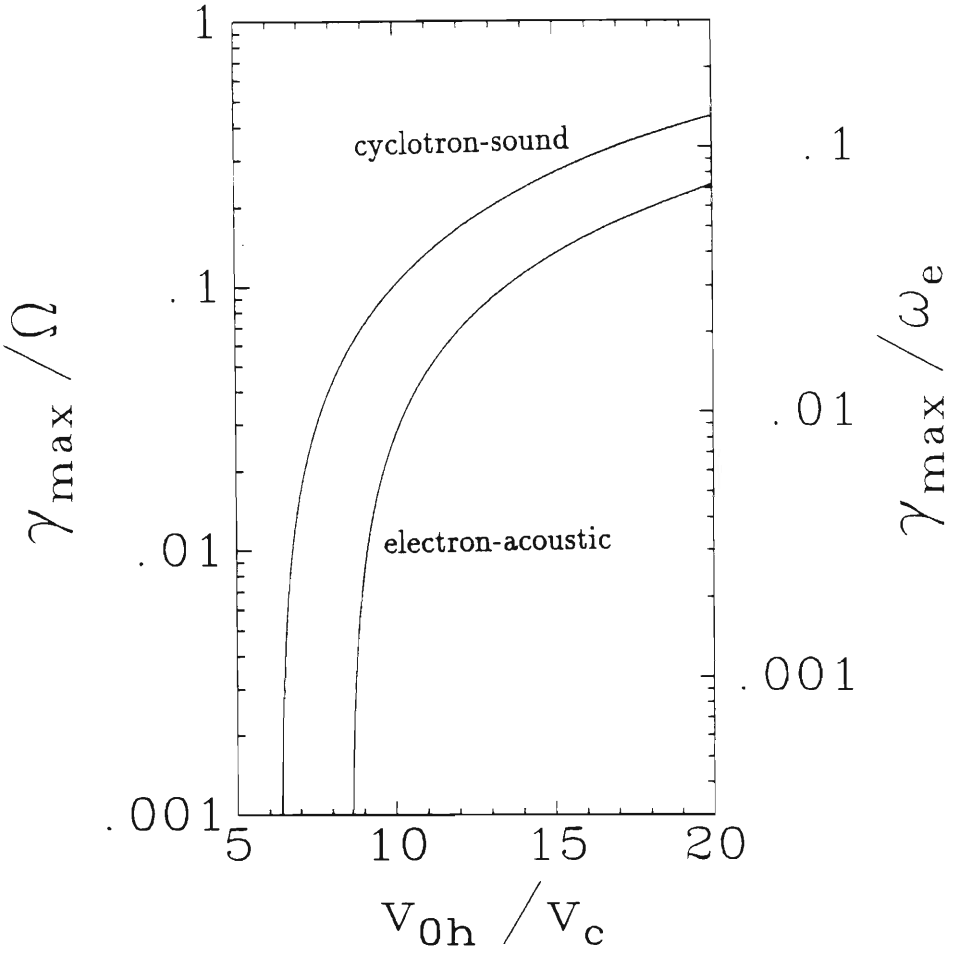

Figure 4.16: A comparison of the maximum growth rate of the electron-cyclotron-sound- and electron-acoustic instabilities for $\theta = 20°$, $\Omega/\omega_c = 0.424$.

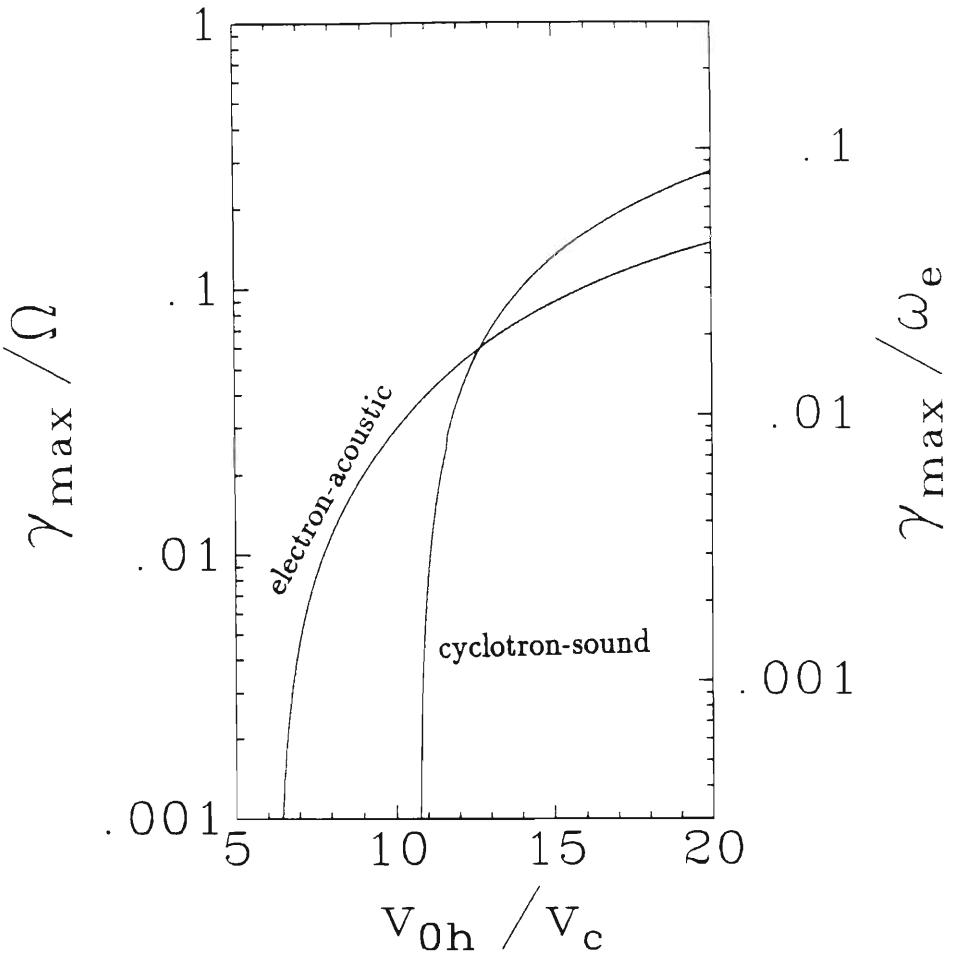

Figure 4.17: A comparison of the maximum growth rate of the electron-cyclotron-sound-like and the electron-acoustic instabilities for $\theta = 40°$, $\Omega/\omega_c = 0.424$.

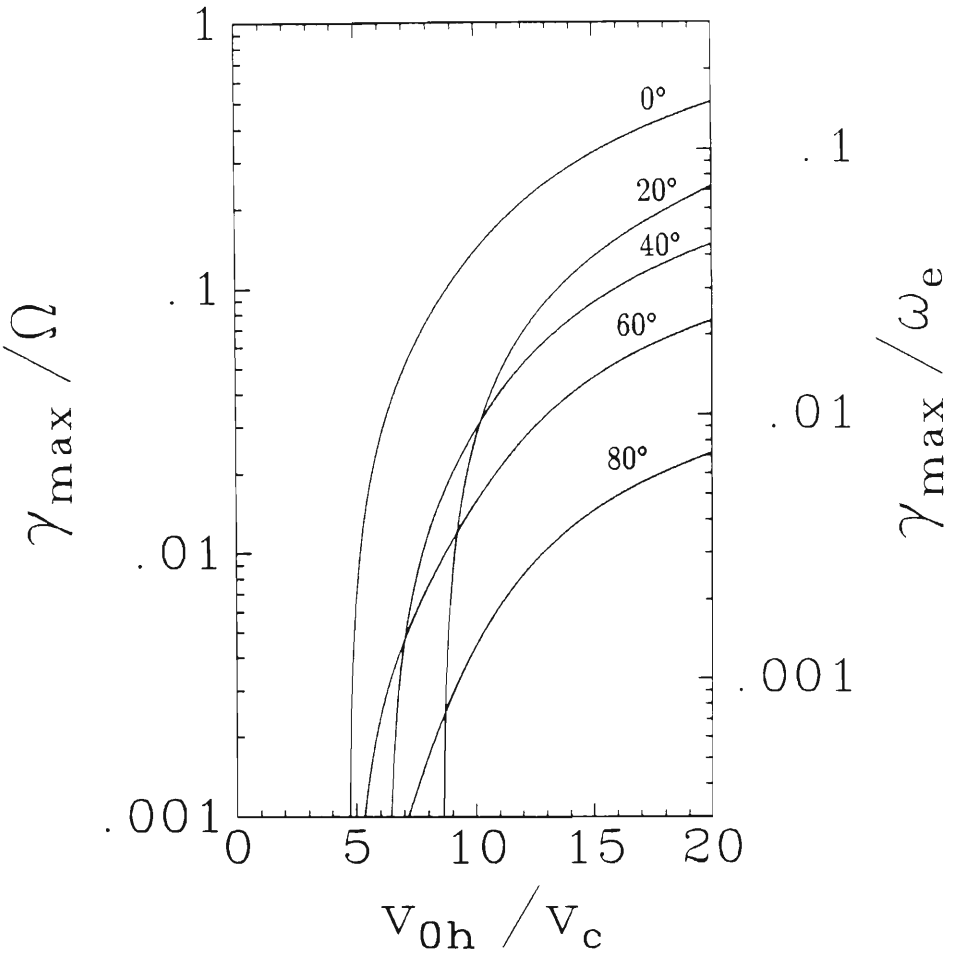

Figure 4.18: The maximum growth rate of the weakly magnetized ($\Omega/\omega_c = 0.424$) electron-acoustic instability as a function of hot electron drift speed for various values of θ (labelling curves).

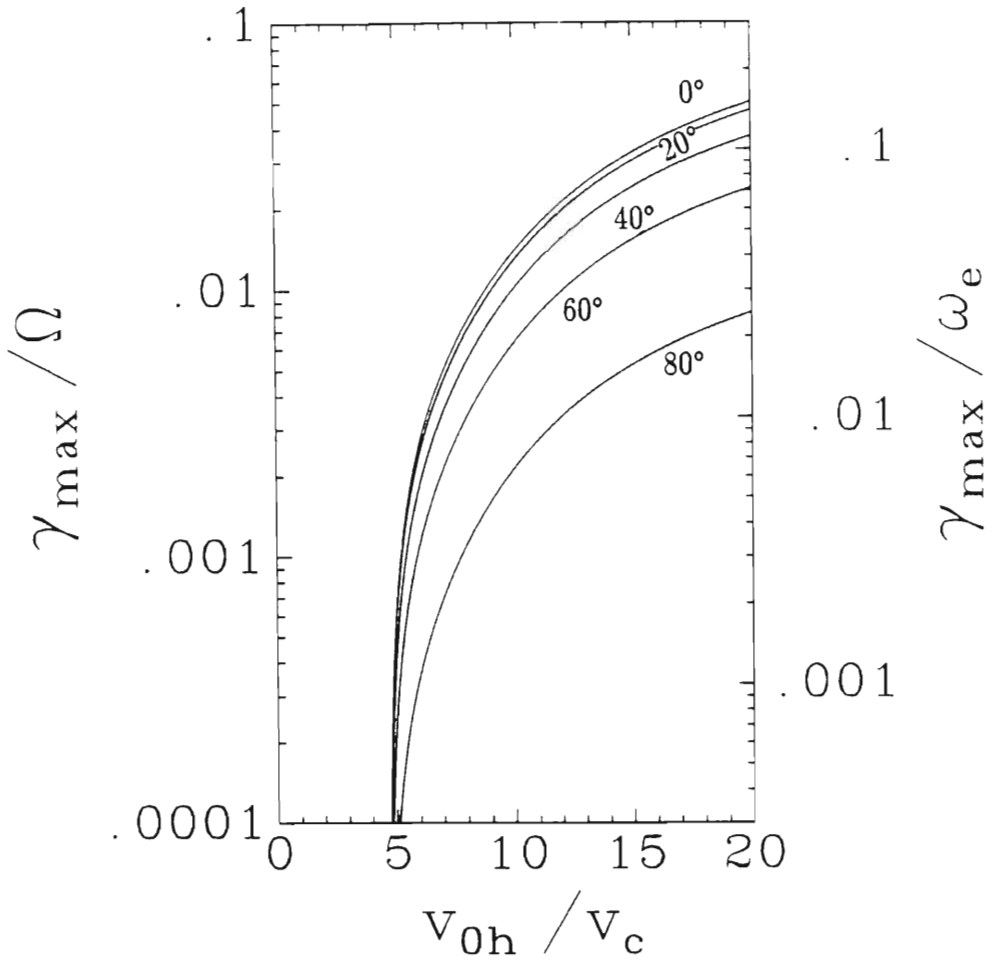

Figure 4.19: The maximum growth rate of the strongly magnetized ($\Omega/\omega_c = 4.24$) electron-acoustic instability as a function of hot electron drift speed. The parameter labelling the curves is θ.

4.4 The hot ion driven instability

It is well known that the modified electron-acoustic mode may be driven unstable by a hot ion drift (Ashour-Abdalla & Okuda, 1986; Schriver & Ashour-Abdalla, 1987). Under the assumption that the phase velocity of the modified electron-acoustic wave satisfies

$$v_c \ll \frac{\omega_r}{k} \ll v_{ib}, v_h, \tag{4.21}$$

Yu & Shukla (1983) showed that the modified electron-acoustic mode has the following dispersion relation in an unmagnetized plasma,

$$\omega_r = \frac{\omega_c}{(1 + 1/k^2\lambda_{Dh}^2 + 1/k^2\lambda_{Dib}^2)^{1/2}},$$

where λ_{Dib} is the Debye length of the hot drifting ion species. However, the condition (4.21) imposes the rather restrictive condition on the ratio of ion-to-cool electron temperature ratio $T_{ib}/T_c \gg m_i/m_e$ (Gary & Tokar 1985). Such large ion-electron temperature ratios rarely occur in space/cosmic plasma situations and are virtually impossible to attain in the laboratory.

Using kinetic theory Schriver & Ashour-Abdalla (1987) were able to show that the situation is not as bleak as a first glance might imply. They showed that the modified electron-acoustic instability emerges when the temperature of the ion beam is of the order of 250 times greater than the cool electron temperature, which represents a significant improvement over the value of 1836. Although this still requires that the ions be very hot, it is certainly more tenable than the formidable temperature ratio of very much larger than m_i/m_e.

Moreover, ion temperatures larger than $250T_c$ are believed to occur in the geomagnetic tail (Schriver & Ashour-Abdalla, 1987) and therefore, the unstable spectrum of modified electron-acoustic waves could be responsible, at least in part, for broadband electrostatic noise (below the electron plasma frequency) observed there. We present in this section a comparison of the hot ion driven instability with that of the hot electron driven instability of the foregoing sections.

A model similar to that of Schriver & Ashour-Abdalla (1987) is employed: the plasma consists of stationary cold unmagnetized ions; hot unmagnetized ions that drift along **B** with drift speed v_{0ib}; hot magnetized electrons; and cold magnetized electrons that are both stationary. Once

again we write the dispersion relation

$$1 + \sum_j K_j = 0,$$

but in this instance the summation includes a term of the form

$$K_{ib} = -\frac{1}{2k^2\lambda_{Dib}^2} Z'\left(\frac{\omega - k_{||} v_{0ib}}{\sqrt{2} k v_{ib}}\right), \tag{4.22}$$

where v_{0ib} is the mean velocity of the drifting hot ions. K_i, K_c and K_h are given by (4.2), (4.3) and (4.20) (with $v_{0h} = 0$), respectively.

In the strongly magnetized regime ($\Omega/\omega_c \gg 1$), the dispersion of the unstable mode satisfies (cf. Yu & Shukla 1983)

$$\omega_r = \frac{\omega_c \cos\theta}{(1 + 1/k^2\lambda_{Dh}^2 + 1/k^2\lambda_{Dib}^2)^{1/2}},$$

and as with the hot electron-driven instability, the effect of the magnetic field is to introduce a factor of $\cos\theta$ into the numerator of the unmagnetized dispersion relation. As the strongly magnetized case has been investigated by Schriver & Ashour-Abdalla we shall concentrate primarily on the weakly magnetized regime $\Omega/\omega_c < 1$.

Figure 4.20 illustrates the dispersion and growth rate of the modified electron-acoustic instability for a propagation angle of $\theta = 0°$. In this case the wave dispersion and growth are unaffected by the magnetic field.

In figure 4.21 the wave propagation angle is $\theta = 25°$. There is a notable change in the dispersion of the mode at $\omega_r \simeq \Omega$ as well as the emergence of a peak in the curve for γ there.

For still larger angles of propagation (figure 4.22, $\theta = 30°$) one observes two modes: one that propagates at $\omega_r < \Omega$; and another that is weakly damped for $\omega_r > \Omega$. This behaviour of the dispersion relation for oblique wave propagation is similar to that of the weakly magnetized electron-acoustic instability, however, there are two main differences. Firstly, the resonance at Ω only affects the dispersion of the modified electron-acoustic instability at larger propagation angles, θ, than it does the electron-acoustic instability in the absence of hot ions. Secondly, the mode that has the higher frequency has constant phase velocity at small wavenumbers ($k\rho_c \ll 1$), whereas, when the hot electrons are drifting they drive a high frequency cyclotron-sound mode that has $\omega_r \simeq n\Omega$ at small $k\rho_c$. A similar instability in a more strongly magnetized plasma, that had constant phase velocity at

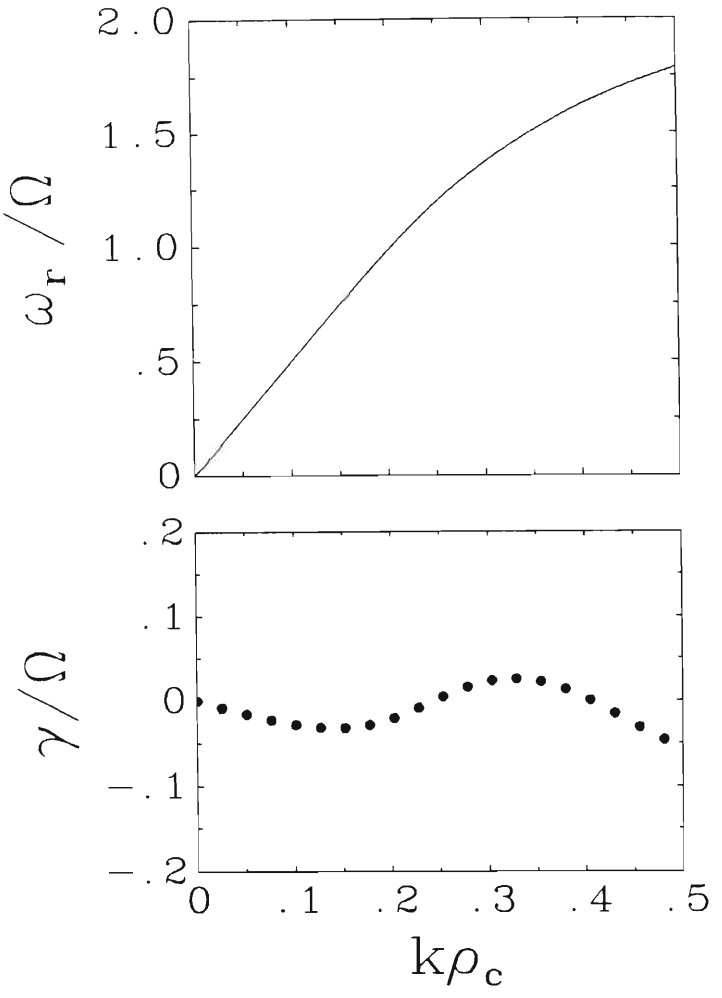

Figure 4.20: The dispersion and growth rate of the weakly-magnetized modified electron-acoustic instability for $\theta = 0°$. Other parameters are $n_c = 0.1n_e$, $T_h = T_{ib} = 500T_c$, $T_i = 125T_c$, $\Omega/\omega_e = 0.2$ and $v_{0ib} = 4.95v_c$. Solid circles correspond to the growth rate of the modified electron-acoustic instability.

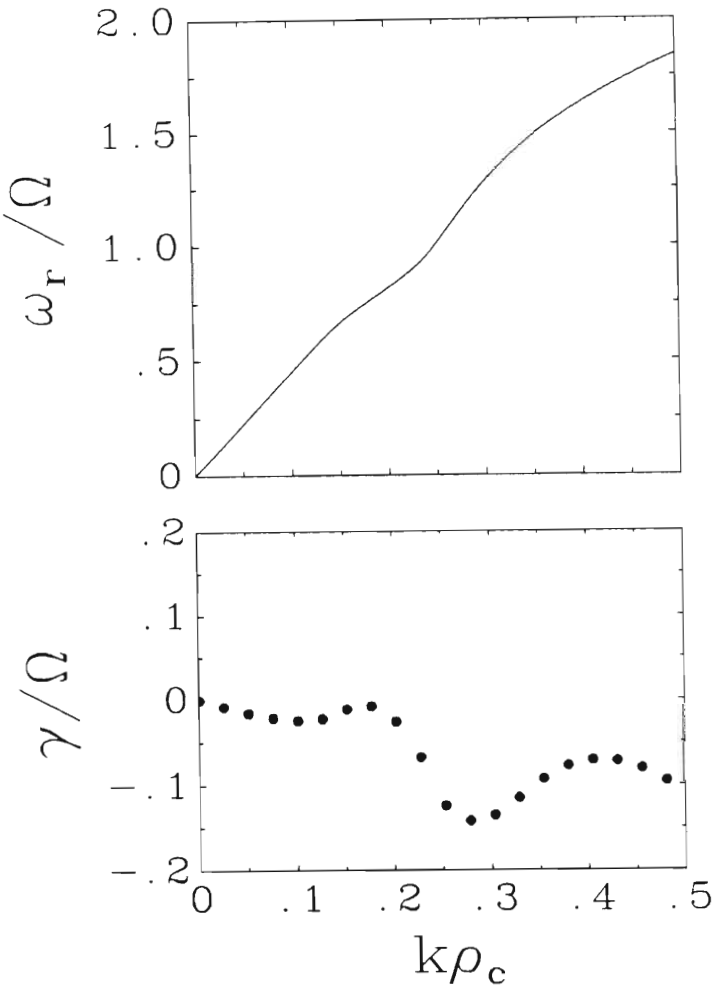

Figure 4.21: The dispersion and growth rate of the weakly-magnetized modified electron-acoustic instability for $\theta = 25°$. Other parameters are as in figure 4.20. Solid circles correspond to the growth rate of the modified electron-acoustic instability.

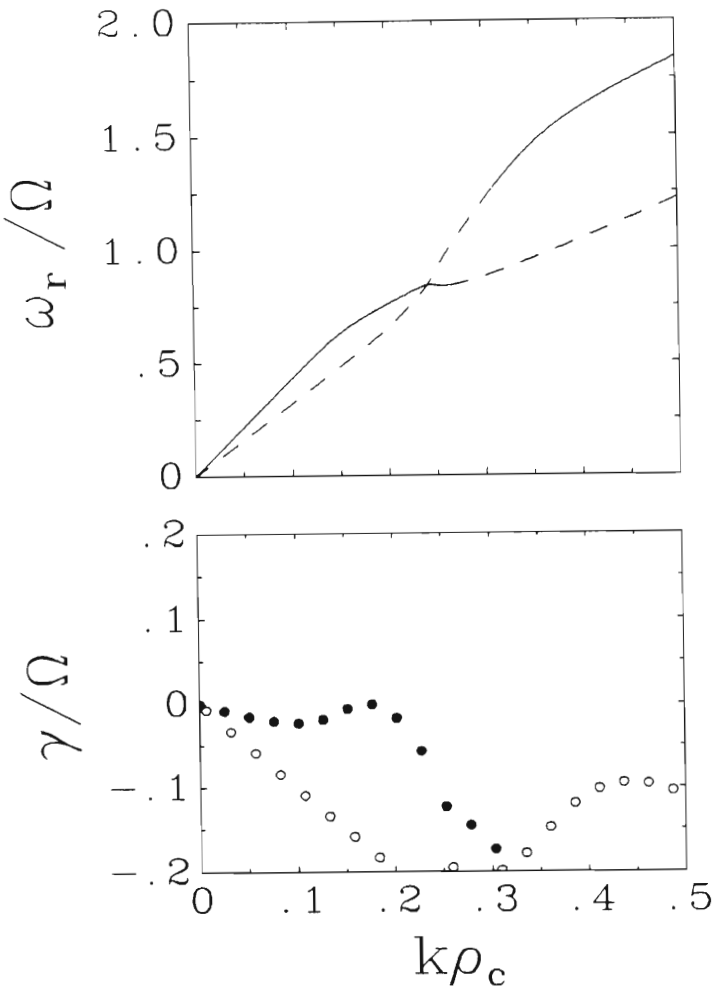

Figure 4.22: The dispersion and growth rate of the weakly-magnetized modified electron-acoustic instability for $\theta = 30°$. Other parameters are as in figure 4.20. Solid circles correspond to the growth rate of the modified electron-acoustic instability.

small wavenumbers was also observed by Schriver & Ashour-Abdalla (1987). They called this instability the beam-resonant instability.

Figure 4.23 illustrates the threshold of the magnetized modified electron-acoustic instability as a function of θ for two values of the ratio Ω/ω_c. The shape of the curves are qualitatively similar to those found in the electron driven case (figure 4.15). For the strongly magnetized ($\Omega/\omega_c > 1$) curve, the threshold drift speed slowly increases with angle of propagation from a starting (parallel propagation) value of $v_{0ib} \sim 4.1 v_c$. In the case of weak magnetization ($\Omega/\omega_c < 1$), we observe two instabilities: an ion beam-resonant instability (Schriver & Ashour-Abdalla 1987) which has lower threshold as $\theta \rightarrow 0$, and a weakly-magnetized modified electron-acoustic instability with larger threshold as $\theta \rightarrow 0$.

The weakly-magnetized modified electron-acoustic instability, has an upper frequency of $\sim \Omega \cos\theta$ (figure 4.22) as does the hot electron-driven electron-acoustic instability. We note also that in the regime $\Omega/\omega_c < 1$, the modified electron-acoustic instability has smallest threshold at intermediate angles θ, only, as does the hot electron-driven electron-acoustic instability.

The maximum growth rate curves (not shown) are qualitatively similar to those of the electron-acoustic instability, but there is a critical velocity above which the modified electron-acoustic instability switches to a beam-resonant instability (Schriver & Ashour-Abdalla, 1987).

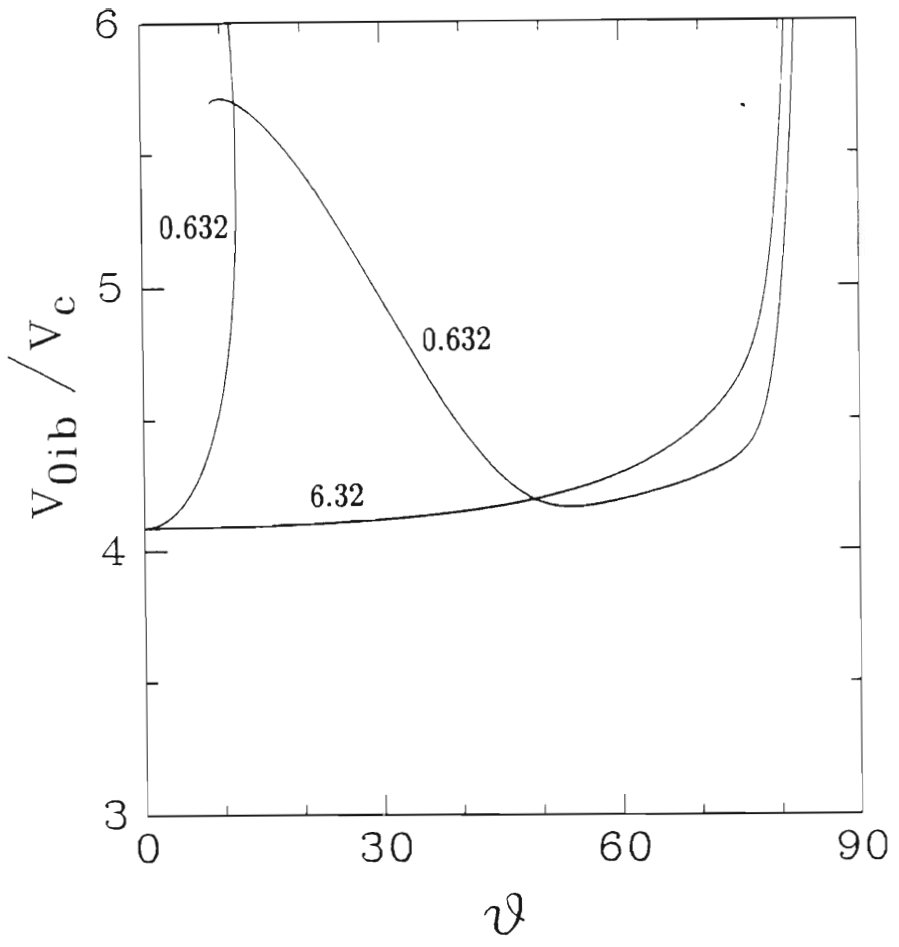

Figure 4.23: The threshold ion drift speed for the magnetized modified electron-acoustic instability as a function of θ. The parameter labelling the curves is Ω/ω_c.

Chapter 5

Conclusion

5.1 Summary

In part I of the thesis we dealt with aspects of the linear theory of the electron-acoustic wave and instability. Chapter 2 was introductory. Chapter 3 dealt with existence criteria for weakly-damped electron-acoustic and Langmuir waves, and chapter 4 was an investigation of the magnetized electron-acoustic instability driven by a relative hot–cool electron drift. The most salient features of the investigation are summarised in the following.

In an extension of the work of Dell, Gledhill & Hellberg (1987) we showed, in chapter 3, that the electron-acoustic wave is distinct from the electron plasma or Langmuir wave. However, for parameters near their critical values, i.e. parameter values at which the dielectric function has saddle points at zero height in its imaginary surface, the dispersion relation of the electron-acoustic wave behaves more like that of an electron plasma wave whose dynamics are based on the cool electron component. It is for this reason that Dell *et al.* (1987) originally identified this wave as a plasma wave with frequency below the electron plasma frequency.

The critical curves also furnish the minimum hot electron density for the occurrence of the electron-acoustic wave. This minimum density of $n_{0h}/n_{0e} \simeq 0.2$ agrees well with that found by independent methods (Gary & Tokar 1985). Furthermore, it was demonstrated, explicitly, that the electron-acoustic wave is only weakly Landau-damped at small wavenumbers for values of the hot electron density n_{0h}/n_{0e} very near to unity, and for large values of the temperature ratio $T_h/T_c > 10$. This too, agrees well with earlier works (Watanabe & Taniuti 1977; Gary & Tokar 1985). In a more

abstract sense the temperature ratio $T_h/T_c = 10$ represents the approximate weak damping criterion for the saddle point introduced by the weighted addition of the Z'–functions in the dispersion relation. In fact this saddle point was shown to play a decisive role in the interplay between the electron plasma and electron-acoustic waves.

The electron-acoustic instability in a magnetized plasma was investigated in chapter 4. This work builds on previous works on the instability. We extend the parameter regime considered by Tokar & Gary (1984) as well as consider the effects of varying the magnetic to plasma pressure ratio. Whereas Gary (1987) considered only parallel wave propagation, we have considered a much wider range of propagation angles which could prove useful in the understanding of BEN in the auroral regions. In contrast to cusp hiss, which is predominantly field-aligned, auroral BEN is fairly isotropic (Dubouloz *et al.* 1991a) and requires a more general instability analysis.

In this chapter it was found that the ratio of the electron-gyrofrequency to cool electron plasma frequency was critical in determining dispersion and damping characteristics of the electron-acoustic wave. Furthermore a cyclotron-sound type instability, which is closely related to the electron-acoustic instability, was identified. At small wave propagation angles relative to the magnetic field, the cyclotron-sound instability is found to have the larger growth rate, but becomes increasingly difficult to destabilize by the field-aligned free energy of the hot electron beam at progressively more oblique angles. At larger propagation angles the electron-acoustic instability exhibits the lower threshold and larger growth rate provided the beam speed is not too large.

At very large values of the electron-gyrofrequency to cool electron plasma frequency ratio it was demonstrated that the cyclotron sound branch is strongly damped and that the electron-acoustic instability is prevalent.

Finally, the similarities between the electron driven and ion driven instabilities were pointed out.

5.2 Suggestions for further work

As far as the saddle point method of chapter 3 is concerned further work might involve the inclusion of the effects of particle drifts and/or the effects of magnetization on higher order electron mode behaviour. Particle drifts have been investigated from the point of view of the saddle point method

by Gledhill (1982), for ion-acoustic waves in a multi-ion-beam plasma. It appears, however, that no such work has been performed for waves in a multi-electron beam plasma.

A further refinement of the saddle point method would be the introduction of a magnetic field. Neither Gledhill (1982) nor Dell (1984) considered this scenario. The problem, however, becomes substantially more involved when a magnetic field is introduced because it greatly increases the number of wave modes. Nevertheless such an investigation may render some interesting results.

In the consideration of the magnetized electron-acoustic instability we have neglected to take into account inhomogeneities. In the polar cusp plasma one would expect some variation of the plasma parameters and magnetic field from place to place. Effects such as density and magnetic field gradients should be investigated for a better undestanding of the electron-acoustic instability in the polar cusp. In fact, bursts of BEN have been shown to be correlated with gradients in the cool electron density (Dubouloz *et al.* 1991a, 1991b).

We have neglected to take into account possible electromagnetic effects. These effects would become especially important when the plasma particle pressure is of the order of the magnetic field pressure, or put another way $\omega_c \sim \Omega_e$. In this frequency regime, were one to include an oscillating magnetic field component one may find intermediate frequency Alfvén and magnetosonic waves that arise due to the inertia of the cooler electron component rather than that of the ion component. This would presumably lead to the identification of new magnetosonic waves.

There still remains a lot of scope for work on the linear electron-acoustic wave/instability itself, especially on the experimental side. As indicated in the introduction (chapter 1) the body of work devoted to the electron-acoustic wave is by far smaller than that afforded to the ion-acoustic wave. Moreover, it appears that very little, if any, experimental work on the electron-acoustic wave has been undertaken in the laboratory.

Whereas it can be said fairly conclusively (Tokar & Gary 1984; Gary 1985; Lin *et al.* 1985; Roth & Hudson 1986; Lin *et al.* 1987; Gary 1987; Pottelette *et al.* 1988, 1990; Dubouloz *et al.* 1991a, 1991b) that electron-acoustic waves occur in the terrestrial polar regions it remains to be conclusively shown that they occur upstream of the earth's bow shock (Thomsen *et al.* 1983; Marsch 1985). This will require further detailed analyses of electron distributions in that region, as well as wave instability analyses modelled on such distributions.

Part II

Nonlinear theory

... the success of any physical investigation depends on the judicious selection of what is to be observed as of primary importance, combined with a voluntary abstraction of the mind from those features which, however attractive they appear, we are not yet sufficiently advanced in science to investigate with profit. (The Scientific Works of James Clerk Maxwell, Vol. II, p. 217)

Chapter 6

Introduction to part II

In the following chapters we shall be concerned primarily with electron-acoustic solitons. These arise, however, as special case solutions of more general nonlinear evolutionary equations of the type first derived by Korteweg & de Vries (1895) in a study of long wavelength water waves in a shallow canal, which often bear their names. For this reason we begin this introduction by way of a discussion of nonlinear dispersive waves in general.

6.1 Nonlinear dispersive waves and solitons

When waves propagate in a medium which is both nonlinear and dispersive they may exhibit some truly remarkable phenomena.

Nonlinearity, or the dependence of the wave packet on its amplitude, as a rule, coordinates the phases and frequencies of the Fourier components of which the wave packet consists. It also leads to the generation of higher wavenumber harmonics, which if unchecked, ultimately bring about the collapse or 'breaking' of the waveform.

Dispersion, or the dependence of the phase velocity of a wave on the wavenumber, results in the shearing of a wave packet caused by phase mixing of the spatial Fourier components with time.

Dispersion causes each new harmonic generated by nonlinearity to travel at a different speed. By this process of phase mixing it can suppress the infinite steepening of an initial wave disturbance, which might otherwise result in a nonlinear, dispersionless medium. On some wave mode branches nonlinearity and dispersion may achieve a delicate balance resulting in wave profiles that propagate unchanged with time over great distances. One such

disturbance in which this fine balance is attained is the solitary-wave or soliton. One might suppose that if the balance is so critical then such entities would be very rare. On the contrary, the detailed balance gives rise to stability. Thus any finite disturbance in a nonlinear, dispersive medium generally leads, in the time asymptotic limit, to an ordered sequence of solitons.

The discovery of the soliton is generally attributed to J. Scott Russell who in 1834 observed such a 'great wave of translation' on the Edinburgh–Glasgow canal (Drazin & Johnson 1989).

Solitons are ubiquitous in nature. They may be subclassified in many ways and into many different types, but a rather important fundamental subclassification is the distinction between topological and nontopological solitons—those that do or do not, respectively, change the state of a system by their passage. A domain wall in a ferromagnet is an example of a topological solitary wave: its passage reverses the direction of magnetization. Russell's water-wave soliton is nontopological: its passage leaves the water behind the 'hump' as before. Recent years have seen the recognition of more and more examples of solitons in physical systems and here we do no more than provide a partial list.

Nontopological solitons include water-wave solitons (Korteweg & de Vries 1895) of several types, ion-acoustic wave solitons (Washimi & Taniuti 1966), nonlinear optics solitons, optical fiber solitons, biomolecular polaron solitons, high-intensity shock solitons and nerve conduction solitons.

Topological solitons include kinks in charge-density waves, some dislocations, epitaxial disclinations, charge localization in low-dimensional conductors, 'bags' and 'lumps' in quantum gauge fields, domain walls in ferroelectrics and in ferro- and antiferromagnets, critical droplets and nucleation, instantons, 'boojums' in superfluids, large scale structures in cosmology and ion-acoustic double layers (Torvén 1981) amongst others.

In plasma physics the distinction between topological and nontopological solitons is hardly ever recognised. Indeed, the definition of a soliton is somewhat narrower than was implied in the above. Generally, in plasma physics a soliton is regarded as a symmetric single peak perturbation of the potential, density, etc. A double layer, which is an abrupt change in the plasma properties over a relatively short length scale, is regarded as a seperate, quite distinct entity. However, the topological nature of the latter is fully exploited within the realms of space and cosmic plasma physics, where it is often invoked to explain the acceleration of charged particles (see the review by Raadu (1989)).

Within the broader definition, the electron-acoustic soliton falls into the nontopological category. The electron-acoustic soliton is an electrostatic phenomenon, which in its most simple aspect consists of a 'slab' of negative space-charge adjacent on either side to slabs of positive space-charge. The surrounding plasma asymptotically approaches the same equilibrium state in either direction, and is charge neutral. This charge density profile is associated, in a self consistent way, with a dip in the plasma potential whose width is of the order of several hot electron Debye lengths and whose depth is $\sim -T_h/e$. The deviation from quasineutrality is caused entirely by variations in the electron fluid densities: the cool ions are massive and slow to respond on electron-acoustic wave time scales. At the soliton centre the cool electrons experience a sharp local increase in number density, whereas the hot electron density undergoes a somewhat slower decrease. The discussion of the electron-acoustic soliton shall be taken up in more detail in chapters 7–9.

Electron-acoustic and ion-acoustic solitons are not the only types of soliton that may occur in a plasma. In fact, much of the interest in plasmas has to do with the multitude of wave types that they can support. Further examples of solitons in plasmas include solitary electrostatic ion cyclotron waves (Yu 1977), Langmuir solitons which take the form of an amplitude modulation of the Langmuir wave (Zakharov 1972), whistler wave solitons governed by a nonlinear Schrödinger equation (Mann 1986) and of course the solitons corresponding to the magnetosonic (Ogino & Takeda 1975) and Alfvén waves (Spangler *et al.* 1982). The latter three examples are electromagnetic phenomena, demonstating that plasma solitons are not necessarily electrostatic in character.

Within the broader definition of a soliton one might also include in this list the various solitary vortices that can occur in plasmas with inhomogeneities (Hasegawa & Mima 1978; Spatschek *et al.* 1990 [and references cited therein]). Furthermore, Bharuthram & Shukla (1988) have investigated monopolar and dipolar vortices based on the modified electron-acoustic wave also.

6.2 Theoretical developments

The idea of Korteweg and de Vries, that the dynamical equations of a physical system may be reduced to a simpler wave equation embodying the essential physics of the phenomenon, has shown, through recurrence of such

equations, that there must be deeply shared concepts underlying many and varied nonlinear phenomena. A much used method of obtaining such evolutionary equations, today, is the so-called reductive perturbation technique of Washimi & Taniuti (1966), which is based on the pioneering work of Gardner & Morikawa (1965).

In this technique one introduces slow time and length scales suggested by the problem at hand, which are usually functions of (say) ϵ—a small parameter. In addition, the wave amplitude is assumed to deviate from its equilibrium state, by at most $O(\epsilon)$ to lowest order. This sets the nonlinearity, and dissipation or dispersion, on an equal footing so that these competing effects may attain a balance. Completing the expansion of the wave amplitude to the desired order in ϵ yields a system of equations, which upon order by order solution, yield the governing evolutionary equation. Such techniques, are not new, however, and can be traced back to antiquity. They (and other techniques) have led to the recognition of a wide variety of one- and multi-dimensional nonlinear wave equations such as nonlinear Schrödinger equations, KdV equations (Washimi & Taniuti 1966), modified KdV equations with both cubic and quadratic nonlinearities (Torvén 1981), Boussinesq equations (Rao, Shukla & Yu 1990) and Benjamin-Bona-Mahoney equations (Broer & Sluijter 1977) to name a few.

The broad class of problems that can be reduced to the solution of such nonlinear evolutionary equations has had a decisive influence on the development of nonlinear wave theory. Elegant analytical techniques have been developed for the solution of the Korteweg–de Vries and other exactly integrable equations. One such much celebrated technique is the method of the inverse scattering transform (Gardner *et al.* 1967). Further developments and methods of solution of the KdV equation as initial-value problem can be found in the work of Drazin & Johnson (1989).

Another common way of approaching the problem of nonlinear waves, especially in plasmas, (Sagdeev 1966; Bharuthram & Shukla 1986; Baboolal, Bharuthram & Hellberg 1988; Baboolal, Bharuthram & Hellberg 1989), is to reduce the problem to the solution of the energy equation for a 'particle' in a potential well. Although, on the one hand, the more general temporal dependence of the evolutionary equation is lost, on the other one gains the advantage of retaining the full nonlinearity of the problem.

In this technique the wave profile is assumed to be time-stationary in some inertial frame of reference. This results in considerable analytical simplification of the dynamical equations, facilitating their reduction to a single equation, which by analogy with classical mechanics, can be thought of

as describing a particle in a potential well. Integration of this equation with suitable 'initial conditions' yields a plethora of simple wave types including cnoidal, soliton and double layer solutions (Lee & Kan 1981; Song, Lee & Huang 1988; Baboolal, Bharuthram & Hellberg 1988; Baboolal, Bharuthram & Hellberg 1989).

6.3 A brief review of nonlinear electron-acoustic waves

Nonlinear ion-acoustic waves and solitons have received much attention in the literature (see Pécseli 1985 and references cited therein). By comparison, the nonlinear electron-acoustic wave has been the subject of relatively few investigations.

In this section we trace the theoretical development of the nonlinear electron-acoustic wave in all its incarnations. In so doing we review the work undertaken on the nonlinear electron-acoustic wave, as well as introduce and compare the various plasma models for nonlinear electron-acoustic waves. As may be expected, many of the models have been met before in part I, and in this section there will necessarily be some overlap with the introduction to that part. However, we have striven to keep such duplication to a minimum. Where material is of a highly specific or technical nature it has been cited in context within the main text. From the point of view of the preceding remarks this section does not represent a comprehensive, up-to-date literature survey.

It appears that Pokroev & Stepanov (1973) first considered the nonlinear evolution of the electron-acoustic wave. Employing a magnetized plasma model similar to that used originally by Sizonenko & Stepanov (1967), Aref'ev (1970) and Lashmore-Davies & Martin (1973), they derived a Boussinesq equation that admits electron-acoustic soliton solutions for quasi-perpendicular propagation directions $\cos\theta \ll (m_e/m_i)^{1/2}$. Some years later Buti, Mohan & Shukla (1980) investigated the same physical situation from the point of view of a pseudo-potential theory incorporating the full nonlinearity of the initial dynamical system at the expense of the Poisson equation. The latter was discarded in favour of the analytical simplification brought about by the assumption of quasineutrality.

Mohan & Buti (1980) derived an evolutionary equation for electron-acoustic waves in the presence of an electron current. By consideration of electron inertia effects they showed that the nonlinear electron acoustic wave

was governed by a 'perturbed' KdV equation which contained an integral damping/growth term. Using the method of inverse scattering it was shown that damping/growth of the wave amplitude led to the formation of a 'tail' behind the soliton. The rate of damping/growth was shown to be strongly dependent on the angle of propagation of the soliton with respect to the background magnetic field.

The works of Pokroev & Stepanov (1973) and Buti, Mohan & Shukla (1980) were generalised by Buti (1980) to include a second hot isothermal ion component. It was found that in such a plasma configuration, in addition to solitons, which correspond to density 'humps', there may also arise supersonic holes (density depressions).

The inclusion of a second electron component was investigated by Yu & Shukla (1983). They showed that if the electrons were non-isothermal, i.e. they comprised two separately isothermal components, then electron acoustic solitons could occur without the necessary introduction of a magnetic field. They called this kind of wave the modified electron-acoustic wave, and the associated soliton, the modified electron-acoustic soliton. The theory of the modified electron-acoustic soliton was generalised by Guha & Dwivedi (1984) to include the effects of a second ion component.

Kinetically modelled electron-acoustic solitons and double layers based on the slow electron-acoustic wave (Stix 1962, Schamel 1979), were investigated by Kim (1983). The electron and ion distribution functions were prescribed *a priori*, from which the Sagdeev or pseudo-potential was constructed. By expanding the Sagdeev potential in the small-amplitude regime, $|\phi| \ll 1$, it was shown that the equations admit solitary wave and double layer solutions.

Double layers based on an Aref'ev (1970) model were constructed using a magnetized fluid theory in which the Poisson equation was replaced by the charge quasi-neutrality condition (Goswami, Kalita & Bujarbarua 1986). Rarefactive and compressive double layers were found when the electrons were isothermal (Boltzmann distribution) and non-isothermal (included a reflected component), respectively.

The effects of higher-order nonlinear terms on electron-acoustic soliton propagation was investigated by Sarma, Kalita & Bujarbarua (1986). They derived a modified KdV equation for the first order potential contribution, and a linear homogeneous equation for the second order potential. The plasma was based on an Aref'ev (1970) model but differed in that the electrons had a drift relative to the ions. Both amplitude and width modifications due to higher order effects on linearly damped and linearly growing

solitons were established by employing the method of renormalisation advanced by Kodama & Taniuti (1978).

The nonlinear excitation of electron-acoustic waves by an electromagnetic pump has also been the subject of a few investigations. Sharma, Ramamurthy & Yu (1984) showed that in a plasma in which the ions are much hotter than the electrons an ordinary or O-mode pump can decay into an upper-hybrid and an electron-acoustic wave. They further pointed out that the excitation threshold of the latter is quite low. In a similar investigation Saleem & Murtaza (1986) demonstrated that an extraordinary electromagnetic pump wave can parametrically decay into an upper-hybrid and an electron-acoustic wave. They obtained the threshold power flux and growth rate of the instability.

Goswami & Bujarbarua (1987) studied weak modified electron-acoustic double layers (MEADLs) in a plasma comprising a hot ion, and two separately isothermal electron components. They find that provided the hot electron distribution function contains free and reflected components, MEADLs can occur. However, if the hot electrons are isothermal (Boltzmann distribution) then no self consistent double layer solutions can be found.

Relativistic solitons have also received passing attention in the literature. Chowdhury, Pakira & Paul (1988) investigated relativistic solitons in what they term an electron-acoustic plasma of fluid ions and warm kinetically determined electrons. In particular they investigate damping effects for comparison with earlier works (Ott & Sudan 1969). It was found that electron Landau damping was increased when relativistic effects were taken into account, because the electron component was able to absorb more mass-energy.

More exotic nonlinear structures based on the modified electron-acoustic wave have been investigated recently. With the inclusion of a magnetic field Bharuthram & Shukla (1988) obtained monopole and dipole solitary vortex solutions for a plasma in which the cool electrons were governed by a fluid guiding centre model, and the densities of the hot electrons and ions were given by the Boltzmann distribution. In addition they investigated spectrum cascading by mode-coupling in the modified electron-acoustic wave turbulence. Such spectral cascade processes were also the subject of an earlier work by Rahman & Shukla (1982)

Dey, Goswami & Bujarbarua (1988) studied modified electron-acoustic double layers and solitons in a four-component plasma consisting of two hot ion components and two, respectively, hot and cool electron components. It was found that if the hot electron component was non-isothermal, i.e.

contained trapped electrons, then in addition to permitting the usual rarefactive modified electron-acoustic soliton solution, the equations also admit compressive soliton and double layer solutions.

Ironically, the more tenable cool ion model of the electron-acoustic wave originally proposed by Watanabe & Taniuti (1977) has received very little attention insofar as nonlinear waves are concerned, even though it was remarked by Watanabe & Taniuti (1977) in their letter that solitary waves might well occur. This initial indifference to the electron-acoustic wave may have been due to a lack of physical applicability of the theory. Since then, however, satellite observations in the dayside polar region have demonstrated that plasmas with hot and cool electron components do occur in the presence of relatively cool ions. The observation of strong electrostatic fluctuations between the ion plasma and electron gyrofrequencies in this region has aroused even further interest in the electron-acoustic wave as proposed by Watanabe & Taniuti (1977).

At the risk of repetition of the introduction to part I, we cite here only a few of the main works supporting the hypothesis of the occurrence of nonlinear electron-acoustic waves in the terrestrial polar region.

The existence of two electron populations of widely disparate temperature, together with intense electrostatic fluctuations below the electron gyrofrequency, in this region, was reported by Lin, Burch, Shawhan & Gurnett (1984) based on data gathered by the *Dynamics Explorer-1* (*DE-1*) satellite. These large amplitude electrostatic fluctuations, which constitute a substantial portion of the so-called cusp auroral hiss, are now widely believed to be of electron-acoustic origin (Tokar & Gary 1984; Lin, Winske & Tokar 1985; Roth & Hudson 1986; Lin & Winske 1987; Gary 1987). Furthermore, recent studies of *Viking* satellite data (Pottelette *et al.* 1988, 1990; Dubouloz *et al* 1991) collected in the dayside polar region at altitudes between 2000 and 10000 km, have added further evidence to suggest that electron-acoustic waves occur in the dayside polar regions. Moreover, the significance of nonlinear effects has been demonstrated (Dubouloz *et al.* 1990). In fact, electron-acoustic solitons passing by the spacecraft have been suggested as possible explanation for the high-frequency part of BEN (Dubouloz *et al.* 1991).

Particle simulations of the electron-acoustic wave in the polar cusp have been undertaken by Lin, Winske & Tokar (1985), Roth & Hudson (1986) and Lin & Winske (1987). The first set of authors observe that at saturation of the electron-acoustic instability the cool electrons exhibit a vortex trapping pattern in phase space implying strongly nonlinear behaviour. The last set

of authors investigated finite beam-dimension effects. A common theme of all the above investigations, however, is the large saturation amplitudes of the electron-acoustic turbulence, conceivably indicating that nonlinear effects become important.

6.4 Outline of part II

The principal concern of part II of this thesis is to investigate the nonlinear electron-acoustic wave in a plasma model based on the plasma constituents found in the terrestrial polar cusp. Of course the models used are often oversimplifications, but this has the advantage of exposing the underlying physics of the phenomena.

In chapter 7 the nonlinear electron-acoustic wave in an unmagnetized plasma is investigated. The work represents an extension to finite wave amplitude, of the linear theory of Gary & Tokar (1985). Both small-amplitude nonlinear waves and arbitrary-amplitude solitons are investigated for a wide range of plasma parameters. For small-amplitude electron-acoustic waves we derive KdV and Kadomtsev–Petviashvili (KP) equations which admit electron-acoustic solitons corresponding to negative potentials. At larger amplitude a pseudo-potential theory based on earlier work by Baboolal, Bharuthram & Hellberg (1989) for ion-acoustic solitons, is presented for electron-acoustic solitons. The soliton solutions predicted by this large amplitude theory reduce to the soliton and planar soliton solutions of the KdV and KP equations, respectively, at small amplitude. At larger amplitudes significant differences in the soliton widths and amplitudes as predicted by each theory, arise. A large part of chapter 7 has been published in an article in *Journal of Plasma Physics.*

Chapter 8 deals with the effects of a strong magnetic field on weakly-nonlinear electron-acoustic waves. Two different fluid models for the ion component are considered: (i) strongly magnetized ions; and (ii) unmagnetized incompressible ions. These two models render quite different results for electron-acoustic soliton propagation, and are compared in detail. Their relative merits and general applicability are also discussed. Furthermore, multi-dimensional electron-acoustic solitons are briefly considered.

In chapter 9 the stationary plasma results of chapter 7 are generalised to allow for nonzero relativistic fluid drifts. In addition to pursuing the more common small-amplitude approach (cf. Nejoh 1987a), a relativistic pseudo-potential theory, which takes into consideration finite fluid temperatures is

presented in full generality. This work too, is to appear in an article in *Journal of Plasma Physics.*

In chapter 10 we investigate the possible existence of electron-acoustic double layers. Both small- and arbitrary-amplitude theories are employed, each yielding contradictory predictions when double layer solutions are assumed. The implications of this for the present and past works on electron-acoustic double layers are discussed.

Finally, we conclude this part with a summary and suggestions for further work.

The analytical details of many of the more tedious derivations are provided in the appendices.

Chapter 7

Nonlinear electron-acoustic waves in an unmagnetized plasma

In this chapter the nonlinear evolution of the electron-acoustic wave in its most simple aspect is investigated employing a fluid model for the plasma components. The work presented here represents a nonlinear extension of the theory of the electron-acoustic wave put forward by Gary & Tokar (1985).

7.1 Model and basic equations

An infinite, one-dimensional, collisionless, homogeneous, unmagnetized fluid plasma consisting of a number of cool fluid components and a single hot Boltzmann electron component

$$n_h = n_{0h} \exp \phi, \tag{7.1}$$

is considered. The validity of the assumption of a Boltzmann component of electrons is subject to the conditions that on the one hand the velocity of a wave-packet be significantly less than the hot electron thermal speed, and on the other hand, that the electron inertia be negligible. The speed of transmission of thermal information of the hot electron component is then far greater than the speed of the waveform or wave-packet and therefore this component may be treated as isothermal. The approximation that the hot

electrons be inertialess may be realised in the case of the electron-acoustic wave, because of the enhanced mobility of the hot electrons over the fluid components, afforded to them via their large thermal velocity. In contrast, the fluid components are assumed to be cool or massive with thermal speeds significantly less than the speed of the waveform and therefore their response is adiabatic.

When the above assumptions are met the system of normalized equations governing the dynamics of the plasma are (cf. (B.6)–(B.8)):

$$\frac{\partial n_j}{\partial t} + \frac{\partial}{\partial x}(n_j u_j) = 0, \tag{7.2}$$

$$n_j m_j \left(\frac{\partial u_j}{\partial t} + u_j \frac{\partial u_j}{\partial x} \right) = -\frac{\partial p_j}{\partial x} - Z_j n_j \frac{\partial \phi}{\partial x}, \tag{7.3}$$

$$\frac{\partial p_j}{\partial t} + u_j \frac{\partial p_j}{\partial x} + 3 p_j \frac{\partial u_j}{\partial x} = 0, \tag{7.4}$$

$$\frac{\partial^2 \phi}{\partial x^2} = n_h - \sum_j Z_j n_j, \tag{7.5}$$

where the subscript j refers to the jth fluid component and the subscript h refers to the hot electrons. In the equilibrium state the plasma is assumed stationary and charge-neutral. At large distances from any disturbances we demand that these equilibrium conditions apply, i.e. we impose the following boundary conditions:

$$\left.\begin{array}{rrr} \phi \to 0, & \dfrac{\partial \phi}{\partial x} \to 0, & \dfrac{\partial^2 \phi}{\partial x^2} \to 0 \\ n_j \to n_{0j}, & p_j \to p_{0j} & u_j \to 0 \end{array}\right\} \quad \text{as} \quad |x| \to \infty. \tag{7.6}$$

These boundary conditions ensure that the solutions of the system (7.1)–(7.5) are localised in space, i.e. they prohibit infinite wavetrain-like solutions. Although such wave train solutions of (7.1)–(7.5) exist under more general conditions they shall be of no concern to us here.

In (7.1)–(7.6) spatial lengths have been normalized by the Debye length $(T_h/4\pi n_{0e}e^2)^{1/2}$, time by $\omega_{pe}^{-1} = (m_e/4\pi n_{0e}e^2)^{1/2}$, densities by the total electron density n_{0e}, pressures by $n_{0e}T_h$, temperatures by T_h, electrostatic potential by T_h/e, velocities by the hot-electron thermal speed $v_h = (T_h/m_e)^{1/2}$, which is closely related to the (characteristic) electron sound speed, $v_{se} = (n_{0c}/n_{0h})^{1/2} v_h$ (Gary & Tokar 1985), masses by m_e; and $Z_j \equiv q_j/e$.

7.2 Small-amplitude electron-acoustic waves

Assuming weak nonlinearity, i.e. assuming that the magnitude of the electrostatic potential is small $|\phi| < 1$, and that the perturbations in the densities, velocities and pressures are all small when compared to unity, one may employ asymptotic (reductive perturbation) techniques based on that of Washimi & Taniuti (1966) to derive from (7.1)–(7.5) evolutionary equations describing weakly-nonlinear electron-acoustic waves.

7.2.1 The 1-D Korteweg–de Vries equation

The derivation is similar to that of Verheest (1988) for ion-acoustic waves and only the salient steps are indicated here; the details of the derivation may be found in appendix D.

Consider a wave-packet propagating along the x–axis. The wavenumbers of the harmonics that constitute the wave-packet are small and satisfy $k\lambda_{Dh} \ll 1$. Then the approximate dispersion relation of the system can be written in the form (cf. equation (2.10))

$$\omega(k) \simeq kv_{se} - \tfrac{1}{2}k^3\lambda_{Dh}^2 v_{se}.$$

Consideration of the phase argument $kx - \omega(k)t$ then yields

$$kx - \omega t = k\lambda_{Dh}\frac{x - v_{se}t}{\lambda_{Dh}} + \tfrac{1}{2}(k\lambda_{Dh})^3\frac{v_{se}}{\lambda_{Dh}}t,$$

which implies the following relative spatial and temporal coordinate dependence

$$\xi = \epsilon^{1/2}(x - Vt), \qquad \tau = \epsilon^{3/2}t. \tag{7.7}$$

The parameter ϵ is a measure of the wave dispersion, which is considered small $\epsilon \ll 1$. The stretchings (7.7), similar to those used by Washimi & Taniuti (1966) in their study of ion-acoustic waves, are based on a Gardner–Morikawa type transformation (Gardner *et al.* 1965; Taniuti 1974; Taniuti & Nishihara 1983).

The densities, velocities, partial pressures and electrostatic potential may all be expanded in terms of some variable related to their amplitude. By choosing the expansion variable to be ϵ we imply a relation between the nonlinearity and dispersion of the wave-packet, effectively tying these two opposing effects so that a balance is attained. We employ the following

expansions of these macroscopic quantities:

$$\left.\begin{aligned} n_j &= n_j^{(0)} + \epsilon n_j^{(1)} + \epsilon^2 n_j^{(2)} + \cdots, \\ u_j &= \epsilon u_j^{(1)} + \epsilon^2 u_j^{(2)} + \cdots, \\ p_j &= p_j^{(0)} + \epsilon p_j^{(1)} + \epsilon^2 p_j^{(2)} + \cdots, \\ \phi &= \epsilon\phi^{(1)} + \epsilon^2\phi^{(2)} + \cdots, \end{aligned}\right\} \tag{7.8}$$

where $n_j^{(0)} \equiv n_{0j}$, $p_j^{(0)} = n_{0j}T_j$, and j refers to the jth fluid component. Note that the deviations of the macroscopic quantities from their equilibrium values are in all cases at most $O(\epsilon)$ and therefore (7.8) satisfies our initial assumptions.

Substituting (7.7) and (7.8) into the the system (7.1)–(7.5) yields an hierarchy of equations in orders of ϵ which may be combined (see appendix D) to yield the Korteweg–de Vries (KdV) equation for the first-order contribution to the electrostatic potential $\phi^{(1)}$:

$$\frac{\partial\phi^{(1)}}{\partial\tau} + a\phi^{(1)}\frac{\partial\phi^{(1)}}{\partial\xi} + b\frac{\partial^3\phi^{(1)}}{\partial\xi^3} = 0. \tag{7.9}$$

The coefficients of the nonlinear and dispersive terms a, b, respectively, are defined as follows:

$$a = \frac{B}{A}; \qquad b = \frac{1}{A}, \tag{7.10}$$

where

$$A = 2\sum_j \frac{Z_j^2}{m_j}\frac{n_j^{(0)}V}{(V^2 - 3\sigma_j)^2} \tag{7.11}$$

$$B = 3\sum_j \frac{Z_j^3}{m_j^2}\frac{n_j^{(0)}(V^2 + \sigma_j)}{(V^2 - 3\sigma_j)^3} - n_{0h}, \tag{7.12}$$

$\sigma_j = T_j/m_j$, and the electron sound speed in the weakly-dispersive limit, V, satisfies the $O(\epsilon)$ "dispersion relation"

$$n_{0h} - \sum_j \frac{Z_j^2 n_j^{(0)}/m_j}{V^2 - 3\sigma_j} = 0. \tag{7.13}$$

The KdV equation (7.9) describes the spatial and temporal evolution of nonlinear, long-wavelength electron-acoustic waves of small amplitude. The

second term of the KdV equation leads to steepening of the leading edge of an initial disturbance by the generation of higher wavenumber harmonics, and the third term governs the dispersion of the wave-packet. These terms, by our initial assumptions, are of the same order of magnitude so that one effect does not dominate over the other. It is noteworthy (see appendix D) that all the other quantities $n_j^{(1)}$, $u_j^{(1)}$, and $p_j^{(1)}$ obey similar KdV equations, the only differences being in the definitions of the coefficients a, b, in each case.

The coefficients a and b are amenable to some simplification if we assume that there is a large disparity in the masses of the ions and electrons, as is usually the case. In this context, $m_i \gg 1$, and terms $O(m_i^{-1})$ in (7.10)–(7.12) can, to a very good approximation, be neglected. This approximation, is validated by our arbitrary-amplitude calculations (see later) and is essentially equivalent to the assumption of a constant ion density (incompressible flow). Under this approximation (7.13) furnishes the following expression for the electron sound speed,

$$V \simeq \left(\frac{n_{0c}}{n_{0h}} + 3T_c \right)^{1/2}. \tag{7.14}$$

Subtitution of (7.14) into (7.10)–(7.12) in the context of the above yields

$$a \simeq -\frac{(n_{0c}/n_{0h})^2 + 3(n_{0c}/n_{0h} + 4T_c)}{2(n_{0c}/n_{0h})(n_{0c}/n_{0h} + 3T_c)^{1/2}}, \tag{7.15}$$

$$b \simeq \frac{(n_{0c}/n_{0h})^2}{2n_{0c}(n_{0c}/n_{0h} + 3T_c)^{1/2}}, \tag{7.16}$$

for the coefficients of the KdV equation. Immediately one notices that for nonzero electron densities $a < 0$ and $b > 0$. Moreover, the coefficient of nonlinearity only vanishes for vanishing cool electron density. Therefore, there are no nonzero critical densities for which this nonlinear coefficient vanishes, as may be the case with ion-acoustic waves in multi-component plasmas (Verheest 1988), and hence there is no need for the elaborate coordinate stretchings that must be introduced to describe soliton propagation at such densities.

Stationary solutions of the KdV equation (7.9) may be sought by writing it in terms of the variable

$$\eta = \xi - U\tau. \tag{7.17}$$

Integrating the resultant ordinary differential equation and imposing the boundary conditions (7.6) yields the solitary-wave solution (Tagare 1973),

$$\phi^{(1)} = \frac{3U}{a}\,\mathrm{sech}^2\left[\left(\frac{U}{4b}\right)^{1/2}(\xi - U\tau)\right], \tag{7.18}$$

In terms of the original coordinates this becomes, using (7.7)

$$\phi = \frac{3\delta V}{a}\,\mathrm{sech}^2\left[\left(\frac{\delta V}{4b}\right)^{1/2}\{x - Mt\}\right], \tag{7.19}$$

where $\delta V \equiv \epsilon U$ and the soliton speed, M, is given by $M = V + \delta V$.

We remark here, parenthetically, that equation (7.18) is not the only solitary-wave solution of (7.9). The latter admits rational soliton solutions (Drazin & Johnson 1989), the first in the hierarchy may be obtained by setting $\partial/\partial\tau = 0$. Then integrating twice yields the solution

$$\phi^{(1)} = \frac{12b}{a\xi^2} \quad \text{or} \quad \phi = \frac{12b}{a}[x - Vt]^{-2}.$$

Although this solution satisfies the boundary conditions it is singular at $\xi = 0$ ($x = Vt$), quite apart from the fact that $|\phi^{(1)}| \gg 1$ for $|\xi| \ll 1$. Such singular rational soliton solutions shall not concern us here, however.

At this juncture some remarks about the properties of the solution (7.19) are in order. The latter takes the form of a solitary wave pulse in which the harmonic producing effects of nonlinearity are delicately balanced against the phase mixing of Fourier components caused by wave dispersion. The amplitude of the soliton is proportional to δV and the width

$$L = \left[\frac{4b}{\delta V}\right]^{1/2},$$

is proportional to $\delta V^{-1/2}$ with the soliton speed given by $V + \delta V$. This means that larger amplitude solitons are narrower and travel faster than their smaller counterparts—which is a general characteristic of soliton solutions of the KdV equation. Computer simulations (Zabusky 1967; Zabusky & Kruskal 1965; Zabusky 1968) have shown that solitons of the form (7.19) interact nonlinearly with each other thereafter retaining their individual identities. Thus a localized initial disturbance at $\tau = 0$ that evolves according to the KdV equation usually emerges, for $\tau \to \infty$, as a finite number

of solitons arranged in order of increasing height. It was because of these quasi-particulate properties that the term soliton was coined for such solutions.

Electron-acoustic solitons given by (7.19) in conjunction with (7.15) and (7.16) are supersonic: they all travel at speeds greater than the electron sound speed defined by (7.14)

$$M > V = \left(\frac{n_{0c}}{n_{0h}} + 3T_c \right)^{1/2} . \tag{7.20}$$

This is evident from the solution (7.19) by noting $b > 0$.

Unlike the classical ion-acoustic soliton in a single electron-ion component plasma (Chen 1984), which exhibits a positive potential (compressive soliton), the electron-acoustic soliton has a potential which is negative, i.e. $\phi < 0$. Such solitons are normally termed "rarefactive". On the other hand, in recent years the observation of two separately isothermal electron components in auroral plasmas has led a number of authors (Baboolal, Bharuthram & Hellberg 1989, Das & Tagare 1975) to investigate ion-acoustic solitons in two-electron-temperature plasmas. One then finds that both compressive and rarefactive ion-acoustic solitons can occur, and in addition, that such a plasma supports ion-acoustic double layers (Bharuthram & Shukla 1986).

Unfortunately, the term rarefactive proves something of a misnomer for electron-acoustic solitons because, as will be observed later, the negative potential is accompanied by an overfilling of that region by cool electrons and in this sense the soliton should be regarded as compressive. However, because of its widespread use we shall accept this "abuse" of terminology, and hereafter when we refer to a rarefactive soliton we mean one that has negative potential amplitude.

The modified electron-acoustic soliton also exhibits a negative potential (Yu & Shukla 1983). The model of the modified electron-acoustic wave employed by the latter authors differs from our plasma model in that the ions in their model are treated as Boltzmann-like. This, however, restricts the range of allowable ion to cool electron temperature ratios to values larger than $T_i/T_c > m_i/m_e$ and because of this it finds sparse application in the terrestrial magnetosphere and well-nigh none in the laboratory. Nevertheless, Yu & Shukla (1983) also observe an overfilling of the negative potential by cool electrons.

The dependence of the soliton width and amplitude on such factors as electron density and temperature is contained within the coefficients a and

b. We defer discussion of these effects till later when we consider arbitrary-amplitude solitons.

7.2.2 The Kadomtsev–Petviashvili equation

The assumption of a wave-packet whose harmonic components propagate *exactly* parallel to the x–axis is something of an idealisation which is hardly ever realised in nature. For purposes of completeness, and to account for the interactions of electron-acoustic solitons which propagate obliquely with respect to one another, we derive the two-dimensional generalization of the KdV equation of the previous subsection.

Historically, the Kadomtsev–Petviashvili (KP) equation has been used to prove the stability of planar one dimensional solitons to perturbations in all directions (Infeld, Rowlands & Hen 1978; Kuznetsov, Spector & Fal'kovich 1984; Gabl, Bulson & Lonngren 1984) and, it appears, has never been derived for electron-acoustic waves.

The two dimensional generalization of the basic dynamical equations are employed

$$\left.\begin{aligned}
&\frac{\partial n_j}{\partial t} + \frac{\partial}{\partial x}(n_j u_j) + \frac{\partial}{\partial y}(n_j v_j) = 0, \\
&n_j m_j \left(\frac{\partial u_j}{\partial t} + u_j \frac{\partial u_j}{\partial x} + v_j \frac{\partial u_j}{\partial y} \right) = -\frac{\partial p_j}{\partial x} - Z_j n_j \frac{\partial \phi}{\partial x}, \\
&n_j m_j \left(\frac{\partial v_j}{\partial t} + u_j \frac{\partial v_j}{\partial x} + v_j \frac{\partial v_j}{\partial y} \right) = -\frac{\partial p_j}{\partial y} - Z_j n_j \frac{\partial \phi}{\partial y}, \\
&\frac{\partial p_j}{\partial t} + u_j \frac{\partial p_j}{\partial x} + v_j \frac{\partial p_j}{\partial y} + 3p_j \left(\frac{\partial u_j}{\partial x} + \frac{\partial v_j}{\partial y} \right) = 0, \\
&\frac{\partial^2 \phi}{\partial x^2} + \frac{\partial^2 \phi}{\partial y^2} = n_h - \sum_j Z_j n_j,
\end{aligned}\right\} \tag{7.21}$$

with n_h given by the Boltzmann distribution (7.1). We impose the same boundary conditions as in the 1-D case.

We now consider a wave packet propagating nearly parallel to the x–axis. The wavenumbers of the various harmonics constituting the wave-packet satisfy the somewhat more general conditions than those used in §7.2.1:

$$k\lambda_{Dh} \ll 1; \qquad k_x \gg k_y. \tag{7.22}$$

It is well known (Petviashvili 1986) that nonlinear acoustic waves steepen (by the generation of higher wavenumber harmonics) in the direction of group propagation, and so the second inequality develops naturally with time. This allows the following expansion of the dispersion relation for the system (cf. equation (2.10))

$$\omega \simeq k_x v_{se} - \tfrac{1}{2} k_x^3 v_{se} \lambda_{Dh}^2 + \frac{k_y^2}{2k_x} v_{se},$$

and by consideration of the phase we adopt the following coordinate stretchings:

$$\xi = \epsilon^{1/2}(x - Vt), \qquad \eta = \epsilon y, \qquad \tau = \epsilon^{3/2} t. \tag{7.23}$$

In view of the second inequality in (7.22) the dependence of the macroscopic variables on x will be much stronger than the dependence on y, therefore we employ the following expansions in terms of ϵ:

$$\left.\begin{aligned} n_j &= n_j^{(0)} + \epsilon n_j^{(1)} + \epsilon^2 n_j^{(2)} + \cdots, \\ u_j &= \epsilon u_j^{(1)} + \epsilon^2 u_j^{(2)} + \cdots, \\ v_j &= \epsilon^{3/2} v_j^{(1)} + \epsilon^{5/2} v_j^{(2)} + \cdots, \\ p_j &= p_j^{(0)} + \epsilon p_j^{(1)} + \epsilon^2 p_j^{(2)} + \cdots, \\ \phi &= \epsilon \phi^{(1)} + \epsilon^2 \phi^{(2)} + \cdots. \end{aligned}\right\} \tag{7.24}$$

in which the motion perpendicular to x appears at higher order than the motion in the x–direction. A similar set of expansions was used by Nejoh (1987b) to derive a Kadomtsev–Petviashvili equation for relativistic ion-acoustic waves.

Substituting the expansions (7.24) and the stretchings (7.23) into the system (7.21), and once again reducing the resultant system of equations into a single equation for $\phi^{(1)}$ (see appendix E) furnishes the Kadomtsev–Petviashvili (KP) equation (Kadomtsev & Petviashvili 1970)

$$\frac{\partial}{\partial \xi}\left\{ \frac{\partial \phi^{(1)}}{\partial \tau} + a\phi^{(1)} \frac{\partial \phi^{(1)}}{\partial \xi} + b \frac{\partial^3 \phi^{(1)}}{\partial \xi^3} \right\} + c \frac{\partial^2 \phi^{(1)}}{\partial \eta^2} = 0. \tag{7.25}$$

The coefficients a and b are the same as those found in the previous subsection and are given by (7.15) and (7.16), respectively; and the coefficient c is given by

$$c = \tfrac{1}{2} V,$$

where V satisfies (7.14). The KP equation above describes the propagation of nonlinear electron-acoustic waves in a direction almost along the x-axis. In addition, with its full time dependence it can account for oblique interactions of planar electron-acoustic solitons.

By analogy with Nejoh (1987b) the one soliton solution to the KP equation is found by writing it in terms of the new variable

$$\chi = K_1\xi + K_2\eta - \Omega\tau.$$

The resulting equation is readily integrated yielding

$$\phi^{(1)} = \frac{3U}{a}\mathrm{sech}^2\left[\left(\frac{U}{4b}\right)^{1/2}\left\{\xi + \frac{K_2}{K_1}\eta - \frac{\Omega}{K_1}\tau\right\}\right], \tag{7.26}$$

where

$$U = \frac{\Omega}{K_1} - c\frac{K_2^2}{K_1^2}. \tag{7.27}$$

In terms of the original coordinates the above solution becomes

$$\phi = \frac{3\epsilon U}{a}\mathrm{sech}^2\left[\left(\frac{\epsilon U}{4b}\right)^{1/2}\left\{x + \epsilon^{1/2}\frac{K_2}{K_1}y - \left[V\left(1 + \epsilon\frac{K_2^2}{2K_1^2}\right) + \epsilon U\right]t\right\}\right] \tag{7.28}$$

which clearly indicates the weak dependence on y. If K_2 is zero then this soliton solution reduces to (7.19), the solution of the one-dimensional KdV equation, whereas for nonzero K_2 the soliton amplitude is smaller than in the former case (at the same soliton speed).

7.3 Arbitrary-amplitude theory

To incorporate stronger nonlinearity and wave dispersion we employ the pseudo-potential approach of Baboolal, Bharuthram & Hellberg (1988, 1989). In short, this involves the reduction of the system (7.1)–(7.5) to a single ordinary differential equation which is integrated with suitable "initial conditions" (more correctly a one sided boundary condition) to yield soliton profiles. Unlike the small-amplitude theory, this approach does not formally allow for time dependence in the wave frame and hence only stationary potential structures are admitted. Furthermore, in this approach there is no prescription of the relation tying the nonlinearity to the wave dispersion which, formally, allows for a richer spectrum of wave profiles. For

example, Baboolal, Bharuthram & Hellberg (1988) have used this method to construct double layer as well as soliton profiles for ion-acoustic waves, and Lee & Kan (1981); Song, Lee & Huang (1988) have also found cnoidal wave-like solutions using a similar approach.

We shall suppose that all the harmonics constituting the wave-packet move along the x–direction, or alternatively, that the plasma is one dimensional. Then the system of equations (7.1) – (7.5) govern the plasma and wave dynamics.

Seeking solitary solutions that retain their original form with the evolution of time we introduce the new coordinate,

$$s = x - Mt, \tag{7.29}$$

upon which, we assume, the various macroscopic quantities depend. This yields a dramatic simplification of the initial partial differential equations which in terms of this new coordinate become a system of coupled ordinary differential equations.

The equation of continuity (7.2) may be integrated at once. Using the latter equation in the pressure equation (7.4) and integrating, the well known adiabatic law

$$p_j n_j^{-3} = p_{0j} n_{0j}^{-3},$$

is recovered, which permits integration of the momentum equation (7.3). In the integrations the transformed boundary conditions have been imposed, viz.

$$\left.\begin{array}{llll} \phi \to 0, & \dfrac{\mathrm{d}\phi}{\mathrm{d}s} \to 0, & u_i \to 0, & u_c \to 0, \\ n_i \to 1, & n_c \to n_{0c}, & p_i \to T_i, & p_c \to n_{0c} T_c \end{array}\right\} \quad \text{as} \quad |s| \to \infty. \tag{7.30}$$

Eliminating p_j and u_j from the resultant system of equations yields:

$$M^2 \left(\frac{n_{0c}}{n_c}\right)^2 + 3T_c \left(\frac{n_c}{n_{0c}}\right)^2 = M^2 + 3T_c + 2\phi, \tag{7.31}$$

$$M^2 \left(\frac{1}{n_i}\right)^2 + 3\frac{T_i}{m_i} n_i^2 = M^2 + 3\frac{T_i}{m_i} - \frac{2\phi}{m_i}, \tag{7.32}$$

for the cool-electron and ion densities, respectively, where it was tacitly assumed that the ion species is hydrogen-like.

Equations (7.31) and (7.32) express the conservation of cool electron and ion momentum, respectively. They are structurally similar to those obtained

by Baboolal *et al.* (1988, 1989) in their investigation of ion-acoustic solitons and double layers. In the cold fluid limit T_c, $T_i \to 0$ they yield on solving for n_c, n_i

$$n_c = \frac{n_{0c}}{(1+2\phi/M^2)^{1/2}}, \tag{7.33}$$

$$n_i = \frac{1}{(1-2\phi/m_iM^2)^{1/2}}, \tag{7.34}$$

respectively, while for T_c, $T_i \neq 0$ one obtains

$$n_c = n_{0c}\left(\frac{1}{6T_c}\right)^{1/2}\left(M^2+3T_c+2\phi \pm \sqrt{(M^2+3T_c+2\phi)^2-12M^2T_c}\right)^{1/2}, \tag{7.35}$$

$$n_i = \left(\frac{m_i}{6T_i}\right)^{1/2}\left(M^2+3\frac{T_i}{m_i}-\frac{2\phi}{m_i} \pm \sqrt{\left(M^2+3\frac{T_i}{m_i}-\frac{2\phi}{m_i}\right)^2-12M^2\frac{T_i}{m_i}}\right)^{1/2}. \tag{7.36}$$

Clearly, for finite fluid temperature the cool electron and ion densities are multi-valued. To select the correct density branch we require, for continuity of the densities, that equations (7.35) and (7.36) coincide with (7.33) and (7.34), respectively, in the limits T_c, $T_i \to 0$. Application of L' Hospital's rule shows that the branches with the positive surd must be discarded. Similar correspondence was used by Baboolal *et al.* (1988, 1989) for the ion densities in a study of ion-acoustic solitons and double layers, however, in their investigation the correct density branch was determined numerically.

Real-valuedness of the densities imposes the following restrictions on ϕ,

$$\tfrac{1}{2}[-M^2-3T_c+M\sqrt{12T_c}] < \phi < \tfrac{1}{2}[m_iM^2+3T_i-M\sqrt{12m_iT_i}],$$

which for T_i, $T_c \to 0$ becomes $-M^2/2 < \phi < m_iM^2/2$, a condition similar to that placed on ϕ in the ion-acoustic case (Baboolal *et al.* 1989). Although these inequalities seem to imply the existence of compressive electron-acoustic solitons we have seen that in the present case such solitons are not found, i.e. there is a further constraint leading to $\phi < 0$.

With (7.29) Poisson's equation becomes

$$\frac{\mathrm{d}^2\phi}{\mathrm{d}s^2} = n_{0h}\exp\phi + n_c - n_i \equiv N(\phi), \tag{7.37}$$

where, following Baboolal *et al.* (1988, 1989), we have defined the normalized charge density by $N(\phi)$. Now, in the usual way, (7.37) can be integrated formally (Baboolal *et al.*, 1988, 1989) to yield

$$\frac{1}{2}\left(\frac{\mathrm{d}\phi}{\mathrm{d}s}\right)^2 + \Psi(\phi) = 0, \tag{7.38}$$

with $\Psi(\phi)$, the Sagdeev potential, defined by

$$\Psi(\phi) = -\int_0^{\phi} N(\phi')\,\mathrm{d}\phi'. \tag{7.39}$$

Equation (7.38) expresses the conservation of total momentum of the system. $\Psi(\phi)$ may be evaluated analytically if the fluids are cold, i.e. $T_c = T_i = 0$: substituting (7.33) and (7.34) into the above equation for Ψ, and integrating, yields

$$\Psi(\phi) = n_{0h}(1 - \exp\phi) + n_{0c}M^2\left(1 - \sqrt{1 + \frac{2\phi}{M^2}}\right) + m_i M^2\left(1 - \sqrt{1 - \frac{2\phi}{m_i M^2}}\right).$$

For nonzero T_c, T_i, the integral in (7.39) must be calculated numerically incorporating the density equations (7.35) and (7.36).

If (7.38) is to admit soliton solutions then the Sagdeev potential, Ψ, must satisfy the usual conditions (Sagdeev, 1966)

$$\Psi(0) = \frac{\mathrm{d}\Psi(0)}{\mathrm{d}\phi} = 0 \tag{7.40}$$

$$\Psi(\phi_0) = 0 \quad \text{for some } \phi_0, \tag{7.41}$$

$$\Psi(\phi) < 0 \quad \text{in } 0 < |\phi| < |\phi_0|. \tag{7.42}$$

It is interesting to investigate the behaviour of equation (7.38) by thinking of it as an energy integral of a particle in a potential well. Then, by analogy with classical mechanics, the equations (7.41) and (7.42) impose the condition that the potential Ψ have a potential well shape, and equation (7.40) ensures that a "particle" starting off at $\phi = 0$ makes a single transit to the point ϕ_0 and then returns to its starting point $\phi = 0$.

Finally, equations (7.33)–(7.36) and (7.39) are used to numerically construct the Sagdeev potential (Baboolal *et al.* 1988), and (7.38) is integrated numerically as an initial-value problem with initial condition

$$\phi(0) = \phi_0,$$

where ϕ_0 is obtained by numerical solution of (7.41).

7.4 Large amplitude theory: numerical results

In this section equations (7.38) and (7.39), incorporating the density equations (7.33)–(7.36) are solved without approximation for stationary soliton structures. Parameter values similar to those used by Tokar & Gary (1984) have been chosen. They are approximately what one might expect for plasma in the polar cusp at altitudes exterior to the upward electron beams. In this numerical work we have defined the Mach number by

$$\mathcal{M} = \frac{M}{(n_{0c}/n_{0h})^{1/2}} = \frac{v}{(n_{0c}/n_{0h})^{1/2} v_h} \tag{7.43}$$

where v is the soliton velocity and $(n_{0c}/n_{0h})^{1/2} v_h \equiv v_{se}$ is the electron sound speed (Gary & Tokar, 1985).

Figures 7.1 and 7.2 illustrate the effect of finite cool-electron and ion temperature on the Sagdeev and real potentials Ψ, ϕ, respectively. As is evident, an increase in the fluid temperatures causes the Sagdeev potential to become shallower and also decreases the magnitude of the maximum soliton potential $|\phi_0|$. These effects are brought about almost entirely by the finite cool-electron temperature, for the ion temperature has virtually no effect on the Sagdeev or soliton potential profiles (cf. (7.15) and (7.16)).

The maximum soliton amplitude was calculated as a function of ion temperature for temperatures ranging from 0 to 500 (not shown). Extremely weak dependence was observed over this range, which is not unexpected, bearing in mind the small contributions of the T_i terms to the KdV equation in §7.2.1. This insensitivity to ion temperature is in accordance with linear theory (Watanabe & Taniuti 1977, Gary & Tokar 1985, Mace & Hellberg 1990) where ion parameters do not appear in the linear dispersion relation for electron-acoustic waves. Thus we deduce that in the nonlinear, as well as in the linear theory of electron-acoustic waves, the only function of the ions is to provide a neutralizing background. The dynamic neutralization is provided by the hot electrons.

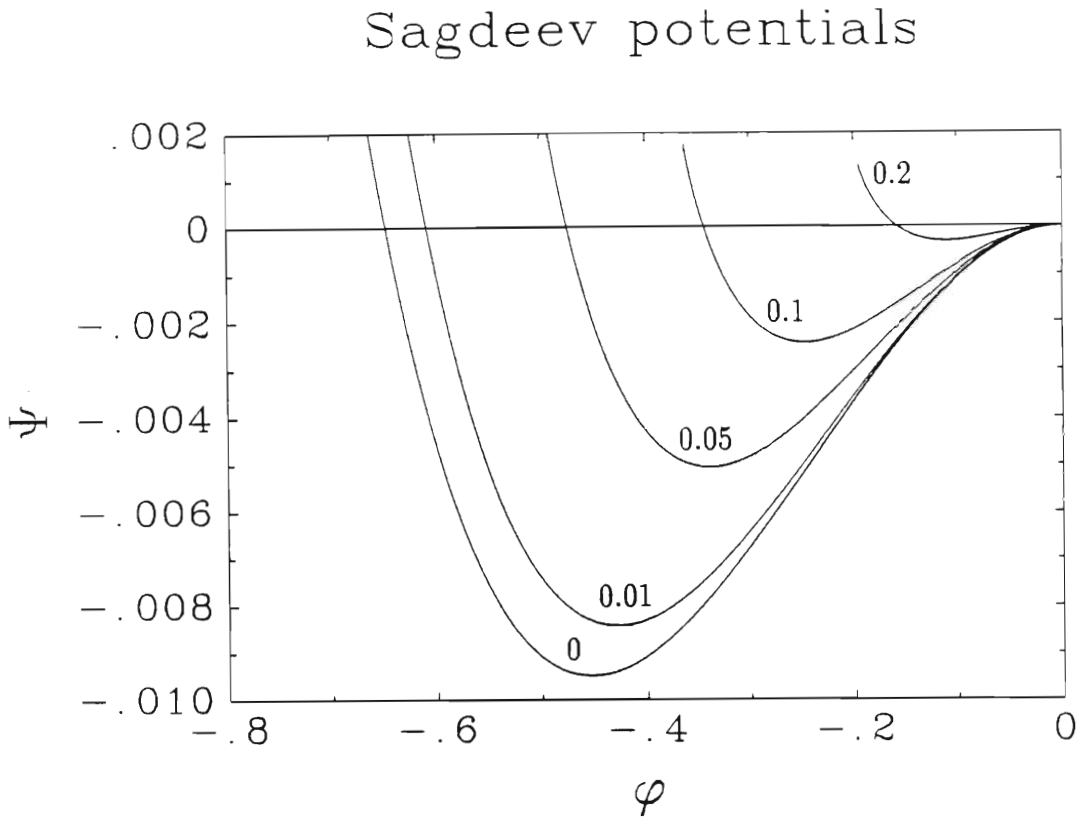

Figure 7.1: Sagdeev potentials corresponding to a Mach number $\mathcal{M} = 1.4$ for a plasma with $n_{0c} = 0.5$. The parameter labelling the curves is the temperature $T_c = T_i$. In all figures in this chapter $m_i = 1836$ and $n_{0i} = 1$, corresponding to a hydrogen plasma.

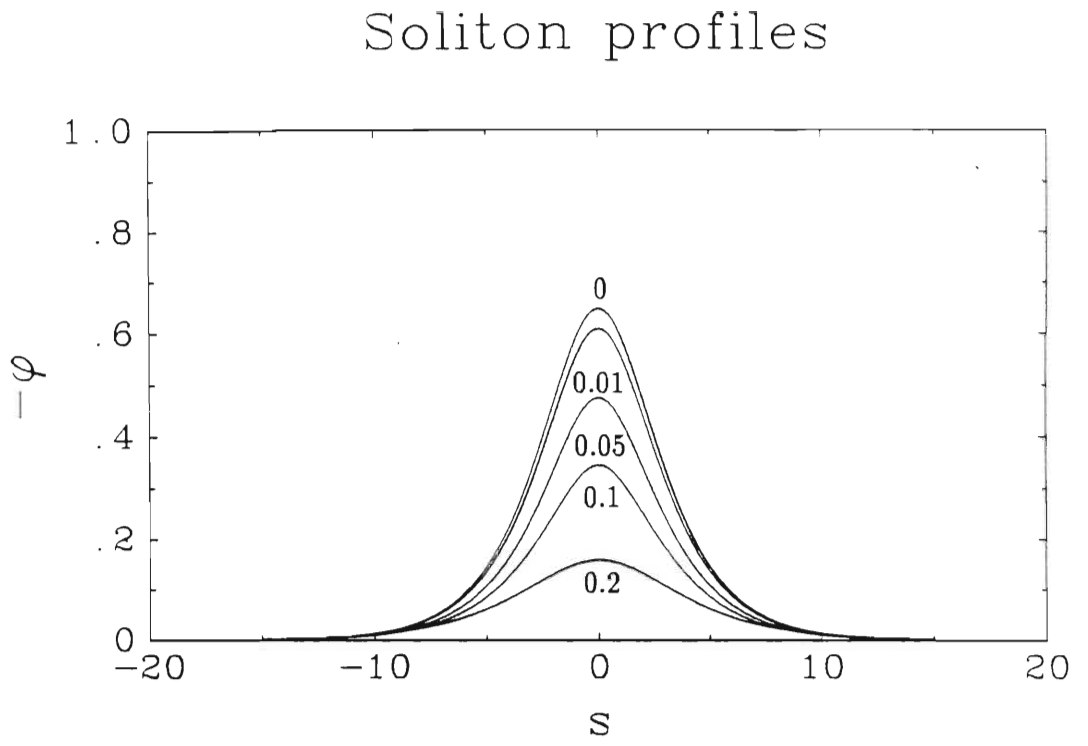

Figure 7.2: The corresponding real potentials associated with the Sagdeev potentials in figure 7.1

Figure 7.3 shows some typical arbitrary-amplitude, finite temperature, electron-acoustic soliton profiles for various Mach numbers. Clearly, the width of the solitons decreases with increasing amplitude, which is related to the Mach number $\mathcal{M}$ (cf. the small-amplitude result (7.19)). Also, the shapes of the larger amplitude solitons, especially the curves for n_c the cool electron density, and ρ the total charge density, differ from those predicted by the small-amplitude theory.

Small-amplitude theory predicts that the perturbation in the cool electron density should be proportional to the perturbation in the electrostatic potential (D.23). In the large-amplitude theory this is clearly not the case and the cool electron density profile becomes very steep for large nonlinearity, indicating that there is a large overfilling of cool electrons near the centre of the soliton, and indicating the generation of very high wavenumber harmonics. This behaviour is also reflected in the total charge density ρ. The ion density is for all practical purposes constant and equal to n_{0i} which lends support to our small-amplitude approximations.

Unlike ion-acoustic solitons, in which the charge separation arises from the disparities in the densities of the ions and cool electrons, in the electron-acoustic soliton the charge separation arises entirely because of the difference in the densities of the hot and cool electron fluids. The former exhibits a depletion in number density, whereas the latter shows a density enhancement at the soliton centre. The final set of curves in this figure, for the total charge density, indicate that the electron-acoustic soliton manifests itelf as a slab of negative space charge "sandwiched" by adjacent wedges of positive space charge. This sytem of charge moves perpendicular to the face of the slab.

It is noteworthy that the curve for $\mathcal{M} = 1.8$ is a large-amplitude soliton, $|\phi_0| > 1$, and as such has no counterpart in the weakly-nonlinear theory where, by assumption, the soliton potential is less than unity.

Figure 7.4 illustrates the influence on the maximum soliton amplitude of increasing the Mach number $\mathcal{M}$. The effect is an approximately linear increase in $|\phi_0|$ with $\mathcal{M}$, the deviation from linearity becoming more profound at larger $\mathcal{M}$ values. As the temperature of the cool electrons and ions is increased, the range of Mach numbers over which soliton solutions can be obtained, decreases. This occurs because above a critical cool-electron temperature (7.31) can only be satisfied by a complex-valued cool-electron density, implying the violation of cool electron momentum "conservation". We have found that in the vicinity of such critical points the nonlinearity generates very high wavenumber harmonics in the cool electron density profile (see previous figure) allowing us to infer that at the critical points there

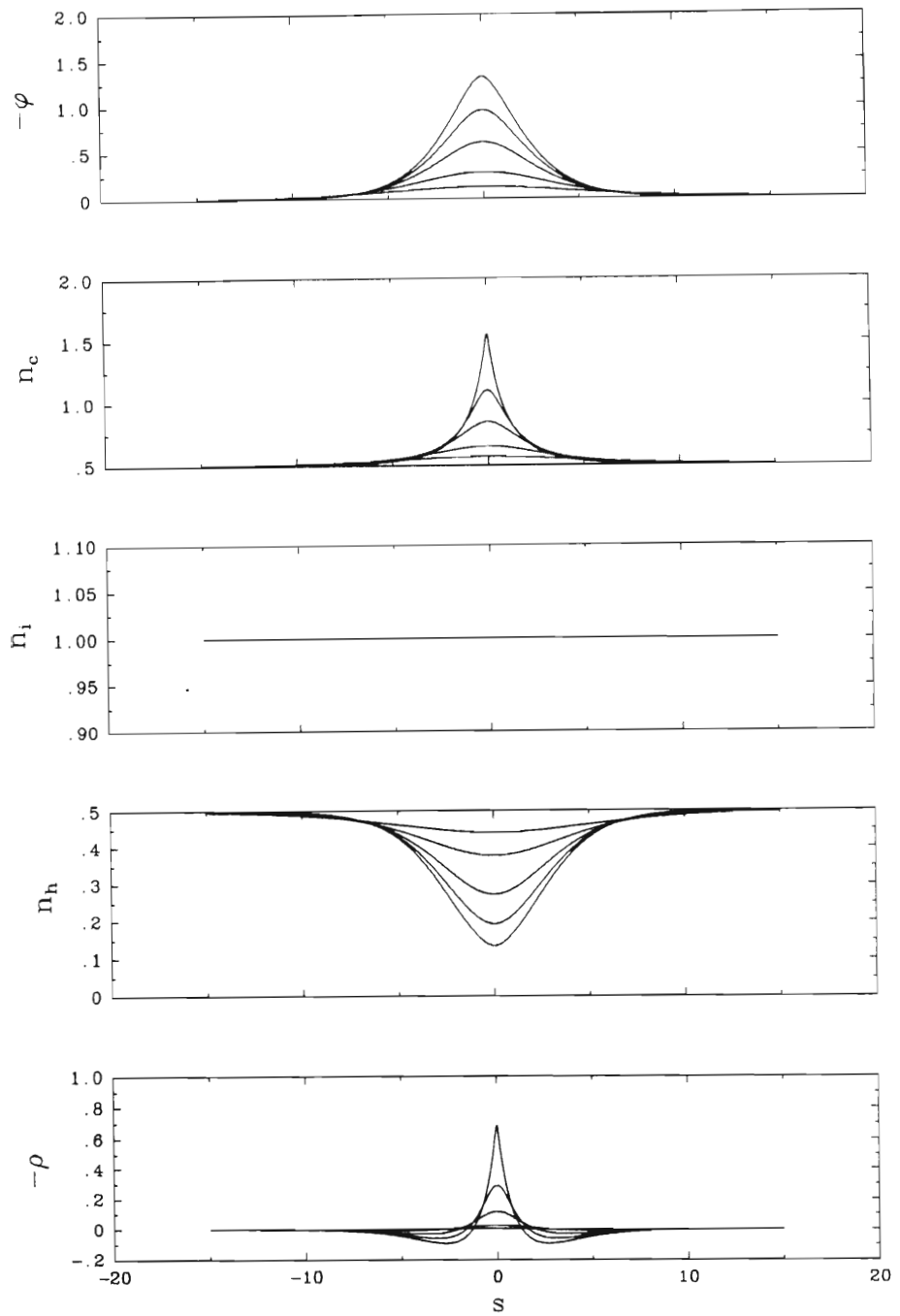

Figure 7.3: Soliton potential, density and charge profiles ranging from small to large amplitude. The Mach numbers depicted are $\mathcal{M} = 1.1, 1.2, 1.4, 1.6, 1.8$. In the $-\phi$, n_c and $-\rho$ plots the soliton amplitude increases monotonically with Mach number, in the n_h plot it decreases monotonically, and in the n_i profiles there is no visible variation with $\mathcal{M}$. Other fixed parameters are: $n_{0c} = 0.5$ and $T_c = T_i = 0.01$.

is a breakdown in the balance between nonlinearity and dispersion: the latter being too weak to balance the former. At these critical points the system (7.1)–(7.5) does not admit single stationary soliton solutions.

On the other end of the Mach number scale it is seen that the threshold Mach number for solitons increases with increasing cool electron temperature. This threshold condition is well described analytically by the small-amplitude existence condition (7.20) in conjunction with (7.14), which in terms of the present normalization is written

$$\mathcal{M} > \left(1 + 3\frac{T_c}{n_{0c}/n_{0h}}\right)^{1/2}. \tag{7.44}$$

In the arbitrary-amplitude theory this condition arises because the Sagdeev potential exhibits a local maximum value at $\phi = 0$, i.e.

$$\left.\frac{\partial^2 \Psi}{\partial \phi^2}\right|_{\phi=0} < 0. \tag{7.45}$$

In terms of the analogy with classical mechanics this condition implies that the particle comes to rest at $\phi = 0$. Differentiating (7.39) twice one then has

$$\frac{\partial^2 \Psi}{\partial \phi^2} = \frac{\partial n_i}{\partial \phi} - \frac{\partial n_c}{\partial \phi} - n_{0h} \exp \phi \simeq -\frac{\partial n_c}{\partial \phi} - n_{0h} \exp \phi, \tag{7.46}$$

and calculating $\partial n_c/\partial \phi$ from either of (7.31) or (7.35) yields

$$\frac{\partial n_c}{\partial \phi} = -\frac{n_c}{M^2(n_{0c}/n_c)^2 + 3T_c(n_c/n_{0c})^2}. \tag{7.47}$$

Finally, substitution of (7.47) and (7.46) into (7.45), and taking $\phi \to 0$ yields (7.44) after renormalization. As discussed by Baboolal (1988), it is not necessary to specify (7.45) *a priori* in order to integrate the Poisson equation, but in this case the condition arises naturally as a consequence of our boundary conditions.

Figure 7.5 illustrates the monotonic decrease in $|\phi_0|$ with cool-electron temperature for various Mach numbers. The effect of a finite cool-electron temperature is to increase the phase velocity of the linear electron-acoustic wave (7.14). An increase in T_c decreases $\delta V \simeq M - (n_{0c}/n_{0h} + 3T_c)^{1/2}$ resulting in weaker nonlinearity. That increasing T_c decreases wave-packet dispersion may be seen by considering the quantity $\Delta \equiv |d\Omega/dK| - |d^2\Omega/dK^2|$

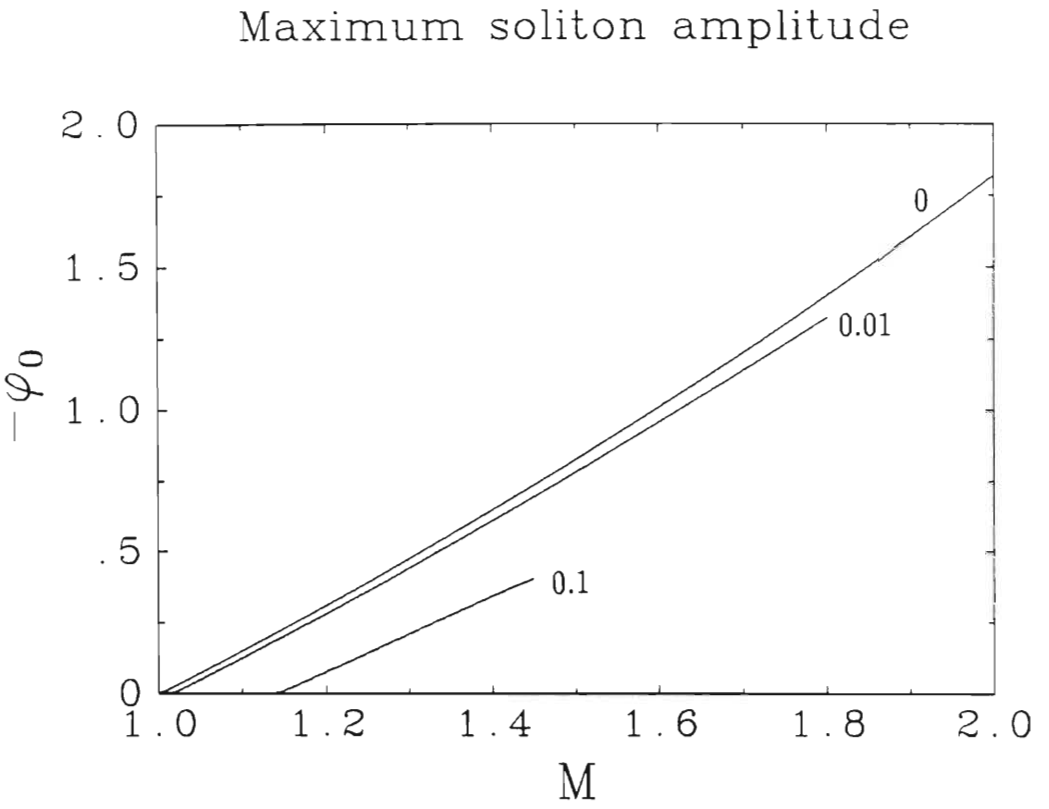

Figure 7.4: The maximum soliton amplitude as a function of Mach number $\mathcal{M}$. The parameter labelling the curves is $T_c = T_i$ and $n_{0c} = 0.5$.

where the larger the value of Δ the weaker the dispersion (Taniuti & Nishihara 1983). The quantities Ω and K are normalised frequency and wavenumber, respectively, such that $V = \Omega/K$. Clearly, in the weakly-dispersive limit equation (7.14) implies

$$\begin{aligned} \frac{\Omega}{K} &= \left(\frac{n_{0c}}{n_{0h}} + 3T_c\right)^{1/2}, \\ &= \frac{d\Omega}{dK}; \\ \frac{d^2\Omega}{dK^2} &= 0, \end{aligned}$$

and therefore

$$\Delta = \left(\frac{n_{0c}}{n_{0h}} + 3T_c\right)^{1/2}.$$

Hence, increasing T_c also increases Δ and therefore decreases the dispersion. Baboolal *et al.* (1989) arrived at an analogous conclusion for ion-acoustic solitons, where it was found that finite ion temperature weakened wave dispersion. It is noteworthy that larger amplitude solitons exist only over progressively smaller values of T_c. Physically this occurs because of the violation of cool electron momentum conservation discussed earlier.

Figure 7.6 illustrates the maximum soliton amplitude as a function of the cool-electron number density for a Mach number of $\mathcal{M} = 1.4$. The maximum value of $|\phi_0|$ increases with increasing n_{0c}. However, it must be borne in mind that our definition of $\mathcal{M}$ (equation (7.43)) includes a factor $n_{0c}^{1/2}$. Thus, for fixed $\mathcal{M}$, the use of progressively larger values of n_{0c} implies that we are considering increasing values of the absolute velocity of the soliton, v, in our calculations. On the other hand, some computations have been carried out in which the soliton velocity v was kept constant. The results confirmed the KdV prediction for this case (cf. equations (7.19) in conjunction with (7.15) and (7.16)) that there should be a decrease in the maximum amplitude with n_{0c} for δV held constant.

Finally, in figures 7.7–7.10 the range of applicability of the small-amplitude KdV theory is illustrated. Curves from figures 7.2–7.6 which were calculated using the arbitrary-amplitude theory have been selected and compared with the corresponding curves predicted by weakly-nonlinear theory. As expected, there is good correspondence for $|\phi| \ll 1$, and in fact even up to values $|\phi| < 0.5$. For intermediate-amplitude solitons $0.5 < |\phi| < 1$ there

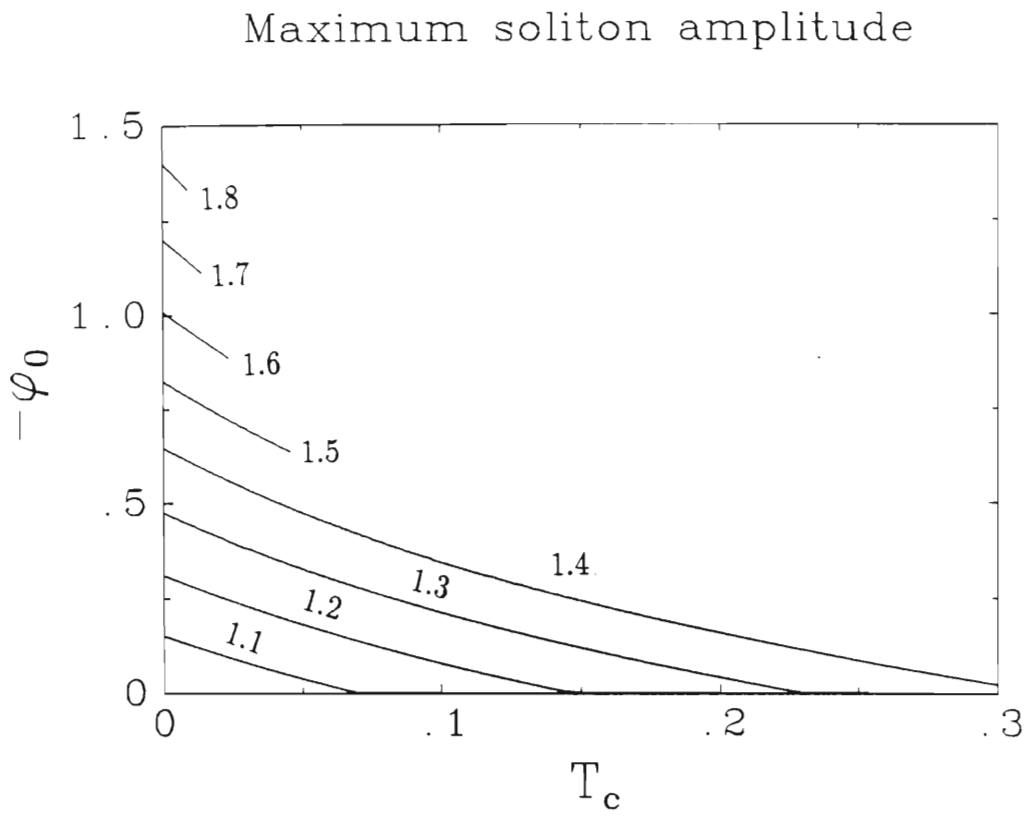

Figure 7.5: Maximum soliton amplitude as a function of T_c. The parameter labelling the curves is $\mathcal{M}$. Other parameters are: $n_{0c} = 0.5$ and $T_i = 0$.

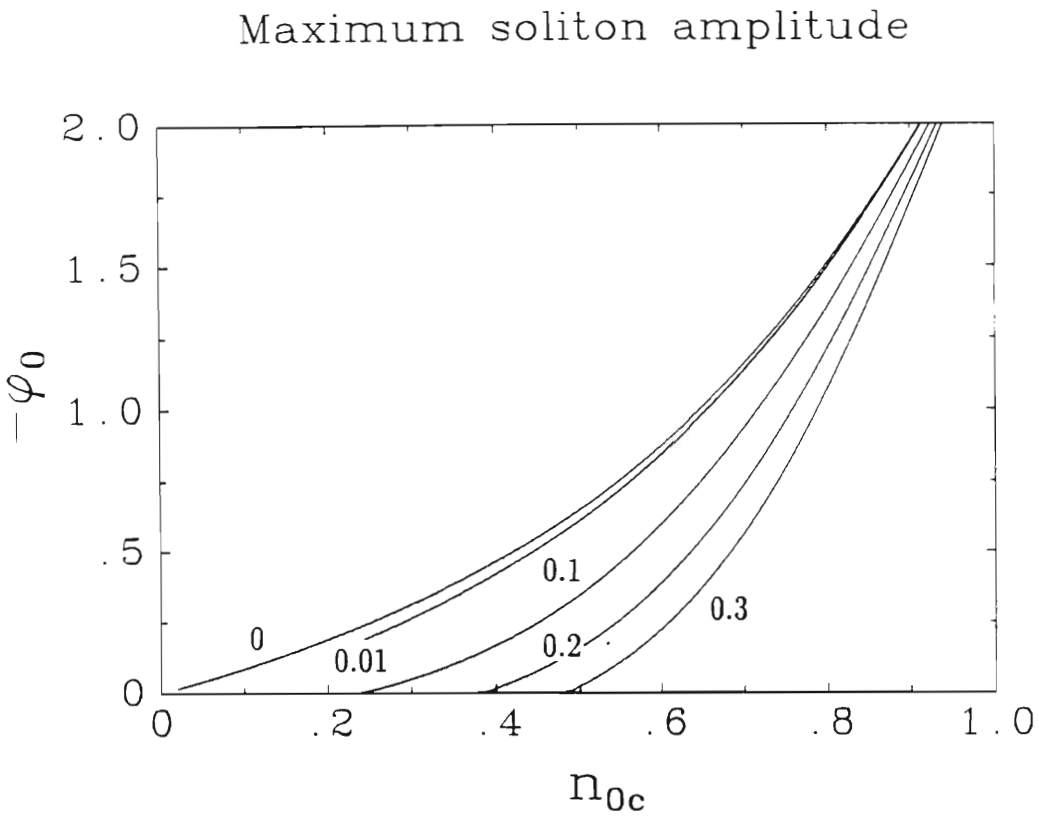

Figure 7.6: Maximum soliton amplitude as a function of n_{0c} for a Mach number $\mathcal{M} = 1.4$. The parameter labelling the curves is $T_c = T_i$. The curve for $T_c = 0.01$ terminates early because the surd in equation (7.35) evaluates to an imaginary number for smaller values of n_{0c}.

is at best only qualitative agreement, whilst for large-amplitude solitons $|\phi| > 1$ the small-amplitude theory breaks down.

In addition, these diagrams illustrate the following noteworthy features. We observe in figure 7.7 that for large-amplitude solitons, the width of the KdV solitons differs markedly from that obtained from the arbitrary-amplitude theory. Furthermore, the maximum amplitude ϕ_0 predicted by the two theories can differ by several percent for large amplitude solitons. This leads us to emphasize that the weakly nonlinear theory of electron-acoustic waves cannot simply be applied without further thought to nonlinear electron-acoustic structures, unless they are really of small amplitude. Finally, and most importantly, the KdV curves in figures 7.8 and 7.9 do not exhibit the cut-offs in temperature that are predicted by the arbitrary-amplitude theory.

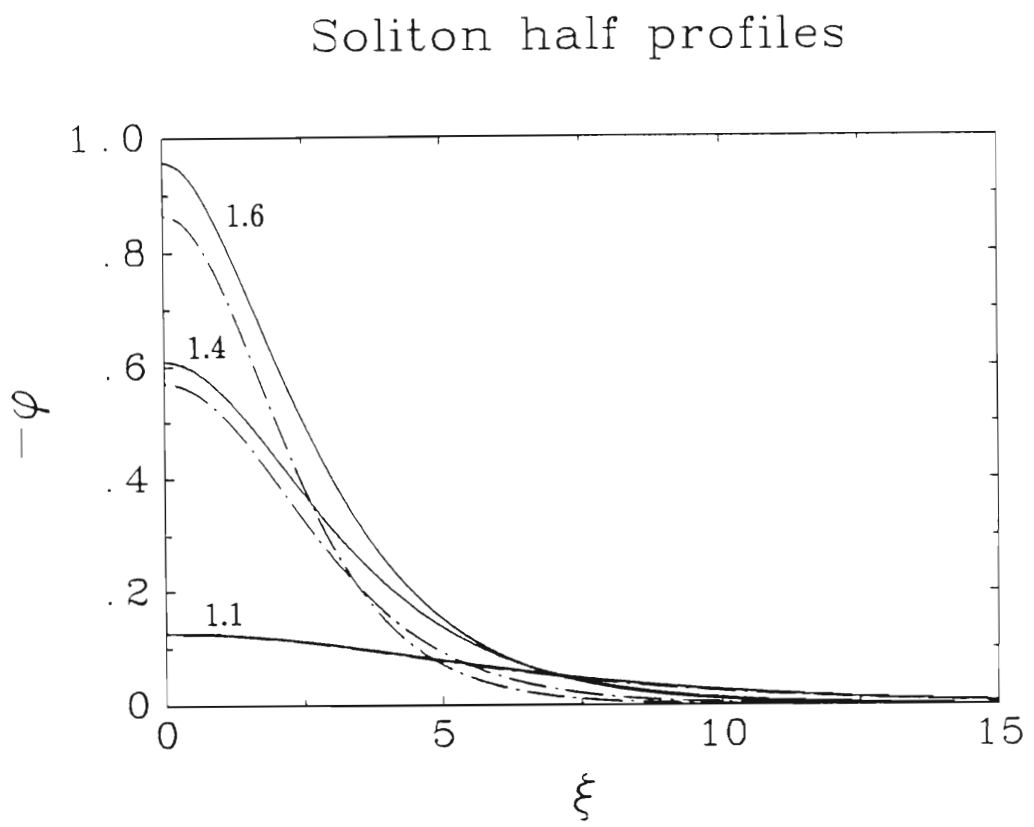

Figure 7.7: A comparison of the soliton half profiles predicted by arbitrary-amplitude theory (solid curves) with those predicted by small amplitude KdV theory (dashed curves). The parameter labelling the curves is $\mathcal{M}$ and other parameters are as in figure 7.3.

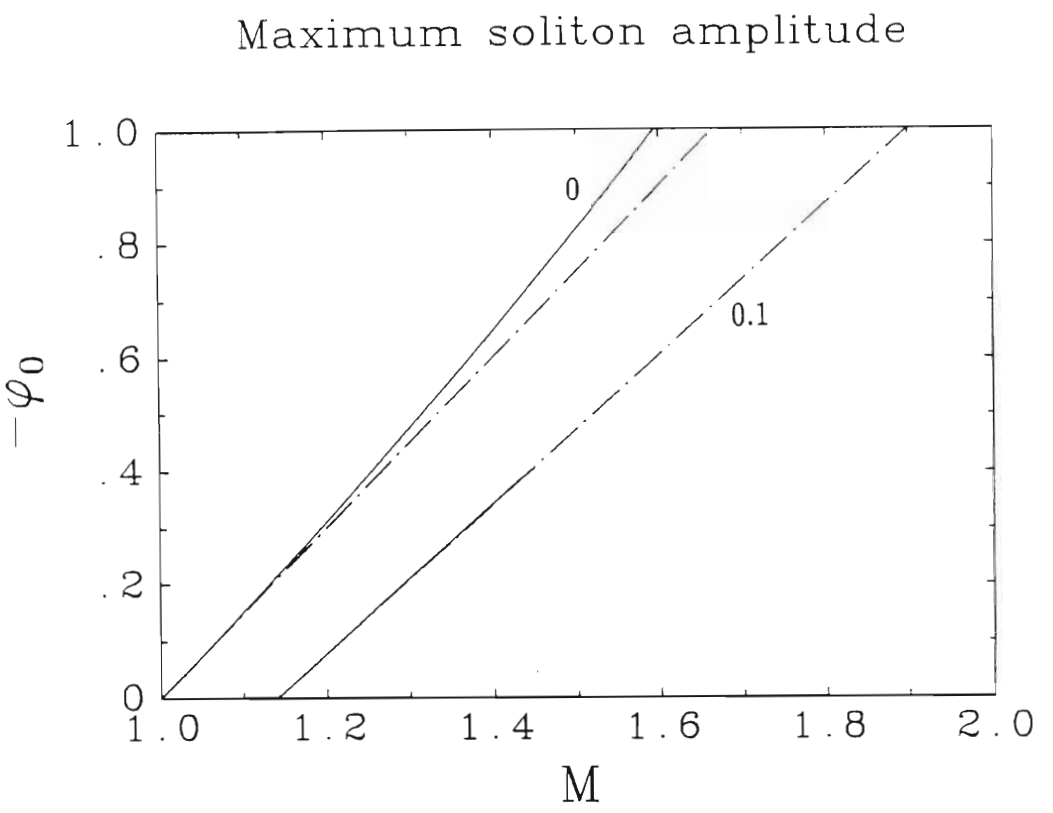

Figure 7.8: A comparison of the maximum soliton amplitude predicted by the arbitrary-amplitude theory with that predicted by the small-amplitude theory as a function of $\mathcal{M}$. The parameters and labelling of curves are as in figure 7.4.

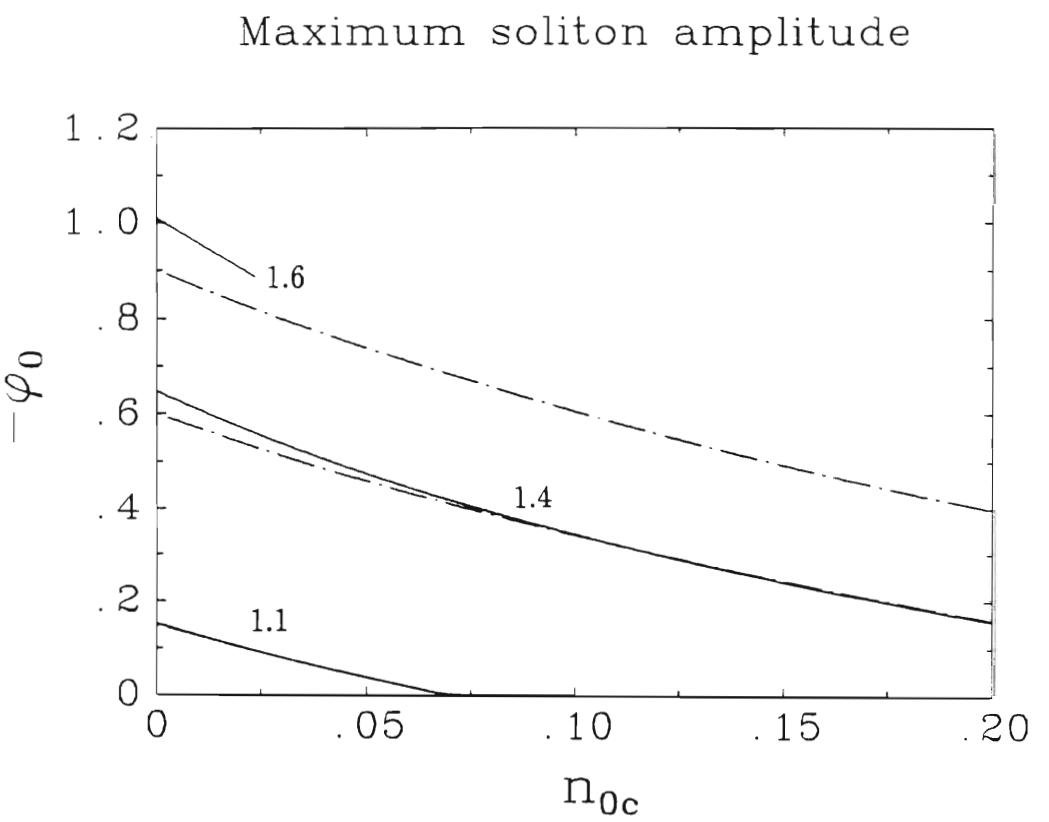

Figure 7.9: A comparison of the maximum soliton amplitude predicted by the arbitrary-amplitude theory with that predicted by the small-amplitude theory, as a function of T_c. The parameters and labelling of curves are as in figure 7.5.

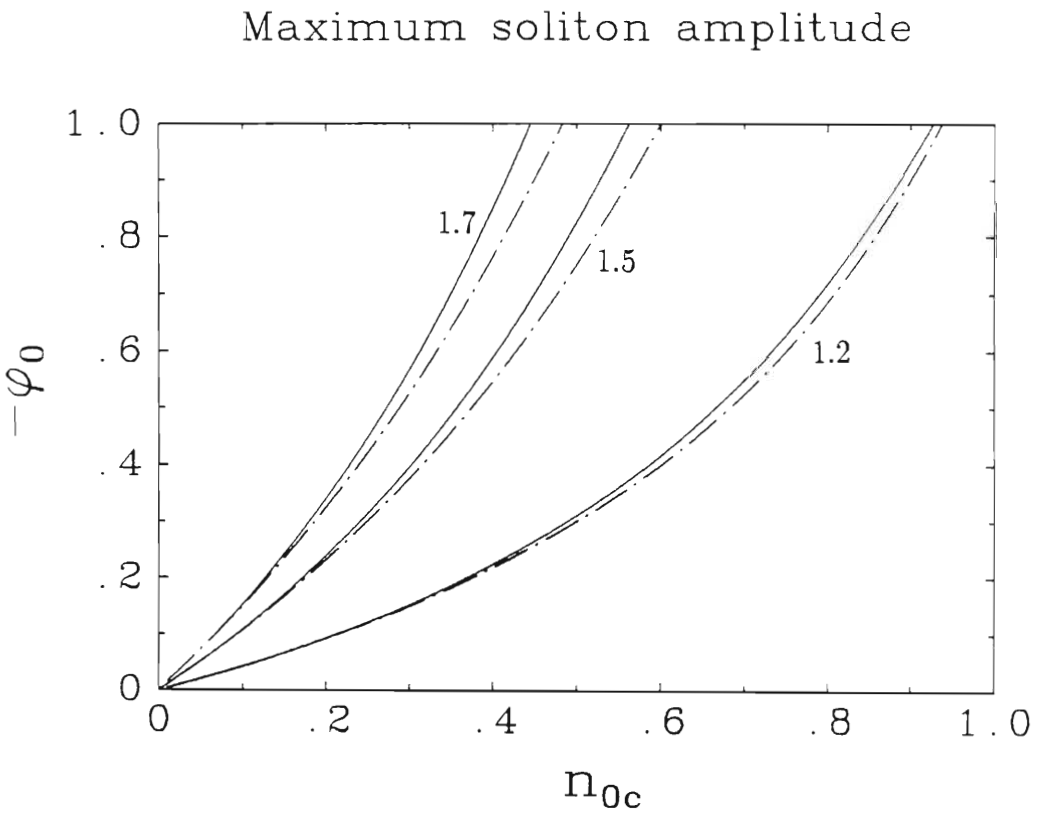

Figure 7.10: A comparison of the maximum soliton amplitude as a function of n_{0c} for various values of $\mathcal{M}$; other parameters are $T_c = T_i = 0$.

Chapter 8

Small-amplitude solitons in magnetized plasma

Because of its occurrence in the polar cusp region, the electron-acoustic wave and the associated plasma dynamics will be influenced by the terrestrial magnetic field unless the plasma pressure completely dominates the magnetic pressure. With the introduction of a magnetic field the plasma acts as an anisotropic medium for electrostatic wave propagation. In this chapter the small-amplitude results of chapter 7 are generalized to include a strong homogeneous, constant, magnetic field. Even for this relatively simple configuration, the presence of a magnetic field so complicates the dynamical equations that no arbitrary-amplitude theory along the lines of that chapter, can be formulated.

Lee & Kan (1981) have constructed a theory of nonlinear ion-acoustic waves in magnetized plasma which involved direct integration of the fluid equations but there they dispensed with Poisson's equation and used the quasineutrality condition instead. Song, Lee & Huang (1988) improved upon this theory by including the Poisson equation, but only after assuming that the deviation from quasineutrality was of order $\epsilon = \Omega_i^2/\omega_{pi}^2 \ll 1$, a very small quantity. We pursue neither of these approaches in this chapter. Rather, we employ the reductive perturbation technique to reduce the system of dynamical equations to an evolutionary equation describing weakly-nonlinear electron-acoustic waves in strongly magnetized plasma.

8.1 Basic equations

An infinite homogeneous, collisionless, magnetized plasma is considered. The magnetic field is in the direction of $\mathbf{e}_z$. The hot electron density is given by the Boltzmann distribution and the dynamics of the fluid components are determined by

$$\frac{\partial n_j}{\partial t} + \nabla \cdot (n_j \mathbf{u}_j) = 0, \tag{8.1}$$

$$m_j n_j \left(\frac{\partial \mathbf{u}_j}{\partial t} + \mathbf{u}_j \cdot \nabla \mathbf{u}_j \right) = -\nabla p_j - Z_j n_j \nabla \phi + Z_j m_j n_j \Omega_j \mathbf{u}_j \times \mathbf{e}_z, \tag{8.2}$$

$$\frac{\partial p_j}{\partial t} + \mathbf{u}_j \cdot \nabla p_j + 3 p_j \nabla \cdot \mathbf{u}_j = 0. \tag{8.3}$$

The system of equations is coupled by the Poisson equation

$$\nabla^2 \phi = n_{0h} \exp \phi - \sum_j Z_j n_j, \tag{8.4}$$

and the index j runs over the fluid components ($j = i, c$). The following normalizations have been used in the above equations: lengths by the 'Debye length' $(T_h/4\pi n_{0e} e^2)^{1/2}$, time by the inverse electron plasma frequency $\omega_{pe}^{-1} = (m_e/4\pi n_{0e} e^2)^{1/2}$, number densities by the total electron density n_{0e}, pressures by $n_{0e} T_h$, temperatures by T_h, velocities by the hot electron thermal speed $(T_h/m_e)^{1/2}$, electrostatic potential by T_h/e, masses by the electron mass m_e; and $Z_j \equiv q_j/e$, $\Omega_j = \Omega_j'/\omega_{pe}$ is the gyrofrequency ($\Omega_j' \equiv eB/m_j c_L$ in unnormalized quantities; c_L is the speed of light) divided by the electron plasma frequency. Furthermore, the usual soliton boundary conditions are imposed in three dimensions

$$\left.\begin{aligned} \phi \to 0, \quad \nabla\phi \to 0, \quad \nabla^2\phi \to 0, \\ n_j \to n_j^{(0)}, \quad p_j \to p_{0j}, \quad \mathbf{u}_j \to 0 \end{aligned}\right\} \quad \text{as} \quad |\mathbf{x}| \to \infty. \tag{8.5}$$

8.2 The KdV–ZK equation

8.2.1 Magnetized ions

In this subsection we follow a procedure similar to that of Das & Verheest (1989) in their study of ion-acoustic waves in plasmas with negative ions, to derive the Korteweg–de Vries–Zakharov–Kuznetszov (KdV–ZK) equation

for electron-acoustic waves in a plasma in which both the electron and ion fluids are magnetized. The essential difference between the work presented here and that of the aforementioned, is that we allow for some of our electron components to be fluid-like (the balance being isothermal or Boltzmann) and therefore our model can describe electron-acoustic waves. A fuller derivation of the results of this section can be found in appendix F.

We consider an electron-acoustic wave packet propagating in some arbitrary direction with respect to the magnetic field. The wavenumbers of the harmonics constituting the wave packet are assumed small relative to the hot electron Debye length, and the the perpendicular wavenumbers are small when compared to the "Larmor" radius ρ_{se}, i.e.

$$k\lambda_{Dh} \ll 1, \quad \text{and} \quad k_\perp \rho_{se} = k_\perp v_{se}/\Omega_e \ll 1.$$

Then the dispersion relation for the system can be written:

$$\omega = k_z v_{se}(1 - \tfrac{1}{2}k^2\lambda_{Dh}^2 - \tfrac{1}{2}k_\perp^2\rho_{se}^2).$$

Furthermore we assume that the ion gyrofrequency, as well as the electron gyrofrequency, is much larger than the characteristic wave frequencies of the harmonics in the wave packet. Then the electron and ion fluids behave as if they were strongly magnetized, moving primarily in the magnetic field direction.

Introducing the coordinate stretchings

$$\xi = \epsilon^{1/2}x, \quad \eta = \epsilon^{1/2}y, \quad \zeta = \epsilon^{1/2}(z - Vt), \quad \tau = \epsilon^{3/2}t, \tag{8.6}$$

into the above dynamical equations yields

$$-\epsilon^{1/2}V\frac{\partial n_j}{\partial \zeta} + \epsilon^{3/2}\frac{\partial n_j}{\partial \tau} + \epsilon^{1/2}\nabla_\xi \cdot (n_j \mathbf{u}_j) = 0, \tag{8.7}$$

$$-\epsilon^{1/2}m_j n_j V\frac{\partial \mathbf{u}_j}{\partial \zeta} + \epsilon^{3/2}m_j n_j\frac{\partial \mathbf{u}_j}{\partial \tau} + \epsilon^{1/2}m_j n_j \mathbf{u}_j \cdot \nabla_\xi \mathbf{u}_j + \epsilon^{1/2}\nabla_\xi p_j$$
$$= -\epsilon^{1/2}Z_j n_j \nabla_\xi \phi + Z_j m_j n_j \Omega_j (\mathbf{u}_j \times \mathbf{e}_z), \tag{8.8}$$

$$-\epsilon^{1/2}V\frac{\partial p_j}{\partial \zeta} + \epsilon^{3/2}\frac{\partial p_j}{\partial \tau} + \epsilon^{1/2}\mathbf{u}_j \cdot \nabla_\xi p_j + \epsilon^{1/2}3p_j\nabla_\xi \cdot \mathbf{u}_j = 0, \tag{8.9}$$

$$\epsilon\nabla_\xi^2\phi = n_{0h}\Big(1 + \phi + \tfrac{1}{2}\phi^2 + \tfrac{1}{6}\phi^3\Big) - \sum_j Z_j n_j, \tag{8.10}$$

where the operator $\nabla_\xi \equiv (\partial/\partial\xi, \partial/\partial\eta, \partial/\partial\zeta)$ and the flow velocity is defined by $\mathbf{u}_j \equiv (u_j, v_j, w_j)$. The stretchings (8.6) reflect the same spatial and

temporal dependence that was employed in chapter 7, however, the number of spatial dimensions has now been increased to three.

We expand the various macroscopic variables as follows

$$n_j = n_j^{(0)} + \epsilon n_j^{(1)} + \epsilon^2 n_j^{(2)} + \cdots, \tag{8.11}$$

$$w_j = \epsilon w_j^{(1)} + \epsilon^2 w_j^{(2)} + \cdots, \tag{8.12}$$

$$p_j = p_j^{(0)} + \epsilon p_j^{(1)} + \epsilon^2 p_j^{(2)} + \cdots, \tag{8.13}$$

$$\phi = \epsilon\phi^{(1)} + \epsilon^2\phi^{(2)} + \cdots, \tag{8.14}$$

$$u_j = \epsilon^{3/2} u_j^{(1)} + \epsilon^2 u_j^{(2)} + \cdots, \tag{8.15}$$

$$v_j = \epsilon^{3/2} v_j^{(1)} + \epsilon^2 v_j^{(2)} + \cdots. \tag{8.16}$$

Observe that the expansions (8.11–8.16) reflect the anisotropy introduced into the system by the strong magnetic field; which is manifested in the fact that the perpendicular motion appears at higher order in ϵ than the motion parallel to $\mathbf{B}$, implying a preferred direction of motion along the magnetic field. This complies with our initial assumption that the perpendicular wavenumbers are small, or alternatively, that the fluids are strongly magnetized.

Upon substitution of (8.11)–(8.16) into (8.7)–(8.10) there results the following set of equations to order $O(\epsilon^{3/2})$:

$$n_j^{(1)} = \frac{Z_j n_j^{(0)}/m_j}{V^2 - 3\sigma_j}\phi^{(1)}, \tag{8.17}$$

$$u_j^{(1)} = -\frac{V^2}{m_j\Omega_j(V^2 - 3\sigma_j)}\frac{\partial\phi^{(1)}}{\partial\eta}, \tag{8.18}$$

$$v_j^{(1)} = \frac{V^2}{m_j\Omega_j(V^2 - 3\sigma_j)}\frac{\partial\phi^{(1)}}{\partial\xi}, \tag{8.19}$$

$$w_j^{(1)} = \frac{Z_j V/m_j}{V^2 - 3\sigma_j}\phi^{(1)}, \tag{8.20}$$

$$p_j^{(1)} = \frac{3Z_j n_j^{(0)}\sigma_j}{V^2 - 3\sigma_j}\phi^{(1)}, \tag{8.21}$$

where σ_j has the same meaning as in chapter 7.

The perpendicular fluid velocity at this order $\mathbf{u}_\perp^{(1)} = u_j^{(1)}\mathbf{e}_x + v_j^{(1)}\mathbf{e}_y$ is proportional to the $\mathbf{E}\times\mathbf{B}$ drift $\mathbf{V}_E$, whereas the velocity parallel to

$\mathbf{B}$, namely $w_j^{(1)}\mathbf{e}_z$, is the same as for the unmagnetized case (see equation (D.22)).

The phase velocity V must satisfy the $O(\epsilon)$ relation

$$n_{0h} - \sum_j \frac{Z_j^2 n_j^{(0)}/m_j}{V^2 - 3\sigma_j} = 0, \tag{8.22}$$

for non-trivial $\phi^{(1)}$. This relation (8.22) is exactly the same as was found in the unmagnetized case in chapter 7, which is not surprising recalling that V is the electron sound speed in the direction of the magnetic field (cf. the stretchings (8.6)).

At $O(\epsilon^2)$ the continuity equation requires

$$\frac{\partial u_j^{(1)}}{\partial \xi} + \frac{\partial v_j^{(1)}}{\partial \eta} = 0,$$

which is satisfied identically by (8.18) and (8.19) above. The ξ– and η–components of momentum at $O(\epsilon^2)$ which now incorporate both $\mathbf{E}\times\mathbf{B}$ and polarization fluid drifts, yield, after partial differentiation by ξ

$$\frac{\partial u_j^{(2)}}{\partial \xi} = \frac{V^3}{Z_j m_j \Omega_j^2 (V^2 - 3\sigma_j)} \frac{\partial^3 \phi^{(1)}}{\partial \zeta\, \partial \xi^2}, \tag{8.23}$$

$$\frac{\partial v_j^{(2)}}{\partial \eta} = \frac{V^3}{Z_j m_j \Omega_j^2 (V^2 - 3\sigma_j)} \frac{\partial^3 \phi^{(1)}}{\partial \zeta\, \partial \eta^2}, \tag{8.24}$$

where (8.18) and (8.19) have been used.

Combining these expressions with the other $O(\epsilon^{5/2})$ equations derived from the momentum and continuity equations yields the following expression for $\partial n_j^{(2)}/\partial \zeta$

$$\begin{aligned}\frac{\partial n_j^{(2)}}{\partial \zeta} = {} & 2\frac{Z_j n_j^{(0)} V/m_j}{(V^2 - 3\sigma_j)^2} \frac{\partial \phi^{(1)}}{\partial \tau} + 3\frac{Z_j^2 n_j^{(0)} (V^2 + \sigma_j)/m_j^2}{(V^2 - 3\sigma_j)^3} \phi^{(1)} \frac{\partial \phi^{(1)}}{\partial \zeta} \\ & + \frac{n_j^{(0)} V^4}{Z_j m_j \Omega_j^2 (V^2 - 3\sigma_j)^2} \frac{\partial}{\partial \zeta} \left(\frac{\partial^2 \phi^{(1)}}{\partial \xi^2} + \frac{\partial^2 \phi^{(1)}}{\partial \eta^2} \right) + \frac{Z_j n_j^{(0)}/m_j}{V^2 - 3\sigma_j} \frac{\partial \phi^{(2)}}{\partial \zeta}.\end{aligned} \tag{8.25}$$

Substitution of the above equation into the $O(\epsilon^{5/2})$ equation derived from Poisson's equation, i.e.

$$\frac{\partial}{\partial\zeta}\left(\frac{\partial^2\phi^{(1)}}{\partial\xi^2}+\frac{\partial^2\phi^{(1)}}{\partial\eta^2}\right)+\frac{\partial^3\phi^{(1)}}{\partial\zeta^3}=n_{0h}\frac{\partial\phi^{(2)}}{\partial\zeta}$$
$$+n_{0h}\phi^{(1)}\frac{\partial\phi^{(1)}}{\partial\zeta}-\sum_j Z_j\frac{\partial n_j^{(2)}}{\partial\zeta}, \tag{8.26}$$

results in the KdV–ZK equation

$$\frac{\partial\phi^{(1)}}{\partial\tau}+a\phi^{(1)}\frac{\partial\phi^{(1)}}{\partial\zeta}+b\frac{\partial^3\phi^{(1)}}{\partial\zeta^3}+c\frac{\partial}{\partial\zeta}\left(\frac{\partial^2\phi^{(1)}}{\partial\xi^2}+\frac{\partial^2\phi^{(1)}}{\partial\eta^2}\right)=0, \tag{8.27}$$

for the first order contribution to the potential $\phi^{(1)}$. The similarity of the above equation to the KdV equation is obvious. The anisotropy inherent in the system is apparent through the appearance of the 2-D Laplacian in the above.

The coefficients a, b and c are defined as follows:

$$a=\frac{B}{A};\qquad b=\frac{1}{A};\qquad c=\frac{C}{A};$$

with

$$A = 2\sum_j\frac{Z_j^2n_j^{(0)}V/m_j}{(V^2-3\sigma_j)^2}, \tag{8.28}$$

$$B = 3\sum_j\frac{Z_j^3}{m_j^2}n_j^{(0)}\frac{(V^2+\sigma_j)}{(V^2-3\sigma_j)^3}-n_{0h}, \tag{8.29}$$

$$C = 1+\sum_j\frac{n_j^{(0)}V^4/m_j}{\Omega_j^2(V^2-3\sigma_j)^2}. \tag{8.30}$$

A and B and hence a and b are the same as in the one dimensional unmagnetized KdV equation. Consequently, ignoring the ion terms which are negligible in comparison to those of the electrons, a and b reduce to those found in chapter 7, viz. (7.15) and (7.16). Because the ion gyrofrequency is a small quantity when compared to the electron gyrofrequency, and because the former appears in the denominator of C, we cannot do away with ion

terms in this coefficient. Also, letting $m_i \to \infty$ causes C to diverge because of the definition of the ion gyrofrequency $eB/[m_i c_L \omega_{pe}]$. One is thus forced to include the ion magnetization in C and therefore c. The inability to ignore ion magnetization comes about as a result of our initial expansions where it was *a priori* assumed that the ion fluid was strongly magnetized. Thus, in view of the above discussion, c is written

$$c = \frac{1}{2}\left\{ \frac{(n_{0c}/n_{0h})^2(1 + n_{0i}/m_i\Omega_i^2)}{n_{0c}(n_{0c}/n_{0h} + 3T_c)^{1/2}} + \frac{(n_{0c}/n_{0h} + 3T_c)^{3/2}}{\Omega_e^2} \right\}, \qquad (8.31)$$

and is most often dominated by the first term involving the ion magnetization. This means that wave dispersion in this case is greatly influenced by the ion magnetization.

8.2.2 Unmagnetized ions

The assumption that the ions are magnetized, i.e. that the ion gyrofrequency is much larger than the characteristic frequencies of the wave packet, is restrictive because it requires the existence of very strong magnetic fields. This is especially relevant for the electron-acoustic wave where the frequency is characteristically larger than the ion plasma frequency. On the other hand, because of their very much larger mass and therefore Larmor radius, and their very much smaller gyrofrequency, it is often a good approximation to assume that the ions are unmagnetized when considering electron-acoustic waves. Furthermore, previous analyses and computations (Tokar & Gary 1984; Mace *et al.* 1991) (see chapters 2–4) have shown that the ion dynamics plays very little role in the physics of the electron-acoustic wave.

In this subsection we shall treat the ions as an incompressible, unmagnetized fluid with constant density

$$n_i = n_{0i}.$$

Here our analysis differs from previous works (Das & Verheest 1989). The former assumption has been used in previous chapters and was shown to be a valid approximation by our arbitrary-amplitude calculations (cf. chapter 7). The assumption that the fluid is unmagnetized requires that the ion gyrofrequency be less than the characteristic frequencies of the electron-acoustic wave packet. In this context Poisson's equation becomes

$$\nabla^2\phi = n_{0h}\exp\phi + n_c - n_{0i}$$

and the equation analogous to (8.26) derived therefrom takes the form:

$$\frac{\partial}{\partial\zeta}\left(\frac{\partial^2\phi^{(1)}}{\partial\xi^2}+\frac{\partial^2\phi^{(1)}}{\partial\eta^2}\right)+\frac{\partial^3\phi^{(1)}}{\partial\zeta^3}=n_{0h}\frac{\partial\phi^{(2)}}{\partial\zeta}+n_{0h}\phi^{(1)}\frac{\partial\phi^{(1)}}{\partial\zeta}+\frac{\partial n_c^{(2)}}{\partial\zeta}. \quad (8.32)$$

The term $\partial n_c^{(2)}/\partial\zeta$ is given by (8.25) with the subscript c substituted for j. Then the weakly-nonlinear waves are once-again governed by a KdV–ZK equation but the quantities A, B and C in this situation become

$$A = \frac{2n_{0c}V}{(V^2-3T_c)^2}, \quad (8.33)$$

$$B = -\frac{3n_{0c}(V^2+T_c)}{(V^2-3T_c)^3}-n_{0h}, \quad (8.34)$$

$$C = 1+\frac{n_{0c}V^4}{\Omega_e^2(V^2-3T_c)^2}, \quad (8.35)$$

where the electron sound speed, V, satisfies the relation

$$n_{0h}-\frac{n_{0c}}{(V^2-3T_c)^2}=0,$$

whose solution is

$$V=\left(\frac{n_{0c}}{n_{0h}}+3T_c\right)^{1/2}. \quad (8.36)$$

On comparing (8.33)–(8.35) with (8.28)–(8.30) we observe that the former are merely a special case of the latter in which the ion terms have been neglected. This is as a result of our assumption that the ion fluid is incompressible. It is noteworthy also, that we could have arrived at (8.33)–(8.35) from (8.28)–(8.30) by letting $m_i \to \infty$, but at the same time making the rather artificial assumption that $\Omega_i = \text{const}$.

Thus, once again a and b are given by (7.15) and (7.16) of chapter 7, but now c takes the form

$$c=\frac{1}{2}\left\{\frac{(n_{0c}/n_{0h})^2}{n_{0c}(n_{0c}/n_{0h}+3T_c)^{1/2}}+\frac{(n_{0c}/n_{0h}+3T_c)^{3/2}}{\Omega_e^2}\right\}. \quad (8.37)$$

and is devoid of ion terms. Note that c contains both the dispersive coefficient b of the KdV equation and a contribution involving Ω_e^2 which arises from the dispersion caused by electron magnetization.

8.3 Solitary-wave solutions of the KdV–ZK equation

8.3.1 One-dimensional solitons

We seek solutions of the KdV–ZK equation that depend on the variable (cf. Das & Verheest 1989)

$$\chi = \zeta \cos\alpha + \xi \sin\alpha - U\tau,$$

where α is the angle between the wavevector and the magnetic field $\mathbf{B}$. No loss of generality is incurred in assuming that the wave propagation direction lies in the ξ-ζ–plane because of the cylindrical symmetry about the ζ axis. Transforming the KdV–ZK equation, using the above, and integrating yields the single soliton solution

$$\phi^{(1)} = \frac{3U}{a\cos\alpha}\mathrm{sech}^2\left[\frac{1}{2}\left(\frac{U}{\cos^3\alpha(b + c\tan^2\alpha)}\right)^{1/2}\chi\right]. \tag{8.38}$$

Defining $\delta V = \epsilon U/\cos\alpha$ and the soliton velocity $M = V + \delta V$, the solution expressed in terms of our original coordinates becomes:

$$\phi = \frac{3\delta V}{a}\mathrm{sech}^2\left[\frac{1}{2}\left(\frac{\delta V}{b\cos^2\alpha + c\sin^2\alpha}\right)^{1/2}\left\{x\sin\alpha + z\cos\alpha - (M\cos\alpha)t\right\}\right]. \tag{8.39}$$

Evidently, as $\alpha \to 0$, i.e. for propagation parallel to the magnetic field, the solution reduces to that obtained in the unmagnetized case and represents a plane soliton propagating in the z–direction with speed M. In contrast to this, for $\alpha \to \pi/2$ we observe that the soliton speed vanishes and therefore it ceases to propagate. For oblique angles and constant nonlinearity, δV, the soliton speed decreases with increasing α. This type of behaviour was also observed in the linear theory of the magnetized electron-acoustic wave where the phase velocity exhibited a $\cos\alpha$ dependence on angle, being maximum for wave propagation along the magnetic field direction, and vanishing for propagation perpendicular to it.

The soliton width is given by (Das & Verheest 1989)

$$L = 2\left[\frac{b\cos^2\alpha + c\sin^2\alpha}{\delta V}\right]^{1/2},$$

and is clearly bounded by $(4b/\delta V)^{1/2} \leq L \leq (4c/\delta V)^{1/2}$ (because $c > b$). Clearly, for fixed δV the soliton width increases with an increase in α. Such behaviour has been noted by other authors (Das & Verheest 1989) in studies of magnetized ion-acoustic solitons. Das & Verheest (1989) have investigated the stability of such solutions to transverse sinusoidal perturbations. We do not address that question here but summarise their findings in the following.

They find that there is always instability if (in the present notation)

$$C \tan^2 \alpha \leq \tfrac{3}{5},$$

and in particular if $\alpha = 0$, i.e. for propagation parallel to **B**. If the above inequality is not satisfied then the condition for instability becomes

$$m^2 - \frac{5C \tan^2 \alpha - 3}{3 \cos^2 \alpha + 3C \sin^2 \alpha} l^2 > 0, \tag{8.40}$$

where l, m, n are the direction cosines of the sinusoidal perturbation. Das and Verheest (1989) have calculated the growth rates of these instabilities and found for the latter case

$$g_R^2 = \frac{4CU^2}{45(\cos^2 \alpha + C \sin^2 \alpha)^2} \Big[m^2(3 \cos^2 \alpha + 3C \sin^2 \alpha) + l^2(3 - 5C \tan^2 \alpha) \Big],$$

and for the particular case $\alpha = 0$ the growth rate obeys

$$g_R^2 = \tfrac{4}{15} CU^2(1 - n^2) = \tfrac{4}{15} CU^2 \sin^2 \chi,$$

where χ is the angle made by the direction of the perturbation with the magnetic field. They showed, in addition, that maximum growth rates occur for perturbations in the plane perpendicular to the direction of propagation of the soliton.

Continuing, some plane soliton solutions of the KdV-ZK equation are shown in figures 8.1–8.3 for the case in which *both* the ion and electron fluids are magnetized. The soliton potential is plotted against $s \equiv x \sin \alpha + z \cos \alpha - (M \cos \alpha)t$. In all the figures the condition $C \tan^2 \alpha > \frac{3}{5}$ is satisfied, viz.

$$\left\{ 1 + \frac{n_{0i}}{m_i \Omega_i^2} + \frac{n_{0c}(n_{0c}/n_{0h} + 3T_c)^2}{\Omega_e^2 (n_{0c}/n_{0h})^2} \right\} \tan^2 \alpha > \frac{3}{5},$$

and hence the solitons are stable (at least so long as condition (8.40) is not satisfied). The figures show that the effect of increasing the magnetization (gyrofrequencies) of the fluids is to cause the solitons to become narrower,

and that the effect of increasing the angle of soliton propagation with respect to **B** is to increase the width of the soliton. The dashed curves represent the "unmagnetized" $\alpha = 0°$ soliton profile. Although this soliton is unstable ($C\tan^2\alpha < \frac{3}{5}$) we have included it in the diagrams as a comparison with the unmagnetized scenario.

Figures 8.4–8.5 depict the scenario when the ion fluid is considered unmagnetized. Using (8.35) the condition for instability can be written

$$\left\{1 + \frac{n_{0c}(n_{0c}/n_{0h} + 3T_c)^2}{\Omega_e^2(n_{0c}/n_{0h})^2}\right\}\tan^2\alpha \leq \frac{3}{5}.$$

In this case the effects of magnetization, which now only apply to the cool electrons, are far less profound. As the electron gyrofrequency is increased beyond unity the profile tends asymptotically (but rather quickly so) to its unmagnetized shape. The relative widths of the solitons in the magnetized as opposed to the unmagnetized ion cases, can be understood by comparing the relative magnitudes of c in each. In the former, for the parameters that we have selected the size of c is of the order of $1/m_i\Omega_i^2 = m_i/\Omega_e^2$ and in the figures Ω_e is not greater than 10. Therefore the value of c ranges over approximately $m_i/100 \leq c \leq m_i$ and represents a large value ($c > 18$). Thus, it is not surprising that in the magnetized ion case the soliton width is large. On the other hand, in the unmagnetized ion case $c > 1$, and thus the soliton width is only maginally greater than that obtained in chapter 7 where the plasma was unmagnetized and isotropic.

It is noteworthy that in the absence of ion magnetization the solitons are unstable at $\alpha = 10°$ for the values used for the other parameters. Hence only propagation angles of 30° and 60° have been shown.

8.3.2 Multi-dimensional solitons

Defining the new normalized coordinates

$$\tau' = \tau, \qquad \xi' = \frac{\xi}{c^{1/2}}, \qquad \eta' = \frac{\eta}{c^{1/2}}, \qquad \zeta' = \frac{\zeta}{b^{1/2}},$$

the KdV–ZK equation may be cast in the form

$$\frac{\partial\phi^{(1)}}{\partial\tau'} + \frac{a}{b^{1/2}}\phi^{(1)}\frac{\partial\phi^{(1)}}{\partial\zeta'} + \frac{1}{b^{1/2}}\frac{\partial}{\partial\zeta'}\nabla_{\xi'}^2\phi^{(1)} = 0, \tag{8.41}$$

where $\nabla_{\xi'}^2 = \partial^2/\partial\xi'^2 + \partial^2/\partial\eta'^2 + \partial^2/\partial\zeta'^2$ is the Laplacian in three dimensions.

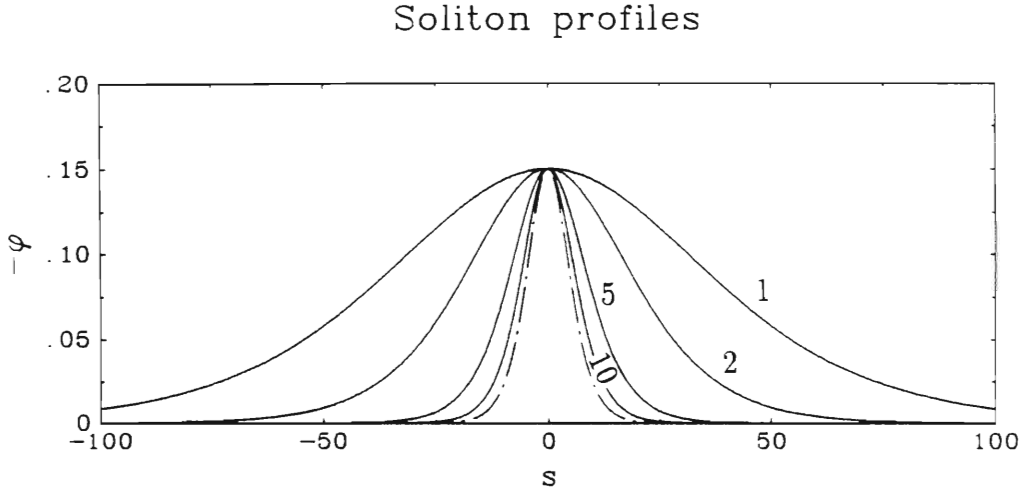

Figure 8.1: The soliton potential for various values of Ω_e (normalized) at a propagation angle of 10° with respect to **B**. The ion and electron fluids are cold ($T_c = T_i = 0$), $M = 1.1$, $n_{0c} = n_{0h} = 0.5$, $n_{0i} = 1$ and $m_i = 1836$. Here, and in figures 8.2–8.5, the curve $(- \cdot -)$ denotes the unmagnetized case.

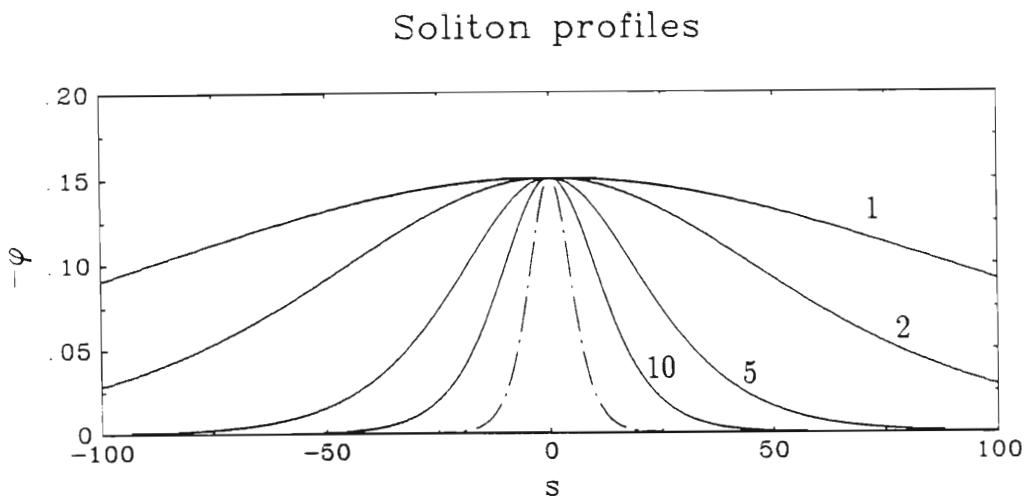

Figure 8.2: The soliton potential for various values of Ω_e (normalized) at a propagation angle of 30° with respect to B. Other parameters are as in figure 8.1.

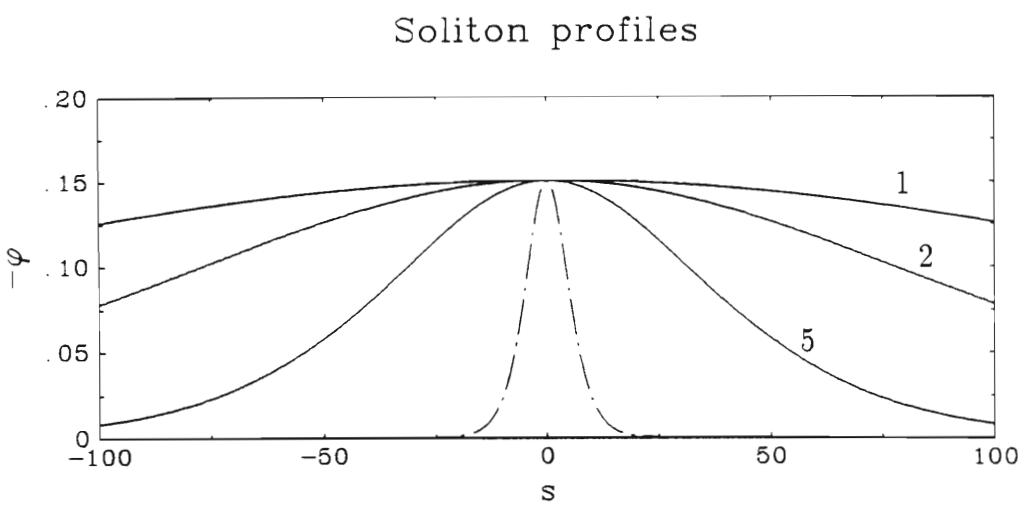

Figure 8.3: The soliton potential for various values of Ω_e (normalized) at a propagation angle of 60° with respect to B. Other parameters are as in figure 8.1.

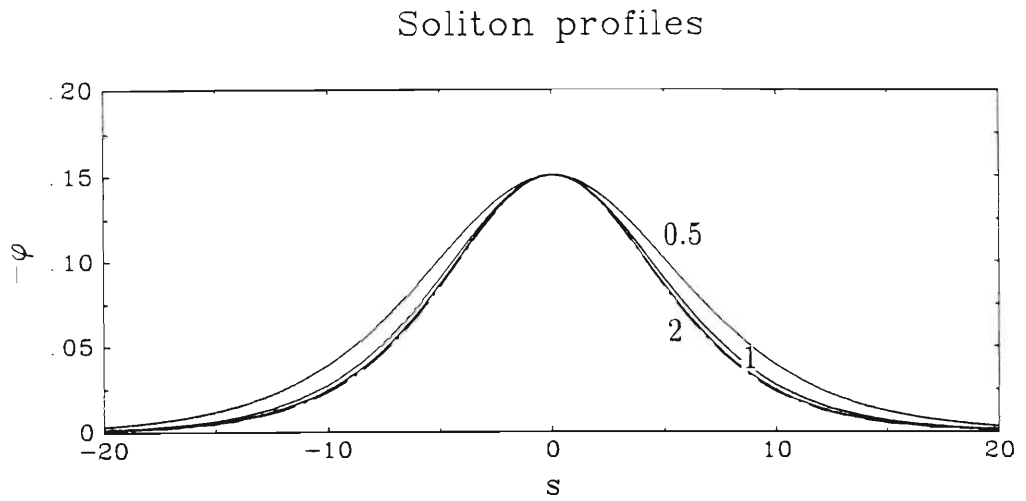

Figure 8.4: The soliton potential for various values of Ω_e (normalized) at a propagation angle of 30° with respect to **B**. Other parameters are as in figure 8.1.

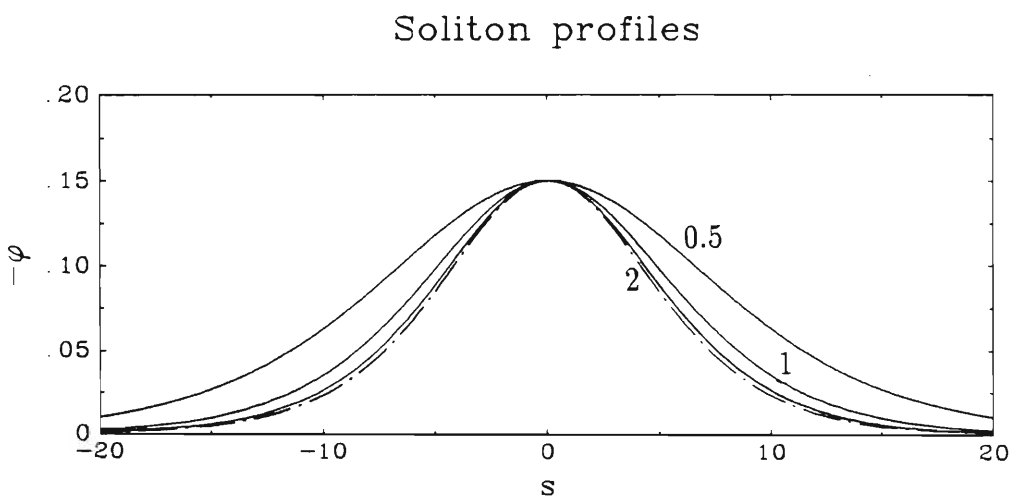

Figure 8.5: The soliton potential for various values of Ω_e (normalized) at a propagation angle of 60° with respect to **B**. Other parameters are as in figure 8.1.

With the change of variable

$$\zeta'' = \zeta' - U\tau',$$

and dropping primes in the sequel, one obtains after integration

$$-U\phi^{(1)} + \frac{a}{b^{1/2}}(\phi^{(1)})^2 + \frac{1}{b^{1/2}}\nabla_\xi^2\phi^{(1)} = 0, \tag{8.42}$$

under the supposition that $\phi^{(1)}$ and its derivatives vanish at $|\zeta| \to \infty$. Seeking spherically symmetric solutions to (8.42), the Laplacian ∇_ξ^2 can be written in the form

$$\nabla_\xi^2 = \frac{1}{r^2}\frac{\partial}{\partial r}r^2\frac{\partial}{\partial r},$$

which when substituted into (8.42) yields the equation

$$\frac{\partial^2\phi^{(1)}}{\partial r^2} + \frac{2}{r}\frac{\partial\phi^{(1)}}{\partial r} - [b^{1/2}U - \tfrac{1}{2}a\phi^{(1)}]\phi^{(1)} = 0. \tag{8.43}$$

This equation is structurally similar to the one derived by Zakharov & Kusnetsov (1975) for ion-acoustic solitons in a low-pressure magnetized plasma. Numerical calculation shows that this equation admits spherical soliton solutions that travel along the magnetic field direction. Zakharov & Kuznetsov (1975) have proven the stability of these three-dimensional soliton solutions, which, in contrast to their plane one-dimensional counterparts, are stable for propagation parallel to **B**.

We have numerically solved (8.43) for spherical solitons and a typical one is shown in figure 8.6.

Because of the normalizations these solitons are actually ellipsoidal in shape and the real transverse radius differs from the longitudinal radius by a factor of $(c/b)^{1/2}$, which means for the electron-acoustic wave, that they are larger in the transverse than in the logitudinal direction. When the magnetized ion model for c is used, then this ellipsoidal shape is more pronounced owing to the much larger value of c in that case. In fact, in that case the solitons are quasi-planar due to the large disparity between c and b. When only electron magnetization is taken into account the solitons are very nearly spherical for strong magnetization, and represent a radially decreasing (in magnitude) potential profile that propagates along the magnetic field.

Frycz & Infeld (1989) have investigated the stability of plane wave solutions of the KdV–ZK equation (8.27) in a form where the differential coefficients are unity by solving it in two dimensions as an initial-value problem.

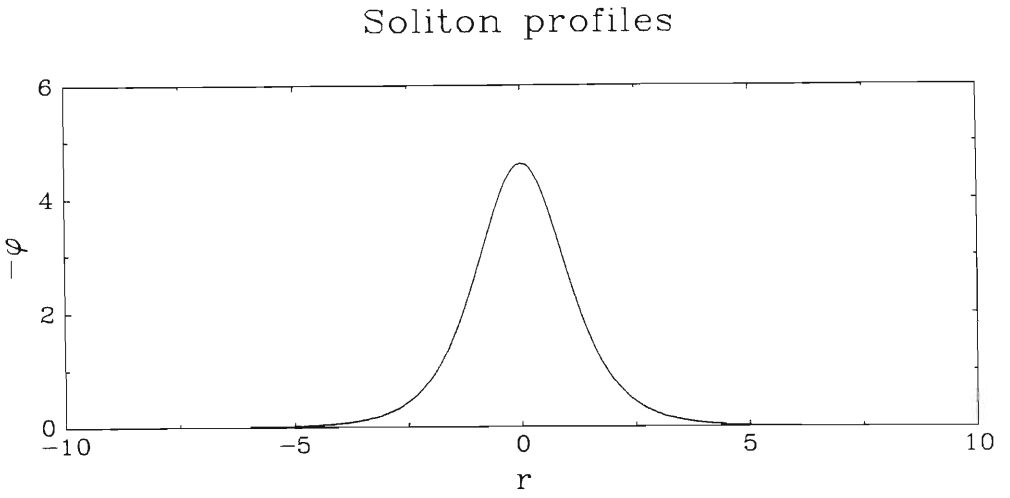

Figure 8.6: A typical spherical soliton solution of the equation (8.43) for $n_{0c} = n_{0h} = 0.5$, $n_{0i} = 1$, $T_c = T_i = 0$, $U = 1.1$, $\Omega_e = 1$, $m_i = 1836$ and the ion fluid is magnetized.

As initial-value they used a plane soliton that was sinusoidaly perturbed in a direction perpendicular to the propagation direction. They found that the perturbations undergo temporal growth with the eventual result that the plane soliton disintegrates into an array of the more stable cylindrical solitons. Unfortunately, the calculations were done in only two spatial dimensions (hence the appearance of cyclindrical solitons), however, they argue that in the full three dimensional situation these would further break up into the still more stable spherical solitons.

Finally, we conclude this chapter with some comments on the model of spherical solitons employed here. In the model we have employed a pressure equation which was derived (see appendix B) by making the assumption that the fluid component underwent one-dimensional compressions. In the case of spherical solitons, however, in which the fluids undergo approximately spherically symmetric compressions it would be more correct to employ the pressure equation

$$\frac{\partial p_j}{\partial t} + \mathbf{u}_j \cdot \nabla p_j + \tfrac{5}{3} \nabla \cdot \mathbf{u}_j = 0.$$

This equation is obtained by assuming that the fluid is ideal and therefore the pressure tensor $\mathbf{P}_j = p_j \mathbf{I}$, and then contracting equation (B.3) of appendix B by the unit tensor $\mathbf{I} = \mathbf{e}_x \otimes \mathbf{e}_x + \mathbf{e}_y \otimes \mathbf{e}_y + \mathbf{e}_z \otimes \mathbf{e}_z$ with respect to both indices.

Thus, for finite fluid pressures and therefore temperatures, the model of 3-D solitons employed here represents only a rough approximation. This does not invalidate our graphical result (figure 8.6), however, in which the fluids were supposed cold.

Chapter 9

Electron-acoustic solitons in a weakly-relativistic electron beam plasma

Relativistic plasmas play an important role in understanding many space and astrophysical phenomena such as plasma processes near black holes, quasars, pulsars, neutron stars and other ultra-dense cosmic bodies.

Of particular relevance to this chapter are the cool electron beams and associated BEN observed upstream of the earth's bow shock (Thomsen *et al.* 1983; Marsch 1985). Although the beams are generally non-relativistic they do border on the relativistic regime (see figures 1 and 2 of Thomsen *et al* 1983 where the beam speeds are $\sim 5 \times 10^8\,\mathrm{cm\,s^{-1}}$) and conceivably, under conditions of intense solar activity become weakly-relativistic. In this chapter we show that relativistic beam effects on electron-acoustic solitons appear at relatively low electron beam speeds $\sim 0.1c$ and therefore may have some importance as far as nonlinear electron-acoustic waves and solitons upstream of the earth's bow shock are concerned.

Although this work was done with the region upstream of the earth's bow shock in mind, the KdV equation derived here could also provide a model for solitons in the pulsar magnetic polar regions wherein an electron-positron plasma is continually produced (Beskin *et al.* 1983). The very strong longitudinal electric fields near the pulsar surface accelerate the plasma components to ultra-relativistic velocities in the cusp region, nevertheless, there may be regions in the pulsar magnetosphere near the poles in which the plasma is weakly relativistic, and where our KdV equation would become

applicable. Moreover, low frequency waves whose dispersion resembles that of the ion-acoustic wave have been found in theoretical studies of electron-positron plasmas (Lominadze, Melikidze & Pataraya 1984). It may be that these waves are describable by a KdV equation similar to the one derived in this chapter.

There have been a number of studies of ion-acoustic solitons in relativistic plasmas (Das & Paul 1985; Roychoudhury & Bhattacharyya 1987; Nejoh 1987a; Nejoh 1987b; Das, Karmakar & Paul 1988; Chowdhury, Pakira & Paul 1989; Yadav & Sharma, 1989; Salahuddin 1990; Singh & Dahiya 1990), however, the electron-acoustic wave has only had passing attention in this respect (Chowdhury, Pakira & Paul 1988). This chapter investigates, in the main, electron-acoustic solitons at both small and large amplitude, in a plasma composed of a weakly-relativistic electron beam as well as stationary hot electrons and ions.

9.1 Basic equations

The equations governing the dynamics of a relativistic (relativistically cool $T \ll mc^2$), infinite, one-dimensional, homogeneous, unmagnetized, collisionless plasma comprising Boltzmann electrons and any number of electron and (positive or negative) ion fluid species are (cf. Nejoh 1987a, appendix G)

$$\frac{\partial n_j}{\partial t} + \frac{\partial}{\partial x}(n_j u_j) = 0, \tag{9.1}$$

$$n_j m_j \left(\frac{\partial}{\partial t} + u_j \frac{\partial}{\partial x}\right)(\gamma_j u_j) = -\frac{\partial p_j}{\partial x} - Z_j n_j \frac{\partial \phi}{\partial x}, \tag{9.2}$$

$$\frac{\partial p_j}{\partial t} + u_j \frac{\partial p_j}{\partial x} + 3p_j \frac{\partial}{\partial x}(\gamma_j u_j) = 0, \tag{9.3}$$

$$\frac{\partial^2 \phi}{\partial x^2} = n_{0h} \exp \phi - \sum_{j=i,c} Z_j n_j. \tag{9.4}$$

Considering only weakly-relativistic effects we expand γ_j as follows

$$\gamma_j = 1 + \frac{1}{2}\frac{u_j^2}{c^2},$$

where the subscript j refers to the jth fluid component.

In addition, we impose the following boundary conditions

$$\left.\begin{array}{lll} \phi \to 0, & \dfrac{\partial \phi}{\partial x} \to 0, & \dfrac{\partial^2 \phi}{\partial x^2} \to 0, \\ n_j \to n_{0j}, & p_j \to p_{0j}, & u_j \to u_{0j}, \end{array}\right\} \quad \text{as} \quad |x| \to \infty. \tag{9.5}$$

It is appropriate to point out that a number of authors (Das & Paul 1985; Nejoh 1987a; Nejoh 1987b; Das, Karkamar & Paul 1988; Singh & Dahiya 1990) have considered plasmas in which there is equilibrium relativistic streaming with velocity u_0, but have imposed the condition that $u \to 0$ as $|x| \to \infty$. We take the view of Roychoudhury & Bhattacharyya (1987) that the boundary conditions are more correctly specified in this case by $u \to u_0$ as $|x| \to \infty$, as in (9.5) above. The normalizations of the above equations are the same as those employed in chapter 7 (Mace *et. al.* 1991b), viz. lengths by the hybrid Debye length $(T_h/4\pi n_{0e}e^2)^{1/2}$, time by the inverse electron plasma frequency $(m_e/4\pi n_{0e}e^2)^{1/2}$, number densities by the total electron density n_{0e}, pressures by $n_{0e}T_h$, temperatures by T_h, electrostatic potential by T_h/e, velocities by $(T_h/m_e)^{1/2}$, masses by the electron proper mass m_e; and $Z_j \equiv q_j/e$.

9.2 Small-amplitude solitons

9.2.1 Multispecies plasma

We employ the now familiar asymptotic technique of reducing the original system of dynamical equations to the KdV equation. The derivation of the relativistic KdV equation is essentially a generalisation of the derivation outlined in chapter 7 and is presented in appendix G.

We consider a weakly-relativistic electron-acoustic wave packet propagating along the x–direction. As before the wavenumbers of the harmonics that constitute the wave packet are assumed small, $k\lambda_{Dh} \ll 1$, allowing the following expansion of the dispersion relation (obtained by a linearisation of (9.1)–(9.4) in unnormalized form),

$$\omega \simeq k u_{0c} + k\frac{v_{se}}{\Gamma_c} - \tfrac{1}{2}k^3\lambda_{Dh}^2\frac{v_{se}}{\Gamma_c},$$

where $\Gamma_c = 1 + \frac{3}{2}(u_{0c}/c)^2$. To comply with the assumption that the waves are weakly-relativistic we furthermore require that $u_{0c} \ll c$.

The above dispersion relation implies the usual one dimensional coordinate stretchings, cf. chapter 7,

$$\xi = \epsilon^{1/2}(x - Vt) \qquad \tau = \epsilon^{3/2}t, \tag{9.6}$$

and we expand the macroscopic quantities in terms of ϵ:

$$\left.\begin{aligned} n_j &= n_j^{(0)} + \epsilon n_j^{(1)} + \epsilon^2 n_j^{(2)} + \cdots, \\ u_j &= u_j^{(0)} + \epsilon u_j^{(1)} + \epsilon^2 u_j^{(2)} + \cdots, \\ p_j &= p_j^{(0)} + \epsilon p_j^{(1)} + \epsilon^2 p_j^{(2)} + \cdots, \\ \phi &= \epsilon\phi^{(1)} + \epsilon^2\phi^{(2)} + \cdots. \end{aligned}\right\} \tag{9.7}$$

We remark here, parenthetically, that although we consider in the main electron-acoustic waves, the following analysis is fairly general, applying to all waves admitted by the plasma, whose dispersion relation can be written $\omega \sim \alpha k + \beta k^3$ in the weakly-dispersive limit (see § 9.2.3).

Following the same procedure that was employed for the non-relativistic case in chapter 7, we substitute the above stretchings (9.6) and expansions (9.7) into (9.1)–(9.4) and solve for $\phi^{(1)}$ (see for e.g. Nejoh 1987a and appendix G) yielding the Korteweg–de Vries (KdV) equation for weakly-relativistic waves:

$$\frac{\partial\phi^{(1)}}{\partial\tau} + a\phi^{(1)}\frac{\partial\phi^{(1)}}{\partial\xi} + b\frac{\partial^3\phi^{(1)}}{\partial\xi^3} = 0. \tag{9.8}$$

The coefficients a and b are given by

$$a = \frac{B}{A}, \qquad b = \frac{1}{A},$$

$$A = 2\sum_j \frac{Z_j^2}{m_j}\frac{n_j^{(0)}\lambda_j}{\Gamma_j(\lambda_j^2 - 3\sigma_j)^2}, \tag{9.9}$$

$$B = 3\sum_j \frac{Z_j^3}{m_j^2}\left\{\frac{n_j^{(0)}(\lambda_j^2 + (3\Gamma_j - 2)\sigma_j)}{\Gamma_j^2(\lambda_j^2 - 3\sigma_j)^3} - \frac{u_j^{(0)}}{c^2}\frac{n_j^{(0)}\lambda_j}{\Gamma_j^3(\lambda_j^2 - 3\sigma_j)^2}\right\} - n_{0h}, \tag{9.10}$$

where

$$\lambda_j = V - u_j^{(0)}, \quad \Gamma_j = 1 + \frac{3}{2}\left(\frac{u_j^{(0)}}{c}\right)^2, \quad \sigma_j = \frac{p_j^{(0)}}{m_j n_j^{(0)}} = \frac{T_j}{m_j},$$

and V, the phase velocity in the weakly-dispersive limit, satisfies the linear ($O(\epsilon)$) dispersion relation

$$n_{0h} - \sum_j \frac{n_j^{(0)} Z_j^2/m_j}{\Gamma_j(\lambda_j^2 - 3\sigma_j)} = 0. \tag{9.11}$$

The KdV equation admits the familiar soliton solution

$$\phi = \frac{3\delta V}{a}\text{sech}^2\left[\left(\frac{\delta V}{4b}\right)^{1/2}\{x - Mt\}\right], \tag{9.12}$$

in terms of the original coordinates. As before the soliton speed is defined by

$$M \equiv V + \delta V = V + \epsilon U,$$

with the soliton amplitude given by

$$\phi_0 \equiv \frac{3\delta V}{a}.$$

The soliton solution (9.12) differs from that obtained in chapter 7 only in the definitions of a and b (A and B).

It is interesting to note that the coefficients a, b only include relativistic contributions due to the zeroth-order drifts u_{0j}. Thus, if $u_{0j} \to 0$ then the relativistic effects disappear altogether (see later). This is fundamentally different to the pseudo-potential (arbitrary-amplitude) approach to be introduced later, where relativistic effects due to the fluid velocity are included to all orders, as well as allowing for the possibility that the soliton speed, itself, may be relativistic even if there is no equilibrium streaming.

It is instructive to consider the following limiting cases of the equations for A and B, viz. the zero drift case,

$$u_j^{(0)} = 0, \qquad \Gamma_j = 1, \qquad \lambda_j = V, \tag{9.13}$$

and the non-relativistic drift situation,

$$\frac{u_j^{(0)}}{c} \to 0, \qquad \Gamma_j \to 1. \tag{9.14}$$

In the first case (9.13), the relativistic effect disappears completely and one recovers (7.11) and (7.12). In the second case (9.14) the coefficients A and

B become

$$A = 2\sum_j \frac{Z_j^2}{m_j}\frac{n_j^{(0)}\lambda_j}{(\lambda_j^2 - 3\sigma_j)^2},$$

$$B = 3\sum_j \frac{Z_j^3}{m_j^2}\frac{n_j^{(0)}(\lambda_j^2 + \sigma_j)}{(\lambda_j^2 - 3\sigma_j)^3} - n_{0h},$$

and the dispersion relation reduces to

$$n_{0h} - \sum_j \frac{n_j^{(0)} Z_j^2/m_j}{\lambda_j^2 - 3\sigma_j} = 0.$$

These equations differ from those obtained in the former case (9.13) by the appearance of $\lambda_j = V - u_{0j}$ in place of V, only, and describe a plasma in which each fluid species j has a non-relativistic drift $u_j^{(0)} \equiv u_{0j}$ parallel/anti-parallel to the direction of wave propagation. They represent still a further generalisation of the KdV equation derived in chapter 7.

Thus the KdV equation incorporating non-relativistic fluid drifts remains similar, in form, to that obtained in the stationary case, provided we introduce the relative velocities λ_j with respect to the jth drifting species to replace V in the stationary theory. On the other hand, the KdV equation incorporating weakly-relativistic drifts exhibits relativistic effects, but only due to the zeroth-order (equilibrium) drift speeds of each particle component.

9.2.2 Case study: electron-acoustic solitons

Restricting the number of fluid components to two—a stationary, massive ion, and a cool, relativistically-streaming electron component—we recover the KdV equation for weakly-nonlinear, weakly-relativistic electron-acoustic waves. Neglecting the ion terms in (9.9), (9.10) and (9.11), as was done in previous chapters, results in considerable simplification: the sound speed reduces to

$$V = u_{0c} + \left(\frac{n_{0c}/n_{0h}}{\Gamma_c} + 3\sigma_c\right)^{1/2}, \tag{9.15}$$

and is illustrated, for a number of cool electron temperatures, in figure 9.1; and the nonlinear and dispersive coefficients of the KdV equation become,

respectively

$$a = \frac{3}{2\Gamma_c^2}\frac{u_{0c}}{c^2} - \frac{(n_{0c}/n_{0h})^2 + 3[n_{0c}/n_{0h} + \sigma_c\Gamma_c(1+3\Gamma_c)]}{2\Gamma_c^{1/2}(n_{0c}/n_{0h})(n_{0c}/n_{0h} + 3\sigma_c\Gamma_c)^{1/2}}, \quad (9.16)$$

$$b = \frac{(n_{0c}/n_{0h})^2}{2\Gamma_c^{1/2} n_{0c}(n_{0c}/n_{0h} + 3\sigma_c\Gamma_c)^{1/2}}. \quad (9.17)$$

(We have used $\sigma_c \equiv T_c$ in the above to avoid confusion of T_c with Γ_c, the temperature and relativistic factor, respectively.)

These coefficients differ in two respects from those found in chapter 7 for the non-drifting situation: (i) they contain the relativistic factor Γ_c due to the cool electron streaming; and (ii) the relativistic beam introduces a positive contribution to the nonlinear coefficient, b. Compressive electron-acoustic solitons are ruled out, however, by the unphysically (and inconsistently) large velocities required for their existence, $u_0 \sim c^2$. The functional form of these coefficients is similar to that found by Nejoh (1987a) for ion-acoustic waves in a weakly-relativistic plasma, but in that case only compressive solitons were found, and the relativistic beam introduced a negative contribution to the nonlinear coefficient.

Thus, on physical grounds we expect $\phi_0 < 0$ and for real-valuedness of our soliton solution, (9.12), we further demand $M > V$, i.e. the weakly-nonlinear, relativistic electron-acoustic solitons are respectively, rarefactive and travel at velocities greater than the linear electron-acoustic sound (phase) speed. We defer discussion of the effects of beam velocity and temperature on the electron-acoustic solitons, until §9.4 where they are discussed in detail.

9.2.3 Case study: solitons in an electron-positron plasma

Considering one of the simpler models for an electron-positron plasma, i.e. assuming that the electrons are hot and Boltzmann-like and that the positrons are cool and fluid-like, and stream relativistically with velocity u_{0p} one obtains from (9.11) (the sum reduces to $j = p$) the sound speed for acoustic waves in a streaming electron-positron plasma:

$$V = u_{0p} + \left(\frac{1}{\Gamma_p} + 3\sigma_p\right)^{1/2}, \quad (9.18)$$

where the subscript p refers to positron parameters. Low frequency sound solutions to the dispersion relation for electrostatic waves in a relativistic

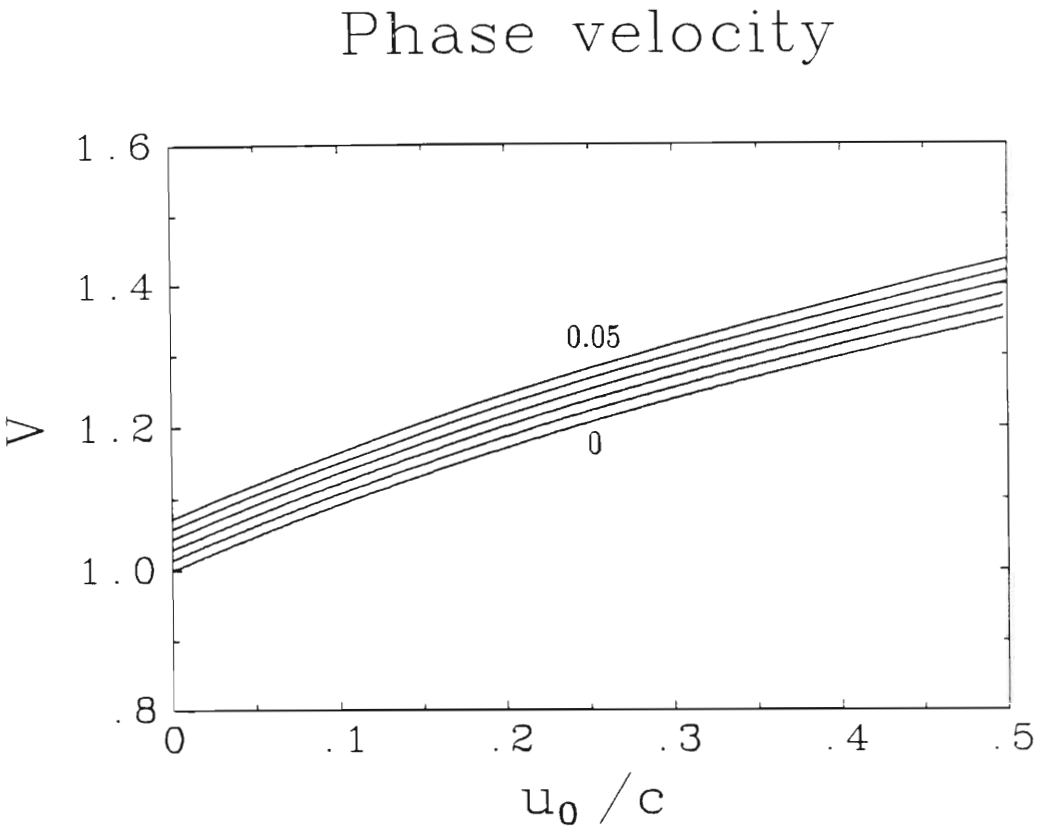

Figure 9.1: The linear phase velocity of the electron-acoustic wave as a function of cool electron beam speed for various cool electron and ion temperatures. The parameter labelling the curves is $T_c = T_i$. The increment in temperature from a lower curve to one immediately above is 0.01.

electron-positron plasma have been found before (Polyakov 1983), however their physical essence is vague (Lominadze *et al.* 1984). Comparing (9.18) with (9.15) one immediately observes the similarity in form.

It is easy to show that in this model the coefficients a and b reduce to

$$a = \frac{1+\frac{3}{2}\sigma_p\Gamma_p(1+3\Gamma_p)}{[\Gamma_p(1+3\sigma_p\Gamma_p)]^{1/2}} - \frac{3}{2}\frac{u_{0p}}{\Gamma_p c^2}, \tag{9.19}$$

$$b = \frac{1}{2[\Gamma_p(1+3\sigma_p\Gamma_p)]^{1/2}}, \tag{9.20}$$

which, are the same coefficients (disregarding multiplicative constants) obtained by Nejoh (1987a) in his investigation of ion acoustic waves in which the ions formed a warm beam component. It must be remembered, however, that our normalizations are based on electron parameters whereas in the former work the normalizations were based on those of the ions. Therefore the phase velocity of the wave in the former is much smaller than that presented here and, in addition, the time-scales implied in the former are much slower than those here.

Inspecting the coefficients a and b it is immediately apparent that for realistic parameters, both are positive. Therefore, solitons given by (9.12) with (9.19) and (9.20) will be compressive, $\phi > 0$, with an overfilling of the positive potential by positrons, and a depletion in the number density of hot electrons in that region. Furthermore, they are supersonic and travel at speeds greater than the sound speed given by (9.18).

9.3 Arbitrary-amplitude formulation

Assuming as in the nonrelativistic theory of chapter 7, that the various macroscopic quantities depend on the variable

$$s = x - Mt,$$

where M is a normalized velocity, enables (9.1) to be integrated immediately, yielding u_j as a function of n_j:

$$u_j = \frac{n_{0j}}{n_j}(u_{0j} - M) + M. \tag{9.21}$$

Substitution of the latter equation into (9.3) and solving for p_j as a function of n_j:

$$p_j = p_{0j}\left(\frac{n_j}{n_{0j}}\right)^{3(1+3M^2/2c^2)}$$

$$\cdot \exp\left\{ \frac{9}{4c^2}(u_{0j} - M)^2 \left(1 - \left(\frac{n_{0j}}{n_j}\right)^2\right) + \frac{9}{c^2} M(u_{0j} - M)\left(1 - \frac{n_{0j}}{n_j}\right)\right\}. \tag{9.22}$$

The above equation is the generalization of the more familiar adiabatic law $p_j n_j^{-3} = p_{0j} n_{0j}^{-3}$ to include the effects of special relativity. The momentum equation (9.2), after integration, may be cast in the form

$$\left[-Mu_j + \frac{1}{2}u_j^2 - \frac{1}{2}\frac{Mu_j^3}{c^2} + \frac{3}{8}\frac{u_j^4}{c^2}\right]_{u_{0j}}^{u_j} + \frac{1}{m_j}\left[\frac{p_j}{n_j}\right]_{n_{0j}}^{n_j} + \frac{1}{m_j}\int_{n_{0j}}^{n_j} \frac{p_j}{n_j^2}\,\mathrm{d}n_j = -\frac{Z_j}{m_j}\phi, \tag{9.23}$$

which, together with (9.21) and (9.22) above, yields an implicit relation for the function $n_j(\phi)$. Recall that in the non-relativistic pseudo-potential theory of chapter 7 we were able to explicitly solve for $n_j(\phi)$ and found that it was double-valued. Plotting (9.23) shows that this is still the case when relativistic effects are included, and as was done in that chapter, we select the smaller root for the definition of $n_j(\phi)$. This ensures the continuity of n_j at $\sigma_j = 0$.

It is noteworthy that both equations (9.22) and (9.23) exhibit weakly relativistic effects even at vanishing beam velocity u_{0j}, which contrasts strongly with the small-amplitude theory (see earlier discussions). In the absence of a relativistic beam these effects may nevertheless arise if the soliton velocity ('Mach number' M) is relativistic.

With $n_j(\phi)$ determined the Poisson equation can be integrated in the usual way by defining the Sagdeev potential

$$\Psi(\phi) = \int_0^{\phi} \left(\sum_j Z_j n_j(\phi') - n_{0h} \exp \phi'\right) \mathrm{d}\phi',$$

yielding (on using the boundary conditions)

$$\frac{1}{2}\left(\frac{\mathrm{d}\phi}{\mathrm{d}s}\right)^2 + \Psi(\phi) = 0. \tag{9.24}$$

Subjecting the Sagdeev potential to the following constraints

$$\Psi(0) = \frac{\mathrm{d}\Psi}{\mathrm{d}\phi}(0) = 0; \quad \Psi(\phi_0) = 0; \quad \Psi(\phi) < 0 \quad \text{for} \quad 0 < |\phi| < |\phi_0|; \tag{9.25}$$

enables soliton solutions of (9.24) to be found by a method similar to that of Mace *et al.* (1991a) and Baboolal *et al.* (1989) which was used in chapter 7.

9.4 Intermediate- to large-amplitude solitons: numerical results

In this section we present the full nonlinear solution of the system of equations (9.21)–(9.25) for intermediate- to strongly-nonlinear solitons. The number of fluid components has been restricted to two—a stationary proton ($u_{0i} = 0$) and a cool, relativistically-streaming electron component (henceforth we omit the c subscript on u_{0c}). This plasma configuration permits the investigation of electron-acoustic solitons in weakly-relativistic plasma. The calculations are performed in the inertial frame of the protons and hot, Boltzmann electrons, hereafter referred to as the laboratory frame. The following standard parameter values have been used in the calculations: $n_{0c} = n_{0h} = 0.5$, $n_{0i} = 1$, $m_i = 1836$ and $u_{0i} = 0$.

Figure 9.2 illustrates the effect on the electron-acoustic soliton profiles, of increasing u_0/c whilst keeping δV, a measure of the nonlinearity (or dispersion) of the system, constant and equal to 0.3. The magnitude of the amplitude of the solitons is found to increase with increasing u_0/c, i.e. relativistic beam speed. This effect is also predicted by KdV theory where the coefficient, a, (9.16) is found to decrease (in magnitude) with u_0 yielding an increase in the magnitude of the soliton amplitude.

In figure 9.3 we quantify this. In addition, we illustrate the effect of varying the beam temperature on the soliton maximum amplitude. The effect of a finite temperature is twofold: it causes a decrease in soliton amplitude $|\phi_0|$ (cf. chapter 7 for the non-relativistic case); but more importantly it restricts the allowable range of u_0 over which soliton solutions can be found. This effect becomes more profound for stronger nonlinearity (see figure 9.4). Although the KdV theory does exhibit the decrease in soliton amplitude with temperature (cf. equation (9.16)), it does not put any further constraints on the value of u_0 other than those necessary to ensure only weak relativistic effects.

We have found that if the beam is cold, $\sigma_c \equiv T_c = 0$, then there is no cutoff value of u_0 within the allowable, weakly-relativistic range ($0 \leq u_0 < 0.5c$). On the other hand, for finite T_c there is an upper limit on u_0 determined by the condition that equation (9.23) is satisfied by a complex value of n_c. This point indicates parameter values for which cool electron

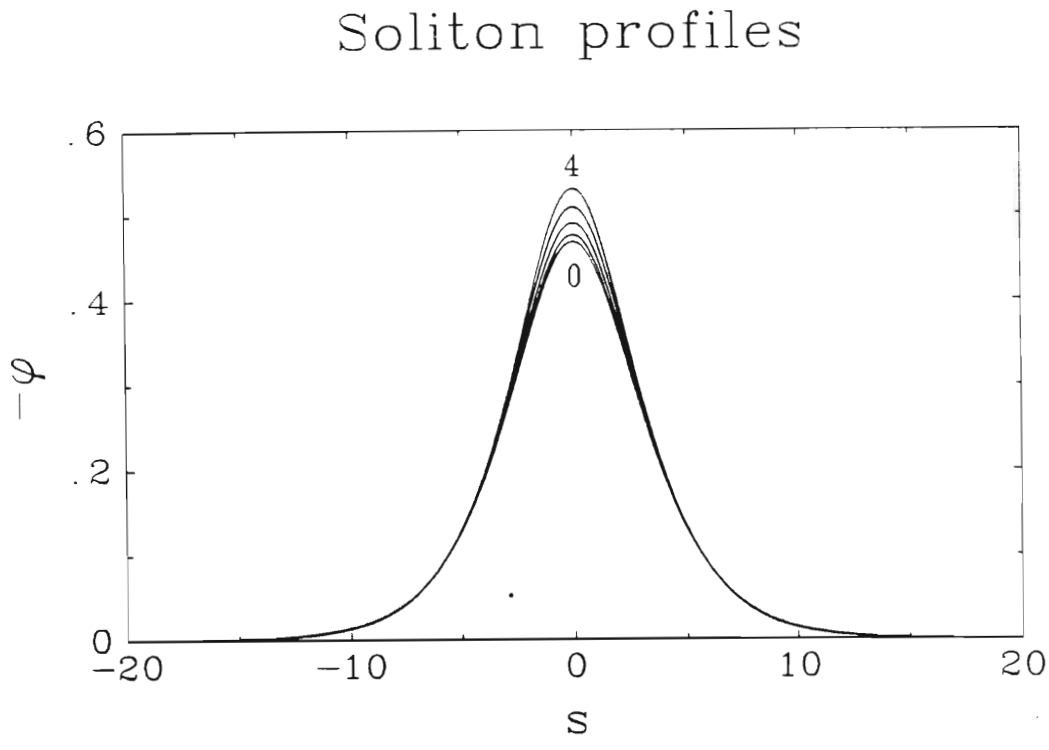

Figure 9.2: Soliton profiles for various cool electron beam speeds: $\delta V = 0.3$, $T_c = T_i = 0.01$, $c = 10$, and the parameter labelling the curves is the beam speed. The increment in beam speed from a lower curve to one immediately above is 1.

momentum "conservation" is violated.

The physical reason for this occurrence lies in the fact that finite beam temperature weakens the wave dispersion, which in turn reduces the phase mixing, of an electron-acoustic wave packet similar to that discussed in chapter 7. This can be seen by consideration of the soliton solution, (9.12). Increasing T_c increases b and hence the soliton width, which is coupled to the decrease in soliton amplitude (increase in a). Thus, we deduce that there has been a reduction in the dispersion of the wave packet which consists primarily of low-k Fourier components.

More generally, this can be seen by analysing the dispersion relation $\Omega(K)$, where Ω and K are normalized frequency and wavenumber, respectively. The larger the quantity $|\mathrm{d}\Omega/\mathrm{d}K| - |\mathrm{d}^2\Omega/\mathrm{d}K^2| \equiv \Delta$, the weaker the wave dispersion and hence the effects of phase mixing (Taniuti & Nishihara 1983). Equation (9.15), valid in the long-wavelength regime, implies

$$\frac{\Omega}{K} = u_{0c} + \left(\frac{n_{0c}/n_{0h}}{\Gamma_c} + 3T_c\right)^{1/2} = \frac{\mathrm{d}\Omega}{\mathrm{d}K},$$

$$\frac{\mathrm{d}^2\Omega}{\mathrm{d}K^2} = 0,$$

and clearly, increasing T_c increases Δ which in turn weakens the wave dispersion. The dispersion relation obtained via linearization of (9.1)–(9.4) and valid at shorter wavelengths,

$$\frac{\Omega}{K} = u_{0c} + \left[\frac{n_{0c}/n_{0h}}{\Gamma_c(1 + K^2/n_{0h})} + 3T_c\right]^{1/2},$$

though rendering more cumbersome expressions, exhibits this same trend.

Now by increasing the beam speed we eventually reach a point at which the dispersion can no longer balance the nonlinearity, and where a single soliton solution ceases to be valid. At such points the soliton structure may break down rendering a train of solitons together with a precursor (Nejoh 1987b).

Although KdV theory does not explicitly yield these critical temperatures and beam speeds (which really lie ouside of the region of applicability of the theory anyway), such points have been predicted by many authors (Das & Paul 1985; Nejoh 1987a; Nejoh 1987b) on the basis of the increase in soliton amplitude with beam velocity exhibited in small-amplitude theories (and by implication, an argument similar to that given above). However,

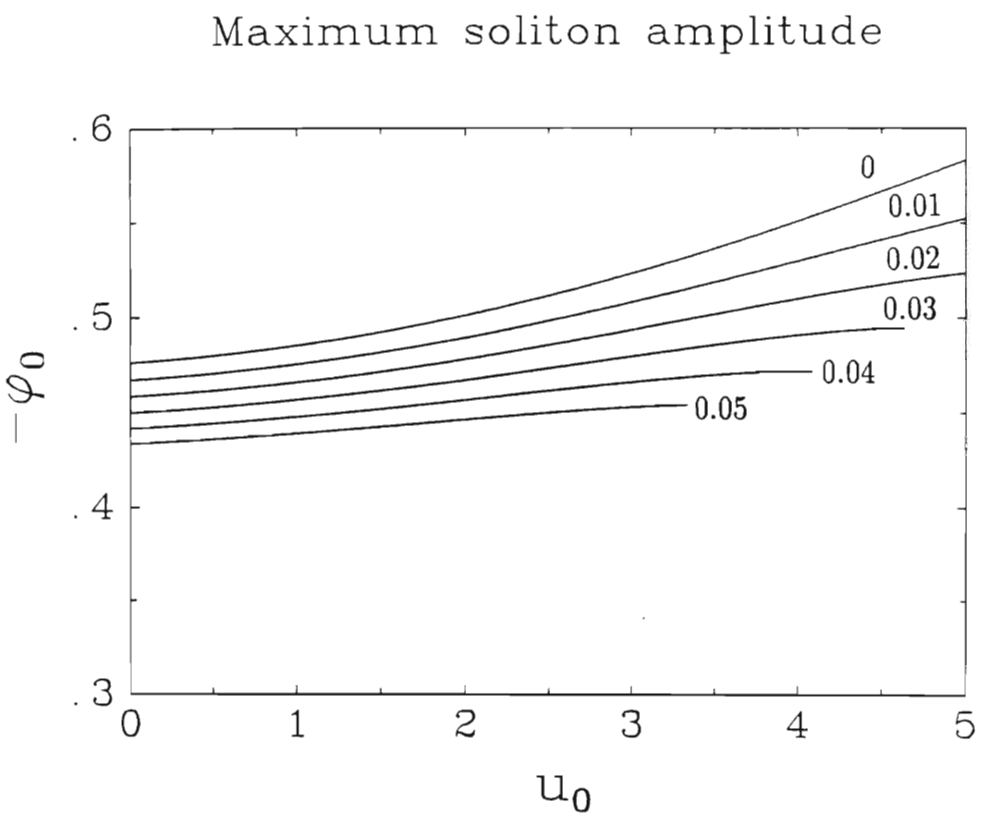

Figure 9.3: Maximum soliton amplitude as a function of beam speed for various cool electron and ion temperatures, for weak nonlinearity $\delta V = 0.3$. The value of $c = 10$ and the parameter labelling the curves is $T_c = T_i$.

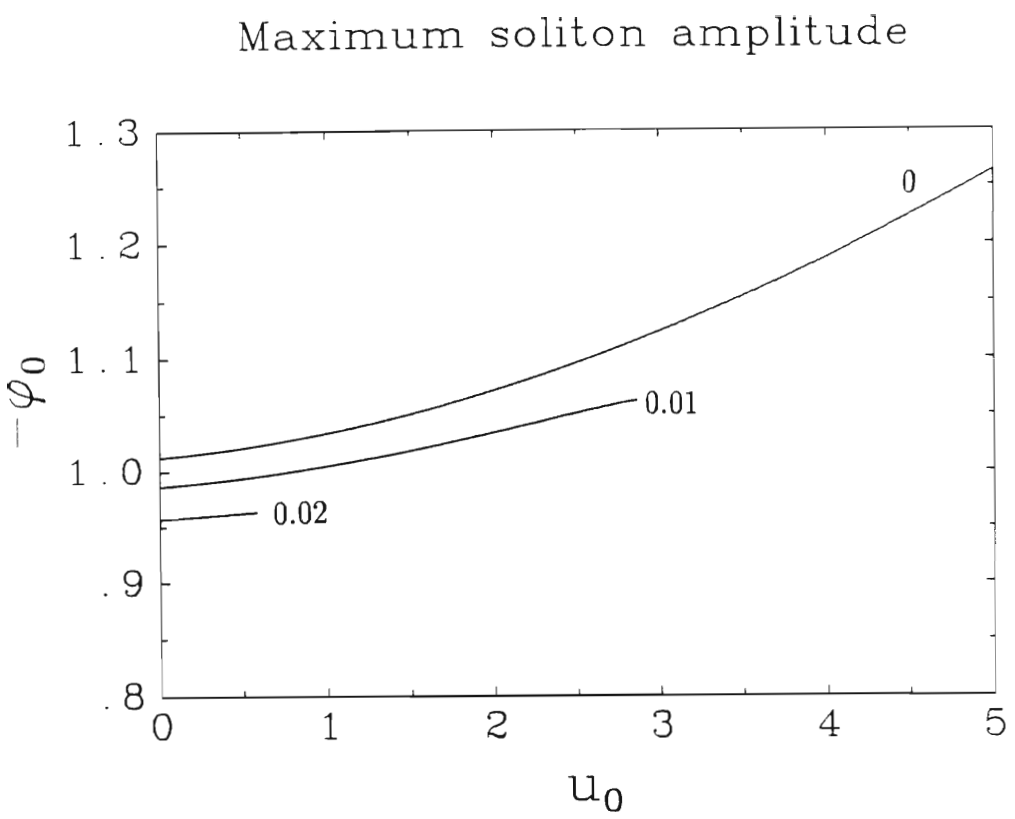

Figure 9.4: Maximum soliton amplitude as a function of beam speed for various cool electron and ion temperatures for relatively large nonlinearity $\delta V = 0.6$. The value of $c = 10$ and the parameter labelling the curves is $T_c = T_i$.

it would appear that until now there has been no quantitative evidence for them in relativistic plasmas, as illustrated here.

Recall that we have normalized all velocities by the hot electron thermal velocity, which for realistic electron density ratios is commensurate with the electron sound speed $v_{se} = (n_{0c}/n_{0h})^{1/2} v_h$. Thus by choosing different values of the speed of light c, one is actually varying the ratio of the speed of light to the hot electron thermal speed. The soliton amplitude as a function of u_0 is illustrated for various values of c in two different scenarios. In figure 9.5, for fixed u_0, one finds that there is a strong dependence of $|\phi_0|$ on c and hence u_0/c, i.e. the strength of the relativistic effect. We note (i) that for $c = 100$, which implies a very weak relativistic effect, there is very little dependence of $|\phi_0|$ on u_0, agreeing with the results for the non-relativistic case (§9.2.1), and (ii) for $c = 10$, the beam velocity $u_0 = 5$ lies at the limits of our approximation.

In figure 9.6 we have plotted the soliton magnitude versus u_0/c. By altering the value of c at constant u_0/c one changes only the value of the hot electron thermal velocity and hence the beam/soliton 'Mach number'. It is observed that increasing c decreases the value of the soliton magnitude, which is in agreement with figure 9.5, however, now the change is not as dramatic as in that case. This may be seen, qualitatively, from equation (9.16), where an increase in c for constant u_0/c yields a small increase in the magnitude of a and hence a decrease in $|\phi_0|$. It is noteworthy that the larger the value of c, the more supersonic/hypersonic the beam speed, e.g., when $c = 100$ and $u_0/c = 0.5$ the 'Mach number' of the beam is 50.

Figure 9.7 provides a comparison of the arbitrary-amplitude theory with the small-amplitude KdV theory. One observes that there is a significant difference in the amplitudes predicted by the two theories, even for the relatively small value of $\delta V = 0.3$ depicted here. More importantly, the small-amplitude theory does not exhibit the cutoff beam speeds where the balance between nonlinearity and dispersion breaks down.

9.5 A note on interpretation

In non-relativistic studies of solitons and/or double layers one often encounters the phrase "...and tranforming into the stationary frame defined by $s = x - Mt$,...". This phrase, although quite correct in non-relativistic theories, is completely incorrect in relativistic theories and for this reason we have judiciously steered away from its use in this chapter. Were we to trans-

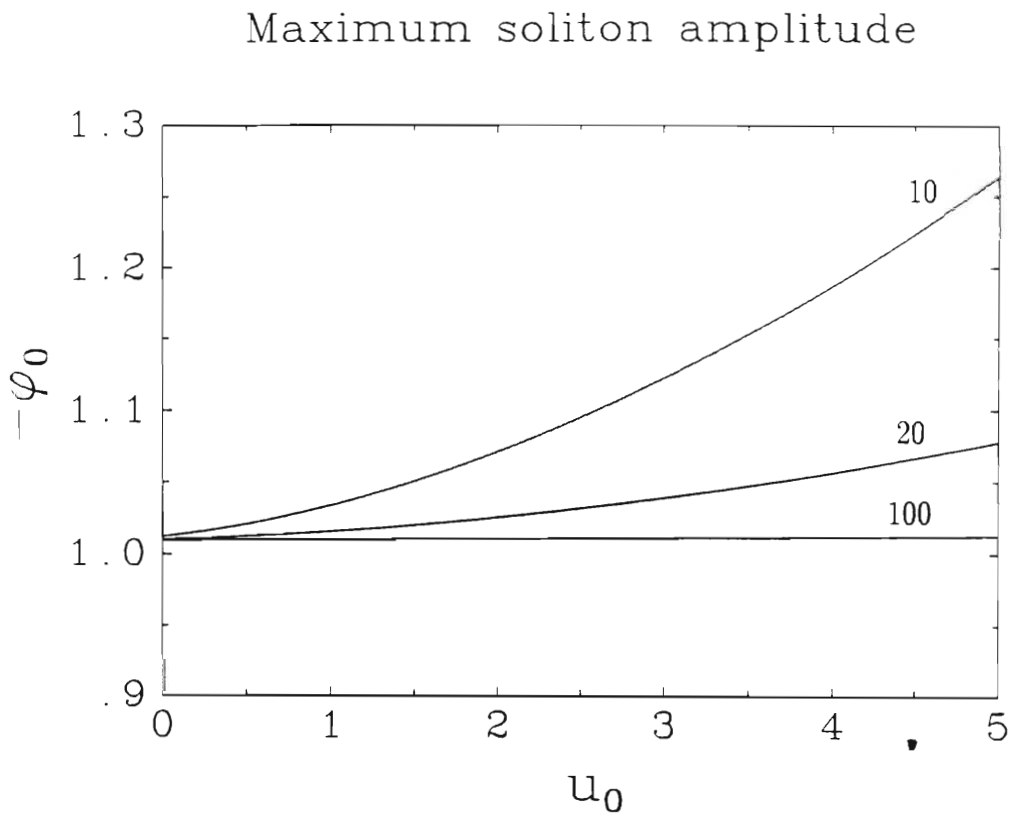

Figure 9.5: Maximum soliton amplitude as a function of beam speed for various values of c. The fluid temperatures are $T_c = T_i = 0$, and $\delta V = 0.6$. The parameter labelling the curves is c.

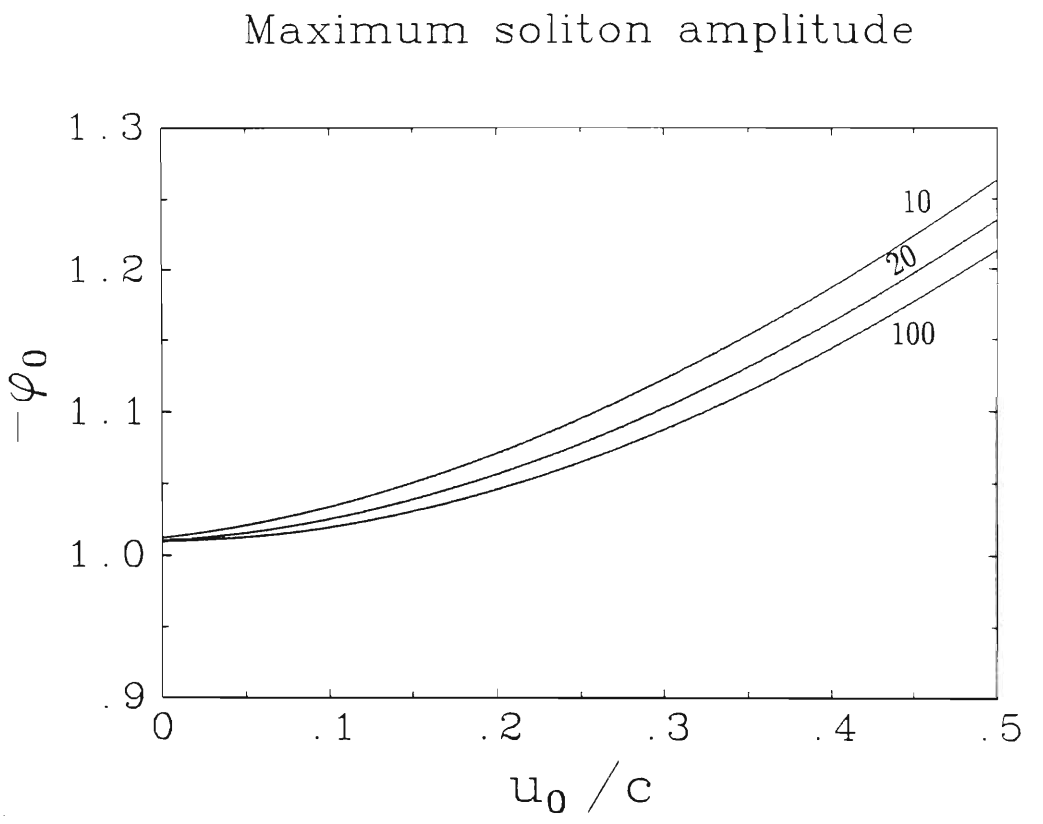

Figure 9.6: Maximum soliton amplitude as a function of beam speed relative to c, for various values of c. The electron and ion fluids are cold $T_c = T_i = 0$, and $\delta V = 0.6$. The parameter labelling the curves is c.

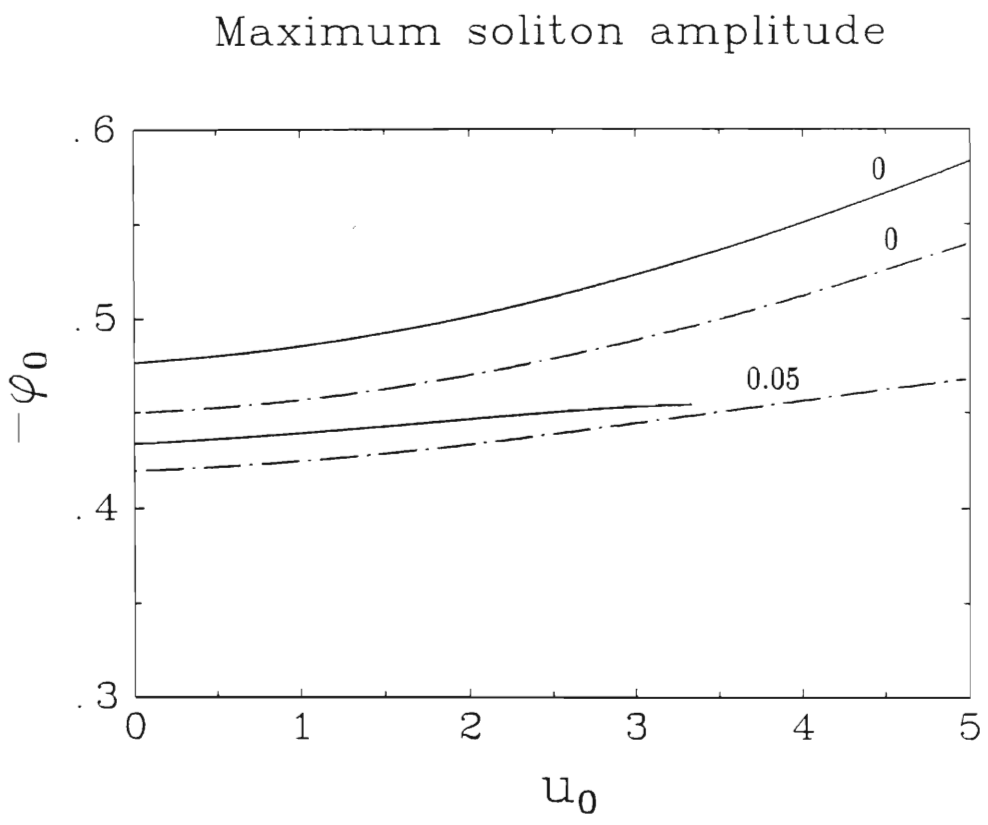

Figure 9.7: Maximum soliton amplitude as a function of beam speed for various cool electron and ion temperatures: $\delta V = 0.3$. The parameter labelling the curves is $T_c = T_i$ and other parameters are $c = 10$. (—) Arbitrary-amplitude theory, $(- \cdot -)$ small-amplitude KdV theory.

form to the "stationary frame", i.e. the soliton rest frame, then we would be transforming away almost all relativistic effects except those arising due to thermal motions, quite apart from the fact that we would require a special Lorentz transform to do so. To clarify, when we assume dependence on the variable

$$s = x - Mt,$$

we do nothing other than prescribe the functional dependence of a macroscopic variable on x and t—we *do not* make any underlying physical assumptions about changing frames of reference in doing so. Having said this, our plots of soliton potential versus s are to be interpreted as "snapshots" of the soliton potential made by an observer located in spacetime at ($x = 0$, $t = 0$), as the soliton passes by the origin.

Chapter 10

On the existence of electron-acoustic double layers

In chapter 7 it was shown that electron-acoustic waves could support nonlinear potential structures whose time-evolution was governed by the Korteweg–de Vries equation; in particular we noted the existence of solitons. It was also observed that the nonlinear coefficient, a, of the KdV equation for electron-acoustic waves could never vanish (for nonzero electron densities), thereby preventing the occurrence of a modified KdV equation with only cubic nonlinearity.

In this chapter we shall nevertheless assume that for some parameter values this coefficient can be made small—$O(\epsilon^{1/2})$—then the term involving this coefficient, i.e.

$$a\phi^{(1)}\frac{\partial\phi^{(1)}}{\partial\xi},$$

will be $O(\epsilon^3)$ which is of higher order than the other terms in the equation ($O(\epsilon^{5/2})$) and consequently higher-order nonlinearities will start to become significant.

It then becomes necessary to seek an evolutionary equation that contains both quadratic and cubic nonlinearities on an equal footing, which can be accomplished by employing a coordinate stretching that allows for a higher degree of nonlinearity (see later). This equation, known as the modified Korteweg–de Vries equation (mKdV) with quadratic and cubic nonlinearity, usually admits double-layer solutions for some parameter values. In a natu-

ral extension of our earlier work then, we seek such solutions in this chapter. However, it will be shown that although such solutions exist formally, they violate the consistency conditions necessary for the validity of the mKdV equation.

Double layers in plasmas are regions of adjacent enhanced positive and negative charge. Within the broader definition of a soliton given in chapter 6 the double layer falls into the category of topological solitons because it alters the state of the plasma by its passage. The charge separation produces a localized electric field whose corresponding potential jumps from some $\phi_{\min}$ to another potential $\phi_{\max}$ over a relatively small spatial distance—typically of the order of tens of electron Debye lengths—and usually propagates through the plasma at supersonic speed. For this reason double layers are sometimes called electrostatic shock waves (Torvén 1981). Ion-acoustic double layers have been found to occur in plasmas whose electrons consist of two separately isothermal components with distinct temperatures (Baboolal, Bharuthram & Hellberg 1988 and references therein).

10.1 Basic equations

As in chapter 7 we shall suppose that the plasma is infinite, homogeneous, unmagnetized and collisionless. The plasma dynamics are then governed by the one-dimensional fluid–Poisson system

$$\frac{\partial n_j}{\partial t} + \frac{\partial}{\partial x}(n_j u_j) = 0, \tag{10.1}$$

$$m_j n_j \left(\frac{\partial u_j}{\partial t} + u_j \frac{\partial u_j}{\partial x} \right) = -\frac{\partial p_j}{\partial x} - Z_j n_j \frac{\partial \phi}{\partial x}, \tag{10.2}$$

$$\frac{\partial p_j}{\partial t} + u_j \frac{\partial p_j}{\partial x} + 3p_j \frac{\partial u_j}{\partial x} = 0, \tag{10.3}$$

$$\frac{\partial^2 \phi}{\partial x^2} = n_{0h} \exp \phi - \sum_j Z_j n_j. \tag{10.4}$$

The usual normalizations have been used. In this chapter we employ the somewhat less stringent boundary conditions

$$\left.\begin{array}{rr} \phi \to 0, & \dfrac{\partial \phi}{\partial x} \to 0, \quad \dfrac{\partial^2 \phi}{\partial x^2} \to 0 \\ n_j \to n_{0j}, & p_j \to p_{0j}, \quad u_j \to 0 \end{array}\right\} \quad \text{as} \quad x \to \infty, \tag{10.5}$$

which are one-sided as opposed to the two-sided boundary conditions imposed previously (cf. equation (7.6)).

10.2 The mKdV equation

Our basic assumptions concerning the wave packet are similar to those used in §7.2.1. We employ the reductive perturbation technique with the following coordinate stretchings

$$\xi = \epsilon(x - Vt), \qquad \tau = \epsilon^3 t, \tag{10.6}$$

which imply that the magnitude of the dispersion effect is $k^2\lambda_{Dh}^2 \sim \epsilon^2$ and differ from those used in chapter 7 in which it was assumed $k^2\lambda_{Dh}^2 \sim \epsilon$. Because $\epsilon \ll 1$ the stretchings (10.6) allow for the incorporation of even higher wavenumber harmonics in the wave-packet, than was permitted there. Consequently they admit stronger wave dispersion, which for balance implies a greater degree of nonlinearity.

We employ the expansions

$$\left.\begin{aligned} n_j &= n_j^{(0)} + \epsilon n_j^{(1)} + \epsilon^2 n_j^{(2)} + \epsilon^3 n_j^{(3)} + \cdots, \\ p_j &= p_j^{(0)} + \epsilon p_j^{(1)} + \epsilon^2 p_j^{(2)} + \epsilon^3 p_j^{(3)} + \cdots, \\ u_j &= \epsilon u_j^{(1)} + \epsilon^2 u_j^{(2)} + \epsilon^3 u_j^{(3)} + \cdots, \\ \phi &= \epsilon\phi^{(1)} + \epsilon^2\phi^{(2)} + \epsilon^3\phi^{(3)} + \cdots, \end{aligned}\right\} \tag{10.7}$$

which in this case are carried out to $O(\epsilon^3)$.

Proceeding as in chapter 7 we obtain to $O(\epsilon^2)$

$$n_j^{(1)} = \frac{Z_j n_j^{(0)}/m_j}{V^2 - 3\sigma_j}\phi^{(1)}, \quad p_j^{(1)} = \frac{3Z_j n_j^{(0)}\sigma_j}{V^2 - 3\sigma_j}\phi^{(1)}, \quad u_j^{(1)} = \frac{Z_j V/m_j}{V^2 - 3\sigma_j}\phi^{(1)}, \tag{10.8}$$

where V, the sound speed, satisfies the long-wavelength linear ($O(\epsilon)$) dispersion relation

$$n_{0h} - \sum_j \frac{Z_j^2 n_j^{(0)}/m_j}{V^2 - 3\sigma_j} = 0. \tag{10.9}$$

Equations (10.8) and (10.9) are none other than the linear perturbations and dispersion relation obtained in the derivation of the KdV equation (see appendix D).

To next highest order $O(\epsilon^3)$ one obtains

$$n_j^{(2)} = \frac{Z_j n_j^{(0)}/m_j}{V^2 - 3\sigma_j}\phi^{(2)} + \frac{3Z_j^2 n_j^{(0)}(V^2 + \sigma_j)/m_j^2}{2(V^2 - 3\sigma_j)^3}(\phi^{(1)})^2, \tag{10.10}$$

$$p_j^{(2)} = \frac{3Z_j n_j^{(0)}\sigma_j}{V^2-3\sigma_j}\phi^{(2)} + \frac{3Z_j^2 n_j^{(0)}\sigma_j(5V^2-3\sigma_j)/m_j}{2(V^2-3\sigma_j)^3}(\phi^{(1)})^2, \quad (10.11)$$

$$u_j^{(2)} = \frac{Z_j V/m_j}{V^2-3\sigma_j}\phi^{(2)} + \frac{Z_j^2 V(V^2+9\sigma_j)/m_j^2}{2(V^2-3\sigma_j)^3}(\phi^{(1)})^2, \quad (10.12)$$

where, in contrast with §7.2.1 (and appendix D), one can immediately solve for the second-order quantities in terms of the first-order potential. To $O(\epsilon^2)$ the Poisson equation yields

$$\frac{1}{2}\left\{ n_{0h} - \sum_j \frac{3Z_j^3 n_j^{(0)}(V^2+\sigma_j)/m_j^2}{(V^2-3\sigma_j)^3} \right\}(\phi^{(1)})^2 = 0. \quad (10.13)$$

We have already noted that the term in braces cannot vanish for electron-acoustic waves and even if it could this condition would severely restrict the range of parameters over which the resulting mKdV equation would be valid.

This $O(\epsilon^2)$ equation may still be satisfied, however, by requiring that the term in braces is $O(\epsilon)$ or higher. The left hand side then becomes $O(\epsilon^3)$ and satisfies (10.13) at $O(\epsilon^2)$. In this case the term involving (10.13) must be retained in the $O(\epsilon^3)$ expansion of the Poisson equation. Thus, the Poisson equation becomes, after partial differentiation by ξ (which increases the order to $O(\epsilon^4)$),

$$\frac{\partial^3\phi^{(1)}}{\partial\xi^3} = n_{0h}\frac{\partial\phi^{(3)}}{\partial\xi} + n_{0h}\frac{\partial}{\partial\xi}(\phi^{(1)}\phi^{(2)}) + \frac{1}{2}\left\{ n_{0h} - \sum_j \frac{3Z_j^3 n_j^{(0)}(V^2+\sigma_j)/m_j^2}{(V^2-3\sigma_j)^3} \right\}\frac{\partial}{\partial\xi}(\phi^{(1)})^2 + \tfrac{1}{6}n_{0h}\frac{\partial}{\partial\xi}(\phi^{(1)})^3 - \sum_j Z_j\frac{\partial}{\partial\xi}n_j^{(3)}. \quad (10.14)$$

At $O(\epsilon^4)$ one obtains from the continuity equation,

$$\frac{\partial n_j^{(1)}}{\partial\tau} - V\frac{\partial n_j^{(3)}}{\partial\xi} + n_j^{(0)}\frac{\partial u_j^{(3)}}{\partial\xi} + \frac{\partial}{\partial\xi}(n_j^{(1)}u_j^{(2)}) + \frac{\partial}{\partial\xi}(n_j^{(2)}u_j^{(1)}) = 0,$$

from the momentum equation,

$$n_j^{(0)}\frac{\partial u_j^{(1)}}{\partial\tau} - n_j^{(0)}V\frac{\partial u_j^{(3)}}{\partial\xi} - n_j^{(1)}V\frac{\partial u_j^{(2)}}{\partial\xi} - n_j^{(2)}V\frac{\partial u_j^{(1)}}{\partial\xi}$$

$$+n_j^{(0)}u_j^{(1)}\frac{\partial u_j^{(2)}}{\partial\xi}+n_j^{(1)}u_j^{(1)}\frac{\partial u_j^{(1)}}{\partial\xi}+n_j^{(0)}u_j^{(2)}\frac{\partial u_j^{(1)}}{\partial\xi}$$
$$=-\frac{Z_j}{m_j}n_j^{(0)}\frac{\partial\phi^{(3)}}{\partial\xi}-\frac{Z_j}{m_j}n_j^{(1)}\frac{\partial\phi^{(2)}}{\partial\xi}-\frac{Z_j}{m_j}n_j^{(2)}\frac{\partial\phi^{(1)}}{\partial\xi}-\frac{1}{m_j}\frac{\partial p_j^{(3)}}{\partial\xi},$$

and

$$\frac{\partial p_j^{(1)}}{\partial\tau}-V\frac{\partial p_j^{(3)}}{\partial\xi}+u_j^{(1)}\frac{\partial p_j^{(2)}}{\partial\xi}+u_j^{(2)}\frac{\partial p_j^{(1)}}{\partial\xi}$$
$$+3p_j^{(0)}\frac{\partial u_j^{(3)}}{\partial\xi}+3p_j^{(1)}\frac{\partial u_j^{(2)}}{\partial\xi}+3p_j^{(2)}\frac{\partial u_j^{(1)}}{\partial\xi}=0,$$

from the pressure equation. Elimination of $u_j^{(3)}$ and $p_j^{(3)}$ from the above equations yields the following equation for $\partial n_j^{(3)}/\partial\xi$ (where (10.8) and (10.10)–(10.12) have been used)

$$\frac{\partial n_j^{(3)}}{\partial\xi}=\frac{2Z_jn_j^{(0)}V/m_j}{(V^2-3\sigma_j)^2}\frac{\partial\phi^{(1)}}{\partial\tau}+\frac{3Z_j^2n_j^{(0)}(V^2+\sigma_j)/m_j^2}{(V^2-3\sigma_j)^3}\frac{\partial}{\partial\xi}(\phi^{(2)}\phi^{(1)})$$
$$+\left\{\frac{3Z_j^3n_j^{(0)}(5V^2+13\sigma_j)/m_j^3}{2(V^2-3\sigma_j)^4}+\frac{48Z_j^3n_j^{(0)}\sigma_j(2V^2+3\sigma_j)/m_j^3}{2(V^2-3\sigma_j)^5}\right\}(\phi^{(1)})^2\frac{\partial\phi^{(1)}}{\partial\xi}$$
$$+\frac{Z_jn_j^{(0)}/m_j}{V^2-3\sigma_j}\frac{\partial\phi^{(3)}}{\partial\xi}.$$

Substituting this equation into the Poisson equation at $O(\epsilon^4)$ and ignoring the $O(\epsilon^5)$ term involving $\partial(\phi^{(1)}\phi^{(2)})/\partial\xi$ one obtains the mKdV equation at $O(\epsilon^4)$

$$\frac{\partial\phi^{(1)}}{\partial\tau}+\tfrac{1}{2}a\frac{\partial}{\partial\xi}(\phi^{(1)})^2+c\frac{\partial}{\partial\xi}(\phi^{(1)})^3+b\frac{\partial^3\phi^{(1)}}{\partial\xi^3}=0, \tag{10.17}$$

where

$$a=\frac{B}{A},\qquad c=\frac{C}{A},\qquad b=\frac{1}{A},$$

and

$$A=\sum_j\frac{2Z_j^2n_j^{(0)}V/m_j}{(V^2-3\sigma_j)^2}, \tag{10.18}$$

$$B = \sum_j \frac{3Z_j^3 n_j^{(0)}(V^2+\sigma_j)/m_j^2}{(V^2-3\sigma_j)^3} - n_{0h}, \tag{10.19}$$

$$C = \sum_j \frac{Z_j^4 n_j^{(0)}(5V^4+30\sigma_j V^2+9\sigma_j^2)/m_j^3}{2(V^2-3\sigma_j)^5} - \tfrac{1}{6}n_{0h}. \tag{10.20}$$

Of course, validity of the mKdV equation is subject to the requirement that

$$\tfrac{1}{2}|B| = \tfrac{1}{2}\left|\frac{a}{b}\right| = O(\epsilon). \tag{10.21}$$

Note that a and b are identical to the corresponding a and b of the KdV equation (chapter 7). For electron-acoustic waves in which the ions are massive the electron sound speed determined by (10.9) becomes

$$V = \left(\frac{n_{0c}}{n_{0h}} + 3T_c\right)^{1/2}, \tag{10.22}$$

and the coefficients can be written

$$a = -\frac{(n_{0c}/n_{0h})^2 + 3(n_{0c}/n_{0h}+4T_c)}{2(n_{0c}/n_{0h})(n_{0c}/n_{0h}+3T_c)^{1/2}},$$

$$c = -\frac{(n_{0c}/n_{0h})^4 - 15(n_{0c}/n_{0h})^2 - 180T_c(n_{0c}/n_{0h}) - 432T_c^2}{12(n_{0c}/n_{0h})^3(n_{0c}/n_{0h}+3T_c)^{1/2}},$$

$$b = \frac{(n_{0c}/n_{0h})^2}{2n_{0c}(n_{0c}/n_{0h}+3T_c)^{1/2}}.$$

These enable us to write the consistency condition (10.21) in the form

$$\tfrac{1}{2}n_{0h}\left[1 + 3\frac{n_{0h}}{n_{0c}} + 12T_c\left(\frac{n_{0h}}{n_{0c}}\right)^2\right] = O(\epsilon). \tag{10.23}$$

It is noteworthy that the left hand side of (10.23) is less than unity only for $n_{0c} > n_{0h}$ which sets a lower bound on the allowable density ratio for the validity of the mKdV equation.

It is at this point that we encounter the first inconsistency. It has nothing to do with the small-amplitude mKdV theory, however, but is of a more fundamental nature. In the density regime $n_{0c}/n_{0h} > 1$ the electron sound speed is larger than the hot electron thermal velocity. This raises serious questions about the validity of the assumption of isothermality for the hot

electrons. On the other hand, because of the large nonlinearity and hence dispersion (for balance) it could be argued that the wavenumbers of the Fourier components constituting the wave packet are large enough so that $\omega/k \simeq v_{se}(1 - \frac{1}{2}k^2\lambda_{Dh}^2) < v_h$, and the assumption of approximate isothermality remains intact. However, let us for the moment take the fluid model for what it is worth and continue unabated.

10.3 Double layer solutions

We seek simple solutions of (10.17) that depend only on the variable $s = \xi - U\tau$. Then the mKdV equation can be integrated twice yielding

$$\frac{1}{2}\Big(\frac{\mathrm{d}\phi^{(1)}}{\mathrm{d}s}\Big)^2 = \frac{U}{2b}(\phi^{(1)})^2 - \frac{a}{6b}(\phi^{(1)})^3 - \frac{c}{4b}(\phi^{(1)})^4 \equiv -\Psi(\phi^{(1)}). \qquad (10.24)$$

The function Ψ must satisfy the following conditions if (10.24) is to admit double layer solutions (Bharuthram & Shukla 1986)

$$\Psi(0) = \Psi(\phi_m^{(1)}) = 0, \qquad \frac{\mathrm{d}\Psi}{\mathrm{d}\phi^{(1)}}\bigg|_{\phi^{(1)}=\phi_m^{(1)}} = \frac{\mathrm{d}\Psi}{\mathrm{d}\phi^{(1)}}\bigg|_{\phi^{(1)}=0} = 0, \qquad (10.25)$$

as well as the usual

$$\frac{\mathrm{d}^2\Psi}{\mathrm{d}(\phi^{(1)})^2}\bigg|_{\phi^{(1)}=0} < 0, \qquad \frac{\mathrm{d}^2\Psi}{\mathrm{d}(\phi^{(1)})^2}\bigg|_{\phi^{(1)}=\phi_m^{(1)}} < 0.$$

By analogy with classical mechanics the derivative condition at $\phi_m^{(1)}$ in (10.25) ensures that the particle starting from $\phi^{(1)} = 0$ will eventually come to rest at $\phi_m^{(1)}$ undergoing no reflection. From a physical point of view this condition demands quasineutrality at $\phi_m^{(1)}$.

Equation (10.25) can be satisfied if

$$\phi_m^{(1)} = -\frac{a}{3c} \quad \text{and} \quad U = -\frac{a^2}{18c}. \qquad (10.26)$$

When these conditions are met then (10.24) formally yields the double layer solution

$$\phi^{(1)} = \tfrac{1}{2}\phi_m^{(1)}[1 - \tanh\beta\{\xi - U\tau\}], \qquad (10.27)$$

where

$$\beta = \left(-\frac{a^2}{72bc}\right)^{1/2}. \qquad (10.28)$$

In terms of the original coordinates the solution (10.27) may be written

$$\phi = -\tfrac{1}{2}\chi\left[1 - \tanh\left\{\left(-\frac{\chi^2 c}{8b}\right)^{1/2}\left\{x - (V - \tfrac{1}{2}\chi^2 c)t\right\}\right\}\right], \qquad (10.29)$$

where we have defined $\chi \equiv \epsilon a/3c$.

From previous results (chapter 7) we know that $a < 0$ and $b > 0$ for electron-acoustic waves. Therefore in order for the solution (10.29) to hold we demand that β be real and hence $c < 0$. We thus arrive at the following necessary condition for the existence of electron-acoustic double layers

$$(n_{0c}/n_{0h})^4 - 15(n_{0c}/n_{0h})^2 - 180T_c(n_{0c}/n_{0h}) - 432T_c^2 > 0. \qquad (10.30)$$

Treating the left hand side of (10.30) as a quadratic in T_c with roots given by

$$T_c = -\frac{180}{864}\left[1 \pm \left\{1 - \frac{1728}{32400}(15 - \delta^2)\right\}^{1/2}\right], \qquad (10.31)$$

where $\delta = n_{0c}/n_{0h}$, we see that both are negative unless $\delta^2 > 15$ in which case the larger root represents an upper bound for the allowable temperature. Note that this criterion, i.e. $n_{0c}/n_{0h} > \sqrt{15}$ satisfies the consistency condition (10.23), but unfortunately places a question mark over the fundamental physical assumptions underlying the fluid model (see earlier remarks).

For such parameter values, however, the double layer solution is invalidated by the excessively large values of $\phi_m^{(1)}$ necessary for its existence. The following table clarifies this ($T_c = 0$ has been chosen for simplicity),

n_{0c}/n_{0h}	$a/2$	c	b	$\phi_m^{(1)}$
4	−0.875	−0.0104	5.00	−56
5	−0.894	−0.0745	6.71	−8
6	−0.919	−0.119	8.57	−5.14

We have refrained from admitting too large values for n_{0c}/n_{0h} for reasons mentioned before.

Immediately we notice the very small magnitude of the coefficient of the cubic nonlinearity $|c|$ when compared to $\frac{1}{2}|a|$. This indicates the very small role of the cubic nonlinearity in the present model of electron-acoustic waves. Furthermore, it gives rise to intolerably large values of $\phi_m^{(1)}$ in the case of electron-acoustic double layers (recall that $\phi_m^{(1)}$ is required to be $O(\epsilon)$ to guarantee convergence of the small-amplitude expansions (10.7)). We are thus led to conclude that (10.27) is not a valid solution of the mKdV equation for electron-acoustic waves in the present model.

10.4 Soliton solutions

Under more general circumstances the mKdV equation admits solitary wave solutions. In appendix H we show that equation (10.24) has the following solitary-wave solution (cf. Yadav & Sharma (1989) in a study of relativistic ion-acoustic waves)

$$\phi^{(1)} = U\left[\pm\left(\frac{a^2}{36}+cU/2\right)^{1/2}\cosh\left\{\left(\frac{U}{b}\right)^{1/2}(\xi-U\tau)\right\}+\frac{a}{6}\right]^{-1}, \quad (10.32)$$

provided

$$U > -\frac{a^2}{18c} \quad \text{if } c>0; \qquad U < -\frac{a^2}{18c} \quad \text{if } c<0. \quad (10.33)$$

The first condition above effectively states that if $c > 0$ then $U > 0$ because the quantity $-a^2/18c$ under these circumstances is negative. On the other hand if $c < 0$ then the second condition in (10.33) places an upper bound for the occurrence of a soliton, on the allowable velocity, U. Furthermore the sign of the first term must be equal to the sign of a if the solution is to be non-singular.

Comparing these conditions with those necessary for the occurrence of a double layer we see that the latter is a rather special solution that occurs if the velocity U takes on the particular value $U = -a^2/18c$, with $c < 0$. However, as was seen in the previous section this value is large in the case of the electron-acoustic wave and the theory breaks down there. The mKdV equation formally admits solutions for even larger values of U, but we do not dicuss these here.

10.5 Discussion

We have investigated the fully nonlinear Sagdeev potential as defined in chapter 7 over an extensive set of parameter values but could not satisfy the tangency criterion $\mathrm{d}\Psi/\mathrm{d}\phi = 0$ at $\phi = \phi_m$.

Comparing this fully nonlinear Sagdeev potential with the small-amplitude approximation defined by (10.24) we find satisfactory agreement between the two if the parameter U is sufficiently small and $n_{0c} > n_{0h}$ (see figure 10.1). In this situation the solutions to the mKdV equation are of the solitary-wave type and are given by (10.32).

However, for those parameters calculated in §10.3 that predict double layers (10.26), the small- and arbitrary-amplitude theories diverge: the full

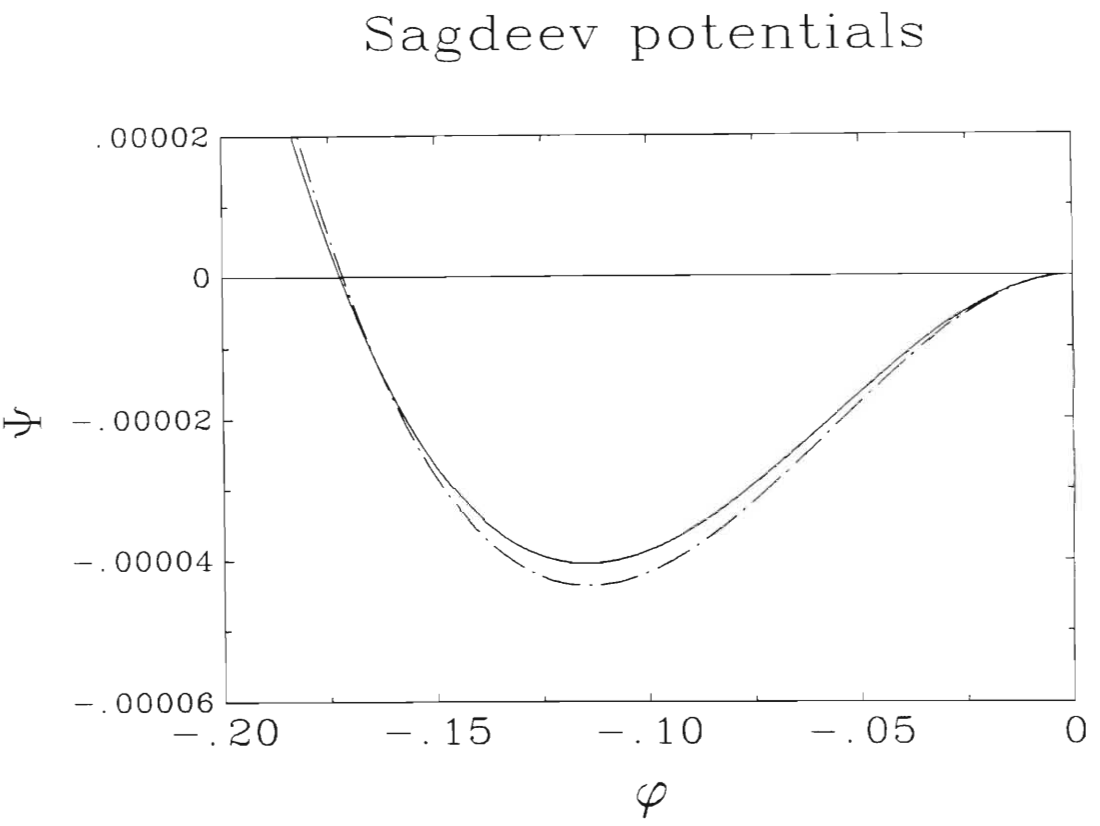

Figure 10.1: The Sagdeev potentials predicted by the full (—) and small-amplitude (− · −) theories for parameter values of $n_{0c} = 0.8$, $U = 0.1$, $T_c = T_i = 0$.

theory indicates that the tangency condition is not met (see figure 10.2), lending further support to our earlier suggestion that weak electron-acoustic double layers do not occur for the two-electron-component model used.

In physical terms the plasma cannot support electron-acoustic double layers because it always sustains a net charge at ϕ_m which destroys the quasineutrality required for the existence of the weak DL, i.e.

$$\left.\frac{d\Psi}{d\phi}\right|_{\phi=\phi_m} = -n_h - n_c + n_i \neq 0, \qquad |\phi_m| > 0.$$

We have been reluctant to investigate very large values of the ratio n_{0c}/n_{0h} for three reasons. Firstly, the wave speed at these large values

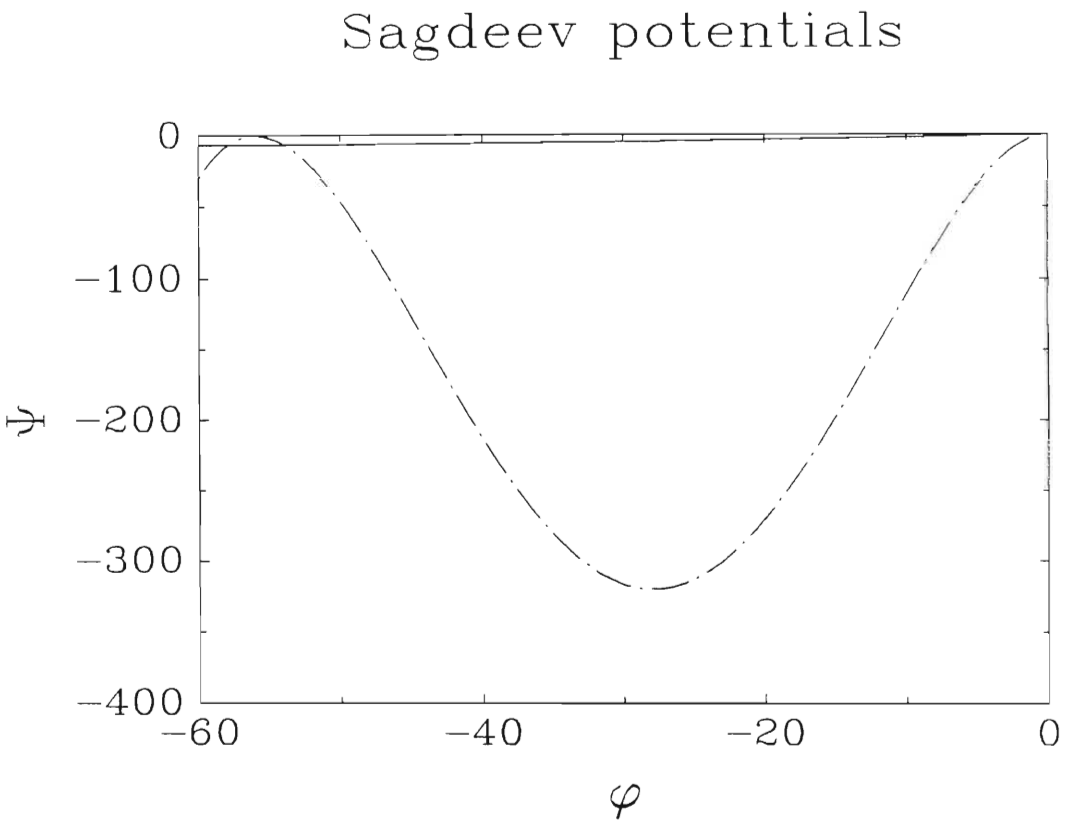

Figure 10.2: The Sagdeev potentials predicted by the full (—) and small-amplitude (− · −) theories for parameter values of $n_{0c} = 0.8$, $U = 16.33333$, $T_c = T_i = 0$.

exceeds the hot electron thermal speed, thus invalidating our fundamental assumtion of isothermality for this component. Secondly, at large values of this ratio the electron-acoustic and electron plasma wave become indistinguishable (see chapter 3). Thirdly, at such large density values the linear Landau damping by the hot electron component would become appreciable (see chapter 2).

Recently, by employing a pseudo-potential approach, Baboolal, Bharuthram & Hellberg (1991) showed that ion-acoustic double layers supported by negative ions do not occur unless the negative ion concentration is negligibly small. Their plasma was similar to that considered here: it consisted of Boltzmann electrons; and any number of positive and negative ion species, which for numerical calculations they limited to one of each. The positive to negative ion mass ratio was of the order of one.

By comparing the $O(\epsilon^4)$ expansion of the Sagdeev potential with that of the closed form they were able to show that the term of $O(\epsilon^5)$ which is neglected in the expansion is of the same order of magnitude as the potential amplitude ϕ_m, and apart from this, the potential does not satisfy the consistency relation $|\phi_m| = O(\epsilon)$ where $\epsilon \ll 1$. In fact the disparity between the pseudo-potentials predicted by mKdV theory and the Sagdeev potential method was pointed out earlier by Watanabe (1984) in a study of ion-acoustic solitons in negative ion plasmas.

Since our model differs from that of Baboolal *et al.* (1991) only in the positive to negative 'ion' mass ratio, and as we have seen, the discrepancies between the arbitrary and small amplitude theories are in accord with the findings of the latter, it is our belief that the result of Baboolal *et al.* (1991) holds approximately even if the negative 'ion' species is substituted by an electron species. Then, using the result of Baboolal *et al.* (1991), we conclude that the the neglect of the $O(\epsilon^5)$ term implied in (10.17) is invalid under most circumstances and in particular for double layers, and gives rise to the discrepancies between the small and large amplitude theories which are observed here.

A number of authors (Goswami & Bujarbarua 1987; Goswami, Kalita & Bujarbarua 1986; Dey, Goswami & Bujarbarua 1988) have considered small-amplitude electron-acoustic double layers in multi-component plasmas. Considering modified electron-acoustic (MEA) waves in a plasma composed of hot electrons, Boltzmann ions and fluid electrons and using a small-amplitude expansion for the MEA Sagdeev potential, Goswami & Bujarbarua (1987) were able to show that no MEA double layers occur when the hot electron species is Boltzmann-like, but when the hot electrons have

both trapped and reflected components then MEA double layers can exist. These results were generalized by Dey, Goswami & Bujarbarua (1988) to a plasma with two Boltzmann ion components. Again double layers were only obtained when the hot electron component was non-isothermal in the sense that it was composed of both trapped and reflected populations. Goswami, Kalita & Bujarbarua (1986) considered modified electron-acoustic double layers in a magnetized plasma composed of Boltzmann ions, hot electrons and fluid cold electrons ($T_c = 0$)—which is essentially a generalization of the Aref'ev (1970) model for electron-acoustic waves. They found that rarefactive and compressive DLs could occur when the hot electron component was considered isothermal (Boltzmann) and non-isothermal, respectively. However, apart from the fact that they use a small-amplitude expansion for their Sagdeev potential, they dispense with the Poisson equation and employ the quasineutrality condition. Such simplification may yield questionable results because of the very nature of the double layer.

As shown by Baboolal, Bharuthram & Hellberg (1991) when negative ions and/or electrons are considered one must be especially careful to ensure that one's solutions meet the criteria for convergence of the original expansions. This aspect has been emphasized in the present work. Having said this it is our view that the works mentioned in the preceding paragraphs require vindication through a full nonlinear treatment of the problems.

Kinetic models of slow electron-acoustic double layers (SEADLs) have been employed by Kim (1983) and Schamel (1983). In these models the electron and ion distribution functions are modelled on data obtained from particle simulations and elsewhere. Such models have yielded the correct form of the real potential but lack the support of experimental evidence in the case of the electron-acoustic wave.

Chapter 11

Conclusion

11.1 Summary

Part II of this thesis has been concerned, in the main, with nonlinear electron-acoustic waves, and in particular solitons. We considered five different physical models of electron-acoustic solitons, each progressively more involved than the next. A common feature of all the models considered, however, is the presence of an isothermal component of hot electrons. We summarise our findings in the following.

The first model, outlined in general in §7.1 and in more detail in §7.2.1, was the simplest: the unmagnetized plasma consisted of cool ions, cool electrons and hot Boltzmann electrons. By considering only one-dimensional waves propagating unidirectionally, we derived a KdV equation for weakly-nonlinear electron-acoustic waves. The soliton solutions of this equation were investigated in detail and compared with those predicted by the full fluid system of equations. This comparison unequivocally shows that for intermediate to large amplitude solitons, $|e\phi/T_h| > 0.5$, the KdV equation gives at best only a qualitative description of electron-acoustic solitons.

Our results demonstrate the importance of the cool electron temperature in determining the characteristics of electron-acoustic solitons as well as in determining their existence domains. This strong dependence of soliton behaviour on the cool electron temperature (relative to the hot) has been a common theme in all of our studies of electron-acoustic solitons. Furthermore, it was found that ion parameters have negligible effect on soliton characteristics. This was borne out in all our investigations except when the ions were treated as strongly magnetized.

In §7.2.2 we allowed for more generality by considering the electron-acoustic wave packet constituting the nonlinear wave to be "weakly" two-dimensional. Under these assumptions we found that nonlinear electron-acoustic waves are governed by a Kadomtsev–Petviashvili (KP) equation. An interesting feature of the KP equation is that two obliquely propagating solitons can produce a third by a resonant interaction (see for example Pécseli (1985)) and therefore we deduce that electron-acoustic solitons can exhibit such behaviour.

Introducing strong fluid magnetization (chapter 8) we derived a three-dimensional generalisation of the KdV equation for electron-acoustic waves in a magnetized plasma: the KdV–ZK equation. In contrast to the preceding work (chapter 7), when strong magnetization is introduced the contribution due to the ion dynamics becomes important for electron-acoustic soliton propagation. On the other hand, if the ions are *a priori* considered unmagnetized because of their large Larmor radii and gyrofrequencies (when compared to those of the electrons), then it is shown that the magnetic field only brings about a relatively small change in the soliton shape. In either case, however, there is a broadening of the soliton profile as the angle of soliton propagation with respect to the magnetic field is increased. This broadening is accompanied by a decrease in the soliton speed. When the angle of propagation with respect to the magnetic field was held constant while increasing the ratio of Ω_e/ω_{pe}, it was found that the soliton width decreased towards the width of an unmagnetized electron-acoustic soliton.

When weakly-relativistic beam effects were investigated (chapter 9) we found some interesting results. We employed a model in which the cool electron fluid streamed relativistically with repect to stationary background ions and isothermal hot electrons. It was found that the amplitude of electron-acoustic solitons is greatly affected by relativistic streaming. The magnitude of the amplitude is found to increase nonlinearly with beam speed, but this is shown to be strongly dependent on the temperature of the cool electron fluid. Such increases in amplitude with beam speed have previously been predicted for ion-acoustic solitons in the presence of a relativistic ion beam by Nejoh (1987a).

Furthermore, we developed a theory which allows direct numerical integration of the relativistic fluid equations incorporating relativistic thermal effects. Although such effects were small by comparison with beam effects, they were nevertheless detectable numerically (being orders of magnitude larger than our numerical precision). This arbitrary-amplitude theory was used to reinforce and extend our small-amplitude (KdV) results, and

moreover, to determine approximate parameter regimes in which relativistic electron-acoustic solitons might occur. In so doing we were able to quantitatively predict (for the first time in relativistic plasma, it appears) points at which the nonlinearity introduced by the beam overcomes the dispersion, leading to break-up of the original soliton into a finite train of solitons. As discussed by Nejoh (1987a, b) this may lead to the formation of a precursor.

Finally in chapter 10, by employing a small-amplitude analysis with the hope of being able to determine parameter regimes in which electron-acoustic double layers might occur, we derived a modified KdV equation for electron-acoustic waves. Whereas this equation formally admits double layer solutions it was found that the conditions under which they are valid are irreconcilable with the conditions under which the mKdV equation was derived. Investigating the Sagdeev potential obtained by reducing the original fluid equations (without approximation) to an 'energy' equation we were able to establish fairly conclusively that the tangency condition required for double layers does not occur, hence preventing the formation of stationary, weak double layers in our fluid model.

This brings us to an important final point. There is an increasing awareness of the shortcomings of small-amplitude theories of solitons and double layers (Baboolal *et al.* 1988; Baboolal *et al.* 1989), especially when negatively charged fluids are present (Baboolal *et al.* 1991). Thus, wherever possible we have substantiated our small-amplitude theories with large/arbitrary-amplitude calculations. Good agreement between the two theories was generally found at small soliton amplitudes $|e\phi/T_h| < 0.5$, however, at larger amplitudes significant differences in soliton widths and amplitudes arose. This suggests that small-amplitude theory only really gives accurate quantitative results for weak nonlinearity, although qualitatively the predictions are the same as those of the larger-amplitude theory over a wide range of nonlinearities. When double layers are considered, however, small-amplitude theories can yield completely incorrect predictions (Baboolal *et al.* 1991).

11.2 Limitations of the present, and suggestions for further work

Many of the remarks made in the conclusion of part I carry over to this part, but in addition, the following questions still need to be addressed.

11.2.1 Damping of solitary-waves

Although we took cognizance of finite fluid temperatures in our analyses through a somewhat idealised model of the pressure tensor, notably conspicuous in the work of part II was our neglect of the effects of wave damping by the interaction of the waveform with resonant particles.

The simplest such interaction is of course the linear Landau damping introduced in part I (chapter 2). Ott & Sudan (1969) considered the effects of linear electron Landau damping on nonlinear ion-acoustic waves and obtained an equation of the form

$$\gamma\frac{\partial\phi}{\partial\tau}+\alpha\phi\frac{\partial\phi}{\partial\xi}+\frac{\partial^3\phi}{\partial\xi^3}-f_0'(V)\,\mathcal{P}\int_{-\infty}^{\infty}\frac{\partial\phi/\partial\eta}{\xi-\eta}\mathrm{d}\eta=0, \qquad (11.1)$$

where $\mathcal{P}$ denotes principal value. Such equations are normally known as perturbed Korteweg–de Vries equations (Pécseli 1985) because often the integral term is treated as being smaller in magnitude than the others. Ott & Sudan (1969) demonstrated that an initial waveform may either steepen or not depending of the relative strengths of the nonlinearity as opposed to linear Landau damping.

Equations of the form (11.1) are only strictly valid for times less than the resonant interaction time τ_R, which for periodic waves corresponds to the trapping time (Pécseli 1985). For times larger than τ_R a modification term based on linear Landau damping becomes inadequate and particle reflection by the soliton must be taken into account. In this regard more complex integral damping terms have been considered by Karpman *et al.* (1979) and Karpman *et al.* (1980) for Trivelpiece–Gould solitons, and by Karpman (1979) for ion-acoustic solitons.

Employing coordinate stretchings that allow for time dependence in the wave velocity, Sanuki & Todoroki (1972) demonstrated that in such a case extra terms are introduced into equation (11.1).

Mohan & Buti (1980) derived a perturbed KdV equation of the form (11.1) for electron acoustic waves propagating across a magnetic field in a current-carrying plasma. The electrons bore a drift perpendicular to **B** and the ions were assumed much hotter that the electrons. Only Landau damping due to the hot ion component was considered. They showed that the Landau damping term gives rise to tail formation behind the soliton. Furthermore, the height of the tail remains almost constant, but the width increases linearly with time. Apart from this work, we are not aware of any other works on the damping of electron-acoustic solitary waves other than

that by Chowdhury, Pakira & Paul (1988), where a relativistic plasma was considered.

In part I it was shown that the linear Landau damping of electron-acoustic waves in the small-wavenumber regime could be quite substantial if the cool electron density n_{0c} was not much less than the hot electron density n_{0h}. One might then expect that for times less than the time of resonant interaction linear Landau damping of electron-acoustic solitons would be important, leading to a modification of our KdV equation to include an integral term as in (11.1). For times larger than τ_R one is forced to consider nonlinear Landau damping for an accurate description of reality, and an analysis analogous to that of Karpman (1979) for ion-acoustic waves might prove interesting.

The collisionless damping of electron-acoustic solitons could lead, perhaps, to the formation of a collisionless electron-acoustic shock wave just as collisonless damping of ion-acoustic waves can lead to ion-acoustic shocks. Electron-acoustic shocks may well be accessible to an arbitrary-amplitude pseudo-potential model similar to that used in chapter 7, but which includes the effects of (collisionless) dissipation. Once again calling on our analogy with classical mechanics, in the case of collisionless shocks the 'particle' would oscillate in the potential well (Chen 1984) as it underwent damping, eventually coming to 'rest' at a potential $\sim \phi_0/2$. Thus we speculate on the grounds of our previous work that a collisionless electron-acoustic shock would constitute a negative dip in the potential which has an oscillatory tail. The dip is associated with a sharp increase in cool electron number density.

Clearly, from the previous discussion there is vast scope for study of nonlinear wave-particle (or wave-wave for that matter) scattering by large amplitude electron-acoustic waves/turbulence. Such investigations would yield valuable information in determining the fate of electron-acoustic solitons and nonlinear waves as studied in part II.

11.2.2 Electron-acoustic double layers

The question of electron-acoustic double layers is still an open one. We have considered only the most simple fluid model of nonlinear electron-acoustic waves in which we showed that the weak electron-acoustic double layer does not exist. The introduction of particle drifts, trapped particle effects—which are essentially kinetic effects, etc. might well lead to the succesful formation of an electron-acoustic double layer. Indeed, slow electron-acoustic double layers (SEADLs), based on the slow electron-acoustic wave (Stix 1962) have

been constructed using kinetic models, by Kim (1983) and Schamel (1983).

Furthermore, we have considered only stationary electron-acoustic double layers. It remains to be seen whether non-stationary electron-acoustic double layers are admitted by our plasma model.

11.2.3 Large-amplitude soliton interactions

Soliton interactions governed by a host of evolutionary equations are now well known (see Drazin & Johnson (1989)). Such evolutionary equations, however, usually result only after some basic assumption as to the magnitude of the wave amplitude (and hence dispersion) has been made.

The arbitrary-amplitude wave model employed in part II for electron-acoustic solitons, and by Baboolal *et al* (1989) for ion-acoustic waves, has shown that whereas the KdV equation is a good approximation for weak nonlinearity, it fails to predict the correct soliton amplitudes and widths for strongly nonlinear solitons. Consequently, we expect the interaction of the fully nonlinear solitons to differ from that predicted by the KdV equation.

Perturbations of solitons due to higher-order nonlinearity ('soliton dress') were considered by e.g. Konno *et al.* (1977). Indeed, such works have been carried out for the modified electron-acoustic soliton (Sarma, Kalita & Bujarbarua 1986) but no time dependent investigation of interactions was carried out by the latter. Notwithstanding these works, it still remains to be seen what kind of interactions occur when the full nonlinearity is taken into account.

11.2.4 Soliton stability

Although it is now a fairly well-established fact that plane soliton solutions of the KdV equation are stable, the same cannot be said of the two- and three-dimensional generalisations. Moreover, it appears that very little (if any) work has been carried out on the three-dimensional stability of large/arbitrary-amplitude solitons as presented in part II. Such a work would necessarily be numerical in nature because of the unavailability of exact soliton solutions of the fully nonlinear fluid-Poisson system. It might entail the numerical solution of the abovementioned system of equations as an initial-value problem with an arbitrarily large amplitude perturbed soliton profile as initial profile. In addition, it might be interesting to investigate the evolution of an arbitrarily large electron-acoustic double layer initial profile.

Appendix A

The dispersion relation for electrostatic waves in a magnetized plasma

In this appendix we derive the dispersion relation for electrostatic waves in a magnetized, multi-species plasma. Because the waves are electostatic we shall assume that the electric field is derivable from a scalar potential

$$\mathbf{E} = -\nabla\phi.$$

The plasma particles are assumed to be drifting parallel/antiparallel to the magnetic field $\mathbf{B}$.

A.1 Basic equations

Our starting equations are the Vlasov-Poisson system of equations:

$$\nabla^2\phi = -4\pi \sum_j n_{0j} q_j \int f_j \, \mathrm{d}\mathbf{v}, \tag{A.1}$$

$$\frac{\partial f_j}{\partial t} + \mathbf{v} \cdot \frac{\partial f_j}{\partial \mathbf{x}} + \frac{q_j}{m_j}(-\nabla\phi + \frac{1}{c}\mathbf{v} \times \mathbf{B}) \cdot \frac{\partial f_j}{\partial \mathbf{v}} = 0, \tag{A.2}$$

where j refers to the jth particle species. Linearizing about a static background, we put $\phi = \phi^{(1)}(\mathbf{x}, t)$, $\mathbf{B} = \mathbf{B}^{(0)}$, and $f_j = f_j^{(0)}(\mathbf{v}) + f_j^{(1)}(\mathbf{x}, \mathbf{v}, t)$,

and obtain to zeroth order

$$4\pi \sum_j n_{0j} q_j \int f_j^{(0)} \, \mathrm{d}\mathbf{v} = 0, \tag{A.3}$$

$$\frac{q_j}{m_j}\left(\frac{1}{c}\mathbf{v} \times \mathbf{B}^{(0)}\right) \cdot \frac{\partial f_j^{(0)}}{\partial \mathbf{v}} = 0, \tag{A.4}$$

and to first order

$$\nabla^2 \phi^{(1)} = -4\pi \sum_j n_{0j} q_j \int f_j^{(1)}(\mathbf{x}, \mathbf{v}, t) \, \mathrm{d}\mathbf{v}, \tag{A.5}$$

$$\left(\frac{\partial}{\partial t} + \mathbf{v} \cdot \frac{\partial}{\partial \mathbf{x}} + \frac{q_j}{m_j}\left(\frac{1}{c}\mathbf{v} \times \mathbf{B}^{(0)}\right) \cdot \frac{\partial}{\partial \mathbf{v}}\right) f_j^{(1)} = \frac{q_j}{m_j} \frac{\partial \phi^{(1)}}{\partial \mathbf{x}} \cdot \frac{\partial f_j^{(0)}}{\partial \mathbf{v}}. \tag{A.6}$$

Equation (A.3) expresses the charge quasineutrality condition and equation (A.4) states that the zeroth-order distribution function is a function of $v_\perp$ and $v_\parallel$, i.e.

$$f_j^{(0)}(\mathbf{v}) = f_j^{(0)}(v_\perp, v_\parallel).$$

A.2 The dispersion relation

The left hand side of equation (A.6) is just the rate of change following an unperturbed orbit in phase space. Thus we may write the latter equation as follows

$$\frac{\mathrm{d}^{(0)}}{\mathrm{d}t} f_j^{(1)} = \frac{q_j}{m_j} \frac{\partial \phi^{(1)}}{\partial \mathbf{x}} \cdot \frac{\partial f_j^{(0)}}{\partial \mathbf{v}},$$

where the operator $\mathrm{d}^{(0)}/\mathrm{d}t$ is the operator on the left hand side of (A.6). The above equation has formal solution

$$\begin{aligned} f_j^{(1)}(\mathbf{x}, \mathbf{v}, t) \;=\; & f_j^{(1)}(\mathbf{X}(t'), \mathbf{V}(t'), t' = -\infty) \\ & + \int_{-\infty}^{t} \mathrm{d}t' \, \frac{q_j}{m_j} \frac{\partial \phi^{(1)}}{\partial \mathbf{x}}(\mathbf{X}(t'), t') \cdot \frac{\partial f_j^{(0)}}{\partial \mathbf{v}}(\mathbf{V}(t')), \end{aligned} \tag{A.7}$$

where the point $\mathbf{X}(t')$, $\mathbf{V}(t')$ is the unperturbed orbit in phase space that will arrive at $\mathbf{x}$, $\mathbf{v}$ at $t' = t$.

Seeking plane-wave solutions we set

$$\left.\begin{aligned} \phi^{(1)}(\mathbf{x}, t) &= \Phi_{\mathbf{k}\omega} \exp i(\mathbf{k} \cdot \mathbf{x} - \omega t) \\ f_j^{(1)}(\mathbf{x}, \mathbf{v}, t) &= f_{j\,\mathbf{k}\omega}(\mathbf{v}) \exp i(\mathbf{k} \cdot \mathbf{x} - \omega t) \end{aligned}\right\}, \tag{A.8}$$

where it is assumed that $\mathrm{Im}\,\omega > 0$. By the latter assumption one must have $f_j^{(1)}(\mathbf{X}(t'), \mathbf{V}(t'), t' = -\infty) = 0$ since a finite amplitude at $t' = t$ implies that the amplitude must tend to zero as t' tends to $-\infty$. Then, by (A.7) above one obtains

$$f_{j\,\mathbf{k}\omega}(\mathbf{v}) = i\Phi_{\mathbf{k}\omega} \int_{-\infty}^{t} \mathrm{d}t' \, \frac{q_j}{m_j} \mathbf{k} \cdot \frac{\partial f_j^{(0)}}{\partial \mathbf{v}}(\mathbf{V}(t')) \exp i\Big[\mathbf{k} \cdot (\mathbf{X} - \mathbf{x}) - \omega(t' - t)\Big], \tag{A.9}$$

which, with the change of variable $\tau = t' - t$, becomes

$$f_{j\,\mathbf{k}\omega} = \frac{i\Phi_{\mathbf{k}\omega} q_j}{m_j} \int_{-\infty}^{0} \mathrm{d}\tau \, \mathbf{k} \cdot \frac{\partial f_j^{(0)}}{\partial \mathbf{v}}(\mathbf{V}(\tau)) \exp i\Big[\mathbf{k} \cdot (\mathbf{X} - \mathbf{x}) - \omega\tau\Big], \tag{A.10}$$

where it is now understood that $\mathbf{X}(\tau)$, $\mathbf{V}(\tau)$ is the unperturbed orbit that will arrive at $\mathbf{x}$, $\mathbf{v}$ at $\tau = 0$.

It is easy to show that a charged particle immersed in, and drifting in the direction of a constant homogeneous magnetic field, $\mathbf{B} = B_0 \mathbf{e}_z$, has velocity

$$\left.\begin{aligned} V_x &= v_\perp \cos(\varphi - \Omega_j \tau), \\ V_y &= v_\perp \sin(\varphi - \Omega_j \tau), \\ V_z &= U + v_\parallel, \end{aligned}\right\} \tag{A.11}$$

where $v_\perp = \sqrt{V_x^2 + V_y^2} = \sqrt{v_x^2 + v_y^2}$, $v_\parallel = V_z - U = v_z - U$, $\Omega_j = q_j B_0 / m_j c$, (Note: φ is the azimuthal coordinate in a cylindrical system and is not to be confused with the electrostatic potential ϕ) with corresponding trajectory

$$\left.\begin{aligned} X &= x + \frac{v_\perp}{\Omega_j} \sin\varphi - \frac{v_\perp}{\Omega_j} \sin(\varphi - \Omega_j \tau), \\ Y &= y - \frac{v_\perp}{\Omega_j} \cos\varphi + \frac{v_\perp}{\Omega_j} \cos(\varphi - \Omega_j \tau), \\ Z &= z + U\tau + v_\parallel \tau, \end{aligned}\right\} \tag{A.12}$$

and clearly these satisfy $\mathbf{X}(0) = \mathbf{x}$, $\mathbf{V}(0) = \mathbf{v}$. Now, because $f_j^{(0)}(\mathbf{v}) = f_j^{(0)}(v_\perp, v_\parallel)$ one obtains

$$\begin{aligned} \frac{\partial f_j^{(0)}}{\partial \mathbf{v}}(\mathbf{V}(\tau)) &= \mathbf{e}_x \frac{\partial f_j^{(0)}}{\partial v_\perp} \frac{\partial v_\perp}{\partial v_x} + \mathbf{e}_y \frac{\partial f_j^{(0)}}{\partial v_\perp} \frac{\partial v_\perp}{\partial v_y} + \mathbf{e}_z \frac{\partial f_j^{(0)}}{\partial v_\parallel} \frac{\partial v_\parallel}{\partial v_z}\bigg|_{V(\tau)}, \\ &= \frac{\partial f_j^{(0)}}{\partial v_\perp} \Big(\mathbf{e}_x \cos(\varphi - \Omega_j \tau) + \mathbf{e}_y \sin(\varphi - \Omega_j \tau)\Big) \end{aligned}$$

$$+\mathbf{e}_z \frac{\partial f_j^{(0)}}{\partial v_{||}}, \tag{A.13}$$

and without loss of generality we assume $\mathbf{k} = k_\perp \mathbf{e}_x + k_{||}\mathbf{e}_z$ then

$$\mathbf{k} \cdot \frac{\partial f_j^{(0)}}{\partial \mathbf{v}}(\mathbf{V}(\tau)) = k_\perp \frac{\partial f_j^{(0)}}{\partial v_\perp} \cos(\varphi - \Omega_j \tau) + k_{||} \frac{\partial f_j^{(0)}}{\partial v_{||}}. \tag{A.14}$$

Substitution of (A.11), (A.12) and (A.14) into (A.10) yields

$$f_{j\mathbf{k}\omega}(\mathbf{v}) = i\frac{q_j}{m_j}\Phi_{\mathbf{k}\omega} \int_{-\infty}^{0} \mathrm{d}\tau \left(k_\perp \frac{\partial f_j^{(0)}}{\partial v_\perp} \cos(\varphi - \Omega_j \tau) + k_{||} \frac{\partial f_j^{(0)}}{\partial v_{||}} \right)$$
$$\cdot \exp i \left(\frac{k_\perp v_\perp}{\Omega_j} \sin\varphi - \frac{k_\perp v_\perp}{\Omega_j} \sin(\varphi - \Omega_j \tau) + k_{||}(U + v_{||})\tau - \omega\tau \right). \tag{A.15}$$

By definition of the cosine in terms of the complex exponential one can write the equation (A.15) in the form

$$\begin{aligned} f_{j\mathbf{k}\omega}(\mathbf{v}) \;=\; & i\frac{q_j}{m_j}\Phi_{\mathbf{k}\omega} \left\{ \int_{-\infty}^{0} \mathrm{d}\tau \left[\tfrac{1}{2} k_\perp \frac{\partial f_j^{(0)}}{\partial v_\perp} \exp i\Big(\varphi - \Omega_j \tau + \frac{k_\perp v_\perp}{\Omega_j} \sin\varphi \right.\right. \\ & \left. - \frac{k_\perp v_\perp}{\Omega_j} \sin(\varphi - \Omega_j \tau) + k_{||}(U + v_{||})\tau - \omega\tau \Big) \right] \\ & + \int_{-\infty}^{0} \mathrm{d}\tau \left[\tfrac{1}{2} k_\perp \frac{\partial f_j^{(0)}}{\partial v_\perp} \exp i\Big(-\varphi + \Omega_j \tau + \frac{k_\perp v_\perp}{\Omega_j} \sin\varphi \right. \\ & \left. - \frac{k_\perp v_\perp}{\Omega_j} \sin(\varphi - \Omega_j \tau) + k_{||}(U + v_{||})\tau - \omega\tau \Big) \right] \\ & + \int_{-\infty}^{0} \mathrm{d}\tau \left[k_{||} \frac{\partial f_j^{(0)}}{\partial v_{||}} \exp i\Big(\frac{k_\perp v_\perp}{\Omega_j} \sin\varphi \right. \\ & \left.\left. - \frac{k_\perp v_\perp}{\Omega_j} \sin(\varphi - \Omega_j \tau) + k_{||}(U + v_{||})\tau - \omega\tau \Big) \right] \right\}. \end{aligned} \tag{A.16}$$

Consider the first integral in (A.16) above. Employing the following identities

$$\exp(ia\sin\varphi) = \sum_{n=-\infty}^{\infty} J_n(a) \exp(in\varphi),$$

$$\exp(-ia\sin\varphi) = \sum_{n=-\infty}^{\infty} J_n(a)\exp(-in\varphi),$$

one can write

$$\begin{aligned}
&\tfrac{1}{2}k_\perp \frac{\partial f_j^{(0)}}{\partial v_\perp} \exp i\varphi \int_{-\infty}^{0} \mathrm{d}\tau \exp\Big[i(k_\parallel(U+v_\parallel) - \Omega_j - \omega)\tau\Big] \\
&\qquad \cdot \sum_{n=-\infty}^{\infty}\sum_{m=-\infty}^{\infty} J_n\Big(\frac{k_\perp v_\perp}{\Omega_j}\Big)\exp(in\varphi) J_m\Big(\frac{k_\perp v_\perp}{\Omega_j}\Big) \\
&\qquad\qquad \cdot \exp[-im\varphi + im\Omega_j\tau] \\
= \;& \tfrac{1}{2}k_\perp \frac{\partial f_j^{(0)}}{\partial v_\perp} \sum_{n=-\infty}^{\infty}\sum_{m=-\infty}^{\infty} \exp[i(1+n-m)\varphi] J_n\Big(\frac{k_\perp v_\perp}{\Omega_j}\Big) J_m\Big(\frac{k_\perp v_\perp}{\Omega_j}\Big) \\
&\qquad \cdot \int_{-\infty}^{0} \mathrm{d}\tau \exp[i(k_\parallel(U+v_\parallel) + (m-1)\Omega_j - \omega)\tau] \\
= \;& \tfrac{1}{2}k_\perp \frac{\partial f_j^{(0)}}{\partial v_\perp} \sum_{n=-\infty}^{\infty}\sum_{m=-\infty}^{\infty} \frac{\exp[i(n-m)\varphi]}{i[k_\parallel(U+v_\parallel) + m\Omega_j - \omega]} \\
&\qquad \cdot J_n\Big(\frac{k_\perp v_\perp}{\Omega_j}\Big) J_{m+1}\Big(\frac{k_\perp v_\perp}{\Omega_j}\Big),
\end{aligned} \tag{A.17}$$

where we have used the assumption $\mathrm{Im}\,\omega > 0$ and made the substitution $m \mapsto m-1$ in the last step. Similarly, the second integral may be written

$$\begin{aligned}
= \;& \tfrac{1}{2}k_\perp \frac{\partial f_j^{(0)}}{\partial v_\perp} \sum_{n=-\infty}^{\infty}\sum_{m=-\infty}^{\infty} \frac{\exp[i(n-m)\varphi]}{i[k_\parallel(U+v_\parallel) + m\Omega_j - \omega]} \\
&\qquad \cdot J_n\Big(\frac{k_\perp v_\perp}{\Omega_j}\Big) J_{m-1}\Big(\frac{k_\perp v_\perp}{\Omega_j}\Big),
\end{aligned} \tag{A.18}$$

and summing these two integrals (A.17) and (A.18)—recalling that

$$J_{n+1}(x) + J_{n-1}(x) = (2n/x)J_n(x),$$

one obtains

$$\begin{aligned}
= \;& \sum_{n=-\infty}^{\infty}\sum_{m=-\infty}^{\infty} \frac{\exp[i(n-m)\varphi]}{i[k_\parallel(U+v_\parallel) + m\Omega_j - \omega]} \\
&\qquad \cdot J_n\Big(\frac{k_\perp v_\perp}{\Omega_j}\Big) J_m\Big(\frac{k_\perp v_\perp}{\Omega_j}\Big) \frac{m\Omega_j}{v_\perp} \frac{\partial f_j^{(0)}}{\partial v_\perp}.
\end{aligned} \tag{A.19}$$

The third integral is handled by much the same procedure; one obtains

$$= \sum_{n=-\infty}^{\infty} \sum_{m=-\infty}^{\infty} \frac{\exp[i(n-m)\varphi]}{i[k_{||}(U+v_{||})+m\Omega_j-\omega]} k_{||} \frac{\partial f_j^{(0)}}{\partial v_{||}} J_n\Big(\frac{k_\perp v_\perp}{\Omega_j}\Big) J_m\Big(\frac{k_\perp v_\perp}{\Omega_j}\Big). \tag{A.20}$$

Finally, summing the three integrals using (A.19) and (A.20) yields the desired expression

$$\begin{aligned} f_{j\mathbf{k}\omega}(\mathbf{V}) \;=\; & \frac{q_j}{m_j}\Phi_{\mathbf{k}\omega} \sum_{n=-\infty}^{\infty} \sum_{m=-\infty}^{\infty} \frac{\exp[i(n-m)\varphi]}{k_{||}(U+v_{||})+m\Omega_j-\omega} \\ & \cdot J_n\Big(\frac{k_\perp v_\perp}{\Omega_j}\Big) J_m\Big(\frac{k_\perp v_\perp}{\Omega_j}\Big) \left(\frac{m\Omega_j}{v_\perp}\frac{\partial f_j^{(0)}}{\partial v_\perp} + k_{||}\frac{\partial f_j^{(0)}}{\partial v_{||}} \right) \end{aligned} \tag{A.21}$$

Substitution of (A.21) into the linearized Poisson equation (A.5), and integrating over φ, noting that

$$\int_0^{2\pi} \exp[i(m-n)\varphi]\,\mathrm{d}\varphi = 2\pi\delta_{mn},$$

yields the dispersion relation

$$\begin{aligned} 1 - 2\pi \sum_j \frac{\omega_j^2}{k^2} \int_0^\infty \mathrm{d}v_\perp\, v_\perp \sum_{n=-\infty}^{\infty} J_n^2\Big(\frac{k_\perp v_\perp}{\Omega_j}\Big) \int_{-\infty}^{\infty} \frac{\mathrm{d}v_{||}}{k_{||}(U+v_{||})+n\Omega_j-\omega} \\ \cdot \left(\frac{n\Omega_j}{v_\perp}\frac{\partial f_j^{(0)}}{\partial v_\perp} + k_{||}\frac{\partial f_j^{(0)}}{\partial v_{||}} \right) = 0 \qquad \mathrm{Im}\,\omega > 0, \end{aligned}$$

where the plasma frequency of the jth component is defined by $\omega_j = (4\pi n_{0j} q_j^2/m_j)^{1/2}$.

The dispersion relation as it stands is only valid in the upper half of the complex ω plain. The integral over $v_{||}$ is in the form of a Hilbert transform. In order for the dispersion relation to be an entire function of ω it must be analytically continued to the lower half of the ω plain. This can be done by prescribing that the integral over $v_{||}$ be taken along a Landau contour as described in, for example, Krall & Trivelpiece (1973). Thus the dispersion relation valid in the entire complex plain is given by

$$1 \;=\; 2\pi \sum_j \frac{\omega_j^2}{k^2} \int_0^\infty \mathrm{d}v_\perp\, v_\perp \int_L \mathrm{d}v_{||} \sum_{n=-\infty}^{\infty} \left(\frac{n\Omega_j}{v_\perp}\frac{\partial f_j^{(0)}}{\partial v_\perp} + k_{||}\frac{\partial f_j^{(0)}}{\partial v_{||}} \right)$$

$$\cdot \frac{J_n^2(k_\perp v_\perp/\Omega_j)}{k_{||}(U+v_{||})+n\Omega_j-\omega}, \tag{A.22}$$

where L denotes the Landau contour which passes under all the poles of the integrand.

A.3 Maxwellian distributions

We seek the dispersion relation when the plasma components have Maxwellian distributions, viz.

$$f_j^{(0)}(v_\perp, v_{||}) = (2\pi v_j)^{-3/2} \exp\left\{-\frac{v_\perp^2+v_{||}^2}{2v_j^2}\right\}. \tag{A.23}$$

Substituting this into (A.22) and considering only the double integral we obtain:

$$\begin{aligned}\iint_2 &= -(2\pi v_j^2)^{-3/2} \int_L \mathrm{d}v_{||} \frac{n\Omega_j/v_j^2 + k_{||}v_{||}/v_j^2}{k_{||}(U+v_{||})+n\Omega_j-\omega} \exp\Big[-\frac{v_{||}^2}{2v_j^2}\Big] \\ &\quad \cdot \int_0^\infty \mathrm{d}v_\perp v_\perp \exp\Big[-\frac{v_\perp^2}{2v_j^2}\Big] J_n^2\Big(\frac{k_\perp v_\perp}{\Omega_j}\Big).\end{aligned} \tag{A.24}$$

The second integral is readily evaluated by employing (Ichimaru 1973)

$$\int_0^\infty x \exp[-a^2x^2] J_n(px) J_n(qx)\,\mathrm{d}x = \frac{1}{2a^2}\exp\Big[-\frac{p^2+q^2}{4a^2}\Big] I_n\Big(\frac{pq}{2a^2}\Big),$$

rendering

$$\int_2 = v_j^2 \exp\Big[-\frac{k_\perp^2 v_j^2}{\Omega_j^2}\Big] I_n\Big(\frac{k_\perp^2 v_j^2}{\Omega_j^2}\Big), \tag{A.25}$$

where $I_n(x)$ is the modified Bessel function of order n.

Consider now the first integral. Defining $s = v_{||}/\sqrt{2}v_j$ it can be cast in the form

$$\begin{aligned}\int_1 &= \frac{\sqrt{2}}{v_j}\int_L \frac{s + n\Omega_j/\sqrt{2}\,k_{||}v_j}{s-(\omega-n\Omega_j-k_{||}U_j)/\sqrt{2}\,k_{||}v_j}\exp[-s^2]\,\mathrm{d}s, \\ &= \frac{\sqrt{2}}{v_j}\int_L \left\{1+\frac{(\omega-k_{||}U_j)/\sqrt{2}\,k_{||}v_j}{s-(\omega-n\Omega_j-k_{||}U_j)/\sqrt{2}\,k_{||}v_j)}\right\}\exp[-s^2]\mathrm{d}s, \\ &= \frac{\sqrt{2\pi}}{v_j}\left\{1+\frac{\omega-k_{||}U_j}{\sqrt{2}k_{||}v_j} Z\left(\frac{\omega-n\Omega_j-k_{||}U_j}{\sqrt{2}\,k_{||}v_j}\right)\right\},\end{aligned} \tag{A.26}$$

where we have used the definition

$$Z(\zeta) \equiv \pi^{-1/2} \int_L \frac{\exp[-s^2]\,\mathrm{d}s}{s-\zeta}.$$

Finally, substituting (A.26) and (A.25) into (A.22) yields the dispersion relation

$$1 + \sum_j \frac{\omega_j^2}{k^2 v_j^2} \sum_{n=-\infty}^{\infty} \exp\Big(-\frac{k_\perp^2 v_j^2}{\Omega_j^2}\Big) I_n\Big(\frac{k_\perp^2 v_j^2}{\Omega_j^2}\Big) \cdot \left\{1 + \frac{\omega - k_\| U_j}{\sqrt{2} k_\| v_j} Z\Big(\frac{\omega - n\Omega_j - k_\| U_j}{\sqrt{2} k_\| v_j}\Big)\right\} = 0, \qquad \text{(A.27)}$$

which on using

$$\sum_{n=-\infty}^{\infty} \exp[-x] I_n(x) = 1,$$

yields

$$1 + \sum_j \frac{\omega_j^2}{k^2 v_j^2} \left\{1 + \frac{\omega - k_\| U_j}{\sqrt{2} k_\| v_j} \exp\Big(-\frac{k_\perp^2 v_j^2}{\Omega_j^2}\Big) \cdot \sum_{n=-\infty}^{\infty} I_n\Big(\frac{k_\perp^2 v_j^2}{\Omega_j^2}\Big) Z\Big(\frac{\omega - n\Omega_j - k_\| U_j}{\sqrt{2} k_\| v_j}\Big)\right\} = 0,$$

A.4 The dispersion relation for electron-acoustic waves

In this section we pursue a derivation analogous to that of Melrose (1986) for ion-acoustic waves in magnetized plasma. We assume that the ions and hot electrons are unaffected by the magnetic field i.e. they are unmagnetized, and that the cool electrons are strongly magnetized. Furthermore, we assume that the phase velocity of the wave satisfies

$$\left|\frac{\omega}{\sqrt{2}\, k v_i}\right| \gg 1, \quad \left|\frac{\omega - n\Omega_e}{\sqrt{2}\, k_\| v_c}\right| \gg 1, \quad \left|\frac{\omega - k_\| v_{0h}}{\sqrt{2}\, k v_h}\right| \ll 1. \qquad \text{(A.28)}$$

The dispersion relation can be written

$$1 + \sum_{j=i,c,h} K_j = 0, \qquad \text{(A.29)}$$

where

$$K_i = -\frac{1}{2k^2\lambda_{Di}^2} Z'\left(\frac{\omega}{\sqrt{2}\,k v_i}\right), \tag{A.30}$$

and the electron contributions are:

$$K_c = \frac{1}{k^2\lambda_{Dc}^2}\left[1 + \frac{\omega}{\sqrt{2}\,k_{\|}v_c}\exp\left(-\frac{k_\perp^2 v_c^2}{\Omega_e^2}\right) \cdot \sum_{n=-\infty}^{\infty} I_n\left(\frac{k_\perp^2 v_c^2}{\Omega_e^2}\right) Z\left(\frac{\omega - n\Omega_e}{\sqrt{2}\,k_{\|}v_c}\right)\right], \tag{A.31}$$

$$K_h = -\frac{1}{2k^2\lambda_{Dh}^2} Z'\left(\frac{\omega - k_{\|}v_{0h}}{\sqrt{2}\,k v_h}\right). \tag{A.32}$$

Consider the term K_c: because $I_n(x) = I_{-n}(x)$ we can write

$$\begin{aligned} K_c = {} & \frac{1}{k^2\lambda_{Dc}^2}\exp\left(-\frac{k_\perp^2 v_c^2}{\Omega_e^2}\right) I_0\left(\frac{k_\perp^2 v_c^2}{\Omega_e^2}\right)\left[1 + \frac{\omega}{\sqrt{2}\,k_{\|}v_c} Z\left(\frac{\omega}{\sqrt{2}k_{\|}v_c}\right)\right] \\ & + \frac{1}{k^2\lambda_{Dc}^2}\sum_{n=1}^{\infty}\exp\left(-\frac{k_\perp^2 v_c^2}{\Omega_e^2}\right) I_n\left(\frac{k_\perp^2 v_c^2}{\Omega_e^2}\right) \\ & \cdot\left[2 + \frac{\omega}{\sqrt{2}k_{\|}v_c}\left\{Z\left(\frac{\omega - n\Omega_e}{\sqrt{2}\,k_{\|}v_c}\right) + Z\left(\frac{\omega + n\Omega_e}{\sqrt{2}\,k_{\|}v_c}\right)\right\}\right]. \end{aligned} \tag{A.33}$$

By (A.28) we employ the following asymptotic expansion of the Z–functions in the above

$$Z(\zeta) = -\frac{1}{\zeta} - \frac{1}{2\zeta^3} - \cdots, \tag{A.34}$$

and we assume that $k_\perp^2 v_c^2/\Omega_e^2 < 1$ which allows the following expansion of the $\exp(-x)I_n(x)$

$$\exp(-x)I_n(x) \simeq \frac{1}{n!}\left(\frac{x}{2}\right)^n. \tag{A.35}$$

The terms in the first set of square brackets in (A.33) are readily expanded yielding

$$\left[1 + \frac{\omega}{\sqrt{2}\,k_{\|}v_c} Z\left(\frac{\omega}{\sqrt{2}\,k_{\|}v_c}\right)\right] \simeq -\frac{k_{\|}^2 v_c^2}{\omega^2}. \tag{A.36}$$

The sum of Z–functions in the second set of square brackets in (A.33) can be written

$$Z\left(\frac{\omega - n\Omega_e}{\sqrt{2}\,k_{||}v_c}\right) + Z\left(\frac{\omega + n\Omega_e}{\sqrt{2}\,k_{||}v_c}\right) = -\sqrt{2}\,k_{||}v_c\left(\frac{1}{\omega - n\Omega_e} + \frac{1}{\omega + n\Omega_e}\right)$$
$$-\sqrt{2}k_{||}^3v_c^3\left(\frac{1}{(\omega - n\Omega_e)^3} + \frac{1}{(\omega + n\Omega_e)^3}\right)$$
$$= -\sqrt{2}k_{||}v_c\frac{2\omega}{\omega^2 - n^2\Omega_e^2} - \sqrt{2}k_{||}^3v_c^3\frac{2\omega^3 + 6\omega n^2\Omega_e^2}{(\omega^2 - n^2\Omega_e^2)^3}. \quad \text{(A.37)}$$

Using (A.35), (A.36) and (A.37) in (A.33) yields

$$K_c \simeq \frac{1}{k^2\lambda_{Dc}^2}$$
$$\cdot\left\{-\frac{k_{||}^2v_c^2}{\omega^2} + \sum_{n=1}^{\infty}\frac{2}{n!}\left(\frac{k_\perp^2v_c^2}{2\Omega_e^2}\right)^n\left[1 - \frac{\omega^2}{\omega^2 - n^2\Omega_e^2} - k_{||}^2v_c^2\frac{\omega^4 + 3\omega^2n^2\Omega_e^2}{(\omega^2 - n^2\Omega_e^2)^3}\right]\right\}.$$

The second term in the above rapidly decreases with increasing n and we take into account only the terms corresponding to $n = 1$ in the sequel. Furthermore, we neglect the last term in square brackets in the above involving $k_{||}^2v_c^2$. Then K_c becomes

$$K_c \simeq -\frac{k_{||}^2}{k^2}\frac{\omega_c^2}{\omega^2} - \frac{k_\perp^2}{k^2}\frac{\omega_c^2}{\omega^2 - \Omega_e^2}. \quad \text{(A.38)}$$

For the K_h term (A.32) we employ the following power series (see (A.28)) expansion of the Z'–function:

$$Z'(\zeta) \simeq -2[1 + i\pi^{1/2}\zeta\exp(-\zeta^2)]. \quad \text{(A.39)}$$

Then K_h becomes

$$K_h \simeq \frac{1}{k^2\lambda_{Dh}^2}\left\{1 + i\pi^{1/2}\frac{\omega - k_{||}v_{0h}}{\sqrt{2}\,kv_h}\exp\left[-\left(\frac{\omega - k_{||}v_{0h}}{\sqrt{2}\,kv_h}\right)^2\right]\right\}. \quad \text{(A.40)}$$

Finally, neglecting the ion contribution K_i, which is comparatively small, yields the following dispersion relation from (A.29) in conjunction with (A.38) and (A.40)

$$1 + \frac{1}{k^2\lambda_{Dh}^2} - \frac{k_{||}^2}{k^2}\frac{\omega_c^2}{\omega^2} + \frac{k_\perp^2}{k^2}\frac{\omega_c^2}{\Omega_e^2 - \omega^2} + i\pi^{1/2}\omega_h^2\frac{\omega - k_{||}v_{0h}}{\sqrt{2}\,k^3v_h^3}\exp\left[-\left(\frac{\omega - k_{||}v_{0h}}{\sqrt{2}\,kv_h}\right)^2\right]. \quad \text{(A.41)}$$

A.4.1 Weakly-magnetized electron-acoustic waves

We seek solutions of (A.41) that are either weakly-damped or weakly-growing, i.e. we set

$$\omega = \omega_r + i\gamma \quad \text{where} \quad |\gamma| \ll |\omega_r|. \tag{A.42}$$

Then employing the binomial theorem yields

$$\begin{aligned} \frac{1}{\omega^2} &= \frac{1}{(\omega_r + i\gamma)^2}, \\ &= \frac{1}{\omega_r^2}\left(1 + i\frac{\gamma}{\omega_r}\right)^{-2}, \\ &\simeq \frac{1}{\omega_r^2}\left(1 - i\frac{2\gamma}{\omega_r} + \cdots\right). \end{aligned} \tag{A.43}$$

Similarly it is easy to show that

$$\begin{aligned} \frac{1}{\Omega_e^2 - \omega^2} &= \frac{1}{(\Omega_e - \omega)(\Omega_e + \omega)} \\ &\simeq \frac{1}{\Omega_e^2 - \omega_r^2}\left(1 + i\frac{2\gamma\omega_r}{\Omega_e^2 - \omega_r^2} + \cdots\right). \end{aligned} \tag{A.44}$$

Substituting (A.42), (A.43) and (A.44) into (A.41) and separating into real and imaginary parts yields

$$1 + \frac{1}{k^2\lambda_{Dh}^2} - \frac{k_\parallel^2}{k^2}\frac{\omega_c^2}{\omega_r^2} + \frac{k_\perp^2}{k^2}\frac{\omega_c^2}{\Omega_e^2 - \omega_r^2} = 0, \tag{A.45}$$

for the real part, and neglecting small quantities one obtains

$$\begin{aligned} \gamma &= \left(\frac{\pi}{8}\right)^{1/2}\frac{\omega_h^2}{\omega_c^2}\frac{(k_\parallel v_{0h} - \omega_r)\omega_r^3}{k^3 v_h^3}\left[\frac{k_\parallel^2}{k^2} + \frac{k_\perp^2}{k^2}\frac{\omega_r^4}{(\Omega_e^2 - \omega_r^2)^2}\right]^{-1} \\ &\quad \cdot \exp\left[-\frac{(k_\parallel v_{0h} - \omega_r)^2}{2k^2 v_h^2}\right], \end{aligned} \tag{A.46}$$

from the imaginary part.

Consider (A.45), multiplying throughout by $\omega_r^2(\Omega_e^2 - \omega_r^2)$ we obtain the following quadratic in ω_r^2:

$$\omega_r^4 - [\Omega_e^2 + \omega_s^2(k)]\omega_r^2 + \omega_s^2(k)\Omega_e^2\cos^2\theta = 0, \tag{A.47}$$

where we have defined $\omega_s(k) = \omega_c/(1 + 1/k^2\lambda_{Dh}^2)^{1/2}$, $\cos\theta = k_{||}/k$, and $\sin\theta = k_\perp/k$. This equation has solutions

$$(\omega_r^{(+,-)})^2 = \tfrac{1}{2}[\Omega_e^2 + \omega_s^2(k) \pm \sqrt{(\Omega_e^2 + \omega_s^2(k))^2 - 4\omega_s^2(k)\Omega_e^2\cos^2\theta}]. \quad \text{(A.48)}$$

We investigate the behaviour of these solutions at small and large wavenumbers. Firstly we rewrite (A.48) in the form

$$\begin{aligned}(\omega_r^{(+,-)})^2 &= \tfrac{1}{2}(\omega_s^2(k) + \Omega_e^2)\left[1 \pm \sqrt{1 - \frac{4\omega_s^2(k)\Omega_e^2\cos^2\theta}{(\omega_s^2(k) + \Omega_e^2)^2}}\right], \\ &\simeq \tfrac{1}{2}(\omega_s^2(k) + \Omega_e^2)\left[1 \pm \left(1 - \frac{2\omega_s^2(k)\Omega_e^2\cos^2\theta}{(\omega_s^2(k) + \Omega_e^2)^2}\right)\right]. \quad \text{(A.49)}\end{aligned}$$

For small wavenumbers, defined by $\omega_s(k) \ll \Omega_e$, we employ the approximation

$$\Omega_e^2/(\omega_s^2(k) + \Omega_e^2) \simeq 1,$$

in $\omega_r^{(+,-)}$ yielding the solution

$$(\omega_r^{(+)})^2 \simeq \Omega_e^2 + \omega_s(k)\sin^2\theta, \quad \text{(A.50)}$$

which implies (using $\omega_s(k) \ll \Omega_e$ and expanding $\omega_s(k)$ for small k):

$$\omega_r^{(+)} \simeq \Omega_e + \frac{k^2 v_{se}^2}{2\Omega_e}\sin^2\theta, \quad \text{(A.51)}$$

where we have used the definition of the electron sound speed, i.e. $v_{se} = (n_{0c}/n_{0h})^{1/2}v_h$. The other root $\omega_r^{(-)}$ is readily calculated from (A.49) yielding

$$\omega_r^{(-)} \simeq \omega_s(k)\cos\theta \simeq k v_{se}\cos\theta. \quad \text{(A.52)}$$

The large-wavenumber regime defined by $\omega_s^2(k) \gg \Omega_e^2$ yields, on approximating

$$\omega_s^2(k)/(\omega_s^2(k) + \Omega_e^2) \simeq 1,$$

from (A.49):

$$(\omega_r^{(+)})^2 \simeq \omega_s^2(k) + \Omega_e^2\sin^2\theta, \quad \text{(A.53)}$$

and therefore

$$\omega_r^{(+)} \simeq \omega_s(k). \quad \text{(A.54)}$$

The other root is given by

$$\omega_r^{(-)} \simeq \Omega_e\cos\theta. \quad \text{(A.55)}$$

A.4.2 Strongly-magnetized electron-acoustic waves

We define the strongly magnetized regime by the condition $\Omega_e \gg |\omega|$. This allows us to write (A.41) in the form

$$1 + \frac{1}{k^2\lambda_{Dh}^2} - \frac{k_{||}^2}{k^2}\frac{\omega_c^2}{\omega^2} + \frac{k_\perp^2}{k^2}\frac{\omega_c^2}{\Omega_e^2} + i\pi^{1/2}\omega_h^2\frac{\omega - k_{||}v_{0h}}{\sqrt{2}\,k^3v_h^3}\exp\left[-\left(\frac{\omega - k_{||}v_{0h}}{\sqrt{2}\,kv_h}\right)^2\right]. \tag{A.56}$$

Then once again seeking solutions that are either weakly-damped or weakly-growing, i.e. those that satisfy (A.42) we may expand ω^{-2} as in (A.43). Substituting (A.43) into (A.56) and separating into real and imaginary parts we obtain

$$\omega_r^2 = \frac{k_{||}^2}{k^2}\frac{\omega_c^2}{1 + 1/k^2\lambda_{Dh}^2 + k_\perp^2\omega_c^2/k^2\Omega_e^2}, \tag{A.57}$$

or

$$\omega_r^2 = \frac{k_{||}^2}{k^2}\frac{k^2v_{se}^2}{1 + k^2\lambda_{Dh}^2 + k_\perp^2\rho_{se}^2}, \tag{A.58}$$

where we have defined $\rho_{se} = v_{se}/\Omega_e$; and

$$\gamma = \left(\frac{\pi}{8}\right)^{1/2}\frac{k^2}{k_{||}^2}\frac{\omega_h^2}{\omega_c^2}\frac{(k_{||}v_{0h} - \omega_r)\omega_r^3}{k^3v_h^3}\exp\left[-\frac{(k_{||}v_{0h} - \omega_r)^2}{2k^2v_h^2}\right]. \tag{A.59}$$

Appendix B

The hydrodynamical equations for a nonrelativistic fluid

Solution of the Vlasov–Maxwell system of equations, even in their linearised form, presents formiddable mathematical difficulties and, one could even say, lies on the bounds of tractability. In some instances, especially when nonlinear effects are considered, it is advantageous to descibe plasma processes within the framework of a macroscopic fluid model. In such a model one discards the microscopic information contained within the distribution function and works with averaged quantities describing the macroscopic behaviour of the fluid.

B.1 The hydrodynamical model

Defining the following averaged quantities

$$
\begin{aligned}
n(\mathbf{x},t) &= \int d\mathbf{v}\, f(\mathbf{x},\mathbf{v},t), \\
\mathbf{u}(\mathbf{x},t) &= \frac{1}{n(\mathbf{x},t)} \int d\mathbf{v}\, \mathbf{v} f(\mathbf{x},\mathbf{v},t), \\
\mathbf{P}(\mathbf{x},t) &= m \int d\mathbf{v} \Big(\mathbf{v} - \mathbf{u}(\mathbf{x},t)\Big)\Big(\mathbf{v} - \mathbf{u}(\mathbf{x},t)\Big) f(\mathbf{x},\mathbf{v},t), \\
\mathcal{Q}(\mathbf{x},t) &= m \int d\mathbf{v} \Big(\mathbf{v} - \mathbf{u}(\mathbf{x},t)\Big)\Big(\mathbf{v} - \mathbf{u}(\mathbf{x},t)\Big)\Big(\mathbf{v} - \mathbf{u}(\mathbf{x},t)\Big) f(\mathbf{x},\mathbf{v},t),
\end{aligned}
$$

and taking velocity moments of the Vlasov equation one obtains an interconnected chain of moment equations (Volkov 1966)

$$\frac{\partial n}{\partial t} + \nabla \cdot (n\mathbf{u}) = 0, \tag{B.1}$$

$$\frac{\partial}{\partial t}(n\mathbf{u}) + \frac{1}{m}\nabla \cdot (nm\mathbf{u} \otimes \mathbf{u} + \mathbf{P}) = \frac{nq}{m}\Big(\mathbf{E} + \frac{1}{c}\mathbf{u} \times \mathbf{B}\Big), \tag{B.2}$$

$$\frac{\partial \mathbf{P}}{\partial t} + \nabla \cdot (\mathcal{Q} + \mathbf{u} \otimes \mathbf{P}) + \mathbf{P} \cdot \nabla \mathbf{u} + (\nabla \mathbf{u})^T \cdot \mathbf{P} = \frac{e}{mc}(\mathbf{P} \times \mathbf{B} - \mathbf{B} \times \mathbf{P}), \tag{B.3}$$

$$\vdots$$

where the macroscopic electric and magnetic fields $\mathbf{E}$ and $\mathbf{B}$ evolve according to Maxwell's equations. These equations describe the spatial and temporal evolution of the averaged quantities n, $\mathbf{u}$, $\mathbf{P}$ and $\mathcal{Q}$.

Clearly, the above system of moment-Maxwell equations is not closed and it is necessary to prescribe certain further constraints to ensure closure. There are two commonly used procedures. The first of these assumes that the divergence of the pressure tensor vanishes $\nabla \cdot \mathbf{P} = 0$, which is called the cold plasma model, and the system above reduces to (B.1)–(B.2). The second procedure allows for finite pressure but now assumes that there is no heat flow so that the divergence of the heat flux tensor $\nabla \cdot \mathcal{Q} = 0$. This is called the warm plasma model. (We adopted the latter model for most of the plasmas studied in part II.) Furthermore, we shall assume that the fluid is ideal and hence the pressure tensor has vanishing off-diagonal elements

$$\mathbf{P} = \begin{pmatrix} p & 0 & 0 \\ 0 & p & 0 \\ 0 & 0 & p \end{pmatrix},$$

which amounts to the assumption that the fluid viscosity is zero.

For longitudinal plane waves the plasma components undergo only one dimensional compressions/rarefactions which, without loss of generality, we may take along the x-direction. Thus, contracting the pressure equation with respect to $\mathbf{e}_x \otimes \mathbf{e}_x$ we obtain, with the above assumptions,

$$\left(\frac{\partial}{\partial t} + \mathbf{u} \cdot \nabla\right) p + 3p\nabla \cdot \mathbf{u} = 0, \tag{B.4}$$

which, upon using the equation of continuity (B.1), yields the adiabatic law for a fluid undergoing one-dimensional compressions

$$\left(\frac{\partial}{\partial t} + \mathbf{u}\cdot\nabla\right)\left(\frac{p}{n^3}\right) = 0. \tag{B.5}$$

The latter equation states that the rate of change of the ratio p/n^3 following a fluid element, remains constant. Also, using the equation of continuity (B.1), one can write the momentum equation in the so-called Euler form. We summarize the three equations here for reference:

$$\frac{\partial n}{\partial t} + \nabla\cdot(n\mathbf{u}) = 0, \tag{B.6}$$

$$n\left(\frac{\partial \mathbf{u}}{\partial t} + \mathbf{u}\cdot\nabla\mathbf{u}\right) = -\frac{1}{m}\nabla p + \frac{nq}{m}\left(\mathbf{E} + \frac{1}{c}\mathbf{u}\times\mathbf{B}\right), \tag{B.7}$$

$$\frac{\partial p}{\partial t} + \mathbf{u}\cdot\nabla p + 3p\nabla\cdot\mathbf{u} = 0. \tag{B.8}$$

For longitudinal electrostatic waves in which the electric field vector lies parallel/antiparallel to the velocity field $\mathbf{u}$, the electric field can be derived from a scalar potential $\mathbf{E} = -\nabla\phi$. Then the only independent Maxwell equation is the Poisson equation

$$\nabla^2\phi = -4\pi\rho, \tag{B.9}$$

where ρ is the total charge density. It is assumed that a set of equations of the form (B.6)–(B.8) hold for each plasma component. These equations provide the basis for most of the analysis performed in part II.

Appendix C

Relativistic fluid equations

In this appendix we follow an analysis similar to that employed by Sakai & Kawata (1980) in deriving the ultra-relativistic fluid equations for a plasma. However, here we reduce the basic equations to their weakly-relativistic limit.

C.1 Basic equations governing the dynamics of a charged relativistic fluid

Suppose M^4 is a four-dimensional Riemannian manifold that possesses metric $g_{\mu\nu}$ with hyperbolic signature $+ - - -$ and invariant line element

$$(\mathrm{d}s)^2 = g_{\mu\nu}\mathrm{d}x^\mu \mathrm{d}x^\nu .$$

Then the equations governing the dynamics of a charged conducting fluid in this curved space-time are:

$$\begin{aligned}
&(nu^\mu)_{;\mu} = 0, && \text{(particle conservation);}\\
&T^{\mu\nu}{}_{;\nu} = 0, && \text{(from Bianchi's identity);}\\
&F^{\mu\nu}{}_{;\nu} = j^\mu, && \text{(Maxwell's equations I);}\\
&F_{\nu\rho;\mu} + F_{\mu\nu;\rho} + F_{\rho\mu;\nu} = 0, && \text{(Maxwell's equations II);}\\
&S^\mu{}_{;\mu} = 0, && \text{(isentropic);}
\end{aligned} \tag{C.1}$$

where n is the proper density of the fluid, $F^{\mu\nu}$ is the Maxwell tensor, S^μ is the entropy flux density, ";" denotes covariant differentiation and

$$T^{\mu\nu} = T^{\mu\nu}_{(M)} + T^{\mu\nu}_{(EM)},$$

is the energy-momentum-stress tensor. We have split the latter into two separate component tensors: $T^{\mu\nu}_{(M)}$ is the energy-momentum tensor of the material fluid; and $T^{\mu\nu}_{(EM)}$ is the energy momentum tensor of the electromagnetic field. The energy-momentum tensor contains contibutions from all sources of energy contained by the fluid because in relativity one loses the distinction between matter and energy, and all forms of energy possess inertia and can act as a source of the gravitational field.

Assuming a perfect, non-viscous fluid the material component of the energy-momentum tensor can be written (see for example Foster & Nightingale (1979))

$$T^{\mu\nu}_{(M)} = (\mu c^2 + p)u^\mu u^\nu - pg^{\mu\nu}, \tag{C.2}$$

where p is the pressure and μ is the proper mass density which includes the internal energy density. The electromagnetic field component is written in terms of the Maxwell tensor,

$$T^{\mu\nu}_{(EM)} = -\frac{1}{4\pi}\Big(F^{\mu\rho}F^{\nu}{}_{\rho} - \tfrac{1}{4}g^{\mu\nu}F_{\rho\sigma}F^{\rho\sigma}\Big), \tag{C.3}$$

The latter is given by

$$F_{\mu\nu} = A_{\nu\,;\mu} - A_{\mu\,;\nu}, \tag{C.4}$$

where A_μ is the vector potential. The four-velocity and four-current are defined by

$$u^\mu = \frac{\mathrm{d}x^\mu}{\mathrm{d}s}, \qquad j_\mu = 4\pi\rho u_\mu, \tag{C.5}$$

respectively, and ρ is the proper charge density.

In a fully relativistic treatment these equations would be supplemented by the Einstein equation

$$R_{\mu\nu} - \tfrac{1}{2}g_{\mu\nu}R = \frac{8\pi G}{c^4}T_{\mu\nu}, \tag{C.6}$$

where $R_{\mu\nu}$ is the Ricci tensor, $R = g^{\mu\nu}R_{\mu\nu}$ is the curvature scalar (Ricci scalar), and $G = 6.67 \times 10^{-8}$ cm^{3}g^{-1}s^{-3} is the gravitational constant.

C.2 The relativistic Euler and energy continuity equations

In this section we shall establish the relativistic Euler and energy continuity equations for a charged conducting fluid.

With this in mind we introduce the projection tensor (Straumann 1984)

$$h_{\mu\nu} = g_{\mu\nu} - u_\mu u_\nu, \tag{C.7}$$

which projects orthogonal to u^μ. It projects into the instantaneous rest-space of an observer moving with world velocity u^μ. Following Straumann (1984) we assert that the equations

$$u_\mu T^{\mu\nu}{}_{;\nu} = 0, \tag{C.8}$$

$$h^\mu_\nu T^{\nu\sigma}{}_{;\sigma} = 0, \tag{C.9}$$

represent the equation of energy continuity and Euler's equation for a charged relativistic fluid, respectively.

To prove the above assertion let us first evaluate the divergences implied in equations (C.8) and (C.9). Consider the divergence of the energy momentum tensor representing the electromagnetic field

$$\begin{aligned} T^\nu_{\mu\,;\nu(EM)} &= -\frac{1}{4\pi}\Big(F_{\mu\rho}F^{\nu\rho} - \tfrac{1}{4}\delta^\nu_\mu F_{\rho\sigma}F^{\rho\sigma}\Big)_{;\nu}, \\ &= -\frac{1}{4\pi}\Big(F_{\mu\rho}F^{\nu\rho}{}_{;\nu} + F_{\mu\rho\,;\nu}F^{\nu\rho} - \tfrac{1}{4}(F_{\rho\sigma}F^{\rho\sigma})_{;\mu}\Big). \end{aligned}$$

By Maxwell I in (C.1) and the antisymmetry of $F^{\mu\nu}$ (cf. (C.4)) we obtain $-F_{\mu\rho}j^\rho$ for the first term in the above. The second term becomes, noting the role of ν and ρ as dummy indices and the former remark about the Maxwell tensor,

$$\begin{aligned} F_{\mu\rho\,;\nu}F^{\nu\rho} &= \tfrac{1}{2}F_{\mu\rho\,;\nu}F^{\nu\rho} + \tfrac{1}{2}F_{\mu\nu\,;\rho}F^{\rho\nu} \\ &= \tfrac{1}{2}(F_{\mu\rho\,;\nu} + F_{\nu\mu\,;\rho})F^{\nu\rho} \\ &= \tfrac{1}{2}F_{\rho\nu\,;\mu}F^{\rho\nu}, \end{aligned}$$

where the Maxwell II equation in (C.1) was used in the last step. This can further be written

$$\tfrac{1}{2}F_{\rho\nu\,;\mu}F^{\rho\nu} = \tfrac{1}{4}(F_{\rho\nu}F^{\rho\nu})_{;\mu},$$

which yields the required result

$$T^{\mu\nu}{}_{;\nu\,(EM)} = \frac{1}{4\pi}F^{\mu\nu}j_\nu. \tag{C.10}$$

Similarly performing the divergence of $T^{\mu\nu}_{(M)}$ and employing (C.10) yields

$$\begin{aligned} T^{\mu\nu}{}_{;\nu} &= \mu c^2(u^\mu{}_{;\nu}u^\nu + u^\mu u^\nu{}_{;\nu}) + u^\mu u^\nu(\mu c^2)_{;\nu} + p(u^\mu{}_{;\nu}u^\nu + u^\mu u^\nu{}_{;\nu}) \\ &\quad +(u^\mu u^\nu - g^{\mu\nu})p_{;\nu} + \frac{1}{4\pi}F^{\mu\nu}j_\nu = 0. \end{aligned} \tag{C.11}$$

Now contracting with respect to u_μ as in (C.8) (noting the normalization condition $u_\mu u^\mu = 1$, $u_\mu u^\mu{}_{;\nu} = 0$ and the antisymmetry of $F_{\mu\nu}$) we obtain the energy continuity equation:

$$(\mu c^2 u^\mu)_{;\mu} + p u^\mu{}_{;\mu} = 0. \tag{C.12}$$

By contracting (C.11) with $h_{\mu\nu}$ as prescribed by (C.9) we obtain the relativistic Euler or momentum equation:

$$(\mu c^2 + p) u^\mu{}_{;\nu} u^\nu - h^{\mu\nu} p_{;\nu} = -\frac{1}{4\pi} F^{\mu\nu} j_\nu. \tag{C.13}$$

We introduce the internal energy density via

$$\mu c^2 = \varrho(c^2 + \varepsilon),$$

where ϱ is the proper density of the mass alone and ε, the specific internal energy density, is given by

$$\varepsilon = \frac{p}{\varrho(\Gamma - 1)}, \tag{C.14}$$

for an ideal fluid; and Γ is the fluid's adiabatic index. With this definition equation (C.12) can be written, using the particle conservation equation (C.1) (in its conservation of proper mass density form),

$$p_{;\mu} u^\mu + \Gamma p u^\mu{}_{;\mu} = 0. \tag{C.15}$$

Upon using (C.15) and particle conservation once more we obtain the adiabatic law for a relativistic fluid,

$$(p n^{-\Gamma})_{;\mu} u^\mu = 0 \quad \text{or} \quad \frac{\mathrm{d}}{\mathrm{d}s}(p n^{-\Gamma}) = 0, \tag{C.16}$$

which shows that the ratio p/n^Γ is conserved along a fluid element's world tube.

C.3 Special relativity and the weakly-relativistic limit

In the rest of this chapter we shall assume that we are far away from any gravitating masses so that the metric can be approximated by the Minkowski

metric of special relativity i.e.

$$(g_{\mu\nu}) = (\eta_{\mu\nu}) = \begin{pmatrix} 1 & 0 & 0 & 0 \\ 0 & -1 & 0 & 0 \\ 0 & 0 & -1 & 0 \\ 0 & 0 & 0 & -1 \end{pmatrix}, \tag{C.17}$$

in a rectilinear coordinate system where the coordinates x^μ are defined by

$$x^0 = ct, \quad x^1 = x, \quad x^2 = y, \quad x^3 = z.$$

In such a coordinate sytem the covariant derivative ";" reduces to the ordinary derivative "," because the affine connections (Christoffel symbols) vanish identically. We shall also make the assumption that the fluid is cool, i.e. $p \ll \varrho c^2$ and that the fluid velocity is not an appreciable fraction of c, i.e. the fluid is weakly-relativistic. We wish to separate the equations into their time and 3-space components, thus, with (C.17), the world-velocity (C.5) becomes

$$u^0 = \frac{1}{\sqrt{1 - v^2/c^2}}, \quad u^j = \frac{v^j}{c\sqrt{1 - v^2/c^2}}, \qquad j = 1, 2, 3, \tag{C.18}$$

where the v^j are the components of the normal three-velocity $\mathbf{v}$.

The antisymmetric Maxwell tensor has covariant components

$$(F_{\mu\nu}) = \begin{pmatrix} 0 & E_1 & E_2 & E_3 \\ -E_1 & 0 & -B_3 & B_2 \\ -E_2 & B_3 & 0 & -B_1 \\ -E_3 & -B_2 & B_1 & 0 \end{pmatrix}, \tag{C.19}$$

where the E_i and B_i are the three-space components of the electric and magnetic fields, $\mathbf{E}$, $\mathbf{B}$, respectively. With our assumption of flat spacetime and by equation (C.14) for the internal energy the Euler equation (C.13) may be cast in the form

$$\left(\varrho c^2 + \frac{\Gamma p}{\Gamma - 1}\right) u^\mu{}_{,\nu} u^\nu - \Gamma p u^\mu u^\nu{}_{,\nu} - \eta^{\mu\nu} p_{,\nu} = -\frac{1}{4\pi} F^{\mu\nu} j_\nu, \tag{C.20}$$

where we have used the pressure equation (C.15). Now separating the above equation into its time and space components and remembering $p/c^2 \ll \varrho$ we obtain for $\mu = 0$

$$\frac{\partial}{\partial t}(\gamma^2 \varrho) + \nabla \cdot (\gamma^2 \varrho \mathbf{v}) = \frac{\gamma \rho}{c^2} \mathbf{E} \cdot \mathbf{v}, \tag{C.21}$$

and for $\mu = 1, 2, 3$

$$\gamma\varrho\left(\frac{\partial}{\partial t} + \mathbf{v}\cdot\nabla\right)(\gamma\mathbf{v}) = -\nabla p + \gamma\rho\left(\mathbf{E} + \frac{1}{c}\mathbf{v}\times\mathbf{B}\right), \tag{C.22}$$

where we have introduced $\gamma = (1 - v^2/c^2)^{-1/2}$.

The latter equation is the relativistic 3-momentum equation for a weakly-relativistic fluid whereas the former equation is like a mass continuity equation with source term. The appearance of the factor γ^2 in these equations is due to two effects: length contraction of an elementary volume element in the direction of motion reduces volumes by a factor of γ^{-1}, and the second factor of γ arises due to the increase in mass of a particle travelling with speed $v > 0$. We therefore define the following quantities: the mass density $\varrho' = \gamma^2\varrho$, the particle number density $n' = \gamma n$, and the charge density $\rho' = \gamma\rho$. It is important to note that these quantities are not scalars in the relativistic theory because they vary depending upon in which inertial reference frame they are measured. With these definitions the above equations become

$$\frac{\partial}{\partial t}\varrho' + \nabla\cdot(\varrho'\mathbf{v}) = \frac{\rho'}{c^2}\mathbf{E}\cdot\mathbf{v}, \tag{C.23}$$

$$mn'\left(\frac{\partial}{\partial t} + \mathbf{v}\cdot\nabla\right)(\gamma\mathbf{v}) = -\nabla p + \rho'\left(\mathbf{E} + \frac{1}{c}\mathbf{v}\times\mathbf{B}\right) \tag{C.24}$$

and the equation of particle continuity reduces to

$$\frac{\partial n'}{\partial t} + \nabla\cdot(n'\mathbf{v}) = 0. \tag{C.25}$$

Returning to (C.15) and writing out in full using the definition of the world velocity (C.18) we obtain

$$\left(\frac{\partial}{\partial t} + \mathbf{v}\cdot\nabla\right)p + \frac{\Gamma p}{\gamma}\left(\frac{\partial\gamma}{\partial t} + \nabla\cdot(\gamma\mathbf{v})\right) = 0.$$

Now, noting $\gamma^{-1} = 1 - \frac{1}{2}v^2/c^2 - \cdots$, $\partial\gamma/\partial t = \gamma^3\mathbf{v}/c^2\cdot\partial\mathbf{v}/\partial t$, and our assumption that the fluid is cool and weakly-relativistic, we neglect the smaller terms to yield the weakly-relativistic pressure equation

$$\left(\frac{\partial}{\partial t} + \mathbf{v}\cdot\nabla\right)p + \Gamma p\nabla\cdot(\gamma\mathbf{v}) = 0. \tag{C.26}$$

Appendix D

The Korteweg–de Vries equation

In this section the reductive perturbation technique (Washimi & Taniuti 1966) is used to derive a Korteweg–de Vries equation for weakly-nonlinear waves in a multi-fluid plasma. The method assumes that the Fourier components constituting the weakly-nonlinear wave packet have a dispersion relation that behaves like

$$\omega \simeq \alpha k + \beta k^3.$$

D.1 Basic equations

An infinite, collisionless, unmagnetized, multi-fluid plasma is assumed (there being little gained in terms of economy, in limiting the number of fluids). The plasma dynamics are governed by the following normalized equations:

$$\frac{\partial n_j}{\partial t} + \frac{\partial}{\partial x}(n_j u_j) = 0, \tag{D.1}$$

$$m_j n_j \left(\frac{\partial u_j}{\partial t} + u_j \frac{\partial u_j}{\partial x} \right) = -\frac{\partial p_j}{\partial x} - Z_j n_j \frac{\partial \phi}{\partial x}, \tag{D.2}$$

$$\frac{\partial p_j}{\partial t} + u_j \frac{\partial p_j}{\partial x} + 3 p_j \frac{\partial u_j}{\partial x} = 0, \tag{D.3}$$

$$\frac{\partial^2 \phi}{\partial x^2} = n_h - \sum_j Z_j n_j, \tag{D.4}$$

and the hot electron density is given by the Boltzmann distribution

$$n_h = n_{0h} \exp \phi. \tag{D.5}$$

The subscript j denotes the jth fluid component, assumed to have thermal velocity much less than the wave phase velocity. The normalizations are as follows: spatial lengths by the length $(T_h/4\pi n_{0e}e^2)^{1/2}$, time by the inverse electron plasma frequency $(m_e/4\pi n_{0e}e^2)^{1/2}$, number densities by the total electron density n_{0e}, pressures by $n_{0e}T_h$, electrostatic potential by T_h/e, velocities by the hot electron thermal speed $(T_h/m_e)^{1/2}$, masses by the electron mass m_e; and $Z_j \equiv q_j/e$.

In addition, we impose the following boundary condtitions

$$\left.\begin{array}{rrr} \phi \to 0, & \dfrac{\partial \phi}{\partial x} \to 0, & \dfrac{\partial^2 \phi}{\partial x^2} \to 0 \\ n_j \to n_{0j}, & p_j \to p_{0j} & u_j \to 0 \end{array}\right\} \quad \text{as} \quad |x| \to \infty. \tag{D.6}$$

D.2 The reductive perturbation technique

We employ the following spatial and temporal stretching of the coordinates (Washimi & Taniuti 1966)

$$\xi = \epsilon^{1/2}(x - Vt), \qquad \tau = \epsilon^{3/2}t, \tag{D.7}$$

where $\epsilon \ll 1$ is a small parameter related to the wave amplitude. In addition, we expand the macroscopic variables in terms of ϵ:

$$\left.\begin{aligned} n_j &= n_j^{(0)} + \epsilon n_j^{(1)} + \epsilon^2 n_j^{(2)} + \cdots \\ p_j &= p_j^{(0)} + \epsilon p_j^{(1)} + \epsilon^2 p_j^{(2)} + \cdots \\ u_j &= \epsilon u_j^{(1)} + \epsilon^2 u_j^{(2)} + \cdots \\ \phi &= \epsilon \phi^{(1)} + \epsilon^2 \phi^{(2)} + \cdots. \end{aligned}\right\} \tag{D.8}$$

In terms of the new coordinates (D.7) the equations (D.1)–(D.4) become

$$-\epsilon^{1/2} V \frac{\partial n_j}{\partial \xi} + \epsilon^{3/2} \frac{\partial n_j}{\partial \tau} + \epsilon^{1/2} \frac{\partial}{\partial \xi}(n_j u_j) = 0, \tag{D.9}$$

$$\begin{aligned} n_j \left(-\epsilon^{1/2} V \frac{\partial u_j}{\partial \xi} + \epsilon^{3/2} \frac{\partial u_j}{\partial \tau} + \epsilon^{1/2} u_j \frac{\partial u_j}{\partial \xi} \right) \\ = -\epsilon^{1/2} \frac{1}{m_j} \frac{\partial p_j}{\partial \xi} - \epsilon^{1/2} \frac{Z_j n_j}{m_j} \frac{\partial \phi}{\partial \xi}, \end{aligned} \tag{D.10}$$

$$-\epsilon^{1/2}V\frac{\partial p_j}{\partial \xi}+\epsilon^{3/2}\frac{\partial p_j}{\partial \tau}+\epsilon^{1/2}u_j\frac{\partial p_j}{\partial \xi}+\epsilon^{1/2}3p_j\frac{\partial u_j}{\partial \xi}=0, \tag{D.11}$$

$$\epsilon\frac{\partial^2\phi}{\partial \xi^2}=n_{0h}(1+\phi+\tfrac{1}{2}\phi^2+\tfrac{1}{6}\phi^3)-\sum_j Z_j n_j. \tag{D.12}$$

Upon substituting the expansions (D.8) into the above system and solving order by order we obtain from Poisson's equation (D.12)

$$O(\epsilon^0) \qquad n_{0h}-\sum_j Z_j n_j^{(0)}=0, \tag{D.13}$$

$$O(\epsilon^1) \qquad n_{0h}\phi^{(1)}-\sum_j Z_j n_j^{(1)}=0, \tag{D.14}$$

$$O(\epsilon^2) \qquad \frac{\partial^2\phi^{(1)}}{\partial \xi^2}=n_{0h}\phi^{(2)}+\frac{1}{2}n_{0h}(\phi^{(1)})^2-\sum_j Z_j n_j^{(2)}, \tag{D.15}$$

from the equation of continuity,

$$O(\epsilon^{3/2}) \qquad -V\frac{\partial n_j^{(1)}}{\partial \xi}+n_j^{(0)}\frac{\partial u_j^{(1)}}{\partial \xi}=0, \tag{D.16}$$

$$O(\epsilon^{5/2}) \qquad -V\frac{\partial n_j^{(2)}}{\partial \xi}+\frac{\partial n_j^{(1)}}{\partial \tau}+n_j^{(1)}\frac{\partial u_j^{(1)}}{\partial \xi}+n_j^{(0)}\frac{\partial u_j^{(2)}}{\partial \xi}$$
$$+u_j^{(1)}\frac{\partial n_j^{(1)}}{\partial \xi}=0, \tag{D.17}$$

from the momentum equation,

$$O(\epsilon^{3/2}) \qquad -Vn_j^{(0)}\frac{\partial u_j^{(1)}}{\partial \xi}=-\frac{Z_j n_j^{(0)}}{m_j}\frac{\partial \phi^{(1)}}{\partial \xi}-\frac{1}{m_j}\frac{\partial p_j^{(1)}}{\partial \xi}, \tag{D.18}$$

$$O(\epsilon^{5/2}) \qquad -Vn_j^{(0)}\frac{\partial u_j^{(2)}}{\partial \xi}-Vn_j^{(1)}\frac{\partial u_j^{(1)}}{\partial \xi}+n_j^{(0)}\frac{\partial u_j^{(1)}}{\partial \tau}+n_j^{(0)}u_j^{(1)}\frac{\partial u_j^{(1)}}{\partial \xi}$$
$$=-\frac{Z_j n_j^{(1)}}{m_j}\frac{\partial \phi^{(1)}}{\partial \xi}-\frac{Z_j n_j^{(0)}}{m_j}\frac{\partial \phi^{(2)}}{\partial \xi}-\frac{1}{m_j}\frac{\partial p_j^{(2)}}{\partial \xi}, \tag{D.19}$$

and

$$O(\epsilon^{3/2}) \qquad -V\frac{\partial p_j^{(1)}}{\partial \xi}+3p_j^{(0)}\frac{\partial u_j^{(1)}}{\partial \xi}=0, \tag{D.20}$$

$$O(\epsilon^{5/2}) \qquad -V\frac{\partial p_j^{(2)}}{\partial \xi} + \frac{\partial p_j^{(1)}}{\partial \tau} + u_j^{(1)}\frac{\partial p_j^{(1)}}{\partial \xi} + 3p_j^{(0)}\frac{\partial u_j^{(2)}}{\partial \xi}$$
$$+3p_j^{(1)}\frac{\partial u_j^{(1)}}{\partial \xi} = 0, \tag{D.21}$$

from the pressure equation.

Note that the $O(\epsilon^{3/2})$ equations (D.16), (D.18) and (D.20) may be integrated at once, using the boundary conditions (D.6), yielding a similar set of equations without the partial derivations in ξ. Substituting the so-derived equation resulting from (D.20) into the corresponding equation resulting from (D.18) one obtains

$$u_j^{(1)} = \frac{Z_j V/m_j}{V^2 - 3\sigma_j}\phi^{(1)}, \tag{D.22}$$

for the first-order velocity of the jth fluid component. The parameter $\sigma_j \equiv p_j^{(0)}/m_j n_j^{(0)} = T_j/m_j$. Employing this equation in the integral of (D.16) yields

$$n_j^{(1)} = \frac{Z_j n_j^{(0)}/m_j}{V^2 - 3\sigma_j}\phi^{(1)}, \tag{D.23}$$

and by (D.20) one has

$$p_j^{(1)} = \frac{3Z_j n_j^{(0)}\sigma_j}{V^2 - 3\sigma_j}\phi^{(1)}. \tag{D.24}$$

Substituting the expression for $n_j^{(1)}$ (D.23) into the $O(\epsilon)$ equation arising from Poisson (D.14) furnishes

$$\left\{ n_{0h} - \sum_j \frac{Z_j^2 n_j^{(0)}/m_j}{V^2 - 3\sigma_j} \right\} \phi^{(1)} = 0,$$

where for non-trivial $\phi^{(1)}$ one must demand that the term in braces vanish, yielding a linear dispersion relation to be satisfied by the long-wavelength phase velocity V,

$$n_{0h} - \sum_j \frac{Z_j^2 n_j^{(0)}/m_j}{V^2 - 3\sigma_j} = 0. \tag{D.25}$$

The $O(\epsilon^{5/2})$ equations are dealt with as follows. The term involving $p_j^{(2)}$ in the momentum equation (D.19) is eliminated by using (D.21). This

results in the following equation for $u_j^{(2)}$

$$
\begin{aligned}
n_j^{(0)}\frac{\partial u_j^{(2)}}{\partial \xi} &= -\frac{V^2}{V^2-3\sigma_j}n_j^{(1)}\frac{\partial u_j^{(1)}}{\partial \xi}+\frac{n_j^{(0)}V}{V^2-3\sigma_j}\frac{\partial u_j^{(1)}}{\partial \tau} \\
&\quad +\frac{n_j^{(0)}V}{V^2-3\sigma_j}u_j^{(1)}\frac{\partial u_j^{(1)}}{\partial \xi}+\frac{Z_jV/m_j}{V^2-3\sigma_j}n_j^{(1)}\frac{\partial \phi^{(1)}}{\partial \xi} \\
&\quad +\frac{Z_jn_j^{(0)}V/m_j}{V^2-3\sigma_j}\frac{\partial \phi^{(2)}}{\partial \xi}+\frac{1/m_j}{V^2-3\sigma_j}\frac{\partial p_j^{(1)}}{\partial \tau} \\
&\quad +\frac{1/m_j}{V^2-3\sigma_j}u_j^{(1)}\frac{\partial p_j^{(1)}}{\partial \xi}+\frac{3/m_j}{V^2-3\sigma_j}p_j^{(1)}\frac{\partial u_j^{(1)}}{\partial \xi}. \qquad \text{(D.26)}
\end{aligned}
$$

Substitution of (D.26) into (D.17) and writing the first order quantities in terms of $\phi^{(1)}$ using (D.22)-(D.24) one obtains

$$
\begin{aligned}
\frac{\partial n_j^{(2)}}{\partial \xi} &= \frac{2Z_jn_j^{(0)}V/m_j}{(V^2-3\sigma_j)^2}\frac{\partial \phi^{(1)}}{\partial \tau} \\
&\quad +\frac{3Z_j^2n_j^{(0)}(V^2+\sigma_j)/m_j^2}{(V^2-3\sigma_j)^3}\phi^{(1)}\frac{\partial \phi^{(1)}}{\partial \xi} \\
&\quad +\frac{Z_jn_j^{(0)}/m_j}{V^2-3\sigma_j}\frac{\partial \phi^{(2)}}{\partial \xi}. \qquad \text{(D.27)}
\end{aligned}
$$

and partially differentiating the $O(\epsilon^2)$ equation (D.15) we obtain to $O(\epsilon^{5/2})$:

$$
\frac{\partial^3\phi^{(1)}}{\partial \xi^3}=n_{0h}\frac{\partial \phi^{(2)}}{\partial \xi}+n_{0h}\phi^{(1)}\frac{\partial \phi^{(1)}}{\partial \xi}-\sum_j Z_j\frac{\partial n_j^{(2)}}{\partial \xi}.
$$

Substitution of (D.27) into the latter equation yields the Korteweg–de Vries equation for the first-order potential $\phi^{(1)}$:

$$
\begin{aligned}
&\sum_j \frac{2Z_j^2n_j^{(0)}V/m_j}{(V^2-3\sigma_j)^2}\frac{\partial \phi^{(1)}}{\partial \tau} \\
&\quad +\left\{\sum_j \frac{3Z_j^3n_j^{(0)}(V^2+\sigma_j)/m_j^2}{(V^2-3\sigma_j)^3}-n_{0h}\right\}\phi^{(1)}\frac{\partial \phi^{(1)}}{\partial \xi} \\
&\quad +\frac{\partial^3\phi^{(1)}}{\partial \xi^3}=0, \qquad \text{(D.28)}
\end{aligned}
$$

where the dispersion relation (D.25) has been used.

Defining

$$A = \sum_j \frac{2Z_j^2 n_j^{(0)} V/m_j}{(V^2 - 3\sigma_j)^2}, \tag{D.29}$$

$$B = \sum_j \frac{3Z_j^3 n_j^{(0)} (V^2 + \sigma_j)/m_j^2}{(V^2 - 3\sigma_j)^3} - n_{0h}, \tag{D.30}$$

with

$$a = \frac{B}{A}, \quad \text{and} \quad b = \frac{1}{A}, \tag{D.31}$$

the Korteweg–de Vries equation may be cast in the form

$$\frac{\partial \phi^{(1)}}{\partial \tau} + a\phi^{(1)} \frac{\partial \phi^{(1)}}{\partial \xi} + b \frac{\partial^3 \phi^{(1)}}{\partial \xi^3} = 0. \tag{D.32}$$

Appendix E

The Kadomtsev–Petviashvili equation

This appendix allows for more generality than appendix D in that the wave packet may have components with wavevectors at small angles to the x–direction. We assume the Fourier components constituting the wave packet have a dispersion relation satisfying

$$\omega \simeq k_x v_{se} - \tfrac{1}{2} k_x^3 v_{se} \lambda_{Dh}^2 + \frac{k_y^2}{2k_x} v_{se}.$$

E.1 Basic equations

As in appendix D we assume an infinite, collisionless, unmagnetized, multi-fluid plasma. The two-dimensional dynamics are governed by the following

system:

$$\left.\begin{aligned}
\frac{\partial n_j}{\partial t} + \frac{\partial}{\partial x}(n_j u_j) + \frac{\partial}{\partial y}(n_j v_j) &= 0, \\
n_j m_j \left(\frac{\partial u_j}{\partial t} + u_j \frac{\partial u_j}{\partial x} + v_j \frac{\partial u_j}{\partial y}\right) &= -\frac{\partial p_j}{\partial x} - Z_j n_j \frac{\partial \phi}{\partial x}, \\
n_j m_j \left(\frac{\partial v_j}{\partial t} + u_j \frac{\partial v_j}{\partial x} + v_j \frac{\partial v_j}{\partial y}\right) &= -\frac{\partial p_j}{\partial y} - Z_j n_j \frac{\partial \phi}{\partial y}, \\
\frac{\partial p_j}{\partial t} + u_j \frac{\partial p_j}{\partial x} + v_j \frac{\partial p_j}{\partial y} + 3p_j \left(\frac{\partial u_j}{\partial x} + \frac{\partial v_j}{\partial y}\right) &= 0, \\
\frac{\partial^2 \phi}{\partial x^2} + \frac{\partial^2 \phi}{\partial y^2} &= n_h - \sum_j Z_j n_j,
\end{aligned}\right\} \qquad \text{(E.1)}$$

and the hot electron density is given by the Boltzmann distribution

$$n_h = n_{0h} \exp \phi. \qquad \text{(E.2)}$$

We have employed the same normalizations and boundary conditions as in appendix D.

E.2 The reductive perturbation technique

The following coordinate stretchings are used (cf. Nejoh 1987b)

$$\xi = \epsilon^{1/2}(x - Vt), \qquad \eta = \epsilon y, \qquad \tau = \epsilon^{3/2} t, \qquad \text{(E.3)}$$

in conjunction with the expansions

$$\left.\begin{aligned}
n_j &= n_j^{(0)} + \epsilon n_j^{(1)} + \epsilon^2 n_j^{(2)} + \cdots, \\
u_j &= \epsilon u_j^{(1)} + \epsilon^2 u_j^{(2)} + \cdots, \\
v_j &= \epsilon^{3/2} v_j^{(1)} + \epsilon^{5/2} v_j^{(2)} + \cdots, \\
p_j &= p_j^{(0)} + \epsilon p_j^{(1)} + \epsilon^2 p_j^{(2)} + \cdots, \\
\phi &= \epsilon \phi^{(1)} + \epsilon^2 \phi^{(2)} + \cdots.
\end{aligned}\right\} \qquad \text{(E.4)}$$

Substituting the stretchings (E.3) into (E.1) yields the following system of equations:

$$
\begin{aligned}
&-\epsilon^{1/2}V\frac{\partial n_j}{\partial \xi}+\epsilon^{3/2}\frac{\partial n_j}{\partial \tau}+\epsilon^{1/2}\frac{\partial}{\partial \xi}(n_j u_j)+\epsilon\frac{\partial}{\partial \eta}(n_j v_j)=0,\\
&n_j\left(-\epsilon^{1/2}V\frac{\partial u_j}{\partial \xi}+\epsilon^{3/2}\frac{\partial u_j}{\partial \tau}+\epsilon^{1/2}u_j\frac{\partial u_j}{\partial \xi}+\epsilon v_j\frac{\partial u_j}{\partial \eta}\right)\\
&\qquad=-\epsilon^{1/2}\frac{1}{m_j}\frac{\partial p_j}{\partial \xi}-\epsilon^{1/2}\frac{Z_j n_j}{m_j}\frac{\partial \phi}{\partial \xi},\\
&n_j\left(-\epsilon^{1/2}V\frac{\partial v_j}{\partial \xi}+\epsilon^{3/2}\frac{\partial v_j}{\partial \tau}+\epsilon^{1/2}u_j\frac{\partial v_j}{\partial \xi}+\epsilon v_j\frac{\partial v_j}{\partial \eta}\right)\\
&\qquad=-\epsilon\frac{1}{m_j}\frac{\partial p_j}{\partial \eta}-\epsilon\frac{Z_j n_j}{m_j}\frac{\partial \phi}{\partial \eta},\\
&-\epsilon^{1/2}V\frac{\partial p_j}{\partial \xi}+\epsilon^{3/2}\frac{\partial p_j}{\partial \tau}+\epsilon^{1/2}u_j\frac{\partial p_j}{\partial \xi}+\epsilon v_j\frac{\partial p_j}{\partial \eta}\\
&\qquad+3p_j\left(\epsilon^{1/2}\frac{\partial u_j}{\partial \xi}+\epsilon\frac{\partial v_j}{\partial \eta}\right)=0,\\
&\epsilon\frac{\partial^2\phi}{\partial \xi^2}+\epsilon^2\frac{\partial^2\phi}{\partial \eta^2}=n_{0h}(1+\phi+\tfrac{1}{2}\phi^2+\tfrac{1}{6}\phi^3)-\sum_j Z_j n_j.
\end{aligned}
$$

Upon substituting the expansions (E.4) into the above system we obtain from Poisson's equation

$$O(\epsilon^0)\qquad n_{0h}-\sum_j Z_j n_j^{(0)}=0, \tag{E.5}$$

$$O(\epsilon^1)\qquad n_{0h}-\sum_j Z_j n_j^{(1)}=0, \tag{E.6}$$

$$O(\epsilon^2)\qquad \frac{\partial^2\phi^{(1)}}{\partial \xi^2}=n_{0h}\phi^{(2)}+\tfrac{1}{2}n_{0h}(\phi^{(1)})^2-\sum_j Z_j n_j^{(2)}. \tag{E.7}$$

The equation of continuity yields the following equations:

$$O(\epsilon^{3/2})\qquad -V\frac{\partial n_j^{(1)}}{\partial \xi}+n_j^{(0)}\frac{\partial u_j^{(1)}}{\partial \xi}=0, \tag{E.8}$$

$$
\begin{aligned}
O(\epsilon^{5/2})\qquad &-V\frac{\partial n_j^{(2)}}{\partial \xi}+\frac{\partial n_j^{(1)}}{\partial \tau}+n_j^{(0)}\frac{\partial u_j^{(2)}}{\partial \xi}+n_j^{(0)}\frac{\partial v_j^{(1)}}{\partial \eta}\\
&+\frac{\partial}{\partial \xi}(n_j^{(1)}u_j^{(1)})=0.
\end{aligned} \tag{E.9}
$$

The ξ–component of the momentum equation yields the equations:

$$O(\epsilon^{3/2}) \qquad -n_j^{(0)} V \frac{\partial u_j^{(1)}}{\partial \xi} = -\frac{1}{m_j}\frac{\partial p_j^{(1)}}{\partial \xi} - \frac{Z_j n_j^{(0)}}{m_j}\frac{\partial \phi^{(1)}}{\partial \xi}, \tag{E.10}$$

$$O(\epsilon^{5/2}) \qquad -n_j^{(0)} V \frac{\partial u_j^{(2)}}{\partial \xi} - n_j^{(1)} V \frac{\partial u_j^{(1)}}{\partial \xi} + n_j^{(0)}\frac{\partial u_j^{(1)}}{\partial \tau} + n_j^{(0)} u_j^{(1)}\frac{\partial u_j^{(1)}}{\partial \xi}$$
$$= -\frac{1}{m_j}\frac{\partial p_j^{(2)}}{\partial \xi} - \frac{Z_j n_j^{(0)}}{m_j}\frac{\partial \phi^{(2)}}{\partial \xi} - \frac{Z_j n_j^{(1)}}{m_j}\frac{\partial \phi^{(1)}}{\partial \xi}. \tag{E.11}$$

The η–component of momentum yields:

$$O(\epsilon^{2}) \qquad -n_j^{(0)} V \frac{\partial v_j^{(1)}}{\partial \xi} = -\frac{1}{m_j}\frac{\partial p_j^{(1)}}{\partial \eta} - \frac{Z_j n_j^{(0)}}{m_j}\frac{\partial \phi^{(1)}}{\partial \eta}, \tag{E.12}$$

$$O(\epsilon^{3}) \qquad -n_j^{(0)} V \frac{\partial v_j^{(2)}}{\partial \xi} - n_j^{(1)} V \frac{\partial v_j^{(1)}}{\partial \xi} + n_j^{(0)}\frac{\partial v_j^{(1)}}{\partial \tau} + n_j^{(0)} u_j^{(1)}\frac{\partial v_j^{(1)}}{\partial \xi}$$
$$= -\frac{1}{m_j}\frac{\partial p_j^{(2)}}{\partial \eta} - \frac{Z_j n_j^{(0)}}{m_j}\frac{\partial \phi^{(2)}}{\partial \eta} - \frac{Z_j n_j^{(1)}}{m_j}\frac{\partial \phi^{(1)}}{\partial \eta}. \tag{E.13}$$

From the pressure equation we obtain:

$$O(\epsilon^{3/2}) \qquad -V\frac{\partial p_j^{(1)}}{\partial \xi} + 3p_j^{(0)}\frac{\partial u_j^{(1)}}{\partial \xi} = 0, \tag{E.14}$$

$$O(\epsilon^{5/2}) \qquad -V\frac{\partial p_j^{(2)}}{\partial \xi} + \frac{\partial p_j^{(1)}}{\partial \tau} + u_j^{(1)}\frac{\partial p_j^{(1)}}{\partial \xi} + 3p_j^{(0)}\frac{\partial u_j^{(2)}}{\partial \xi} + 3p_j^{(1)}\frac{\partial u_j^{(1)}}{\partial \xi}$$
$$+3p_j^{(0)}\frac{\partial v_j^{(1)}}{\partial \eta} = 0. \tag{E.15}$$

Integrating the $O(\epsilon^{3/2})$ equations (E.8), (E.10) and (E.14), and solving in terms of $\phi^{(1)}$ yields

$$u_j^{(1)} = \frac{Z_j V/m_j}{V^2 - 3\sigma_j}\phi^{(1)}, \tag{E.16}$$

$$n_j^{(1)} = \frac{Z_j n_j^{(0)}/m_j}{V^2 - 3\sigma_j}\phi^{(1)}, \tag{E.17}$$

$$p_j^{(1)} = \frac{3Z_j n_j^{(0)}\sigma_j}{V^2 - 3\sigma_j}\phi^{(1)}, \tag{E.18}$$

where we have defined $\sigma_j = p_j^{(0)}/n_j^{(0)}m_j$ as before.

Employing (E.17) in (E.6) we obtain the following relation if $\phi^{(1)}$ is to be non-trivial

$$n_{0h} - \sum_j \frac{Z_j^2 n_j^{(0)}/m_j}{V^2 - 3\sigma_j} = 0, \tag{E.19}$$

which is to be satsfied by the velocity V.

At $O(\epsilon^2)$ we substitute (E.18) into (E.12) yielding

$$\frac{\partial v^{(1)}}{\partial \xi} = \frac{Z_j V/m_j}{V^2 - 3\sigma_j}\frac{\partial \phi^{(1)}}{\partial \eta}. \tag{E.20}$$

We deal with the $O(\epsilon^{5/2})$ equations as follows: we substitute (E.16)–(E.18) into equations (E.11), (E.15) and (E.9); and after some manipulation we obtain

$$\begin{aligned}\frac{\partial n_j^{(2)}}{\partial \xi} &= \frac{2Z_j n_j^{(0)} V/m_j}{(V^2 - 3\sigma_j)^2}\frac{\partial \phi^{(1)}}{\partial \tau} + \frac{3Z_j^2 n_j^{(0)}(V^2 + \sigma_j)/m_j^2}{(V^2 - 3\sigma_j)^3}\phi^{(1)}\frac{\partial \phi^{(1)}}{\partial \xi} \\ &\quad + \frac{n_j^{(0)} V}{V^2 - 3\sigma_j}\frac{\partial v_j^{(1)}}{\partial \eta} + \frac{Z_j n_j^{(0)}/m_j}{V^2 - 3\sigma_j}\frac{\partial \phi^{(2)}}{\partial \xi}.\end{aligned} \tag{E.21}$$

Differentiating (E.7) with respect to ξ and using the above equation and (E.19) yields

$$\begin{aligned}\frac{\partial^3 \phi^{(1)}}{\partial \xi^3} &= \left\{ n_{0h} - \sum_j \frac{3Z_j^3 n_j^{(0)}(V^2 + \sigma_j)/m_j^2}{(V^2 - 3\sigma_j)^3} \right\} \phi^{(1)}\frac{\partial \phi^{(1)}}{\partial \xi} \\ &\quad - \sum_j \frac{2Z_j^2 n_j^{(0)} V/m_j}{(V^2 - 3\sigma_j)^2}\frac{\partial \phi^{(1)}}{\partial \tau} - \sum_j \frac{Z_j n_j^{(0)} V}{V^2 - 3\sigma_j}\frac{\partial v_j^{(1)}}{\partial \eta}.\end{aligned} \tag{E.22}$$

Finally, differentiating the above equation with respect to ξ and using (E.20) yields the Kadomtsev–Petviashvili (KP) equation

$$\begin{aligned}\frac{\partial}{\partial \xi}\Bigg\{ &\sum_j \frac{2Z_j^2 n_j^{(0)} V/m_j}{(V^2 - 3\sigma_j)^2}\frac{\partial \phi^{(1)}}{\partial \tau} \\ &+ \left[\sum_j \frac{3Z_j^3 n_j^{(0)}(V^2 + \sigma_j)/m_j^2}{(V^2 - 3\sigma_j)^3} - n_{0h}\right]\phi^{(1)}\frac{\partial \phi^{(1)}}{\partial \xi} + \frac{\partial^3 \phi^{(1)}}{\partial \xi^3}\Bigg\}\end{aligned}$$

$$+\sum_j \frac{Z_j^2 n_j^{(0)} V^2/m_j}{(V^2-3\sigma_j)^2}\frac{\partial^2\phi^{(1)}}{\partial\eta^2} = 0. \tag{E.23}$$

Defining

$$A = \sum_j \frac{2Z_j^2 n_j^{(0)} V/m_j}{(V^2-3\sigma_j)^2}, \tag{E.24}$$

$$B = \sum_j \frac{3Z_j^3 n_j^{(0)}(V^2+\sigma_j)/m_j^2}{(V^2-3\sigma_j)^3} - n_{0h}, \tag{E.25}$$

with

$$a = \frac{B}{A}, \quad b = \frac{1}{A} \quad \text{and} \quad c = \tfrac{1}{2}V, \tag{E.26}$$

the KP equation may be cast in the form

$$\frac{\partial}{\partial\xi}\left\{\frac{\partial\phi^{(1)}}{\partial\tau} + a\phi^{(1)}\frac{\partial\phi^{(1)}}{\partial\xi} + b\frac{\partial^3\phi^{(1)}}{\partial\xi^3}\right\} + c\frac{\partial^2\phi^{(1)}}{\partial\eta^2} = 0. \tag{E.27}$$

Appendix F

The Korteweg–de Vries–Zakharov–Kuznetszov equation

In this appendix we derive the Korteweg–de Vries–Zakharov–Kuznetszov (KdV–ZK) equation for electron-acoustic waves. The derivation is essentially similar to Das & Verheest (1989) but we have filled in the missing steps.

We assume the Fourier components constituting the wave packet obey the following dispersion relation in the small amplitude limit

$$\omega = k_z v_{se}(1 - \tfrac{1}{2}k^2\lambda_{Dh}^2 - \tfrac{1}{2}k_\perp^2\rho_{se}^2).$$

For the definitions of symbols see chapter 8.

F.1 Basic equations

An infinite homogeneous, collisionless, magnetized plasma is considered. The magnetic field is in the direction of $\mathbf{e}_z$. The hot electron density is given by the Boltzmann distribution and the dynamics of the fluid components are determined by

$$\frac{\partial n_j}{\partial t} + \nabla \cdot (n_j \mathbf{u}_j) = 0, \tag{F.1}$$

$$m_j n_j \left(\frac{\partial \mathbf{u}_j}{\partial t} + \mathbf{u}_j \cdot \nabla \mathbf{u}_j \right) = -\nabla p_j - Z_j n_j \nabla \phi + Z_j m_j n_j \Omega_j \mathbf{u}_j \times \mathbf{e}_z, \tag{F.2}$$

$$\frac{\partial p_j}{\partial t} + \mathbf{u}_j \cdot \nabla p_j + 3p_j \nabla \cdot \mathbf{u}_j = 0. \tag{F.3}$$

The system of equations is coupled by the Poisson equation

$$\nabla^2 \phi = n_{0h} \exp \phi - \sum_j Z_j n_j, \tag{F.4}$$

and the index j runs over the fluid components ($j = i, c$). The following normalizations have been used in the above equations: lengths by the 'Debye length' $(T_h/4\pi n_{0e}e^2)^{1/2}$; time by the inverse electron plasma frequency $\omega_{pe}^{-1} = (m_e/4\pi n_{0e}e^2)^{1/2}$; number densities by the total electron density n_{0e}; pressures by $n_{0e}T_h$; temperatures by T_h; velocities by the hot electron thermal speed $(T_h/m_e)^{1/2}$; electrostatic potential by T_h/e; masses by the electron mass m_e; and $Z_j \equiv q_j/e$; $\Omega_j = \Omega_j'/\omega_{pe}$ is the gyrofrequency ($\Omega_j' \equiv eB/m_j c_L$ in unnormalized quantities; c_L is the speed of light) divided by the electron plasma frequency. Furthermore, the usual soliton boundary conditions are imposed in three dimensions

$$\left.\begin{array}{lll} \phi \to 0, & \nabla\phi \to 0, & \nabla^2\phi \to 0, \\ n_j \to n_j^{(0)}, & p_j \to p_{0j}, & \mathbf{u}_j \to 0 \end{array}\right\} \quad \text{as} \quad |\mathbf{x}| \to \infty. \tag{F.5}$$

F.2 The reductive perturbation technique

Introducing the coordinate stretchings

$$\xi = \epsilon^{1/2}x, \quad \eta = \epsilon^{1/2}y, \quad \zeta = \epsilon^{1/2}(z - Vt), \quad \tau = \epsilon^{3/2}t, \tag{F.6}$$

into the above dynamical equations yields

$$-\epsilon^{1/2}V\frac{\partial n_j}{\partial \zeta} + \epsilon^{3/2}\frac{\partial n_j}{\partial \tau} + \epsilon^{1/2}\nabla_\xi \cdot (n_j \mathbf{u}_j) = 0, \tag{F.7}$$

$$-\epsilon^{1/2}m_j n_j V\frac{\partial \mathbf{u}_j}{\partial \zeta} + \epsilon^{3/2}m_j n_j \frac{\partial \mathbf{u}_j}{\partial \tau} + \epsilon^{1/2}m_j n_j \mathbf{u}_j \cdot \nabla_\xi \mathbf{u}_j + \epsilon^{1/2}\nabla_\xi p_j = -\epsilon^{1/2}Z_j n_j \nabla_\xi \phi + Z_j m_j n_j \Omega_j (\mathbf{u}_j \times \mathbf{e}_z), \tag{F.8}$$

$$-\epsilon^{1/2}V\frac{\partial p_j}{\partial \zeta} + \epsilon^{3/2}\frac{\partial p_j}{\partial \tau} + \epsilon^{1/2}\mathbf{u}_j \cdot \nabla_\xi p_j + \epsilon^{1/2}3p_j \nabla_\xi \cdot \mathbf{u}_j = 0, \tag{F.9}$$

$$\epsilon\nabla_\xi^2 \phi = n_{0h}\Big(1 + \phi + \tfrac{1}{2}\phi^2 + \tfrac{1}{6}\phi^3\Big) - \sum_j Z_j n_j, \tag{F.10}$$

where the operator $\nabla_\xi \equiv (\partial/\partial\xi, \partial/\partial\eta, \partial/\partial\zeta)$ and the flow velocity $\mathbf{u}_j \equiv (u_j, v_j, w_j)$. The stretchings (F.6) reflect the same spatial and temporal dependence that was employed in appendix D, however, the number of spatial dimensions has now been increased to three. Upon substitution of the expansions

$$n_j = n_j^{(0)} + \epsilon n_j^{(1)} + \epsilon^2 n_j^{(2)} + \cdots, \tag{F.11}$$

$$w_j = \epsilon w_j^{(1)} + \epsilon^2 w_j^{(2)} + \cdots, \tag{F.12}$$

$$p_j = p_j^{(0)} + \epsilon p_j^{(1)} + \epsilon^2 p_j^{(2)} + \cdots, \tag{F.13}$$

$$\phi = \epsilon\phi^{(1)} + \epsilon^2\phi^{(2)} + \cdots, \tag{F.14}$$

$$u_j = \epsilon^{3/2} u_j^{(1)} + \epsilon^2 u_j^{(2)} + \cdots, \tag{F.15}$$

$$v_j = \epsilon^{3/2} v_j^{(1)} + \epsilon^2 v_j^{(2)} + \cdots, \tag{F.16}$$

into the above equations and solving order by order we obtain from Poisson's equation

$$O(\epsilon^0) \qquad n_{0h} - \sum_j Z_j n_j^{(0)} = 0, \tag{F.17}$$

$$O(\epsilon^1) \qquad n_{0h}\phi^{(1)} - \sum_j Z_j n_j^{(1)} = 0, \tag{F.18}$$

$$O(\epsilon^2) \qquad \frac{\partial^2\phi^{(1)}}{\partial\xi^2} + \frac{\partial^2\phi^{(1)}}{\partial\eta^2} + \frac{\partial^2\phi^{(1)}}{\partial\zeta^2} = n_{0h}\phi^{(2)} + \tfrac{1}{2} n_{0h}(\phi^{(1)})^2 - \sum_j Z_j n_j^{(2)}, \tag{F.19}$$

from the equation of continuity

$$O(\epsilon^{3/2}) \qquad -V\frac{\partial n_j^{(1)}}{\partial\zeta} + \frac{\partial}{\partial\zeta}(n_j^{(0)} w_j^{(1)}) = 0, \tag{F.20}$$

$$O(\epsilon^2) \qquad n_j^{(0)}\frac{\partial u_j^{(1)}}{\partial\xi} + n_j^{(0)}\frac{\partial v_j^{(1)}}{\partial\eta} = 0, \tag{F.21}$$

$$O(\epsilon^{5/2}) \qquad -V\frac{\partial n_j^{(2)}}{\partial\zeta} + \frac{\partial n_j^{(1)}}{\partial\tau} + n_j^{(0)}\frac{\partial u_j^{(2)}}{\partial\xi} + n_j^{(0)}\frac{\partial v_j^{(2)}}{\partial\eta} + n_j^{(0)}\frac{\partial w_j^{(2)}}{\partial\zeta} + \frac{\partial}{\partial\zeta}(n_j^{(1)} w_j^{(1)}) = 0, \tag{F.22}$$

from the ξ–component of momentum

$$O(\epsilon^{3/2}) \qquad \frac{1}{m_j}\frac{\partial p_j^{(1)}}{\partial \xi} = -\frac{Z_j n_j^{(0)}}{m_j}\frac{\partial \phi^{(1)}}{\partial \xi} + Z_j n_j^{(0)} \Omega_j v_j^{(1)}, \quad \text{(F.23)}$$

$$O(\epsilon^{2}) \qquad -n_j^{(0)} V \frac{\partial u_j^{(1)}}{\partial \zeta} = Z_j n_j^{(0)} \Omega_j v_j^{(2)}, \quad \text{(F.24)}$$

from the η–component of momentum

$$O(\epsilon^{3/2}) \qquad \frac{1}{m_j}\frac{\partial p_j^{(1)}}{\partial \eta} = -\frac{Z_j n_j^{(0)}}{m_j}\frac{\partial \phi^{(1)}}{\partial \eta} - Z_j n_j^{(0)} \Omega_j u_j^{(1)}, \quad \text{(F.25)}$$

$$O(\epsilon^{2}) \qquad -n_j^{(0)} V \frac{\partial v_j^{(1)}}{\partial \zeta} = -Z_j n_j^{(0)} \Omega_j u_j^{(2)}, \quad \text{(F.26)}$$

from the ζ–component of momentum

$$O(\epsilon^{3/2}) \qquad -n_j^{(0)} V \frac{\partial w_j^{(1)}}{\partial \zeta} + \frac{1}{m_j}\frac{\partial p_j^{(1)}}{\partial \zeta} = -\frac{Z_j n_j^{(0)}}{m_j}\frac{\partial \phi^{(1)}}{\partial \zeta}, \quad \text{(F.27)}$$

$$O(\epsilon^{5/2}) \qquad -n_j^{(0)} V \frac{\partial w_j^{(2)}}{\partial \zeta} - V n_j^{(1)} \frac{\partial w_j^{(1)}}{\partial \zeta} + n_j^{(0)} \frac{\partial w_j^{(1)}}{\partial \tau} + n_j^{(0)} w_j^{(1)} \frac{\partial w_j^{(1)}}{\partial \zeta}$$
$$+\frac{1}{m_j}\frac{\partial p_j^{(2)}}{\partial \zeta} = -\frac{Z_j n_j^{(0)}}{m_j}\frac{\partial \phi^{(2)}}{\partial \zeta} - \frac{Z_j}{m_j} n_j^{(1)} \frac{\partial \phi^{(1)}}{\partial \zeta}, \quad \text{(F.28)}$$

and finally, from the pressure equation

$$O(\epsilon^{3/2}) \qquad -V\frac{\partial p_j^{(1)}}{\partial \zeta} + 3p_j^{(0)}\frac{\partial w_j^{(1)}}{\partial \zeta} = 0, \quad \text{(F.29)}$$

$$O(\epsilon^{5/2}) \qquad -V\frac{\partial p_j^{(2)}}{\partial \zeta} + \frac{\partial p_j^{(1)}}{\partial \tau} + w_j^{(1)}\frac{\partial p_j^{(1)}}{\partial \zeta} + 3p_j^{(0)}\left(\frac{\partial u_j^{(2)}}{\partial \xi} + \frac{\partial v_j^{(2)}}{\partial \eta}\right)$$
$$+3p_j^{(0)}\frac{\partial w_j^{(2)}}{\partial \zeta} + 3p_j^{(1)}\frac{\partial w_j^{(1)}}{\partial \zeta} = 0. \quad \text{(F.30)}$$

The $O(\epsilon^{3/2})$ equations (F.20), (F.27) and (F.29) may be integrated immediately using the boundary conditions (F.5). Substituting the equation so obtained from (F.29) into that so obtained from (F.27) and solving for $w_j^{(1)}$ we obtain:

$$w_j^{(1)} = \frac{Z_j V/m_j}{V^2 - 3\sigma_j}\phi^{(1)}, \quad \text{(F.31)}$$

where $\sigma_j \equiv p_j^{(0)}/m_j n_j^{(0)}$. Substituting (F.31) into the remaining equations obtained from (F.20) and (F.29) yields

$$n_j^{(1)} = \frac{Z_j n_j^{(0)}/m_j}{V^2 - 3\sigma_j}\phi^{(1)}, \tag{F.32}$$

and for the first-order pressure

$$p_j^{(1)} = \frac{3Z_j n_j^{(0)}\sigma_j}{V^2 - 3\sigma_j}\phi^{(1)}. \tag{F.33}$$

From the other $O(\epsilon^{3/2})$ equations, namely (F.23) and (F.25), we can write $u_j^{(1)}$ and $v_j^{(1)}$ in terms of derivatives of $\phi^{(1)}$ by employing (F.33), yielding

$$u_j^{(1)} = -\frac{V^2}{m_j\Omega_j(V^2 - 3\sigma_j)}\frac{\partial\phi^{(1)}}{\partial\eta}, \tag{F.34}$$

and

$$v_j^{(1)} = \frac{V^2}{m_j\Omega_j(V^2 - 3\sigma_j)}\frac{\partial\phi^{(1)}}{\partial\xi}. \tag{F.35}$$

Employing the Poisson equation at $O(\epsilon)$ and using (F.32) yields the following equation determining V (on supposing non-trivial $\phi^{(1)}$):

$$n_{0h} - \sum_j \frac{Z_j^2 n_j^{(0)}/m_j}{V^2 - 3\sigma_j} = 0. \tag{F.36}$$

At next highest order we proceed as follows. Firstly note that (F.21) is satisfied identically by (F.34) and (F.35). The other $O(\epsilon^2)$ equations (F.24) and (F.26) yield on using (F.34) and (F.35)

$$\frac{\partial u_j^{(2)}}{\partial\xi} = \frac{V^3}{Z_j m_j\Omega_j^2(V^2 - 3\sigma_j)}\frac{\partial^3\phi^{(1)}}{\partial\zeta\,\partial\xi^2}, \tag{F.37}$$

and

$$\frac{\partial v_j^{(2)}}{\partial\eta} = \frac{V^3}{Z_j m_j\Omega_j^2(V^2 - 3\sigma_j)}\frac{\partial^3\phi^{(1)}}{\partial\zeta\,\partial\eta^2}. \tag{F.38}$$

At $O(\epsilon^{5/2})$ we eliminate $p_j^{(2)}$ from (F.28) by using (F.30) yielding (on using (F.31)–(F.33) and (F.37), (F.38))

$$
\begin{aligned}
n_j^{(0)}\frac{\partial w_j^{(2)}}{\partial \zeta} &= \frac{Z_j n_j^{(0)}(V^2+3\sigma_j)/m_j}{(V^2-3\sigma_j)^2}\frac{\partial \phi^{(1)}}{\partial \tau} \\
&\quad + \frac{Z_j^2 n_j^{(0)} V(V^2+9\sigma_j)/m_j^2}{(V^2-3\sigma_j)^3}\phi^{(1)}\frac{\partial \phi^{(1)}}{\partial \zeta} \\
&\quad + \frac{3n_j^{(0)}V^3\sigma_j}{Z_j m_j \Omega_j^2 (V^2-3\sigma_j)^2}\frac{\partial}{\partial \zeta}\left(\frac{\partial^2\phi^{(1)}}{\partial \xi^2}+\frac{\partial^2\phi^{(1)}}{\partial \eta^2}\right) \\
&\quad + \frac{Z_j n_j^{(0)} V/m_j}{V^2-3\sigma_j}\frac{\partial \phi^{(2)}}{\partial \zeta}. \qquad \text{(F.39)}
\end{aligned}
$$

Substituting this into (F.22) where again we use (F.31)–(F.33) and (F.37), (F.38) yields

$$
\begin{aligned}
\frac{\partial n_j^{(2)}}{\partial \zeta} &= \frac{2Z_j n_j^{(0)} V/m_j}{(V^2-3\sigma_j)^2}\frac{\partial \phi^{(1)}}{\partial \tau} + \frac{3Z_j^2 n_j^{(0)}(V^2+\sigma_j)/m_j^2}{(V^2-3\sigma_j)^3}\phi^{(1)}\frac{\partial \phi^{(1)}}{\partial \zeta} \\
&\quad + \frac{n_j^{(0)}V^4}{Z_j m_j \Omega_j^2 (V^2-3\sigma_j)^2}\frac{\partial}{\partial \zeta}\left(\frac{\partial^2\phi^{(1)}}{\partial \xi^2}+\frac{\partial^2\phi^{(1)}}{\partial \eta^2}\right) \\
&\quad + \frac{Z_j n_j^{(0)}/m_j}{V^2-3\sigma_j}\frac{\partial \phi^{(2)}}{\partial \zeta}. \qquad \text{(F.40)}
\end{aligned}
$$

Finally, differentiating (F.19) with respect to ζ and substituting the above into it; and using (F.36) to eliminate the term involving $\phi^{(2)}$ yields

$$
\begin{aligned}
&2\sum_j \frac{Z_j^2 n_j^{(0)} V/m_j}{(V^2-3\sigma_j)^2}\frac{\partial \phi^{(1)}}{\partial \tau} \\
&\quad + \left\{\sum_j \frac{3Z_j^3 n_j^{(0)}(V^2+\sigma_j)/m_j^2}{(V^2-3\sigma_j)^3} - n_{0h}\right\}\phi^{(1)}\frac{\partial \phi^{(1)}}{\partial \zeta} + \frac{\partial^3 \phi^{(1)}}{\partial \zeta^3} \\
&\quad + \left\{1+\sum_j \frac{n_j^{(0)}V^4}{m_j\Omega_j^2(V^2-3\sigma_j)^2}\right\}\frac{\partial}{\partial \zeta}\left(\frac{\partial^2\phi^{(1)}}{\partial \xi^2}+\frac{\partial^2\phi^{(1)}}{\partial \eta^2}\right) = 0. \qquad \text{(F.41)}
\end{aligned}
$$

Defining

$$A = 2\sum_j \frac{Z_j^2 n_j^{(0)} V/m_j}{(V^2-3\sigma_j)^2}, \tag{F.42}$$

$$B = 3\sum_j \frac{Z_j^3}{m_j^2} n_j^{(0)} \frac{(V^2+\sigma_j)}{(V^2-3\sigma_j)^3} - n_{0h}, \tag{F.43}$$

$$C = 1+\sum_j \frac{n_j^{(0)} V^4/m_j}{\Omega_j^2 (V^2-3\sigma_j)^2}, \tag{F.44}$$

with

$$a = \frac{B}{A}, \qquad b = \frac{1}{A}, \qquad c = \frac{C}{A},$$

the KdV–ZK equation may be cast in the form

$$\frac{\partial \phi^{(1)}}{\partial \tau} + a\phi^{(1)}\frac{\partial \phi^{(1)}}{\partial \zeta} + b\frac{\partial^3 \phi^{(1)}}{\partial \zeta^3} + c\frac{\partial}{\partial \zeta}\left(\frac{\partial^2 \phi^{(1)}}{\partial \xi^2} + \frac{\partial^2 \phi^{(1)}}{\partial \eta^2}\right) = 0. \tag{F.45}$$

Appendix G

The Korteweg–de Vries equation for relativistic, streaming plasma

In this appendix we employ the reductive perturbation technique to derive a KdV equation for a relativistic streaming plasma. The derivation represents a generalization of that done previously in appendix D, and is moreover, a generalization of the work of Nejoh (1987a) to a plasma consisting of k fluid components.

G.1 Basic equations

An infinite, collisionless, unmagnetized, weakly-relativistic ($T_j \ll m_j c^2$), multi-fluid plasma is assumed. The plasma dynamics are governed by the following normalized equations (see appendix C; Nejoh 1987a):

$$\frac{\partial n_j}{\partial t} + \frac{\partial}{\partial x}(n_j u_j) = 0, \tag{G.1}$$

$$n_j \left(\frac{\partial}{\partial t} + u_j \frac{\partial}{\partial x} \right) (\gamma_j u_j) = -\frac{1}{m_j} \frac{\partial p_j}{\partial x} - \frac{Z_j n_j}{m_j} \frac{\partial \phi}{\partial x}, \tag{G.2}$$

$$\frac{\partial p_j}{\partial t} + u_j \frac{\partial p_j}{\partial x} + 3 p_j \frac{\partial}{\partial x}(\gamma_j u_j) = 0, \tag{G.3}$$

$$\frac{\partial^2 \phi}{\partial x^2} = n_h - \sum_j Z_j n_j, \tag{G.4}$$

$$n_h = n_{0h} \exp \phi, \tag{G.5}$$

where j denotes the jth fluid component, whose thermal velocity is assumed to be much less than the wave phase velocity. The normalizations are as follows: spatial lengths by the length $(T_h/4\pi n_{0e}e^2)^{1/2}$, time by the inverse electron plasma frequency $(m_e/4\pi n_{0e}e^2)^{1/2}$, number densities by the total electron density n_{0e}, pressures by $n_{0e}T_h$, electrostatic potential by T_h/e, velocities by the hot electron thermal speed $(T_h/m_e)^{1/2}$, masses by the electron proper mass m_e, and $Z_j \equiv q_j/e$.

In addition, the following boundary conditions are imposed

$$\left.\begin{array}{rrr} \phi \to 0, & \dfrac{\partial \phi}{\partial x} \to 0, & \dfrac{\partial^2 \phi}{\partial x^2} \to 0, \\ n_j \to n_{0j}, & p_j \to p_{0j}, & u_j \to u_{0j}, \end{array}\right\} \quad \text{as} \quad |x| \to \infty. \tag{G.6}$$

G.2 The reductive perturbation technique

As in the nonrelativistic case, the following coordinate stretchings

$$\xi = \epsilon^{1/2}(x - Vt), \qquad \tau = \epsilon^{3/2}t, \tag{G.7}$$

and expansions

$$\left.\begin{aligned} n_j &= n_j^{(0)} + \epsilon n_j^{(1)} + \epsilon^2 n_j^{(2)} + \cdots, \\ u_j &= u_j^{(0)} + \epsilon u_j^{(1)} + \epsilon^2 u_j^{(2)} + \cdots, \\ p_j &= p_j^{(0)} + \epsilon p_j^{(1)} + \epsilon^2 p_j^{(2)} + \cdots, \\ \phi &= \epsilon\phi^{(1)} + \epsilon^2\phi^{(2)} + \cdots, \end{aligned}\right\} \tag{G.8}$$

are employed. In terms of the new coordinates the equations (G.1)–(G.4) become

$$-\epsilon^{1/2}V\frac{\partial n_j}{\partial \xi} + \epsilon^{3/2}\frac{\partial n_j}{\partial \tau} + \epsilon^{1/2}\frac{\partial}{\partial \xi}(n_j u_j) = 0, \tag{G.9}$$

$$n_j\left(-\epsilon^{1/2}(V - u_j)\frac{\partial}{\partial \xi}(\gamma_j u_j) + \epsilon^{3/2}\frac{\partial}{\partial \tau}(\gamma_j u_j)\right) = -\epsilon^{1/2}\frac{1}{m_j}\frac{\partial p_j}{\partial \xi} - \epsilon^{1/2}\frac{Z_j n_j}{m_j}\frac{\partial \phi}{\partial \xi}, \tag{G.10}$$

$$-\epsilon^{1/2}(V - u_j)\frac{\partial p_j}{\partial \xi} + \epsilon^{3/2}\frac{\partial p_j}{\partial \tau} + \epsilon^{1/2}3p_j\frac{\partial}{\partial \xi}(\gamma_j u_j) = 0, \tag{G.11}$$

$$\epsilon\frac{\partial^2\phi}{\partial\xi^2} = n_{0h}(1+\phi+\tfrac{1}{2}\phi^2+\tfrac{1}{6}\phi^3) - \sum_j Z_j n_j. \tag{G.12}$$

The "world velocity", $\gamma_j u_j$, is expanded as follows

$$\begin{aligned}\gamma_j u_j &= u_j^{(0)} + \epsilon u_j^{(1)} + \epsilon^2 u_j^{(2)} + \frac{1}{2c^2}\left\{(u_j^{(0)})^3 + 3\epsilon(u_j^{(0)})^2 u_j^{(1)}\right.\\ &\qquad \left. + 3\epsilon^2((u_j^{(0)})^2 u_j^{(2)} + (u_j^{(1)})^2 u_j^{(0)})\right\},\\ &= \left\{1+\frac{1}{2c^2}(u_j^{(0)})^2\right\} u_j^{(0)} + \epsilon\Gamma_j u_j^{(1)} + \epsilon^2\Gamma_j u_j^{(2)}\\ &\qquad +\epsilon^2\frac{3}{2c^2}u_j^{(0)}(u_j^{(1)})^2,\end{aligned} \tag{G.13}$$

where we have defined

$$\Gamma_j = 1 + \frac{3}{2}\left(\frac{u_j^{(0)}}{c}\right)^2.$$

Upon substituting the expansions (G.8) and (G.13) into the above system, and solving order by order we obtain the following: from Poisson's equation

$$O(\epsilon^0) \qquad n_{0h} - \sum_j Z_j n_j^{(0)} = 0, \tag{G.14}$$

$$O(\epsilon^1) \qquad n_{0h}\phi^{(1)} - \sum_j Z_j n_j^{(1)} = 0, \tag{G.15}$$

$$O(\epsilon^2) \qquad \frac{\partial^2\phi^{(1)}}{\partial\xi^2} = n_{0h}\phi^{(2)} + \frac{1}{2}n_{0h}(\phi^{(1)})^2 - \sum_j Z_j n_j^{(2)}, \tag{G.16}$$

from the equation of continuity

$$O(\epsilon^{3/2}) \qquad -\lambda_j\frac{\partial n_j^{(1)}}{\partial\xi} + n_j^{(0)}\frac{\partial u_j^{(1)}}{\partial\xi} = 0, \tag{G.17}$$

$$O(\epsilon^{5/2}) \qquad -\lambda_j\frac{\partial n_j^{(2)}}{\partial\xi} + \frac{\partial n_j^{(1)}}{\partial\tau} + n_j^{(0)}\frac{\partial u_j^{(2)}}{\partial\xi} + \frac{\partial}{\partial\xi}(n_j^{(1)}u_j^{(1)}) = 0, \tag{G.18}$$

from the momentum equation,

$$O(\epsilon^{3/2}) \qquad -n_j^{(0)}\lambda_j\Gamma_j\frac{\partial u_j^{(1)}}{\partial\xi} = -\frac{1}{m_j}\frac{\partial p_j^{(1)}}{\partial\xi} - \frac{Z_j n_j^{(0)}}{m_j}\frac{\partial\phi^{(1)}}{\partial\xi} \tag{G.19}$$

$$O(\epsilon^{5/2}) \qquad -n_j^{(0)}\lambda_j\Gamma_j\frac{\partial u_j^{(2)}}{\partial\xi} - \frac{3}{2c^2}n_j^{(0)}u_j^{(0)}\lambda_j\frac{\partial}{\partial\xi}(u_j^{(1)})^2 - n_j^{(1)}\lambda_j\Gamma_j\frac{\partial u_j^{(1)}}{\partial\xi}$$
$$+n_j^{(0)}\Gamma_j u_j^{(1)}\frac{\partial u_j^{(1)}}{\partial\xi} + n_j^{(0)}\Gamma_j\frac{\partial u_j^{(1)}}{\partial\tau} = -\frac{1}{m_j}\frac{\partial p_j^{(2)}}{\partial\xi}$$
$$-\frac{Z_j n_j^{(1)}}{m_j}\frac{\partial\phi^{(1)}}{\partial\xi} - \frac{Z_j n_j^{(0)}}{m_j}\frac{\partial\phi^{(2)}}{\partial\xi} \tag{G.20}$$

and

$$O(\epsilon^{3/2}) \qquad -\lambda_j\frac{\partial p_j^{(1)}}{\partial\xi} + 3p_j^{(0)}\Gamma_j\frac{\partial u_j^{(1)}}{\partial\xi} = 0, \tag{G.21}$$

$$O(\epsilon^{5/2}) \qquad -\lambda_j\frac{\partial p_j^{(2)}}{\partial\xi} + \frac{\partial p_j^{(1)}}{\partial\tau} + u_j^{(1)}\frac{\partial p_j^{(1)}}{\partial\xi} + 3p_j^{(0)}\Gamma_j\frac{\partial u_j^{(2)}}{\partial\xi}$$
$$+\frac{9}{2c^2}p_j^{(0)}u_j^{(0)}\frac{\partial}{\partial\xi}(u_j^{(1)})^2 + 3p_j^{(1)}\Gamma_j\frac{\partial u_j^{(1)}}{\partial\xi} = 0, \tag{G.22}$$

from the pressure equation. The parameter λ_j is defined by $\lambda_j \equiv V - u_j^{(0)}$.

Note that as in the non-relativistic case, the $O(\epsilon^{3/2})$ equations (G.17), (G.19) and (G.21) may be integrated at once using the boundary conditions (G.6), yielding a similar set of equations without the partial derivations in ξ. Following a similar proceedure to that employed in appendix D, i.e. substituting the so-derived equation resulting from (G.21) into the corresponding equation resulting from (G.19) we obtain

$$u_j^{(1)} = \frac{Z_j\lambda_j/m_j}{\Gamma_j(\lambda_j^2 - 3\sigma_j)}\phi^{(1)}, \tag{G.23}$$

for the first-order velocity of the jth fluid component. The parameter $\sigma_j \equiv p_j^{(0)}/m_j n_j^{(0)} = T_j/m_j$. Employing this equation in the integral of (G.17) yields

$$n_j^{(1)} = \frac{Z_j n_j^{(0)}/m_j}{\Gamma_j(\lambda_j^2 - 3\sigma_j)}\phi^{(1)}, \tag{G.24}$$

and by (G.21) one has

$$p_j^{(1)} = \frac{3Z_j n_j^{(0)}\sigma_j}{\lambda_j^2 - 3\sigma_j}\phi^{(1)}. \tag{G.25}$$

Substituting the expression for $n_j^{(1)}$ into the $O(\epsilon)$ equation (G.15) arising from the Poisson equation furnishes

$$\left\{ n_{0h} - \sum_j \frac{Z_j^2 n_j^{(0)}/m_j}{\Gamma_j(\lambda_j^2 - 3\sigma_j)} \right\} \phi^{(1)} = 0, \tag{G.26}$$

where for non-trivial $\phi^{(1)}$ we demand that the term in braces vanish, yielding a linear dispersion relation to be satisfied by the long-wavelength phase velocity V.

The higher-order equations are dealt with in a manner similar to that in appendix D. However, we now have to contend with the extra algebraic baggage introduced by the zeroth order drifts.

The term involving $p_j^{(2)}$ in the momentum equation (G.20) is eliminated by substitution from the $O(\epsilon^{5/2})$ pressure equation (G.22). This yields the following equation

$$\begin{aligned} n_j^{(0)} \frac{\partial u_j^{(2)}}{\partial \xi} \;=\; & -\frac{3n_j^{(0)} u_j^{(0)}}{c^2 \Gamma_j} u_j^{(1)} \frac{\partial u_j^{(1)}}{\partial \xi} - \frac{\lambda_j^2}{\lambda_j^2 - 3\sigma_j} n_j^{(1)} \frac{\partial u_j^{(1)}}{\partial \xi} \\ & + \frac{n_j^{(0)} \lambda_j}{\lambda_j^2 - 3\sigma_j} u_j^{(1)} \frac{\partial u_j^{(1)}}{\partial \xi} + \frac{n_j^{(0)} \lambda_j}{\lambda_j^2 - 3\sigma_j} \frac{\partial u_j^{(1)}}{\partial \tau} \\ & + \frac{1/m_j}{\Gamma_j(\lambda_j^2 - 3\sigma_j)} u_j^{(1)} \frac{\partial p_j^{(1)}}{\partial \xi} + \frac{1/m_j}{\Gamma_j(\lambda_j^2 - 3\sigma_j)} \frac{\partial p_j^{(1)}}{\partial \tau} \\ & + \frac{3/m_j}{\lambda_j^2 - 3\sigma_j} p_j^{(1)} \frac{\partial u_j^{(1)}}{\partial \xi} + \frac{Z_j \lambda_j / m_j}{\Gamma_j(\lambda_j^2 - 3\sigma_j)} n_j^{(1)} \frac{\partial \phi^{(1)}}{\partial \xi} \\ & + \frac{Z_j n_j^{(0)} \lambda_j / m_j}{\Gamma_j(\lambda_j^2 - 3\sigma_j)} \frac{\partial \phi^{(2)}}{\partial \xi} \end{aligned} \tag{G.27}$$

Substitution of this equation into equation (G.18) and writing the first order quantities in terms of $\phi^{(1)}$ using (G.23)-(G.25) we obtain

$$\begin{aligned} \frac{\partial n_j^{(2)}}{\partial \xi} \;=\; & \frac{2 Z_j n_j^{(0)} \lambda_j / m_j}{\Gamma_j(\lambda_j^2 - 3\sigma_j)^2} \frac{\partial \phi^{(1)}}{\partial \tau} \\ & + 3 \left\{ \frac{Z_j^2 n_j^{(0)} (\lambda_j^2 + (3\Gamma_j - 2)\sigma_j)/m_j^2}{\Gamma_j^2 (\lambda_j^2 - 3\sigma_j)^3} \right. \end{aligned}$$

$$- \frac{u_j^{(0)}}{c^2} \frac{Z_j^2 n_j^{(0)} \lambda_j / m_j^2}{\Gamma_j^3 (\lambda_j^2 - 3\sigma_j)^2} \Bigg\} \phi^{(1)} \frac{\partial \phi^{(1)}}{\partial \xi}$$

$$+ \frac{Z_j n_j^{(0)} / m_j}{\Gamma_j (\lambda_j^2 - 3\sigma_j)} \frac{\partial \phi^{(2)}}{\partial \xi}. \quad \text{(G.28)}$$

Partially differentiating the $O(\epsilon^2)$ equation (G.16) obtained from the Poisson equation, one obtains to $O(\epsilon^{5/2})$:

$$\frac{\partial^3 \phi^{(1)}}{\partial \xi^3} = n_{0h} \frac{\partial \phi^{(2)}}{\partial \xi} + n_{0h} \phi^{(1)} \frac{\partial \phi^{(1)}}{\partial \xi} - \sum_j Z_j \frac{\partial n_j^{(2)}}{\partial \xi}.$$

Substitution of (G.28) into the latter equation yields the Korteweg–de Vries equation for the first-order potential $\phi^{(1)}$:

$$\sum_j \frac{2 Z_j^2 n_j^{(0)} \lambda_j / m_j}{\Gamma_j (\lambda_j^2 - 3\sigma_j)^2} \frac{\partial \phi^{(1)}}{\partial \tau}$$

$$+ \Bigg\{ \sum_j \frac{3 Z_j^3 n_j^{(0)} (\lambda_j^2 + (3\Gamma_j - 2)\sigma_j) / m_j^2}{\Gamma_j^2 (\lambda_j^2 - 3\sigma_j)^3}$$

$$- \frac{u_j^{(0)}}{c^2} \frac{3 Z_j^3 n_j^{(0)} \lambda_j / m_j^2}{\Gamma_j^3 (\lambda_j^2 - 3\sigma_j)^2} - n_{0h} \Bigg\} \phi^{(1)} \frac{\partial \phi^{(1)}}{\partial \xi}$$

$$+ \frac{\partial^3 \phi^{(1)}}{\partial \xi^3} = 0, \quad \text{(G.29)}$$

where the dispersion relation (G.26) was used. Defining

$$A = 2 \sum_j \frac{Z_j^2}{m_j} \frac{n_j^{(0)} \lambda_j}{\Gamma_j (\lambda_j^2 - 3\sigma_j)^2}, \quad \text{(G.30)}$$

$$B = 3 \sum_j \frac{3 Z_j^3}{m_j^2} \left\{ \frac{n_j^{(0)} (\lambda_j^2 + (3\Gamma_j - 2)\sigma_j)}{\Gamma_j^2 (\lambda_j^2 - 3\sigma_j)^3} - \frac{u_j^{(0)}}{c^2} \frac{n_j^{(0)} \lambda_j}{\Gamma_j^3 (\lambda_j^2 - 3\sigma_j)^2} \right\}$$

$$- n_{0h}, \quad \text{(G.31)}$$

with

$$a = \frac{B}{A}, \quad \text{and} \quad b = \frac{1}{A}, \quad \text{(G.32)}$$

the Korteweg–de Vries equation may be cast in the form

$$\frac{\partial \phi^{(1)}}{\partial \tau} + a\phi^{(1)}\frac{\partial \phi^{(1)}}{\partial \xi} + b\frac{\partial^3 \phi^{(1)}}{\partial \xi^3} = 0. \qquad \text{(G.33)}$$

Appendix H

Simple wave solutions of the KdV and mKdV equations

H.1 Solution of the KdV equation

We consider the following problem

$$\frac{\partial \phi}{\partial \tau} + a\phi \frac{\partial \phi}{\partial \xi} + b\frac{\partial^3 \phi}{\partial \xi^3} = 0, \tag{H.1}$$

subject to the boundary conditions

$$\phi, \frac{\partial \phi}{\partial \xi}, \frac{\partial^2 \phi}{\partial \xi^2} \to 0 \quad \text{as} \quad |\xi| \to \infty. \tag{H.2}$$

By simple waves we mean solutions of the form

$$\phi = \phi(s) = \phi(\xi - U\tau), \tag{H.3}$$

where U is some velocity. Assuming solutions of the form (H.3) we can write the KdV equation in the form

$$-U\frac{\mathrm{d}\phi}{\mathrm{d}s} + \tfrac{1}{2}a\frac{\mathrm{d}}{\mathrm{d}s}\phi^2 + b\frac{\mathrm{d}^3\phi}{\mathrm{d}s^3} = 0. \tag{H.4}$$

Integrating twice using (H.2) yields

$$\left(\frac{\mathrm{d}\phi}{\mathrm{d}s}\right)^2 = \frac{U}{b}\phi^2 - \frac{a}{3b}\phi^3 \tag{H.5}$$

which is readily rearranged and integrated (formally) with respect to s yielding

$$\pm\left(\frac{b}{U}\right)^{1/2}\int\frac{\mathrm{d}\phi}{\phi[1-(a/3U)\phi]^{1/2}}=s+A, \tag{H.6}$$

where A is an arbitrary constant. With the substitution

$$\psi=\sqrt{\frac{a}{3U}}\phi \tag{H.7}$$

equation (H.6) becomes

$$\pm\left(\frac{4b}{U}\right)^{1/2}\int\frac{\mathrm{d}\psi}{\psi[1-\psi^2]^{1/2}}=s+A. \tag{H.8}$$

The left hand side is now in the standard form

$$-\int\frac{\mathrm{d}x}{x\sqrt{1-x^2}}=\operatorname{arcsech}x$$

yielding

$$\pm\operatorname{arcsech}\psi=\left(\frac{U}{4b}\right)^{1/2}(s+A). \tag{H.9}$$

Inverting and using (H.7) yields the required result

$$\phi=\frac{3U}{a}\operatorname{sech}^2\left\{\left(\frac{U}{4b}\right)^{1/2}(s+A)\right\} \tag{H.10}$$

or in terms of the original coordinates

$$\phi=\frac{3U}{a}\operatorname{sech}^2\left\{\left(\frac{U}{4b}\right)^{1/2}(x-U\tau+A)\right\}. \tag{H.11}$$

Of course validity of the solution requires $b>0$.

H.2 Solutions of the mKdV equation

We seek solutions of the mKdV equation

$$\frac{\partial\phi}{\partial\tau}+\tfrac{1}{2}a\frac{\partial}{\partial\xi}\phi^2+c\frac{\partial}{\partial\xi}\phi^3+b\frac{\partial^3}{\partial\xi^3}\phi=0, \tag{H.12}$$

that satisfy

$$\phi, \frac{\mathrm{d}\phi}{\mathrm{d}s}, \frac{\mathrm{d}^2\phi}{\mathrm{d}s^2} \to 0 \quad \text{as} \quad s \to \infty. \tag{H.13}$$

Seeking solutions of the form

$$\phi = \phi(s) = \phi(\xi - U\tau), \tag{H.14}$$

where U is some velocity, we write the mKdV equation in the form

$$-U\frac{\mathrm{d}\phi}{\mathrm{d}s} + \tfrac{1}{2}a\frac{\mathrm{d}}{\mathrm{d}s}\phi^2 + c\frac{\mathrm{d}}{\mathrm{d}s}\phi^3 + b\frac{\mathrm{d}^3\phi}{\mathrm{d}s^3} = 0. \tag{H.15}$$

Then equation (H.15) is readily integrated (twice) yielding on using the boundary conditions,

$$\left(\frac{\mathrm{d}\phi}{\mathrm{d}s}\right)^2 = \frac{U}{b}\phi^2 - \frac{a}{3b}\phi^3 - \frac{c}{2b}\phi^4. \tag{H.16}$$

H.2.1 Solitary-wave solutions

Taking the square root of both sides of (H.16) and manipulating this equation is easily cast in the form

$$\pm\left(\frac{b}{U}\right)^{1/2}\int \frac{\mathrm{d}\phi}{\phi[1-(a/3U)\phi-(c/2U)\phi^2]^{1/2}} = s + A, \tag{H.17}$$

where we have integrated with respect to s (A is an arbitrary constant).

The substitution

$$\theta = \frac{1}{\phi} \tag{H.18}$$

transforms the integral on the right hand side of the above into the form

$$\pm\left(\frac{b}{U}\right)^{1/2}\int \frac{\mathrm{d}\theta}{[\theta^2-(a/3U)\theta-c/2U]^{1/2}} \tag{H.19}$$

and after completing the square in the denominator we obtain

$$\pm\left(\frac{b}{U}\right)^{1/2}\int \frac{\mathrm{d}\theta}{[(\theta-a/6U)^2-(a^2/36U^2+c/2U)]^{1/2}}. \tag{H.20}$$

This is readily cast in the standard form

$$\int \frac{\mathrm{d}x}{\sqrt{x^2-\alpha^2}} = \operatorname{arccosh}\left(\frac{x}{\alpha}\right),$$

by the transformation

$$\psi = \theta - \frac{a}{6U}, \tag{H.21}$$

yielding

$$\pm \left(\frac{b}{U}\right)^{1/2} \operatorname{arccosh} \left\{ \frac{\psi}{\pm[a^2/36U^2 + c/2U]^{1/2}} \right\} = s + A. \tag{H.22}$$

However, this is subject to the condition that

$$\frac{a^2}{36U^2} + \frac{c}{2U} > 0. \tag{H.23}$$

Upon using (H.18) and (H.21) and inverting we obtain the solution (in terms of the original coordinates)

$$\phi = U \left[\pm \left(\frac{a^2}{36} + \frac{cU}{2} \right)^{1/2} \cosh \left\{ \left(\frac{U}{b} \right)^{1/2} (\xi - U\tau + A) \right\} + \frac{a}{6} \right]^{-1}, \tag{H.24}$$

subject to (H.23).

H.2.2 Double layer solutions

If it happens that

$$\frac{a^2}{36U^2} + \frac{c}{2U} = 0,$$

which may be satisfied if $U = -a^2/18c$, then the solution (H.24) is invalidated and we are forced to pursue a different approach. In this case equation (H.16) can be written in the form

$$\left(\frac{\mathrm{d}\phi}{\mathrm{d}s} \right)^2 = -\frac{c}{2b} \phi^2 \left(\phi + \frac{a}{3c} \right)^2. \tag{H.25}$$

Upon taking the square-root and completing the square on the right hand side we obtain on integration with respect to s

$$-\left(-\frac{2b}{c} \right)^{1/2} \int \frac{\mathrm{d}\phi}{(a/6c)^2 - (\phi + a/6c)^2} = \pm(s + A). \tag{H.26}$$

The substitution

$$\psi = \phi + \frac{a}{6c}, \tag{H.27}$$

renders the integral on the left hand side of (H.26) in the standard form

$$\int \frac{\alpha}{\alpha^2 - x^2} \mathrm{d}x = \operatorname{arctanh}\left(\frac{x}{\alpha}\right)$$

which may be inverted yielding

$$\psi = \pm \frac{a}{6c} \tanh\left\{\left(-\frac{a^2}{72bc}\right)^{1/2} (s + A)\right\}. \tag{H.28}$$

In terms of the original coordinates the solutions become

$$\phi = -\frac{a}{6c}\left[1 \pm \tanh\left\{\left(-\frac{a^2}{72bc}\right)^{1/2} (\xi - U\tau + A)\right\}\right], \tag{H.29}$$

where we discard the solution with the upper sign because it does not satisfy the boundary conditions.

References

AKHIEZER, A.I., AKHIEZER, I.A., POLOVIN, R.V., SITENKO, A.G., STEPANOV, K.N. 1975 *Plasma Electrodynamics, Volume 1: Linear Theory*, Pergamon Press: Oxford, p. 265.

AREF'EV, V.I. 1970 *Soviet Phys. Tech. Phys.* **14**, 1487.

ASHOUR-ABDALLA, M. & OKUDA, H. 1986 *Geophys. Res. Lett.* **13**, 366.

BABOOLAL, S. 1988 *Ph.D Thesis*, University of Natal, Durban, South Africa.

BABOOLAL, S., BHARUTHRAM, R. & HELLBERG, M.A. 1988 *J. Plasma Phys.* **40**, 163.

BABOOLAL, S., BHARUTHRAM, R. & HELLBERG, M.A. 1989 *J. Plasma Phys.* **41**, 341.

BABOOLAL, S., BHARUTHRAM, R. & HELLBERG, M.A. 1991 Submitted to *J. Plasma Phys.*

BEGELMAN, M.C. & KIRK, J.G. 1990 *Astrophys. J.* **353**, 66.

BESKIN, V.S., GUREVICH, A.V., ISTOMIN YA. N. 1983 *Sov. Phys. JETP* **58**, 235.

BHARUTHRAM, R. 1991a *J. Plasma Phys.* In press.

BHARUTHRAM, R. 1991b Submitted to *J. Plasma Phys.*

BHARUTHRAM, R. & SHUKLA, P.K. 1986 *Phys. Fluids* **29**, 3214.

BHARUTHRAM, R. & SHUKLA, P.K. 1988 *Astrophysics and Space Science* **149**, 127.

BROER, L.J.F. & SLUIJTER, F.W. 1977 *Phys. Fluids* **20**, 1458.

BUTI, B. 1980 *J. Plasma Phys.* **24**, 169.

BUTI, B., MOHAN, M. & SHUKLA, P.K. 1980 *J. Plasma Phys.* **23**, 341.

CALLEN, J.D. & GUEST, G.E. 1971 *Phys. Fluids* **14**, 1588.

CHEN, F.F. 1984 *Introduction to plasma physics and controlled fusion*, Plenum: New York, p. 299.

CHOWDHURY, A.R., PAKIRA, G.P. & PAUL, S.N. 1988 *Physica C* **151**, 518.

CHOWDHURY, A.R., PAKIRA, G.P. & PAUL, S.N. 1989 *IEEE Trans. Plasma Sci.* **17**, 1989.

CUPERMAN, S. 1981 in *Modern plasma physics: Trieste course, 1979*, IAEA: Vienna, p 125.

DAS, G.C., KARMAKAR, B. & PAUL, S.N. 1988 *IEEE Trans. Plasma Sci.* **16**, 1988.

DAS, G.C. & PAUL, S.N. 1985 *Phys. Fluids* **28**, 823.

DAS, G.C. & TAGARE, S.G. 1975 *Plasma Phys.* **17**, 1025.

DAS, K.P. & VERHEEST, F. 1989 *J. Plasma Phys.* **41**, 139.

DASH, S.S., SHARMA, A.S. & BUTI, B. 1984 *J. Plasma Physics* **32**, 255.

DE ANGELIS, U., FORMISANO, V. & GIORDANO, M. 1988 *J. Plasma Phys.* **40**, 399.

DELL, M.P. 1984 *M.Sc. Thesis*, University of Natal, Durban, South Africa.

DELL, M.P., GLEDHILL, I.M.A. & HELLBERG, M.A. 1987 *Z. Naturforschung* **42a**, 1175.

DENAVIT, J. 1965 *Phys. Fluids* **8**, 471.

DEY, M., GOSWAMI, K.S. & BUJARBARUA, S. 1988 *Physica B* **152**, 385.

DRAZIN, P.G. & JOHNSON, R.S. 1989 *Solitons: an introduction*, Cambridge University Press: Cambridge, p. 7.

DUBOULOZ, N., POTTELETTE, R., MALINGRE, M. HOLMGREN, G. & LINDQVIST, P.A. 1991a *J. Geophys. Res.* **96**, 3565.

DUBOULOZ, N., POTTELETTE, R., MALINGRE, M. & TREUMANN, R.A. 1991b *Geophys. Res. Lett.* **18**, 155.

DUSENBERY, P.B. 1986 *J. Geophys. Res.* **91**, 12005.

DUSENBERY, P.B. & LYONS, L.R. 1985 *J. Geophys. Res* **90**, 10935.

FOSTER, J. & NIGHTINGALE, J.D. 1979 *A short course in general relativity*, Longman Group, p. 73.

FRIED, B.D. & CONTE, S.D. 1961 *The plasma dispersion function*, Academic press: New York

FRIED, B.D. & GOULD, R.W. 1961 *Phys. Fluids* **4**, 139.

FRIED, B.D., WHITE, R.B. & SAMEC, T.K. 1971 *Phys. Fluids* **14**, 2388.

FRYCZ, P. & INFELD, E. 1989 *Phys. Rev. Lett.* **63**, 384.

GABL, E.F., BULSON, J.M. & LONNGREN, K.E. 1984 *Phys. Fluids* **27**, 269.

GARDNER, C.S., GREENE, J.M., KRUSKAL, M.D. & MIURA, R.M. 1967 *Phys. Rev. Lett.* **19**, 1095.

GARDNER, C.S. & MORIKAWA, G.K. 1965 *Comm. Pure Appl. Math.* **XVIII**, 35.

GARY, S.P. 1971 *J. Plasma Phys.* **6**, 561.

GARY, S.P. 1987 *Phys. Fluids* **30**, 2745.

GARY, S.P. & TOKAR, R.L. 1985 *Phys. Fluids* **28**, 2439.

GLEDHILL, I.M.A. 1982 *Ph.D. Thesis*, University of Natal, Durban, South Africa.

GLEDHILL, I. M. A. & HELLBERG M. A. 1986 *J. Plasma Phys.* **36**, 75.

GOEDBLOED, J.P., PYATAK, A.I. & SIZONENKO, V.L. 1973 *Sov. Phys. JETP* **37**, 1051.

GOLD, T. 1969 *Nature* **218**, 731.

GOSWAMI, K.S. & BUJARBARUA, S. 1987 *Il Nuovo Cimento* **9D**, 1133.

GOSWAMI, K.S., KALITA, M.K. & BUJARBARUA, S. 1986 *Plasma Phys. Contr. Fusion* **28**, 289.

GRABBE, C.L. 1985 *Geophys. Res. Lett.* **12**, 483.

GRABBE, C.L. & EASTMANN, T.E. 1984 *J. Geophys. Res.* **89**, 3865.

GUHA, S. & DWIVEDI, C.B. 1984 *J. Plasma Phys.* **32**, 283.

GURNETT, D.A. 1966 *J. Geophys. Res.* **71**, 5599.

GURNETT, D.A. & FRANK, L.A. 1972 *J. Geophys. Res.* **77**, 172.

GURNETT, D.A. & FRANK, L.A. 1977 *J. Geophys. Res.* **82**, 1031.

GURNETT, D.A. & FRANK, L.A. 1978 *J. Geophys. Res.* **83**, 58.

GURNETT, D.A., FRANK, L.A. & LEPPING, R.P. 1976 *J. Geophys. Res.* **81**, 6059.

GURNETT, D.A., SHAWHAN, S.D. & SHAW, R.R. 1983 *J. Geophys. Res.* **88**, 329.

HASEGAWA, A. & MIMA, K. 1978 *Phys. Fluids* **21**, 87.

HEPPNER, J.P. 1969 in *Atmospheric emissions*, edited by B.M. McCormac & A. Omholt, Rheinhold: New York, p251.

HOFFMAN, R.A. & LAASPERE, T. 1972 *J. Geophys. Res.* **77**, 640.

ICHIMARU, S. 1973 *Basic Principles of Plasma Physics: A Stastical Approach*, W.A. Benjamin Inc.: Reading, Mass., p. 73.

INFELD, E., ROWLANDS, G. & HEN, M. 1978 *Acta Phys. Polon.* **A54**, 131.

JONES, W.D., LEE, A., GLEMAN, M. & DOUCET, H.J. 1975 *Phys. Rev. Lett.* **35**, 1349.

KADOMTSEV, B.B. & PETVIASHVILI, V.I. 1970 *Sov. Phys. Dokl.* **15**, 539.

KARPMAN, V.I. 1979 *Sov. Phys. JETP* **50**, 695.

KARPMAN, V.I., LYNOV, J.P., MICHELSEN, P., PÉCSELI, H.L., & RASMUSSEN, J.J. 1979 *Phys. Rev. Lett.* **43**, 210.

KARPMAN, V.I., LYNOV, J.P., MICHELSEN, P., PÉCSELI, H.L., & RASMUSSEN, J.J. 1980 *Phys. Fluids* **23**, 1782.

KIM, K.Y. 1983 *Phys. Lett.* **97A**, 45.

KIRK, J.G. & SCHNEIDER, P. 1987 *Astrophys. J.* **315**, 425.

KITSENKO, A.B., PANCHENKO, V.I. & STEPANOV, K.N. 1974a *Sov. Phys. Tech. Phys.* **18**, 905.

KITSENKO, A.B., PANCHENKO, V.I. & STEPANOV, K.N. 1974b *Sov. Phys. Tech. Phys.* **18**, 911.

KODAMA, Y. & TANIUTI, T.J. 1978 *J. Phys. Soc. Japan* **45**, 298.

KONNO, K., MITSUHASHI, T. & ICHIKAWA, Y.H. 1977 *J. Phys. Soc. Japan* **43**, 669.

KORTEWEG, D.J. & DE VRIES, G. 1895 *Phil. Mag.* **39**, 422.

KRALL, N.A. & TRIVELPIECE, A.W. 1973 *Principles of Plasma Physics*, McGraw-Hill: New York, p. 376.

KUZNETSOV, E.A., SPECTOR, M.D. & FAL'KOVICH, G.E. 1984 *Physica* **10D**, 379.

LASHMORE-DAVIES, C.N. & MARTIN, T.J. 1973 *Nucl. Fus.* **13**, 193.

LEE, L.C. & KAN, K.R. 1981 *Phys. Fluids* **24**, 430.

LIN, C.S., BURCH, J.L., SHAWHAN, S.D., & GURNETT, D.A. 1984 *J. Geophys. Res.* **89**, 925.

LIN, C.S. & HOFFMAN, R.A. 1982 *Space Sci. Rev.* **33**, 415.

LIN, C.S., WINSKE, D., & TOKAR, R.L. 1985 *J. Geophys. Res.* **90**, 8269.

LIN, C.S.& WINSKE, D. 1987 *J. Geophys. Res.* **92**, 7569.

LOMINADZE, J.G., MELIKIDZE, G.I., PATARAYA, A.D. 1984 *International Conference on Plasma Physics, Lausanne, Switzerland* **2**, 1043.

MACE, R.L. & HELLBERG, M.A. 1990 *J. Plasma Phys.* **43**, 239.

MACE, R.L., BABOOLAL, S., BHARUTHRAM, R. & HELLBERG, M.A. 1991a *J. Plasma Phys.* **45**, 323.

MACE, R.L., HELLBERG, M.A., BHARUTHRAM, R. & BABOOLAL, S. 1991b *J. Plasma Phys.* In press.

MANN, G. 1986 *J. Plasma. Phys.* **36**, 25.

MARSCH, E. 1985 *J. Geophys. Res.* **90**, 6327.

MELROSE, D.B. 1986 *Instabilities in space and laboratory plasmas,* Cambridge University Press: Cambridge, p. 209, p. 169.

MOHAN, M. & BUTI, B. 1980 *Plasma Phys.* **22**, 873.

MOHAN, M. & YU, M.Y. 1983 *J. Plasma Physics* **29**, 127.

MONTGOMERY, D.C. 1971 *Theory of the Unmagnetized Plasma* Gordon & Breach: New York, p. 69.

NEJOH, Y. 1987a *J. Plasma Phys.* **37**, 487.

NEJOH, Y. 1987b *J. Plasma Phys.* **38**, 439.

NESS, N.F., SCEARCE, C.S. & SEEK, J.B. 1964 *J. Geophys. Res.* **69**, 3531.

OGINO, T., & TAKEDA, S. 1975 *J. Phys. Soc. Jpn.* **39**, 1365.

OTT, E., & SUDAN, R.N. 1969 *Phys. Fluids* **12**, 2388.

PÉCSELI, H.L. 1985 *IEEE Trans. Plasma Sci.* **PS–13**, 53.

PETVIASHVILI, V.I. 1986 *Reviews of Plasma Physics*, vol 9 (ed. M.A. Leontovich), Consultants Bureau, p. 59.

POKROEV, A.G. & STEPANOV, K.N. 1973 *Sov. Phys. Tech. Phys* **18**, 461.

POLYAKOV, P.A. 1983 *Sov. Phys. JETP* **58**, 922.

POTTELETTE, R., MALINGRE, M., BAHNSEN, A., ELIASSON, L., STACIEWICZ, K., ERLANDSON, R.E. & MARKLUND, G. 1988 *Ann. Geophys.* **6**, 573.

POTTELETTE, R., MALINGRE, M., DUBOULOZ, N., APARICIO, B., LUNDIN, R., HOLMGREN, G. & MARKLUND, G. 1990 *J. Geophys. Res.* **95**, 5957.

RAADU, M.A. 1989 *Physics Reports* **178**, 25.

RAHMAN, H.U., & SHUKLA, P.K. 1982 *Phys. Lett.* **89A**, 13.

RAO, N.N., SHUKLA, P.K. & YU, M. Y. 1990 *Planet. Space Sci.* **38**, 543.

RODRIGUEZ, P. & GURNETT, D.A. 1975 *J. Geophys. Res.* **80**, 19.

ROTH, I & HUDSON, M.K. 1986 *J. Geophys. Res.* **91**, 8001.

ROYCHOUDHURY, R.K. & BHATTACHARYYA, S. 1987 *Phys. Fluids* **30**, 2582.

SAGDEEV, R.Z. 1966 *Reviews of Plasma Physics*, vol. 4 ed. M.A. Leontovich), Consultants Bureau, p. 23.

SAKAI, J. & KAWATA, T. 1980 *J. Phys. Soc. Japan* **49**, 747.

SALAHUDDIN, M. 1990 *Plasma Phys. and Contr. Fusion* **32**, 33.

SALAS, S.L. & HILLE, E. 1978 *Calculus of one and several variables part 2*, Wiley & Sons Inc.: New York, p. 732.

SALEEM, H. & MURTAZA, G. 1986 *J. Plasma Phys.* **36**, 295.

SANUKI, H. & TOKOROKI, J. 1972 *J. Phys. Soc. Japan* **32**, 517.

SARMA, S.N., KALITA, M.K. & BUJARBARUA, S. 1986 *Contrib. Plasma Phys.* **26**, 367.

SCHAMEL, H. 1979 *Physica Scripta* **20**, 336.

SCHAMEL, H. 1983 *Z. Naturforsch. Teil A* **38A**, 1170.

SCHRIVER, D. & ASHOUR-ABDALLA, M. 1987 *J. Geophys. Res.* **92**, 5807.

SHARMA, R.P., RAMAMURTHY, K. & YU, M.Y. 1984 *Phys. Fluids* **27**, 399.

SHAWHAN, S.D. 1979 *Rev. Geophys. Space Phys.* **17**, 705.

SINGH, S. & DAHIYA, R.P. 1990 *Phys. Fluids B* **2**, 901.

SIZONENKO, V.L. & STEPANOV, K.N. 1967 *Nucl. Fus.* **7**, 131.

SONG, L.T., LEE, L.C. & HUANG, L. 1988 *Phys. Fluids* **31**, 1549.

SPANGLER, S.R. & SHEERIN, J.P. 1982 *J. Plasma Phys.* **27**, 193.

SPATSCHEK, K.H., LAEDKE, E.W., MARQUARDT, CHR., MUSHER, S. & WENK, H. 1990 *Phys. Rev. Lett.* **64**, 3027.

STIX, T.H. 1962 *The Theory of Plasma Waves*, Mc Graw-Hill: New York, p 218.

STRAUMANN, N. 1984 *General Relativity and Relativistic Astrophysics*, Springer: Berlin, p. 92.

STURROCK, P.A. 1971 *Astrophys. J.* **164**, 527.

SWANSON, D.G. 1989 *Plasma waves*, Academic press: Boston, p. 178.

TAGARE, S.G. 1973 *Plasma Phys.* **15**, 1247.

TANIUTI, T. 1974 *Progr. Theor. Phys. (Suppl.)* **55**, 1.

TANIUTI, T. & NISHIHARA, K. 1983 *Nonlinear Waves* , Pitman, p. 100.

THOMSEN, M.F., BARR, H.C., GARY, S.P., FELDMAN, W.C. & COLE, T.E. 1983 *J. Geophys. Res* **88**, 3035.

TOKAR, R.L. & GARY, S.P. 1984 *Geophys. Res. Lett.* **11**, 1180.

TORVÉN 1981 *Phys. Rev. Lett.* **47**, 1053.

VERHEEST, F. 1988 *J. Plasma Phys.* **39**, 71.

VOLKOV, T.F. 1966 in *Reviews of Plasma Physics*, vol 4 (ed. M.A. Leontovich), Consultants Bureau, p. 1.

WASHIMI, H. & TANIUTI, T. 1966 *Phys. Rev. Lett.* **17**, 996.

WATANABE, K. & TANIUTI, T. 1977 *J. Phys. Soc. Japan* **43**, 1819.

WATANABE, S. 1984 *J. Phys. Soc. Japan* **53**, 950.

YADAV, L.L. & SHARMA, S.R. 1989 *International Conference on Plasma Physics, New Delhi, India* **2**, 781.

YU, M. 1977 *J. Plasma Phys.* **18**, 139.

YU, M.Y. & SHUKLA, P.K. 1983 *J. Plasma Phys.* **29**, 409.

ZABUSKY, N.J. 1967 in *Nonlinear Partial Differential Equations* (W. Ames, ed.) Academic Press: New York.

ZABUSKY, N.J. 1968 *Phys. Rev. Lett.* **168**, 124.

ZABUSKY, N.J. & KRUSKAL, M.D. 1965 *Phys. Rev. Lett.* **15**, 240.

ZAKHAROV, V.E. 1972 *Sov. Phys. JETP* **35**, 908.

ZAKHAROV, V.E., & KUZNETSOV, E.A. 1975 *Sov. Phys. JETP* **39**, 285.

List of commonly used symbols

Latin alphabet

a, b, c	coefficients of KdV, KP, KdV–ZK and mKdV equations
A, B, C, D	coefficients of KdV, KP, KdV–ZK and mKdV equations
$\mathbf{B}$	magnetic field
c, c_L	speed of light
e	electronic charge
$\mathbf{e}_x, \mathbf{e}_y, \mathbf{e}_z$	cartesian unit vectors
$\mathbf{E}$	electric field
$f_j(\mathbf{x}, \mathbf{v}, t), f_j$	distribution function for particle species j
$F_{\mu\nu}$	Maxwell tensor
$g_{\mu\nu}$	metric tensor
I	unit tensor
$I_n(x)$	modified Bessel function
Im	imaginary part
j^μ	four-current density
$J_n(x)$	Bessel function
$\mathbf{k}, k$	wavevector and its magnitude
k_x, k_y, k_z	cartesian components of $\mathbf{k}$
$k_\parallel, k_\perp$	parallel and perpendicular components of $\mathbf{k}$
K	normalised wavevector magnitude
m_j	mass of particle species j
$M, \mathcal{M}$	soliton speed (Mach number)
n_j	number density of particle species j
n_{0j}	background number density (part II) of species j
$N(\phi)$	normalised charge density
$O(x)$	of order x
p_j	partial pressure of particle species j
P_j	pressure tensor for particle species j
q_j	charge of particle species j
r	radial coordinate
Re	real part
s	moving coordinate
T_j	temperature (in energy units) of particle species j
$T_{\mu\nu}$	energy-momentum tensor
$\mathbf{u}_j, u_j$	fluid velocity of particle fluid j, and its magnitude
u_j, v_j, w_j	cartesian components of $\mathbf{u}_j$

u^μ	world velocity (four-velocity)
$\mathbf{v}$	particle velocity
v_j	(part I) thermal speed of particle species j
v_{0j}	mean drift speed of particle species j
v_{0ib}	ion beam mean drift speed
$\mathbf{v}_g$	group velocity
v_{se}	electron sound speed
v_{si}	ion sound speed
V	sound speed
$\mathbf{V}_E$	$\mathbf{E} \times \mathbf{B}$ drift
$\mathbf{x}$	position vector
$\mathbf{X}(t)$	particle orbit
$Z(\zeta)$	plasma dispersion function
$Z'(\zeta)$	derivative of $Z(\zeta)$
Z_j	normalized charge of particle species j

Greek alphabet

γ	imaginary part of ω
γ_j, Γ_j	relativistic factors for particle species j
ϵ	(part II) expansion parameter
$\epsilon(\mathbf{k}, \omega)$	dielectric function
θ	angle of wavevector w.r.t $\mathbf{B}$
λ_j, λ_{Dj}	Debye lengths of particle species j
λ_{Dib}	ion beam Debye length
λ_j	(chapter 9) phase relative to drift speed of particle species j
μ	proper mass (energy) density
ϱ	mass density
ρ_j	Larmor radius of particle species j
ρ	(proper) charge density
ρ_{se}	effective Larmor radius
σ_j	square of the normalised thermal speed of particle species j
τ, ξ, η, ζ	stretched variables
ϕ	electrostatic potential
ϕ_0	maximum (in modulus) soliton amplitude
ϕ_m	double layer "potential" (§10.3)
$\Psi(\phi), \Psi$	Sagdeev (pseudo) potential

ω	complex wave frequency
ω_j, ω_{pj}	plasma frequency of particle species j
ω_r	real part of ω
$\omega_s(k)$	dispersion relation for electron-acoustic waves
Ω_j	gyrofrequency of particle species j
Ω	electron gyrofrequency; (part II) normalised wave frequency